JRC Scientific and Technical Reports

THEORY - 1

Proceedings of the Scientific Workshop on Nuclear Fission Dynamics and the Emission of Prompt Neutrons and Gamma Rays
27 – 29 September, 2010
Sinaia, Romania

Edited by F.-J. Hambsch and N. Carjan

EUR 24802 EN - 2011

JRC EUROPEAN COMMISSION

Institute for Reference Materials and Measurements

The mission of the JRC-IRMM is to promote a common and reliable European measurement system in support of EU policies.

European Commission
Joint Research Centre
Institute for Reference Materials and Measurements

Contact information
F.-J. Hambsch
European Commission
Joint Research Centre
Institute for Reference Materials and Measurements
Retieseweg 111
B - 2440 Geel
Belgium

E-mail: Franz-Josef.Hambsch@ec.europa.eu
Tel.: +32 (0) 14 571351
Fax: +32 (0) 14 571376

http://irmm.jrc.ec.europa.eu/
http://www.jrc.ec.europa.eu/

JRC 64789

EUR 24802 EN
ISBN 978-92-79-20048-9 (print version)
ISBN 978-92-79-20049-6 (pdf version)
ISSN 1018-5593 (print version)
ISSN 1831-9424 (online version)
doi:10.2787/4298 (print version)

Luxembourg: Publications Office of the European Union

Printed in Belgium

THEORY - 1

Proceedings of the Scientific Workshop on Nuclear Fission Dynamics and the Emission of Prompt Neutrons and Gamma Rays

27 – 29 September, 2010

Sinaia, Romania

Edited by F.-J. Hambsch and N. Carjan

Foreword

On September 27 – 29, 2010 a Scientific Workshop on Nuclear Fission Dynamics and the Emission of Prompt Neutrons and Gamma Rays (THEORY – 1) was held in Sinaia, Romania. The workshop was co-organized by the Neutron Physics Unit of JRC-IRMM and the National Institute of Physics and Nuclear Engineering-Horia-Hulubei, Bucharest, Romania. The organisers were assisted by a Programme Advisory Committee consisting of V. Avrigeanu (NIPNE-HH, Romania), R. Capote (IAEA, Austria), F. Gönnenwein (U. Tübingen, Germany), S. Oberstedt (EC-JRC-IRMM, Belgium), O. Serot (CEA-Cadarache, France), P. Talou (LANL, USA) and A. Tudora (Bucharest University, Romania).

The purpose of the workshop was to provide a comprehensive overview of the dynamical aspects of nuclear fission and their consequences on the fission fragment properties. The contributions have highlighted recent theoretical advancements in the field of nuclear fission and in particular for the emission of prompt neutrons and gamma rays.

Both invited presentations and normal contributions have been given. The success of the workshop must be attributed to the 26 contributions and more than 35 participants, many of which were post-doctoral fellows and PhD students.

The workshop was organised and financed within the Enlargement and Integration activity of JRC. The general aim of this activity is to support the EU enlargement and integration process by fostering collaboration with target countries' governmental organisations (or the like), which will have an institutional role for providing Science and Technology support to the implementation of policies, particularly through the associated scientific and technical organisations.

We would like to express our gratitude to the program advisory committee, for their help to choose key topics to debate and to the speakers for their carefully prepared presentations. A very special thank you goes to the perfect local organisational support of C. Cabanillas Platero.

Franz-Josef Hambsch and Nicolae Carjan
April 2011

Group photo of the participants

Contents

Complementary deuteron breakup and induced activation analysis

M. Avrigeanu, V. Avrigeanu

'Horia Hulubei' National Institute for Physics and Nuclear Engineering, P.O. Box MG-6, 77125 Bucharest-Magurele, Romania
mavrig@ifin.nipne.ro

Abstract: An extended analysis of the reaction mechanisms involved within deuterons interaction with light and medium nuclei, ^{27}Al, ^{59}Co, ^{63,65}Cu, ^{93}Nb, at incident energies up to 60 MeV, starting with elastic scattering until the evaporation from fully equilibrated compound system, forms the object of this work. An increased attention is devoted to the breakup mechanism, all its components, namely the elastic (BE), inelastic (fusion) (BF), and total breakup (BU), being carefully analysed. Furthermore, the corresponding stripping and pick-up mechanisms contributions to the *(d,p)*, *(d,n)*, and *(d,t)* reaction cross sections through population of discrete levels of the residual nuclei, have been analyzed using the Coupled-Reaction Channels (CRC) method. Finally, the pre-equilibrium (PE) and compound-nucleus (CN) cross sections, corrected for the breakup, stripping, and pick-up decrease of the total reaction cross section, completed the deuteron activation cross sections analysis.

Introduction

Description of the deuteron-nucleus interaction represents an important test for the quality of the nuclear reaction models as well as for the associated computers codes used for evaluation of nuclear data requested especially for the fusion reactor technology. The weak binding of the deuteron (2.2 MeV) is responsible for the high complexity of the interaction process involving supplementary a variety of reactions initiated by the neutrons and protons coming from its breakup. The difficulties to interpret the deuteron-induced reaction data in terms of the usual reaction mechanism models have recently been investigated [1-7] looking for a consistent way to include the breakup contribution within the activation cross section calculations too.

Actually, the deuteron-induced reactions at low and medium energies have a great importance for the assessment of the induced radioactivity of the fusion reactor as well as of the International Fusion Materials Irradiation Facility (IFMIF) components. Moreover, recent calculations of the deuteron activation have shown that the deuterons are more important than the neutrons due to a value of about 70 for the ratio of the deuteron- and neutron-induced activity, respectively. On the other hand, it is known that the current calculations and measured deuteron reaction cross sections are less extensive and accurate than for neutrons, so that improved model calculations and further measurements are needed if the deuteron libraries are to approach the standard of the established neutron ones.

OMP analysis

The simultaneous analysis of the deuteron elastic scattering and induced activation appears essential for a consistent input of nuclear model calculations [4-7], a prime interest for the optical model potential (OMP) parameters being motivated by their further use in the calculation of deuteron interaction cross sections.

The few measurements of angular distributions of elastic scattered deuterons on ^{59}Co, ^{63,65}Cu, and ^{93}Nb [8] did not make possible an extended OMP analysis. On the other hand, while previous OMP analysis on ^{6,7}Li [2,3], and ^{27}Al [4,5] shows that no global OMP describes reasonably well the elastic scattering data in the energy range up to 20 MeV, the adjustment of Daehnick et al. [9] parametrization led to a good description of the data for ^{59}Co, ^{63,63,nat}Cu, and ^{93}Nb target nuclei. The comparison of the experimental elastic-scattering angular distributions for the ^{59}Co, ^{63,63,nat}Cu, and ^{93}Nb target nuclei and the calculated values obtained by using these adjusted OMP parameters (solid curves), the global optical potential [9] (dot-dashed curves), and TALYS-1.2 code [10] default option (dashed curves) based on the Watanabe folding approach [11] are shown in Fig. 1. The elastic-scattering cross section calculations have been performed using the computer code SCAT2 [12].

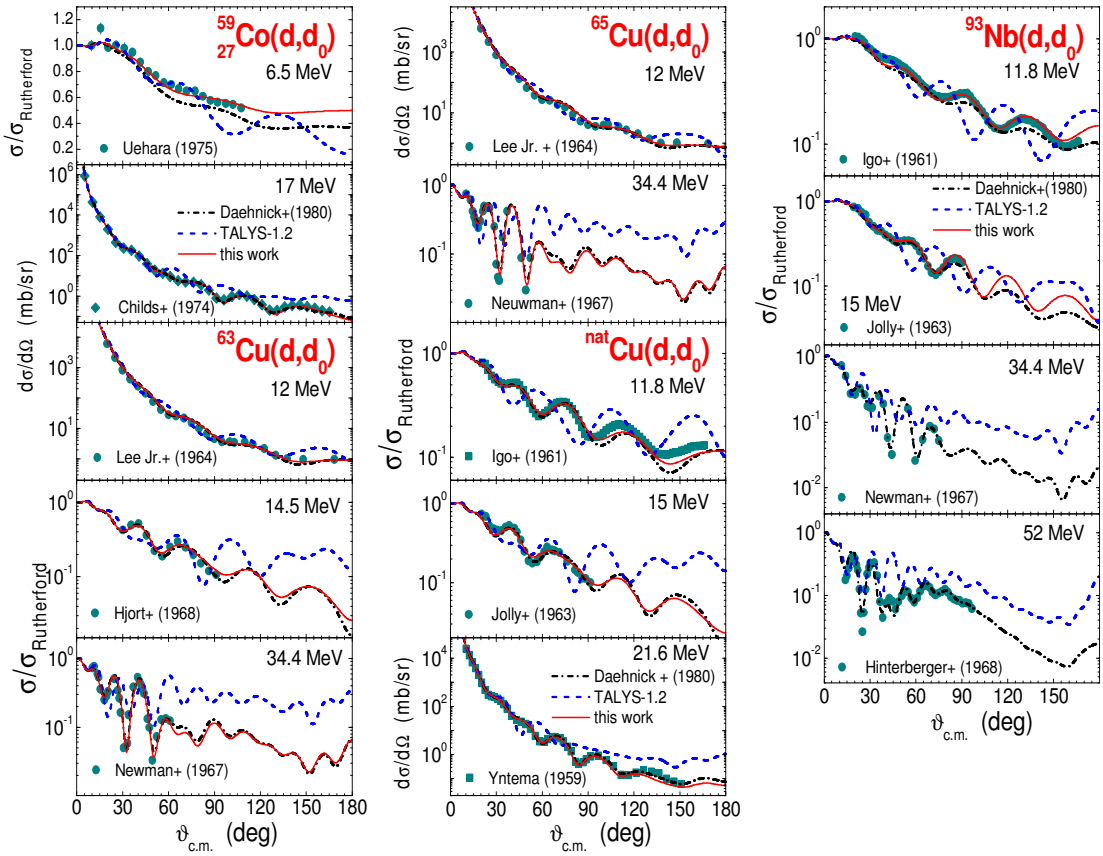

Figure 1. *(Color online) Comparison of the experimental [8] and calculated angular distributions of the elastic scattering of deuterons on ^{59}Co, ^{63,65}Cu, and ^{93}Nb by using the adjusted phenomenological OMP (solid curves), Daehnick et al. [9] OMP (dash-dotted curves) and the default potential for deuterons within TALYS-1.2 code (dashed curves).*

Deuteron breakup

The physical picture of the deuteron breakup in the Coulomb and nuclear fields of the target nucleus considers two distinct processes, namely the elastic breakup (EB), in which the target nucleus remains in its ground state and none of the deuteron constituents interacts with it, and the inelastic breakup or breakup fusion (BF), where one of these deuteron constituents interacts with the target nucleus while the remaining one is detected. Despite the important theoretical studies devoted to the breakup processes (see review papers [13] and references therein), only the elastic breakup contribution can be accurately calculated so far within the Continuum-Discretized Coupled-Channels (CDCC) method [14].

Therefore, the total and inelastic breakup components are typically estimated empirically. Kalbach [1] gives parametrizations for the total proton- and neutron-emission breakup cross section (σ_p^{BU} and σ_n^{BU}), while a second parametrization [4,6,7] considers equal breakup contributions for proton and neutron emission but supplementary gives all breakup components, i.e. the total $\sigma_{p,n}^{BU}$, elastic σ^{BE}, and inelastic $\sigma_{p,n}^{BF}$ breakup cross sections. It can be seen in Fig. 2 that both parametrizations for ^{27}Al, ^{59}Co, ^{63,65}Cu, and ^{93}Nb target nuclei are close for deuteron incident energies above ~7 MeV, while decreasing the incident energy the total proton-emission breakup cross sections given by Kalbach parametrization [1] remain higher than even the deuteron total reaction cross sections (thin solid curves in Fig. 2).

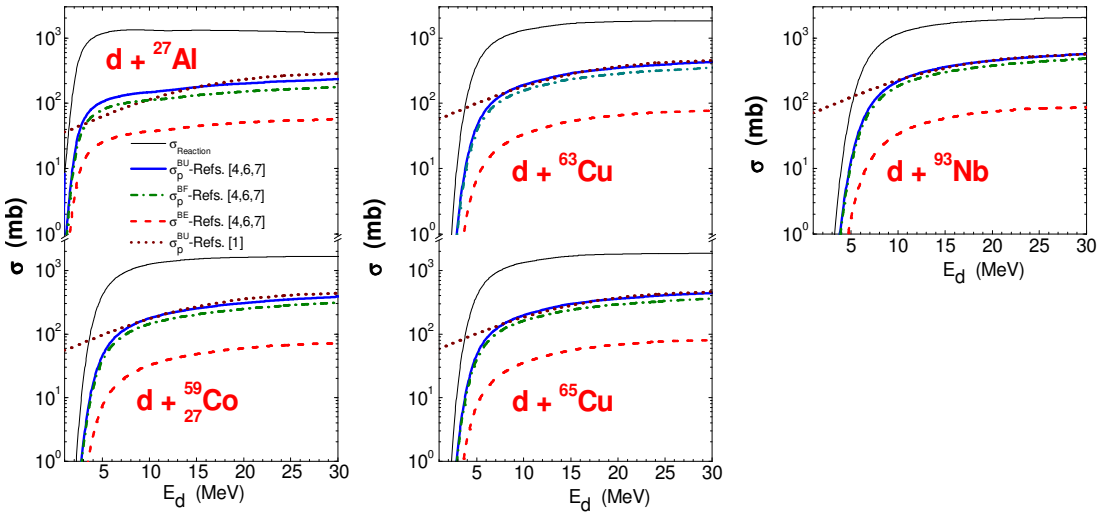

Figure 2. *(Color online) The energy dependence of the total (thick solid), the elastic (dashed), the inelastic (dot-dashed) proton-emission breakup cross sections given by [4] and of the total proton-emission breakup cross sections [1] (dotted) from the deuterons interactions with ^{27}Al, ^{59}Co, ^{63,65}Cu, and ^{93}Nb. The corresponding reaction cross section is shown by thin curve.*

Given the interest of the deuteron activation cross sections for incident energies up to 60 MeV, the extension of the elastic breakup parametrization [4] at higher incident energies beyond the energies formerly considered should be checked [15]. Therefore, in the absence of any available experimental deuteron elastic-breakup cross section at incident energies above 30 MeV, the correctness of an eventual parametrization extrapolation have been analyzed by comparison of its predictions with the CDCC calculations results [15] obtained with the FRESCO code [16]. Finally, as can be seen from Fig. 3 at deuteron energies over 30 MeV the microscopic CDCC results should replace the extrapolation of empirical parametrization of elastic breakup cross sections.

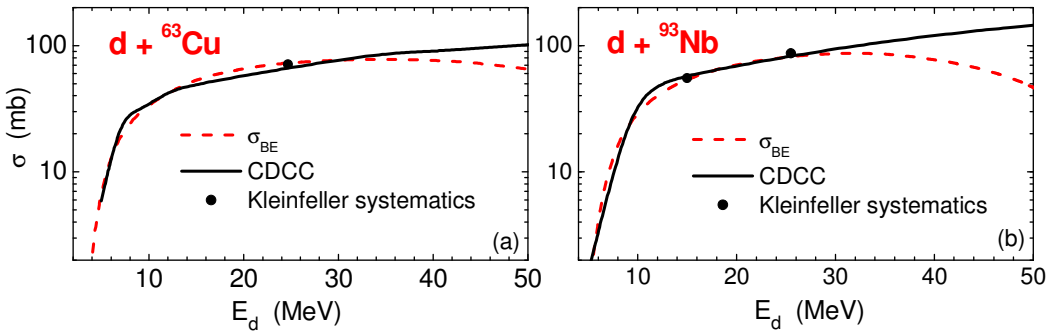

Figure 3. *(Color online) Energy dependence of the empirical [4] (dashed curve) and CDCC [15] (solid line) elastic breakup cross sections for deuteron scattering on ^{63}Cu and ^{93}Nb. The solid circle is the value from Kleinfeller systematics [17].*

On the whole, the deuteron total breakup reaction cross section reduces the amount of the total reaction cross section that should be shared among different outgoing channels. On the other hand, the inelastic breakup process, where one of deuteron constituents interacts with the target leading to a secondary composite nucleus, brings contributions to different reaction channels, enhancing mostly the secondary-chance emission of particles from the original d-target interaction.

Therefore the absorbed neutron following the breakup proton emission contributes to the enhancement of the *(d,p)* as well as *(d,2p)*, *(d,pα)*, *(d,p2n)*, *i.e. (d,xp)* reaction cross sections.

In order to calculate this enhancement, the inelastic breakup cross section, σ_p^{BF}, has been multiplied by the corresponding fraction leading to the above-mentioned reactions, i.e $\sigma(n,x)/\sigma_T$. Here σ_T is the neutron total cross section and x stands for γ, n,p, or α outgoing channels [5,6,7]. A similar procedure has been followed in order to obtain the contribution to the *(d,2n)*, *(d,p2n)*, (d,α2n), i.e. *(d,xn)* reaction cross sections due to the protons which, following the breakup neutron emission, are absorbed in further interactions with the target nucleus. In Fig. 4(a,c) are presented the excitation functions corresponding to *(n,2n)* and respectively *(p,d)* reactions initiated by neutrons and protons, responsible for the inelastic breakup enhancement of the $^{93}Nb(d,x)^{92m}Nb$ activation cross sections, Fig. 4(b).

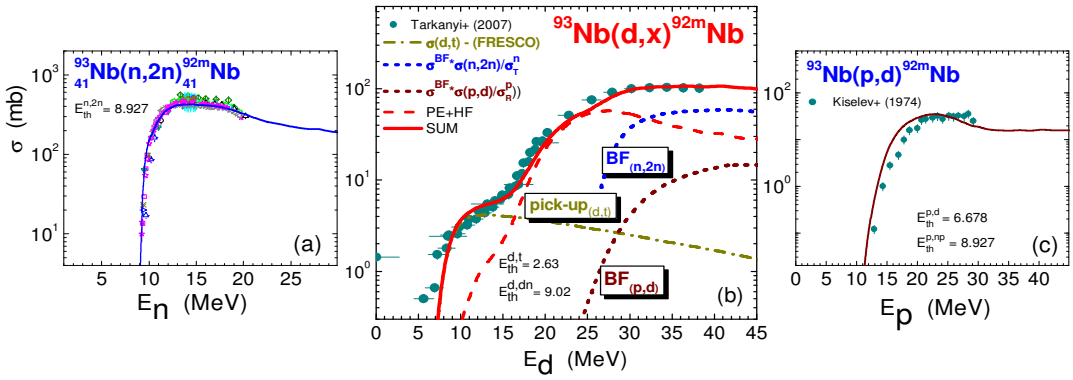

Figure 4. *(Color online)* 4(b) *Comparison of measured [18] and calculated deuteron activation cross sections (thick solid) provided by present analysis taking into account the deuteron inelastic breakup (dotted), the pick-up (dash-dotted), and the PE+CN (dashed) reaction mechanism contributions involved in the deuteron interaction with ^{93}Nb; 4(a), 4(c): Comparison of measured [8] and calculated activation cross sections initiated by neutrons and protons respectively, and responsible for the breakup enhancement of the deuterons activation (see text for more explanations).*

The inelastic breakup component still remains difficult to be handled in the reaction calculations by using the available codes. Thus, Kalbach's parametrization [1] is taken into account in the TALYS code [10] only for the first-chance neutron and respectively proton emission spectra while the consideration of a particular contribution following the absorption of one *BF* proton or neutron by the target remains an open question.

Stripping and pick-up

Apart from the breakup contributions to deuterons interaction process, other direct reactions mechanisms like stripping and pick-up have to be properly considered in order to describe the low energy range of the *(d,p), (d,n) [5-7],* and *(d,t)* excitation functions. Therefore the lowest energy domain of the experimental excitation functions of $^{93}Nb(d,x)^{92m}Nb$, Fig. 4(b), can not be described unless the *(d,t)* pick-up specific contribution is considered. Similar important contributions to the low energy region of excitation function have the stripping reactions (d,p) [5,6] as it is shown in Figs. 5 (a,d). The pick-up excitation function has been calculated here with the FRESCO code [16] based on the Coupled-Reaction Channels (CRC) method. The above-mentioned deuteron phenomenological OMP has been used for the incident channel while Becchetti-Greenlees [19,20] OMP describes triton outgoing channel. The *d-n* interaction in triton has been described with the ^{3}He potential [13] of Woods-Saxon shape, which parameters were determined by fit of the 5.50 MeV ^{3}He binding energy, relatively close to 6.3 MeV corresponding to ^{3}H. Like in the stripping case [4-6], the transferred neutron bound states were generated in a Woods-Saxon real potential too with parameters adjusted to the

nucleon binding energies in the residual nucleus. The spectroscopic factor involved in the transition amplitude of the pick-up process was that obtained experimentally from the analysis of triton angular-distribution corresponding to the population of the 0.136 MeV isomer state in ^{92m}Nb residual nucleus [21].

Preequilibrium and statistical emission

The interaction of deuterons with the target nuclei proceeds largely through direct reaction (DR) processes, for deuteron energies below and around the Coulomb barrier, while increasing the incident energy reaction mechanisms like preequilibrium emission (PE) or evaporation from the fully equilibrated compound nucleus (CN) become also important. The PE and CN cross sections, corrected for the breakup, stripping and pick-up decrease of the total reaction cross section, have been calculated here by using both STAPRE-H95 [22] and the TALYS [10] computer codes.

The formerly adjusted OMPs parameters for deuterons have been used, as well as Koning-Delaroche [20,23], Becchetti-Greenless [19,20] and McFadden-Satchler OMP potentials [20.24] for nucleons, tritons, and respectively alpha-particles outgoing channels. Slight adjustment of the level density parameter *a* derived on the basis of the back-shifted Fermi gas (BSFG) as well as of the neutron and proton single-particle state density parameters, g_n and g_p, were necessary in order to improve the data description.

The measured [8] and the calculated activation cross sections for ^{63,65}Cu targets nuclei (thick curves) as a sum of the inelastic breakup contribution, the DR cross sections provided by the FRESCO code and the PE+CN contributions provided by STAPRE-H95 code are shown in Fig. 5, together with the TALYS predictions (thin curves).

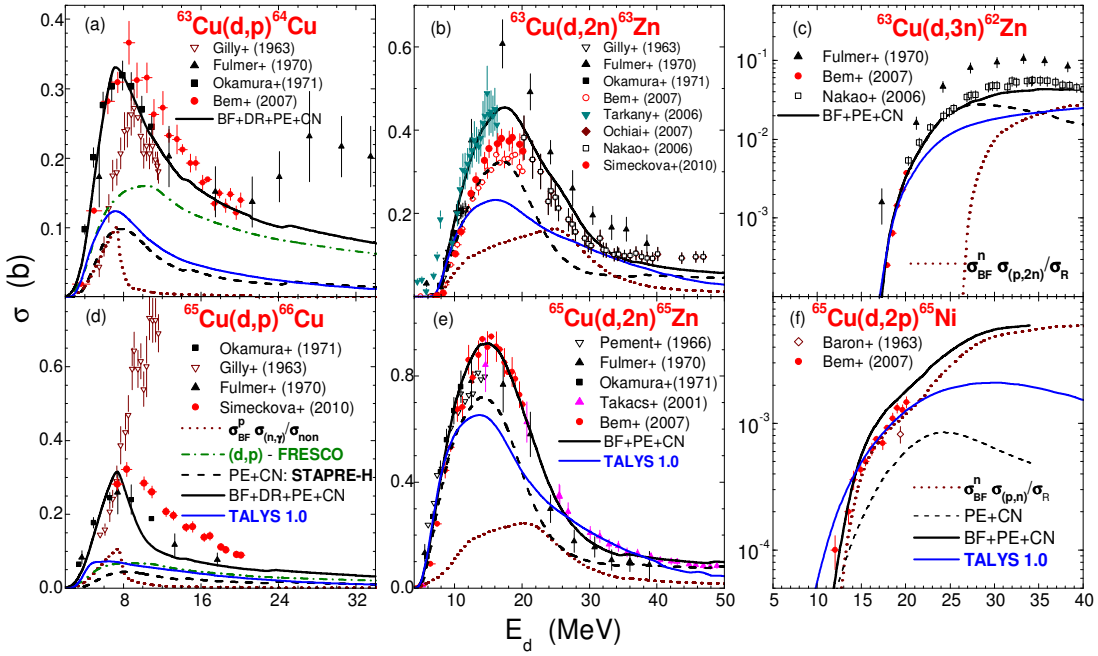

Figure 5. *(Color online) Comparison of measured [8] and calculated activation cross sections for deuterons on ^{63,65}Cu, provided by the code TALYS-1.0 (thin solid curves), and local analysis (thick solid) using the stripping (DR) contribution (dash-dotted) for the (d,p) reaction, the deuteron breakup (BF) (dotted), and the PE+CN for components (dashed).*

Conclusions

This work aims to present an unitary analysis of the nuclear reaction mechanisms responsible for the complex process of the deuteron interactions with nuclei. The comparison of the

present calculations with global predictions of the TALYS code stresses out the importance of an appropriate consideration of the deuteron breakup as well as of the stripping and pick-up reactions mechanism contribution to the activation cross section calculations. These direct mechanisms affect different energy range of the activation excitation functions. While the stripping and pick-up mechanisms contributions are essentials at low deuterons incident energies the deuteron-breakup contributions are important for the description of the high energy part of the activation excitation functions. The agreement between the measured data and model calculations presented here proves the correctness of the nuclear mechanism description taken into account for the deuteron-nucleus interaction.

Acknowledgments
This work was partly supported by CNCSIS-Bucharest, Romania project PN-II-IDEI-43/2008.

References

[1] C. Kalbach Walker, TUNL Prog. Rep. XLII, 2002-2003, pp. 80-83, www.tunl.duke.edu/publications/tunlprogress/2003/.
[2] M. Avrigeanu, W. von Oertzen, U. Fischer, and V. Avrigeanu, Nucl. Phys. A759, 327 (2005).
[3] M. Avrigeanu, W. von Oertzen, H. Leeb, F.L. Roman, and V. Avrigeanu, Proc. 11th Int. Conf. on Nuclear Reaction Mechanisms, June 2006, Varenna, Italy, edited by E. Gadioli (Milan, Ricerca Scientifica ed Educazione Permanente, 2006), p. 123.
[4] M. Avrigeanu, W. von Oertzen, R.A. Forrest, A.C. Obreja, F.L. Roman, and V. Avrigeanu, Fusion Eng. Design 84, 418 (2009).
[5] P. Bem, E. Simeckova, M. Honusek, U. Fischer, S.P. Simakov, R.A. Forrest, M. Avrigeanu, A.C. Obreja, F.L. Roman, and V. Avrigeanu, Phys. Rev. C 79, 044610 (2009).
[6] M. Avrigeanu and V. Avrigeanu, EPJ Web of Conferences 2, 01004 (2010).
[7] M. Avrigeanu and V. Avrigeanu, J. Phys: Conference Series 205, 012014 (2010).
[8] Experimental Nuclear Reaction Data (EXFOR); www-nds.iaea.or.at/exfor.
[9] W.W. Daehnick, J.D. Childs, and Z.Vrcelj, Phys. Rev. C 21, 2253(1980).
[10] A.J. Koning, S. Hilaire, M. C. Duijvestijn, Proc. Int. Conf. on Nuclear Data for Science and Technology, Nice, 2007 (EDP Sciences, Paris, 2008), p. 211; version TALYS-1.2, Dec. 2009.
[11] S. Watanabe, Nucl. Phys. 8, 484 (1958).
[12] O. Bersillon, Note CEA-N-2227, 1992.
[13] G. Baur, F. Rosel, D. Trautmann, and R. Shyam, Phys. Rep. 5, 333(1984); M. Kamimura, M. Yahiro, Y. Iseri, Y. Sakuragi, H. Kameyama, and M. Kawai, Prog. Theor. Phys. 89, Suppl. 1 (1986); N. Austern, Y. Iseri, M. Kamimura, M. Kawai, G. Rawitscher, and M. Yahiro, Phys. Rep. 154, 125 (1987).
[14] R. A. D. Piyadasa, M. Kawai, M. Kamimura, and M. Yahiro, Phys. Rev. C 60, 044611 (1999); J. A. Tostevin, F. M. Nunes, and I. J. Thompson, Phys. Rev. C 63, 024617 (2001); A. M. Moro and F. M. Nunes, Nucl. Phys. A767, 138 (2006); A. M. Moro, F. M. Nunes, and R. C. Johnson, Phys. Rev. C 80, 064606 (2009).
[15] M. Avrigeanu and A.M. Moro, Phys. Rev. C 82, 037601 (2010).
[16] J. Thompson, Comput. Phys. Rep. 7, 167 (1988); v. FRES 2.3 (2007).
[17] J. Kleinfeller, J. Bisplinghoff, J. Ernst, T. Mayer-Kuckuk, G. Baur, B. Hoffmann, R. Shyam, F. Rosel, and D. Trautmann, Nucl. Phys. A370, 205 (1981).
[18] F. Tarkanyi, A. Hermanne, F. Ditroi, S. Takacs, B. Kiraly, M. Baba, T. Ohtsuki, S. F. Kovalev, A.V. A. V.Ignatyuk, Nucl. Instr. Meth. B 255, 297 (2007); F. Ditroi, F. Tarkanyi, M. A. Ali, Nucl. Instr. Meth. B 161, 178 (2000).
[19] F. D. Becchetti Jr and G. W. Greenlees, Annual Report, J.H. Wiliams Laboratory, University of Minesota, 1969.
[20] R. Capote et al., RIPL-Reference Input Parameters Library for Calculations of Nuclear Reactions and Nuclear Data Evaluations, Nuclear Data Sheets 110, 3107 (2009).
[21] T. S. Bhatia, W. W. Daehnick, and T. R. Canada, Phys. Rev. C 3, 13612(1971).
[22] M. Avrigeanu and V. Avrigeanu, IPNE Report NP- 86-1995, Bucharest, 1995, and Refs. therein; News NEA Data Bank 17, 22 (1995).
[23] A.J. Koning and J.P. Delaroche, Nucl. Phys. A713, 231 (2003).
[24] L. McFadden and G. R. Satchler, Nucl. Phys. 84, 177 (1966).

Electromagnetic strength in heavy nuclei – experiments and a global fit

R. Beyer[1)], E. Birgersson[1)], A. R. Junghans[1)], R. Massarczyk[1)], G. Schramm[1)], R. Schwengner[1)], E. Grosse[1,2)]

1) Forschungszentrum Dresden-Rossendorf (FZD), Bautzner Landstr. 400, 01328 Dresden, Germany
2) FZD and IKTP, Technische Universität Dresden, Germany
e.grosse@fzd.de

Abstract: A global parameterization is presented for the electromagnetic strength in heavy nuclei which gives a rather good fit to respective data in nuclei with mass numbers A between 50 and 240. It relies on a Lorentzian description of the isovector giant dipole resonance and it needs only a very small number of parameters to describe the electric dipole strength down to low excitation energy of importance for radiative capture processes. The resonance energies are chosen to be in accordance to liquid drop model parameters adjusted to ground state masses and to rotation invariant determinations of ground state deformation and triaxiality. By a straightforward use of this information a surprisingly smooth variation of the GDR width with A and Z is found and a full agreement to the predictions of the electromagnetic sum rule is assured. Predictions for radiative neutron capture cross sections compare well to respective data, when the proposed photon strength function is combined with standard prescriptions for the level density in the product nuclei.

Introduction

The interaction of neutrons with heavy nuclei is of major interest for the understanding of the cosmic synthesis of the elements as well as for nuclear energy applications. In the latter field the problem of the radioactive waste emerging from power reactors has initiated new research on neutron induced fission as well as on radiative capture of neutrons in heavy nuclei. In nuclear fuel containing ^{238}U the latter process may result in the production of isotopes of Pu and actinides of higher atomic charge Z. These 'minor actinides' are very much unwanted waste as they contain α-emitting radionuclides of half-lives which are long as compared to times for which a safe storage can be assured. This is why modern nuclear reactor concepts aim to minimize radiative capture as compared to neutron induced fission e.g. by a proper selection of the average neutron energy. Here the cross sections for capture and fission and their dependence on the neutron energy are of major interest. As respective measurements for targets from short lived actinide nuclides or fission products may be very difficult or even impossible reliable predictions are needed. Parameterizations are valuable for such predictions, when they fit well to existing data in a global manner, i.e. in an extended range of nuclear mass number A, charge Z and excitation energy E_x. It is not primarily fundamental theory what is needed here, but rather prescriptions based on generally accepted principles, which allow for the extrapolation and generalization of data obtained in nuclei more easily available for experimental study.

In the past decades various data for many nuclei have been obtained by

a) photonuclear reactions in the range of the giant dipole resonance (GDR);
b) inelastic photon scattering yielding strength information below the threshold for photo-dissociation;
c) average radiative capture widths, i.e. the sum of primary de-excitation photon widths;
d) spectra of the photon cascades following the abovementioned processes.

Although these data cover different ranges in E_x and E_γ a consistent description of them can be obtained by introducing the concept of the photon strength function f_λ which is directly related to the photon absorption cross section as well as to the photon decay width. The latter has to be normalized to the phase space open to the photon and to the density $\rho(E_u)$ of the decaying levels. Assuming the validity of the Axel-Brink hypothesis [1] the photon strength function [2] which describes absorption of photons with $E_\gamma = E_x$ as well as electro-magnetic decay does not depend on the energies of the upper and lower levels E_x (respectively E_u) and E_l but only on the transition energy $E_\gamma = E_u - E_l$.

For dipole radiation one has:

$$f_1 = \frac{\overline{\sigma}_{\gamma\text{-}abs}(0 \to E_x)}{3(\pi\hbar c)^2 E_x} = \frac{\overline{\Gamma}_\gamma(E_u \to E_l)\,\rho(E_u)}{E_\gamma{}^3} \qquad (1)$$

In this approximation all processes involving radiation can be derived from the known strength function f_λ and the density ρ of involved levels. In the following it will be discussed, what experimental information is available and how it enters into parameterizations, which of course have to be in accordance to theoretical arguments.

A well studied model case: ^{208}Pb

A heavy nucleus very well investigated theoretically and experimentally is ^{208}Pb. The dipole strength function shown in Fig. 1 as studied by photo-neutron production covers the range of the isovector giant resonance GDR as well as the region above – up to the energy at which a photo-production of pions becomes possible.

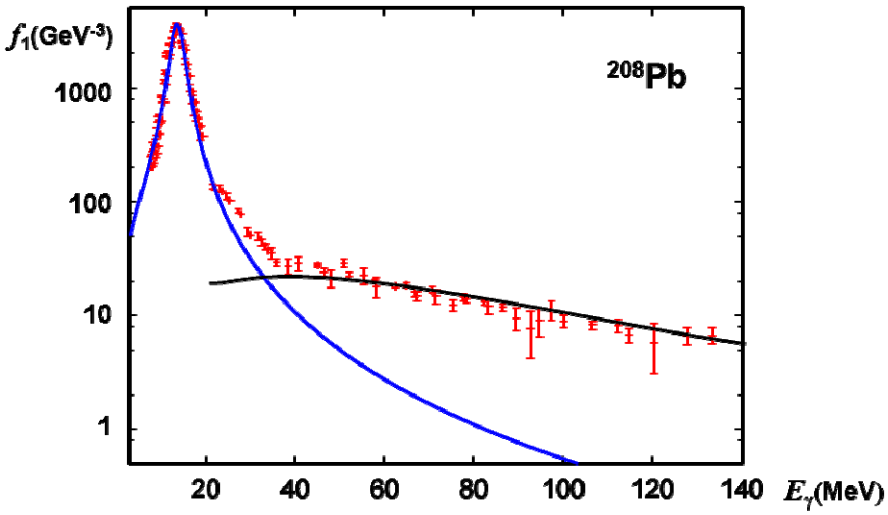

Figure 1. *Photon strength in ^{208}Pb observed as described in the text. The curves depict the electric dipole strength for the GDR as parameterized here (cf. eq. 3; blue) and as calculated for the quasi-deuteron effect (black).*

Using the very general arguments of causality and unitarity [3] it was shown, that up to the pion threshold the main term in the energy weighted sum rule

$$\int \sigma dE = 2\pi^2 \frac{\alpha\hbar^2}{m_N}\frac{ZN}{A} = 5.97\,\frac{ZN}{A}\ \text{MeV fm}^2 \qquad (2)$$

cannot be exceeded by more than 40%. The curve close to the data [4] at low energy depicts a calculation on the basis of eq. 2 and the GDR parameterization based on systematic studies as discussed later. It has been pointed out [5,6], that a Lorentzian may be used to describe the photon absorption cross section in the GDR albeit it is not representing a single level

decaying into the vacuum. The other curve depicts the neutron emission from photons hitting a deuteron in the nuclear medium and it corresponds to a global parameterization [7,8] of the so called quasi-deuteron effect. The sum of the two contributions is calculated to be 100+35 % of the value given in eq. 2 with an error of 7% due to the ambiguous upper bound. Following the findings of a recent experiment [9,10,11] at the superconducting linac ELBE at Dresden-Rossendorf the data shown in Fig. 1 were renormalized by a factor of 0.87 — in accordance to a previous independent study [12]. Apparently there is not much room for GDR strength in addition to eq. 2.

Whereas the photon strength function shown in Fig. 1 was determined by the observation of neutrons emitted from the photo-excited nucleus, the strength of importance for radiative capture lies below the neutron separation energy S_n and it may be measured by photon scattering. For ^{208}Pb various such studies were performed using quasi-monochromatic [4] or bremsstrahlung [13] beams. Using electron beams of various energies from ELBE information was obtained with bremsstrahlung as produced in a thin Nb radiator and scattered from a ^{208}Pb target. Although the set-up was optimized [13] to suppress background radiation of non nuclear origin, which is especially strong at low photon energies, it is still present and it increases with the endpoint energy. As can be seen in Figure 2 an additional quasi-continuum constitutes a considerable part of the scattering yield already in the region between 6 MeV and S_n= 7.37 MeV, where it drops considerably. The spectra also indicate the rise of the dipole strength caused by the GDR peak at 13.6 MeV, albeit there the neutron channel collects most of the yield. The HPGe-detectors were surrounded by escape suppression shields [13] to veto signals not depositing the full photon energy in the detector, and we were able to determine the contribution of such processes to the quasi-continuum for the data taken at 9 MeV. The full energy part of the line shape is close to a Gaussian with σ < 3 keV and from the analysis of the spectra the scattering yield outside the narrow peaks is determined. It results from the decay of strongly excited levels (and isolated resonances above S_n) and will be discussed below.

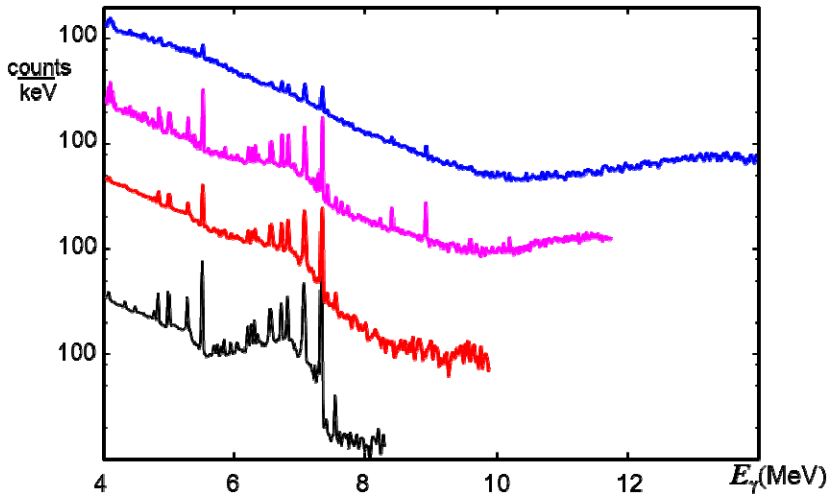

Figure 2. *Photon spectra taken with bremsstrahlung endpoint energies of 9, 12, 15 and 17 MeV (bottom to top) as scattered from an enriched ^{208}Pb target to a detection angle of 127° with respect to the beam.*

The quasi-continuous part occurring at photon energies above 6 MeV and observed best at the lower endpoint energies is partially due to incomplete energy deposition in the detector. However, it may also contain a contribution from many weak resonances overlapping increasingly with excitation energy E_x due to the increasing level density. In that case it would belong to the photon strength in the low energy tail of the GDR. Directly above S_n the mean

distance between $J=1^-$ resonances was determined [14] to be ~30 keV. The result of a detailed analysis with a deconvolution of the spectra taken at 9 MeV endpoint energy is shown in Fig.3. The continuous strength is assumed to be due to the deexcitation of the ~30 levels per MeV already present below $E=S_n$. Non-resonant Thomson scattering from Pb has a cross section of below 1 mb and thus it is very much weaker as compared to the observations.

The level density also influences the results obtained with a completely different set-up at ELBE. A 10 mm thick target of liquid Pb was bombarded with electrons of 25 MeV which produce bremsstrahlung and these generate neutrons in the subsequent Pb(γ,n) reaction. After a flight path of ~ 5 m the neutrons were observed in 1cm thick plastic scintillators [15]. As described in a previous paper [16] this set-up is well suited as a source of pulsed neutrons to be used for various studies using the time-of-flight technique. At this set-up a kinetic energy resolution of less than 5 keV is reached in a study of ^{nat}Pb for S_n= 7.37 MeV <E_x< 10 MeV. Figure 3 shows a preliminary analysis of a neutron spectrum which delivers some information about the strongly fluctuating photon strength directly above S_n. Comparable information – but reaching to 12.5 MeV – can be derived from a high resolution study [17] of the ^{208}Pb(γ,n) reaction, from which a spectrum is also shown in Fig.3. Again, several peaks are seen on top of a smooth increase of the yield. All three data sets shown in Fig.3 have a similar appearance: Superimposed on an increasing strength strong peaks are observed with the distance between them greatly exceeding the distance of neutron capture resonances [14]. Some of the intensity may be due to E2 strength [17], but only by a careful analysis Porter-Thomas fluctuations can be excluded as their origin. The steep drop of the (γ,n) data above and the (γ,γ) data below S_n is well understood as being due to the much larger flux going into the respective channel. The general trend of the total yield (continuum plus peaks) represents the photo-absorption cross section and is reasonably well described by the Lorentzian tail (blue). It remains open, if in addition to pygmy [2] structure at 5.5 MeV extra E1-strength is needed to explain the data.

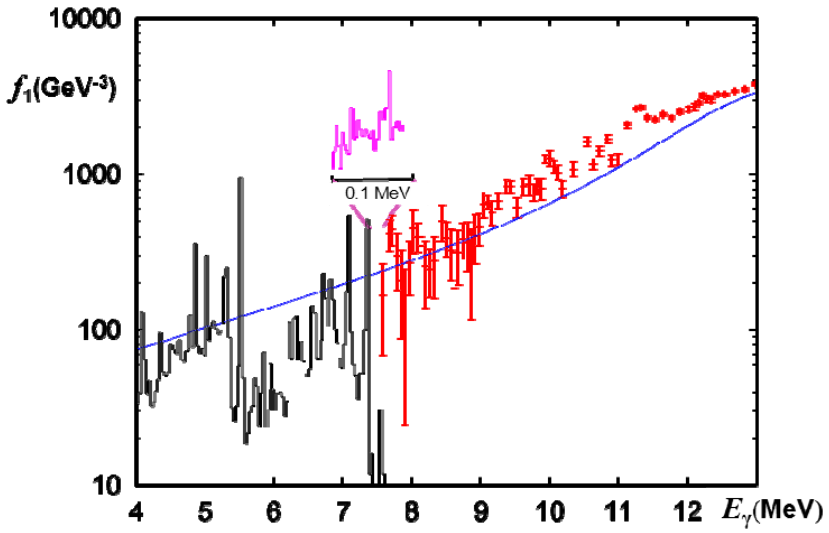

Figure 3. *Dipole strength function observed by photon scattering (black) and in photo-neutron studies; these are based on neutron detection in 4π with variable photon energy (red) and neutron time of flight (magenta, x and y scale multiplied by 10).*

At this point a comparison to theoretical work may be helpful. A very detailed shell model calculation [18] is available for ^{208}Pb, which includes particle-hole as well as 2p-2h-configurations, which are quite numerous. In spite of its large configuration space it under-predicts the level density, e.g. by a factor of 4 for the region near S_n. But, as already shown [18], it describes the overall trend of the E1 strength very well. As shown in Fig. 4 the

comparison of the calculated absorption cross section with the Lorentzian of Fig.1 affirms this conclusion.

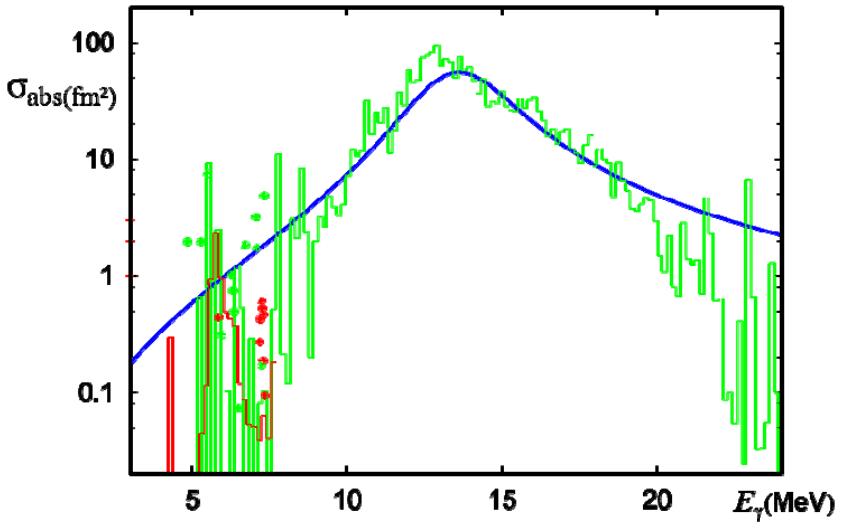

Figure 4. *Dipole absorption from a shell model with configuration mixing for ^{208}Pb [18; green: E1, red: M1]. For comparison a Lorentzian (Fig. 1) is superimposed as well as experimental photon scattering intensities [19; ⌀].*

The abovementioned shell model calculations also deliver the magnetic dipole strength and the corresponding cross section is depicted in red. The absorption cross section in the range of 6 MeV is predicted to be not very different for the electric and magnetic dipole modes. Very recently a photon scattering experiment [19] was performed with quasi-monochromatic, linearly polarized photons generated by inverse Compton scattering of laser light with relativistic electrons circulating in a storage ring. In accordance to data taken previously at ELBE [13] the parity was determined for around 20 levels with 4.5< E_γ <7.5 MeV and in Fig. 4 these data are included; the E2 strength also observed in this experiment results in even less photon absorption. As shown [19] the magnetic strength between 7 and 9 MeV, i.e. in the spin flip region, adds up to 17 (1) μ_N^2, including results from above S_n. This result compares well to what was found in a systematic study [20] and confirms the conclusion that the spin flip M1 strength is of minor importance for photon absorption in heavy nuclei.

Quadrupole strength and the shape of heavy nuclei

The electric quadrupole modes contribute little to the energy weighted photon strength, but their low energy part carries important information on nuclear shapes. It was pointed out [21] that such information can be extracted from reduced E2 matrix elements in a rotation invariant way such that values obtained in the laboratory can be directly transferred to the nuclear rest frame. The sum of all B(E2)-values connected to the ground state is a measure of the breaking of spherical symmetry and a sum over all products of three E2 matrix elements ending at the ground state describes the breaking of axial symmetry. For about 160 heavy nuclei sufficient experimental data have been collected by Coulomb excitation [22-24] and other methods [25] and significant conclusions about their ground state shape can be drawn. Assuming volume conservation and a homogeneous charge distribution they can be expressed as the axis lengths of a triaxial body. The deviations of the axes from the average radius are inversely proportional to the pole energies of the three GDR components in comparison to the centroid energy, if the triaxiality for GDR energies is the same as near the ground state.

The finding of triaxial nuclear shapes in quasi all heavy nuclei away from the doubly magic ^{208}Pb leads us to describe the GDR shapes by three peaks of equal size and with their summed strength according to the sum rule (eq.2). As the existing data do not allow a triple Lorentzian fit independently for each nucleus, we use the rotation invariant information for the ground state triaxiality and we generalize it to all heavy nuclei. Relating the B(E2) to the first excited 2^+ state [26,27] to the triaxiality γ as observed a simple empirical relation is derived: $\cos 3\gamma = \pm 0.55\, B(E2\uparrow)^{0.24}$. In accordance to the finding, that triaxiality usually is more obvious in nuclei with small deformation, a correlation between the two deformation parameters β and γ was already noted previously [28], but the numerical relation given here covers a wider range in A. Of course, the values resulting from it are subject to quantum-mechanical zero point oscillations and detailed studies are needed to study the effect of these; a first investigation [29] along these lines has demonstrated that only the detailed shape of the GDR peak depends on the stiffness of the shape parameters, but the low energy tail does not.

Giant resonances and dipole strength

Photon absorption by heavy nuclei is dominated by the electric dipole mode and this is governed by the GDR. The GDR energies are closely related to the symmetry energy of nuclear matter and the surface stiffness of nuclei [30]; both parameters are well determined by the finite range droplet model [31]. By interpolating between the two models [32] proposed for medium mass and heavy nuclei a prescription was found [5] to predict the centroid GDR energy for all nuclei with 50<A<240 from these two parameters plus an effective nucleon mass which we adjusted by comparison to photo-neutron data to m*= 874 MeV/c². A recent detailed attempt [33,34] to fit the shape of GDR peaks by Lorentzians reports the need of using two poles for obtaining a satisfactory fit in about half of the nuclei studied, whereas in the other half only one was shown to suffice. This local fit delivers widths for the different nuclei which lie between 2 and 12 MeV and which vary strongly in dependence of Z and A. For the energy integrated GDR strength a similar scatter is found with factors ranging from 0.4 to 2.6 when compared to the sum rule (eq. 2). The very large scatter as resulting from fitting only one or two peaks to the GDR data indicates a severe deficiency of this procedure.

In contrast, we propose to use generally three poles related to the three body axes and this results in a triple Lorentzian (TLO) parameterization [5] for the GDR and using eq. 1 one gets for the electric dipole strength f_{E1}:

$$f_{\mathrm{E1}} = \frac{2}{\pi}\cdot\frac{1.99\,MeV^{-3}}{(\pi\hbar c)^2}\cdot\frac{Z\,\mathrm{N}}{\mathrm{A}}\sum_{k=1,3}\frac{E\,\Gamma_k}{(E_k^2-E^2)^2+E^2\Gamma_k^2} \qquad (3)$$

TLO-calculations as performed for a large number of heavy nuclei agree well [5] to GDR data and the widths and integrated strengths vary only smoothly with A and Z while eq. 2 is fully obeyed. For the widths the relation [5,35] between the peak width and its energy $\Gamma_k = a\,E_k^{1.6}$ is used with the exponent derived from hydrodynamical considerations [35]. By comparing with data for many nuclei the proportionality factor was optimized [5] to a = 0.05 when E and Γ_k are given in MeV. This relation is used for describing the GDRs in all investigated nuclei as well as for the three peaks in one nucleus. The resulting description of the absorption cross section in the region of the GDR maxima agrees astonishingly well to the data from various (γ,n) experiments [5,9-11] without any free parameters in addition to a, m*= 874 MeV/c² and the quantities describing the ground state shape. As already mentioned for ^{208}Pb, the photo-neutron data from a certain laboratory [4] had to be renormalized by 0.87, a factor determined by comparison to (γ,n)-data from another source [12] as well as by photo-activation measurements performed at the FZD [9-11]. Also for a few MeV below the neutron separation energies, where the photon absorption was determined from scattering, a good agreement is seen [9-11,36]. Here we make the simplified ansatz [5], that the low energy slope of the dipole

strength is described by the same Lorentzian function as the peak without introducing any energy dependence of the widths Γ_k or any additional term. Finally, comparing the TLO parameterization to particle-photon coincidence data obtained for even smaller excitation energy [37] one observes reasonable agreement, when account is made for the different spin distributions.

In most cases – and especially in nuclei which are falsely considered spherical symmetric – our description with a triple Lorentzian (TLO) leads to a considerably smaller width as compared to the one resulting [33,34] from a fit with only one or two Lorentzians to the GDR peak. In respect to that finding it is of interest to discuss the contribution of the neutron escape to the width, i.e. the natural line width. In Fig.5 the result is shown of a shell model calculation (in Tamm-Dancoff approximation) with explicit coupling to the continuum [38]. There is only one strong component within the first few MeV above S_n with an escape width above 0.5 MeV and all the other configurations are much narrower.

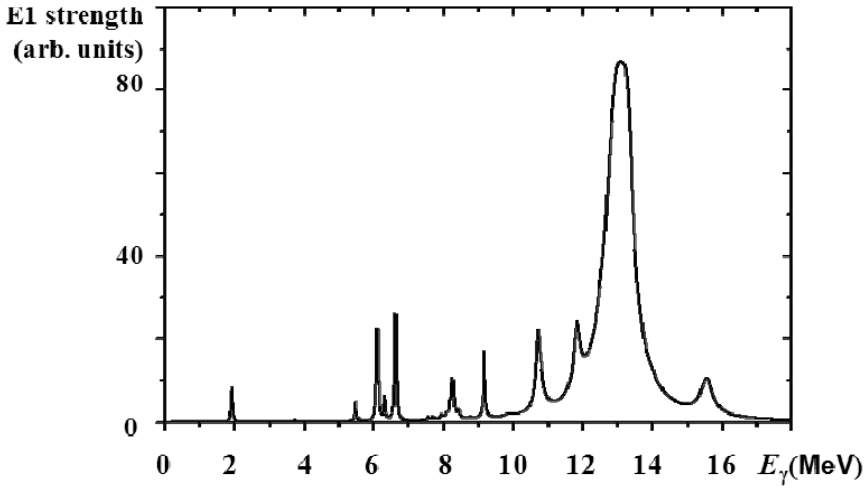

Figure 5. *Electric dipole strength in ^{208}Pb from a continuum shell model calculation folded with 50 keV.*

We thus consider the width used in the TLO-parameterization to be an experimental measure for the spreading of the GDR strength into the many complex states forming the underlying quasi-continuum. The rather small value of this width corresponds to a reduced value of the absorption cross section in the wing region far apart from E_k. This is not only of importance for the sum rule integral but also for predictions concerning the radiative capture. For each resonance the cross section of this process is proportional to the average radiative width, which increases with the energy of the first photons in the decay cascades, and the level density in the final nucleus, decreasing with E_x. Folding the two probabilities leads to a sensitivity curve, which peaks at an intermediate energy near $S_n/2$. Thus a detailed study of the dipole strength in this energy range is important for reliable predictions of radiative neutron capture cross sections which determine reaction rates in stellar plasmae as well as the accumulation of actinide nuclides in fission reactors.

Conclusion: Photon strength, level densities and radiative capture

In principle, three factors enter the predictions for radiative capture: the neutron and photon strength functions and the level density in the final nucleus. For all three the absolute value as well as the energy dependence are important and have to be determined. We aim for a first order prediction by extrapolating our TLO dipole strength to low photon energies and combining it to a model which assumes a simple exponential dependence of the level density on excitation energy. If additionally a semi-classical ansatz [39] is used for the neutron channel one gets for the capture cross section averaged over many resonances R –

assuming a factor 3 for the number of spins to be reached by E1-transitions from 1$^-$-resonances:

$$\left\langle \sigma_R(n,\gamma) \right\rangle \approx 2(2\ell+1)\pi^2 \lambda\!\!\!^{-2}_n \rho(E_R) \left\langle \Gamma_{R\gamma} \right\rangle$$

$$\text{with} \left\langle \Gamma_{R\gamma} \right\rangle = \left\langle \sum_{\mathrm{f}} \Gamma_\gamma(R \to \mathrm{f}) \right\rangle = 3 \int_0^{E_R} E_\gamma^3 f_1(E_\gamma) e^{-\frac{E_\gamma}{T}} dE_\gamma \qquad (4)$$

To get to the aspired prediction for the capture cross section information is needed for the photon strength and the level density in the energy range intermediate between 0 and S_n. In many nuclei the density of resonances populated by neutron capture is well studied [40], such that with knowledge of the dipole strength only the parameter T remains free, the constant 'temperature' in the level density formula, describing the energy dependence. For this parameter local as well as global fits have been performed [41,42] and the assumptions made can be tested for a wide range of nuclei with 50 < A < 240. As a comprehensive overview a plot of average photon widths for 50<A<240 is shown in Fig. 6 as derived from two predictions for T(A). The experimental widths result from radiative capture data compiled within the RIPL project [33,40] of IAEA.

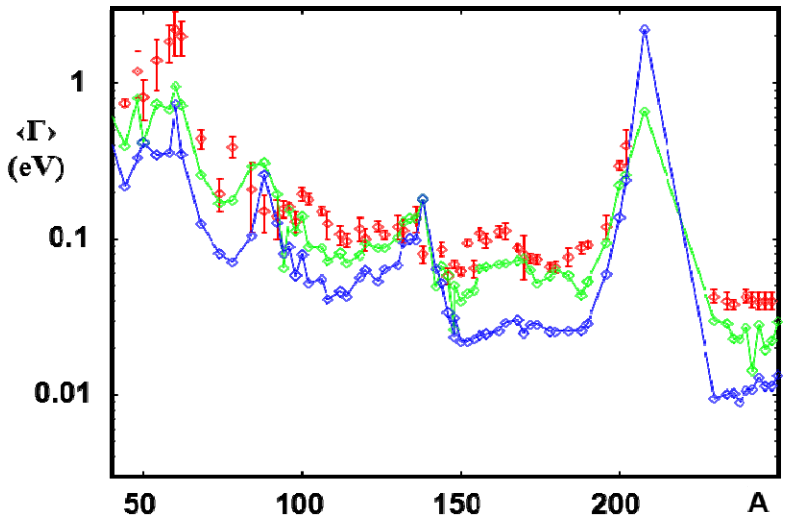

Figure 6. *Average photon widths for even nuclei with mass A: Data (red ◊) are compared to predictions based on a combination (eq. 4) of the triple Lorentzian (TLO) to two values for the `temperature' T(A), describing the energy dependence of the level density (local fit [41], green o, and global fit [42], blue ◊).*

Obviously the local prediction [41] for T(A) yields a somewhat better agreement to the data than a global one [42] and the inclusion of shell effects is of major importance. A good agreement between the experimental data for heavy nuclei and the calculations made with reasonable values for T is found on absolute scale for a wide range of A. This strongly supports the parameterization for the dipole strength f_1 as outlined above. It implies a strength function in accordance to the sum rule and it is based on GDR-widths and strengths, which are varying very smoothly with A and Z. They are derived by properly accounting for the broken spherical and axial symmetry of the nuclear ground states. Actually the triaxiality varies smoothly with the quadrupolar deformation as well and also the 'temperature' T is a smooth function of A with a steep increase only near ^{48}Ca and ^{208}Pb only. Thus we conclude that parameters for GDR and level density, which vary only smoothly with A and Z, allow to well predict average photon widths – and thus radiative neutron capture cross sections. This is achieved without breaking the dipole sum rule [3], and quasi-deuteron absorption and triaxial nuclear deformation are properly accounted for.

Acknowledgements

We very much thank Prof. A. Brown and Dr. R. Wünsch for allowing us to use results of their calculations for ^{208}Pb, and the support from Drs. P. Michel, G. Rusev, K.D. Schilling and A. Wagner is gratefully acknowledged.

References

[1] P. Axel, Phys. Rev. 126, 671 (1962); D. Brink, Ph.D. thesis, Oxford
[2] G. A. Bartholomew et al., Adv. Nucl. Phys. 7 (1972) 229
[3] M. Gell-Mann et al., Phys. Rev. 95 (1954) 1612
[4] A. Veyssiere et al., Nucl.Phys. A159 (1970) 561; A. Lepretre et al., Nucl.Phys. A 367, 237 (1981)
[5] A. R. Junghans et al., Phys. Lett. B 670, 200 (2008)
[6] C.B. Dover et al., Ann. Phys. (N.Y.) 70 (1972) 458
[7] M.B. Chadwick et al, Phys. Rev. C 44, 814 (1991)
[8] A.J. Koning, S. Hilaire and M.C. Duijvestijn, .TALYS-1.0., Nuclear Data for Science and Technology, eds. O.Bersillon et al., (EDP Sciences, Nice, 211, 2008)
[9] C. Nair et al., Phys. Rev. C 78, 055802 (2008)
[10] M. Erhard et al., Phys. Rev. C 81, 034319 (2010)
[11] C. Nair et al., Phys. Rev. C 81, 055806 (2010)
[12] B. L. Berman et al., Phys. Rev. C 36, 1286 (1987)
[13] R. Schwengner et al.,Nucl. Inst. Meth. A555, 211 (2005); id., Phys.Rev. C 81, 054315 (2010)
[14] P. Koehler et al, Phys. Rev. C **35**, 1646 (1987)
[15] R. Beyer et al., Nucl. Instr. Meth. A575 (2007) 449; R. Nolte et al., Nucl. Sci. Eng. 156, 197(2007)
[16] E. Altstadt et al., Ann. Nucl. Energy 34 (2007) 36; J. Klug et al., Nucl. Instr. Meth. A577 (2007) 641
[17] V.V.Varlamov et al., Yad. Konst. 1, 52 (1993), nndc.bnl.gov/exfor; R. Van de Vyver, Z. Physik A 284, 91 (1978)
[18] B.A.Brown, Phys. Rev. Lett. 85 (2000) 5300 , cf. R.Schwengner et al., Phys. Rev. C 81, 054315 (2010)
[19] T. Shizuma et al., Phys. Rev. C 78 (2008) 061303
[20] A. Richter, Prog. Part. Nucl. Phys. 34 (1995) 261; K. Heyde et al., Rev. Mod. Phys. **82**, 2365 (2010)
[21] K. Kumar, Phys. Rev. Lett. 28 (1972) 249; D. Cline, Ann.Rev.Nucl.Part.Sci. 36 (1986) 683
[22] J. Stachel et al., Nucl. Phys. A 419 (1984) 589; C. Y. Wu et al., Nucl. Phys. A 533 (1991) 359
[23] C. Y. Wu et al., Nucl. Phys. A 607 (1996) 178, C. Y. Wu and D. Cline, Phys. Rev. C 54 (1996) 2356
[24] M. Zielinska et al., Nucl. Phys. A 712 (2002) 3; J. Srebnry et al., Nucl. Phys. A 766 (2006) 25
[25] L. Esser et al., Phys. Rev. C 55 (1997) 206; V. Werner et al., Phys. Rev. C 71, 054314 (2005)
[26] S. Raman et al., At. Data Nucl. Data Tabl. 78 (2001) 1
[27] N. Pietralla et al., Phys. Rev. Lett. 73, 2962 (1994)
[28] W. Andrejtscheff and P. Petkov, Phys. Rev. C 48, 2531 (1993), id., Phys. Lett. B 329 (1994) 1
[29] S. Q. Zhang et al., Phys. Rev. C 80 (2009) 021307
[30] W.D. Myers et al., Phys. Rev. C 15 (1977) 2032
[31] P. Möller, J.R. Nix, W. D. Myers and W. J. Swiatecki, At. Data Nucl. Data Tables 59 (1995) 185
[32]. M. Goldhaber and E. Teller, Phys. Rev. **74**, 1046 (1948); H. Steinwedel and H. Jensen, Z.f.Nf. **52**, 413 (1950)
[33] V.A. Pluiko, www-nds.iaea.org/RIPL-3/gamma/gdrparameters-exp.dat, subm. to At. Data Nucl. Data Tables;
[34] R. Capote et al., Nucl. Data Sheets 110 (2009) 3107
[35] B. Bush and Y. Alhassid, Nucl. Phys. A 531 (1991) 27
[36] G. Rusev et al., Phys. Rev. C 77, 064321 (2008)

[37]. H.T. Nyhus et al., Phys. Rev. C 81 (2010) 024325
[38]. H.W.Barz, I.Rotter and J.Höhn, Nucl. Phys. A 275 (1977) 111; R. Wünsch, priv. comm.
[39] D.J. Hughes et al., Phys. Rev. 91(1953)1423; H. Feshbach et al., Phys. Rev. 71(1947)145
[40] A. Ignatyuk, IAEA-TECDOC-1506, RIPL-2 (2006), § 3, Resonances; T. Belgya et al., www-nds.iaea.org/ripl-2/
[41] T. von Egidy and D. Bucurescu, Phys. Rev.C 80, 054310 (2009)
[42] A. Koning et al., Nucl. Phys. A 810 (2008) 13.

Neutron-induced cross sections via the surrogate reaction method

G. Boutoux[1)],, B. Jurado[1)], V. Méot[2)], O. Roig[2)], M. Aïche[1)], A. Bail[2)] , G. Barreau[1)], E. Bauge[2)], J.T. Burke[8)], N. Capellan [1)], I. Companis[1)], S.Czajkowski[1)], J.M. Daugas [2)], X. Derkx[5)] , T. Faul[2)] , L. Gaudefroy [2)], F. Gunsing[4)], B. Haas[1)], G. Kessedjian[7)], L. Mathieu[1)], P. Morel[2)], N. Pillet[2)], P. Romain[2)], K.-H. Schmidt[1)], O. Sérot[3)], J. Taieb[2)], L. Tassan-Got[6)], I. Tsekhanovich[1)]

1) Centre d'Etudes Nucléaires de Bordeaux Gradignan, CNRS/IN2P3, Université Bordeaux 1, FRANCE
2) CEA, DAM, DIF, F-91297 ARPAJON, FRANCE
3) CEA – Cadarache , DEN/DER/SPRC/LEPh, FRANCE
4) CEA – Saclay , DSM/DAPNIA/SPhN, FRANCE
5) Grand Accélérateur National d'Ions Lourds, CNRS/CEA, FRANCE
6) Institut de Physique Nucléaire d'Orsay, CNRS/IN2P3, FRANCE
7) LPSC Grenoble, CNRS/IN2P3, FRANCE
8) Lawrence Livermore National Laboratory, California, USA

boutoux@cenbg.in2p3.fr

Abstract: The surrogate reaction method is an indirect way of determining cross sections for nuclear reactions that proceed through a compound nucleus. Nevertheless, because of the dependence of the populated spin-parity distribution of the entrance channel, the validity of the surrogate method has to be investigated. The CENBG collaboration has applied this technique to determine the **(n,f) cross sections** of several short-lived nuclei. Recently, we performed the ^{243}Am(^{3}He,α), ^{243}Am(^{3}He,t), ^{243}Am(^{3}He,d) reactions as surrogates for respectively ^{241}Am, ^{243}Cm, ^{244}Cm (n,f) cross sections. We are now investigating whether this technique can also be used to determine **(n,γ) cross sections**. For this purpose, we use the surrogate reaction ^{174}Yb(^{3}He,p)^{176}Lu* to infer the well known ^{175}Lu(n,γ) cross section. Preliminary results show clear discrepancies between our surrogate results and the already existing neutron-induced data. In this experiment, we are also able to infer various γ-rays intensities ratios which are powerful observables to constrain angular momentum distribution populated in the surrogate reaction.

How to measure neutron-induced cross sections of very short-lived nuclei?

The "surrogate" reaction method enables cross sections to be extracted for nuclear reactions on short-lived nuclei, that otherwise can not be measured. This method was first proposed by J.D.Cramer and H.C.Britt[1] in the seventies and is schematically represented in figure 1.

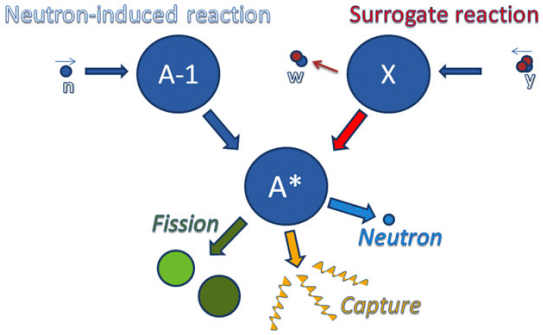

Figure 1. *Schematic representation of the surrogate reaction method. The surrogate reaction is here a transfer reaction X(y,w)A*. Three possible exit channels (fission, capture and neutron emission) are also represented.*

The left part of figure 1 illustrates a « direct » neutron-induced reaction on the target A-1, which leads to the compound-nucleus A at an excitation energy E*. The nucleus A can decay through different exit channels: fission, γ, neutron emission, etc… On the right part of figure 1, in the surrogate reaction method, the same compound nucleus A is produced by a transfer reaction between a projectile y (a light charged particle) and a target X. In the context of short-lived nuclei, the interest of this method is to use targets which are less radioactive than the target A-1. The transfer reaction ($y+X \rightarrow A+w$) leads to a heavy recoil nucleus A and an outgoing particle w (proton, deuteron, triton, etc…). The identification of the ejectile w permits to determine the mass A and charge Z of the decaying nucleus. In addition, we can deduce the excitation energy E^* of the compound nucleus A by measuring the kinetic energy and the emission angle of the ejectile w. Experimentally, the detection of the ejectile w, in coincidence or not, with a given decay product (fission fragments or gamma rays) of the compound nucleus A* gives the decay probability $\overline{P}_{decay}^{A,\exp}$ of the given reaction channel. According to the surrogate reaction method, this measurement of the fission or capture probability permits to determine the neutron-induced cross section for the nucleus A-1 according to the equation:

$$\sigma_{decay}^{A-1}(En) \cong \sigma_{CN}^{A}(En).P_{decay}^{A,\exp}(E^*) \quad (1)$$

where σ_{CN}^{A} is the compound nuclear formation cross section in the desired reaction (formation of the nucleus A after a neutron absorption with an energy En). In our case, σ_{CN}^{A} is obtained from the optical model calculations using TALYS. The relation between incident neutron energy En and the excitation energy E* of the compound nucleus A can be written:

$$E^* = S_n + E_n \cdot \frac{A-1}{A} \quad (2)$$

where S_n is the one-neutron separation energy in the nucleus A.

About the validity of the surrogate reaction method

The neutron-induced reaction and the transfer reaction permit to produce the same (in Z and A) compound nucleus. However, the angular momentum (J) and parity (π) distribution populated by a transfer reaction may not be the same as the one populated in a neutron-induced reaction. The issue is that, at low E*, fission and capture probabilities depend strongly on the Jπ of the compound nucleus. Actually, the surrogate reaction method can only be applied if the decay probabilities from the neutron-induced and transfer reactions are similar:

$$P_{neutron,decay} = P_{transfer,decay} \quad (3)$$

According to the Bohr hypothesis for the compound nucleus, these decay probabilities are given by:

$$P_{neutron,decay}(E^*) = \sum_{J^\pi} P_{neutron}^{form}(E^*, J^\pi) \cdot G_{decay}(E^*, J^\pi) \quad (4)$$

$$P_{transfer,decay}(E^*) = \sum_{J^\pi} P_{transfer}^{form}(E^*, J^\pi) \cdot G_{decay}(E^*, J^\pi) \quad (5)$$

where $P_{neutron}^{form}(E^*, J^\pi)$ and $P_{transfer}^{form}(E^*, J^\pi)$ correspond to the probability that the compound nucleus is formed with spin J and parity π in the neutron-induced and in the transfer reaction, respectively. $G_{decay}(E^*, J^\pi)$ are the branching ratios for a given decay channel. Equation (3) may be valid in two cases:

First hypothesis : Obviously, eq. (3) is valid if the J^π distributions populated in both techniques are similar:

$$P_{neutron}^{form}(E^*, J^\pi) \approx P_{transfer}^{form}(E^*, J^\pi) \quad (6)$$

Unfortunately, angular momentum populations are still poorly known experimentally and theoretically. An important effort from theoreticians and experimentalists should be done in order to determine these distributions.

Second hypothesis : The compound-nuclear decay probabilities are independent of J and π. By writing,

$$G_{decay}(E^*, J^\pi) = G_{decay}(E^*) \quad (7)$$

we denote the Jπ-independent decay probability for the exit channel which can be taken out of the summation signs in equations (5) and (6). Note that $\sum_{J,\pi} P^{form}_{reaction}(E^*, J^\pi) = 1$ and the cross section for the desired reaction takes the simple product form of the equation (1). This second hypothesis is known as the **Weisskopf-Ewing (W-E) approximation** [2] and is justified for high excitation energies where the decay of the compound-nucleus is dominated by statistical level densities. Almost all applications of the surrogate method have made use of this approximation. At lower excitation energy, the decay probabilities strongly depend of the spin of discrete states, whose population depends on the reaction mechanism used to produce the compound nucleus A*.

Surrogate fission measurements

Recently, we used the surrogate reaction method to determine the neutron-induced fission cross sections of ^{242}Cm($T_{1/2}$=162.8 d), ^{243}Cm($T_{1/2}$=29.1 y) and ^{241}Am($T_{1/2}$=432.2 y). These cross sections are of interest for nuclear waste transmutation. However, in the case of the Cm isotopes, the available data are rather scarce or inconsistent and the international evaluations used for reactor simulations present important differences. To reach and study these nuclei we employed few-nucleon transfer reactions using a ^{3}He projectile on a ^{243}Am($T_{1/2}$=7370 y) target. All details are given in [3]. A good agreement was observed between already existing neutron-induced data and our surrogate measurements (even at the lowest neutron energies!). The reason is that the excitation energy of the fissioning nuclei was high enough for the Weisskopf-Ewing approximation to be valid. Consequently, the reaction was not sensitive to the differences between the spin distributions populated in transfer and neutron-induced reactions.

Surrogate capture measurements

Compared to fission, capture reactions may be more sensitive to the differences between the spin-parity distributions [4]. Moreover, in the case of actinides, one need to distinguish between gamma rays originating from the fission fragments and capture gamma rays. This can make capture measurements extremely complicated. Therefore as a first step we have chosen to investigate the validity of the surrogate method for capture reactions on rare earth nuclei. Our aim is to study the transfer reaction ^{174}Yb (^{3}He,pγ)^{176}Lu as surrogate for the ^{175}Lu(n,γ) cross sections, see Fig.2. We have considered the ^{175}Lu(n,γ) cross section because it presents the advantage to be very well known, see for example [5,6].

Experimental Set-Up

We performed this measurement at the Tandem accelerator at the IPN Orsay in March 2010. We used an incident ^{3}He beam with an energy of 24 MeV. The beam intensity was 20 particle nA. To infer the capture probability, gamma rays were detected in coincidence with the ejectiles. The latter were fully identified by two large area ΔE-E telescopes placed symmetrically at 130° with regard to the ^{3}He beam. The E detectors were two Si(Li) detectors of 3 mm thickness. The ΔE detectors were two 300 µm silicon position sensitive detectors, whose 16*16 X-Y strips provided the angle of the detected particle with an angular coverage of 108° to 152°. We shielded the Si detectors against delta electrons coming from the target with a thin Mylar(Al) mask polarized at -300V. Four C_6D_6 liquid scintillators were used for gamma detection to infer the capture probability. The total number of gamma cascades can be obtained with these detectors by using the total energy detection principle in combination with the pulse height weighting technique. The same technique was used to obtain the ^{233}Pa(n,γ) cross section [7,8]. Notice that the coupling of these detectors to a pulse shape discriminator permits to separate between photons and neutrons interacting within the scintillators. The ^{174}Yb target was also surrounded by six germanium detectors. They were used to measure low-lying γ-ray transition intensities as a function of the compound nucleus

excitation energy, which is an additional way to investigate the difference in spin distributions between transfer and neutron-induced reactions. Fig.3 illustrates our experimental set-up.

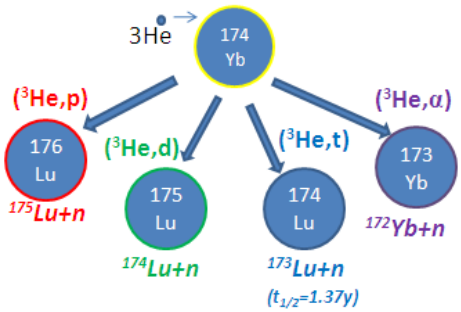

Figure 2. *Transfer channels investigated in the reaction ^{3}He+^{174}Yb and the corresponding neutron-induced capture reactions.*

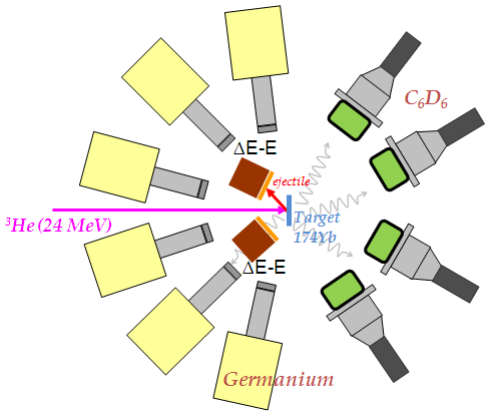

Figure 3. *Top view of the set-up for capture probability measurements.*

Preliminary results

The experimental capture probability Pγ(E*) of ^{176}Lu can then be obtained in the following way:

$$P_{\gamma}(E^*) = \frac{N_{\text{coinc}}(E^*)}{N_{\text{single}}(E^*)} \cdot \frac{1}{\varepsilon(E^*)} \qquad (8)$$

where ε(E*) represents the C6D6 cascade detection efficiency, N_{coinc}(E*) are the number of protons detected in coincidence with the C_6D_6 detectors and N_{single}(E*) the total number of protons, i.e. the number of ^{176}Lu formed. The N_{single}(E*) spectrum is corrected for the protons coming from transfer reactions between the ^{3}He beam and the carbon backing, as illustrated in Fig.4. Since the nucleus ^{176}Lu is formed by a transfer reaction, it is possible to extend our investigation below the neutron separation energy Sn corresponding to E*=6.29 MeV where only γ-rays can be emitted and consequently the measured emission probability should be 1. Below the neutron separation threshold, the ratio N*coinc*(E*)/N*single*(E*) gives the total efficiency of the C6D6 detectors. Applying a 500 keV gamma threshold in order to suppress the contribution of the opening (^{3}He,pnγ)^{175}Lu* neutron-inelastic decay channel, this ratio is of around 3.8% (+-0.3%) and remains constant from E*=5.5 MeV to Sn. Assuming that this value for the efficiency is constant and independent of excitation energy also above Sn, we obtain the probability for emitting a gamma cascade of ^{176}Lu as a function of *E**, see Fig. 5. Our data are compared with TALYS calculations for the neutron-induced capture probability of ^{175}Lu and also for the gamma-induced reaction of ^{176}Lu. The parameters of the code have been tuned to best reproduced the experimental data for the ^{175}Lu(n,γ) cross sections, as illustrated in Fig.6. The preliminary results of Fig.5 show that our surrogate data present big discrepancies with respect to the neutron-induced data, while we observe an excellent agreement with the ^{176}Lu(γ,γ) calculation. As a first conclusion, the Jπ distribution populated in the (^{3}He,p) surrogate reaction seems to be close to the one populated in the photon-induced reaction, which populates higher spins. As an illustration, Fig. 7 shows schematic distributions populated in neutron-induced and gamma-induced reactions. The ground state Jπ of ^{175}Lu and ^{176}Lu are respectively 7/2+ and 7-. The big discrepancies at low E* can be explained by the deviations between the spin distributions populated in transfer and neutron-induced reactions. For energies below the first excited state of ^{175}Lu (113keV,9/2+), the (n,γ) decay channel is only in competition with the compound elastic channel (n,n). Since the nucleus decays to only one state (i.e. by definition the ground state) with a well-defined spin (7/2+ here), this particular exit channel is extremely sensitive to the spin of the compound nucleus ^{176}Lu*. As shown in Fig. 7, it is reasonable to expect that the spin induced by transfer is higher than the one induced by a low-energy neutron leading to a suppression of the compound elastic channel when ^{176}Lu is produced in the (^{3}He,p) reaction. Talys calculations show that the (n,n) channel remains rather strong up to about 7MeV. The selectivity of the (n,n) decay channel could be at the origin of the large discrepancies observed between

surrogate and neutron-induced measurements. In Fig. 6, the resulting ^{175}Lu(n,γ) cross section is compared to neutron-induced measurements. The surrogate cross sections are too large, on average, by roughly a factor 4. High discrepancies have been also observed for ^{155}Gd and ^{157}Gd capture cross sections obtained via the surrogate method involving (p,p') inelastic reactions [9].

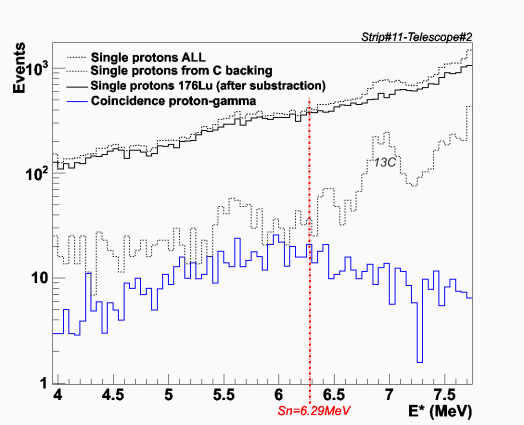

***Figure 4**. Number of single protons $N_{sing}(E^*)$ (i.e ^{176}Lu formed) before and after the substraction of the carbon backing contribution. The number of γ-proton coincidence is also represented in blue.*

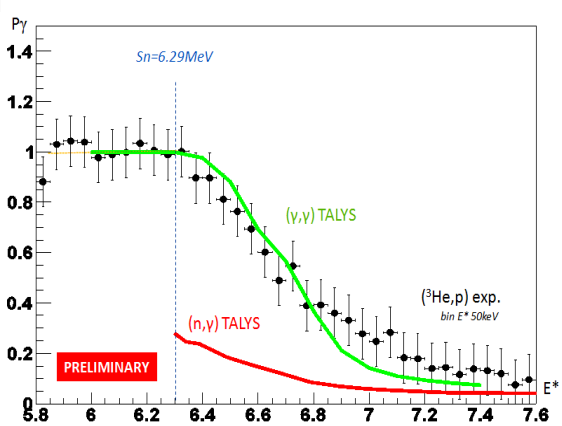

***Figure 5.** Probability of gamma emission obtained in ^{174}Yb(^{3}He,p)^{176}Lu* (black) compared to TALYS calculations for ^{175}Lu(n,γ)^{176}Lu* and ^{176}Lu(γ,γ)^{176}Lu.*

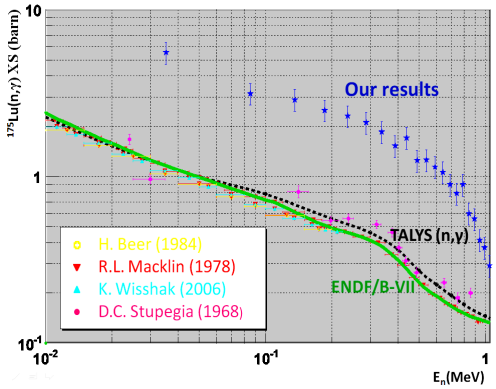

***Figure 6.** Capture cross sections obtained with the surrogate method (blue points) in comparison with neutron-induced data, ENDF evaluation and a TALYS calculation.*

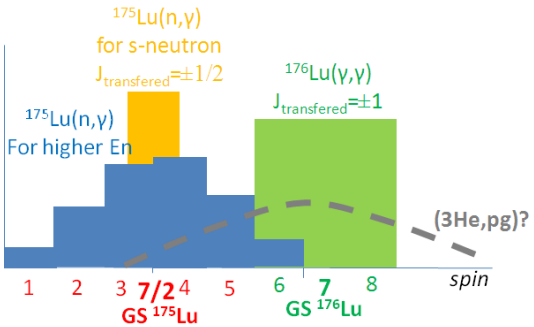

***Figure 7**. Schematic spin distribution related to the ^{175}Lu(n,γ)^{176}Lu* and ^{176}Lu(γ,γ)^{176}Lu* reactions. A reasonable guess of the spin distribution induced in the transfer reaction is presented.*

On the other side, Ge detectors are used for the detection of discrete low-lying γ-rays emitted by the residual nucleus in coincidence with the proton. Gamma spectra as a function of E* (Fig.8) permit us to identify the decaying nucleus relative to the (^{3}He,pγ)^{176}Lu* and (^{3}He,pnγ)^{175}Lu* reactions. In the future, we will extract several γ-ray intensity ratios. These observables are very sensitive to the spin. This information will be useful to constrain reaction deexcitation models and to extract information on the spin distribution. We will use the TALYS code to find the spin-parity distribution that reproduces our experimental data for the (^{3}He,p) reaction, i.e. the γ-ray intensity ratios and the capture decay probability. In this way we will infer the Jπ distribution populated in our surrogate reaction.

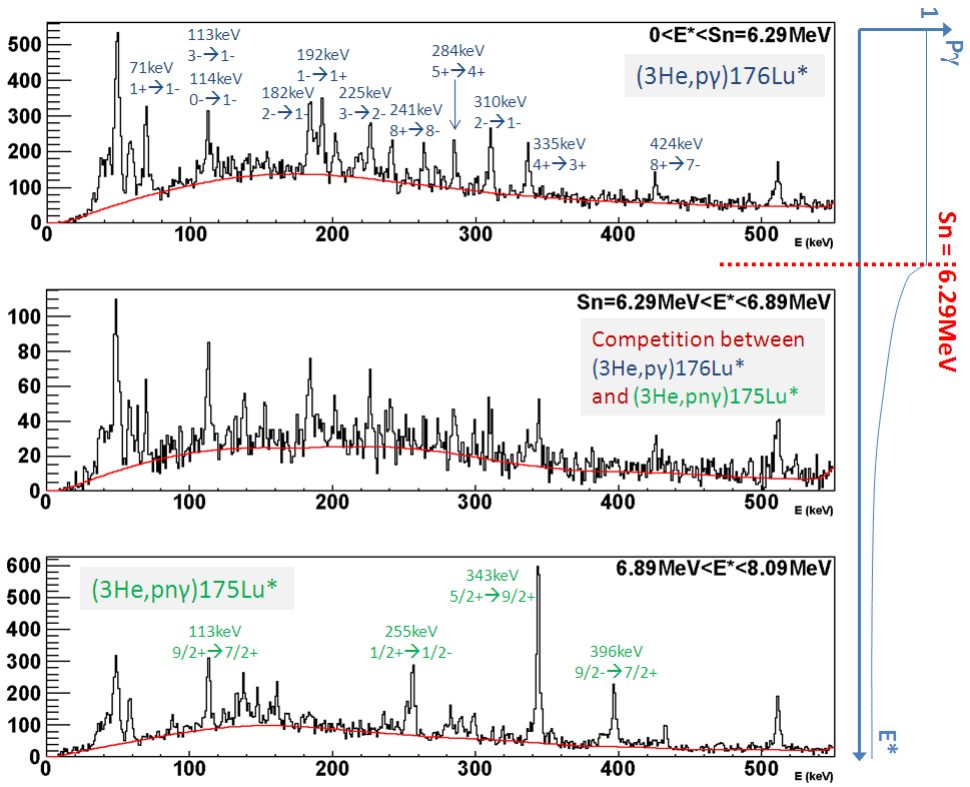

Figure 8. *Gamma spectra for three ranges of E*. One can identify the main γ-ray transitions related to the (^{3}He,pγ)^{176}Lu* and (^{3}He,pnγ)^{175}Lu* exit channels. The background is shown in red. A schematic gamma decay probability is shown on the right.*

Conclusion

We have performed an experiment to study the validity of the surrogate method for extracting capture cross sections. We have used the well known ^{175}Lu(n,γ) cross section to test the ^{174}Yb(^{3}He,pγ)^{176}Lu* reaction. Deviations between the spin distributions populated in transfer and neutron-induced reactions are responsible for the big discrepancies observed in our surrogate capture measurement. At low excitation energy, the compound elastic (n,n) decay channel is predominant and has the particularity to be extremely sensitive to the spin and the parity. This study is extremely important in view of the application of the surrogate method to infer capture cross sections of minor actinides. In the future, we plan to use the ^{238}U(n,γ) and (n,f) cross sections to investigate ^{238}U(d,p)^{239}U surrogate reaction. Note that the (d,p) reaction is very important for future experiments in inverse kinematics.

Acknowledgements

This work is supported by the CNRS program PACEN/GEDEPEON and the EURATOM - European Facilities for Nuclear Data Measurements (EFNUDAT), contract n° FP6-036434.

References

[1] J.D. Cramer, H.C. Britt, Nucl. Sci. and Eng. 41 (1970) 177
[2] V. Weisskopf and D.H. Ewing, Phys. Rev. 57, 472 (1940)
[3] G. Kessedjian et al., Phys. Lett. B 692 (2010) 297-301
[4] J.E. Escher et F.S.Dietrich, Phys. Rev. C 81, (2010) 024612
[5] R.L. Macklin et al., Nucl Sci. and Eng. 95 (1987) 189
[6] K. Wisshak et al., Phys. Rev. C 73 (2006) 015807
[7] S. Boyer et al., Nucl. Phys. A 775 (2006)175
[8] J. N. Wilson et al., Nucl. Instr. Meth. A 511 (2003) 388
[9] N.D. Scielzo et al., Phys. Rev. C 81 (2010) 034608

Neutron emission in fission process by n-n correlation function measurement

I. Companis[1,2], A. Isbasescu[1], M. Mirea[1], H. Petrascu[1]

1) Horia Hulubei National Institute for Physics and Nuclear Engineering, P. O. Box MG-6, 077125 Bucharest-Magurele, Romania
2) Université Bordeaux 1, CNRS/IN2P3, Centre d'Etudes Nucléaires de Bordeaux Gradignan, CENBG, Chemin du Solarium, BP120, 33175 Gradignan, France

companis@cenbg.in2p3.fr

Abstract: Investigation of prompt neutrons emission is a challenging issue pertaining to the fundamental aspects of nuclear fission process. In view to search the origin of the prompt scission neutrons the n-n correlation function, very sensitive to the space-time proximity from which the neutrons are emitted, was used. Quantities of interest as the correlation function strength in the momentum space within a model of independent one-particle pointlike sources, with a Gaussian distribution for the neutron generation points are obtained in a preliminary investigation. The strength of the n-n correlation function for the scission neutron significantly larger than the one for the neutrons emitted from the fission fragments was obtained. Due to this result, we might say that these neutrons could be separated. For the n-n correlation measurement, a new approach based on time of flight method with an array neutron detector and VME complex neutron system it will be used in a (p,xnf) reaction on an actinide target at Bucharest Tandem accelerator.

Introduction

Emission of the prompt neutrons has been extensively studied by both theorist and experimentalists but our understanding of fission process is still far from been complete. Following fission process prompt neutrons are released but their distribution is still uncertain. Most of the prompt neutrons, called post-scission neutrons, are emitted during the acceleration of the Fission Fragments (FF) and from the fully accelerated FF after their separation. A small part of them are emitted from the excited fissioning nucleus, before fission occurs, called pre-scission neutrons or from the neck between FF, in the moment of rupture called scission neutrons. Starting with the pioneering study of scission neutrons emission [1], several experiments and different analysis have been done in an effort to find these neutrons. The results are rather contradictory due to some arbitrary assumptions made in various analyses. Recent experiments based on fission induced by polarized neutrons have been proposed in view to answer to this intriguing subject [2-4]. Exploiting the dependence between neutron spatial orientation and FF flight direction, the total neutron yield found varies from 10 to 15 % [3,4]. This approach is extremely difficult mostly because of the reduced events statistics.

An alternative method could be the correlation analysis of the prompt neutrons in the fission process [5]. Until now the method of pair momentum correlations of identical particles has been successfully used by us in the investigation of the neutron pair pre-emitted from halo Borromean nuclei [6-8]. This method allows to determine the space-time dimension of the neutrons source and to distinguish between the post-scission and scission neutrons due to the strength of the n-n correlation function. Other important characteristics in the investigation of prompt fission neutrons emission are the neutron multiplicity and the neutron spectrum. These observables lead to a better understanding of nucleon-nuclei interaction mechanisms and the fission process properties.

Our purpose is to investigate the prompt fission neutrons emission in ^{233,235,238}U (p,xnf) reactions using time of flight method. The measurements will be held at Bucharest Tandem accelerator in the energy range E_p varying from 6 to 16 MeV. An experimental set-up consisting on array neutron detector combined with a VME acquisition system will be used the first time for this purpose. This array neutron detector with 81 scintillator cells, initial build for to investigate pair neutron pre-emission from halo nuclei has been adapted to work conditions of Bucharest Tandem.

Correlation function method

The investigation of n-n correlations is accomplished with the two-particle interferometry technique, based on the principle that the wave function of the relative motion of identical particles (n) emitted from source of a certain space-time configuration is modified through the Final State Interaction (FSI) and by the Symmetries of Quantum Statistics (SQS) [9]. Bought techniques are very sensitive to the space-time dimension from which the neutrons are emitted. Starting from 1954, when the stellar interferometry was discovered through the effect Hanbury-Brown-Twiss (HBT), the method was adopted for interferometry in high energy particles physics. Later, the method was developed in nuclear physics, focusing on particles pair correlations. Theoretical improvements in the analysis of the correlation functions were realised by Dubna group [10,11] and improved in [12,13] by taking into account the FSI. In the present work it will be used the analytical approach [12,13] that describe the neutron narrow pair correlations at small relative momentum q, within a model of independent pointlike sources, taking into account the Fermi statistics and the s-wave strong interaction. The neutron generation points are assumed independent and their distribution a Gaussian. The normalized correlation function of two neutrons with momenta $p_1 = \{E_1, \mathbf{p_1}\}$ and $p_2 = \{E_2, \mathbf{p_2}\}$ is defined as the ratio between the yield of coincidence events and the yield of uncorrelated events, $C_{nn}(q,p) = k\, N_c(q,p) / N_{nc}(q,p)$ where $q = (p_1 - p_2)/2$ and $p = (p_1 - p_2)/2$. As mentioned, the method has been successfully used by us to investigate the neutron pairs pre-emitted from ^{11}Li halo nuclei, using an array neutron detector [6,7]. Thereby, it was possible to distinguish between the neutron pairs pre-emitted from ^{11}Li halo nuclei and the neutrons emitted from the fusion process. In this context, the C_{nn} theoretical value for the neutron pairs pre-emitted from ^{11}Li halo nuclei had the value 10, while the experimental one was 7-8. This last value is affected by the residual correlations. For neutrons emitted in the fussion process this value reached the value 2 [8]. Motivated by these results, we consider that the method of n-n correlation is also adequate in the fission studies, in order to separate the scission neutrons from the post-scission neutrons. As predicted by hydrodynamical models, the fission neck between FF, in the final state configuration behaves as a filament of neutron matter. A few number of prompt neutrons strongly correlated could be emitted in the moment when the two FF are separated, while for post-scission neutrons the n-n correlations are almost absent.
The calculations realized in the following were made considering the experimental data for ^{233,235,238}U (p,xnf) [14-16], taking into account the most probable fragmentation method [17]. This fragmentation is obtained from the weighted mean mass numbers using relation (2) of Ref. [15]. The most probable charge Z_{pH} and Z_{pL} for heavy and light fragments, respectively, is considered the unchanged charge distribution assumption given by formulas (4) and (5) from Ref. [18]. For the C_{nn} calculation applied to post-scission neutrons, the mean square radius for each light and heavy FF was also obtained by exploiting the most probable fragmentation method. The average prompt neutron multiplicity and the neutron spectrum of the fission process are obtained in the frame of the Los Alamos (LA) model [17,19,20]. It has a good predictive power and requires few input parameters in comparison with other models used for prompt neutron fission data evaluation. The model is taking into account the distribution of FF excitation energy, the energy dependence of the inverse process and the multiple chance fission.

Results and discussions

Estimation of the C_{nn} strength for scission neutrons

The C_{nn} (q,p) was calculated using the analytical formula (24) of Ref. [13] for nonrelativistic neutrons, assuming that the scission neutrons are emitted from a neck formed between the FF, in the final state of the fission process [5]. The dependence of C_{nn} (q,p) versus the relative moment q of the neutron pairs, r_0 being the variance of the Gaussian distribution [12,13] is illustrated in figure 1. A scattering length of the neutrons pair in the singlet state f_0=17 fm and an effective range d_0 = 2.7 fm are considered. The distance between the two neutrons is given by the root mean square radius $r^{rms}=\sqrt{3}\, r_0$. We performed the evaluation for different r_0 values ranging from (1.88-3) fm. These values are justified by the calculations of the tip distance between the FF at scission in the frame of a microscopic-macroscopic model applied to ^{236}Np Compound Nucleus (CN) obtained from ^{235}U(p,f). The tip distance for fissioning nucleus ^{236}Np has been evaluated [21]. We started from the nuclear shape parameterization characterized by 5 degrees of freedom, one being related to the curvature of the necking C,

and another one being the elongation given by the distance between the centres of the FF denoted R. To obtain the scission configuration, the fission trajectory in the five-dimensional configuration space is determined by minimizing the action integral.

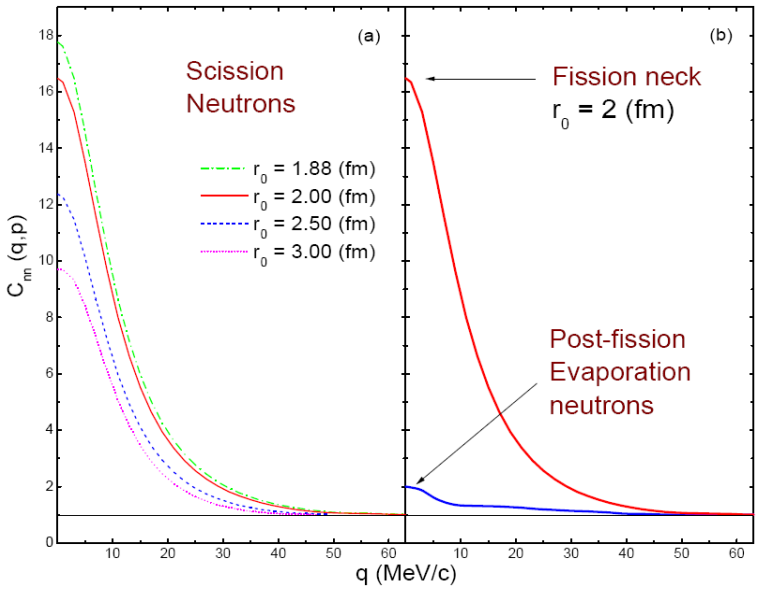

Figure 1. *$C_{nn}(q,p)$ for prompt fission neutrons as a function of relative momentum q(MeV/c). (a) $C_{nn}(q,p)$ for scission neutrons for different values of r_0. (b) Comparison between $C_{nn}(q,p)$ for scission neutrons and $C_{nn}(q,p)$ for neutrons emitted from fully accelerated FF.*

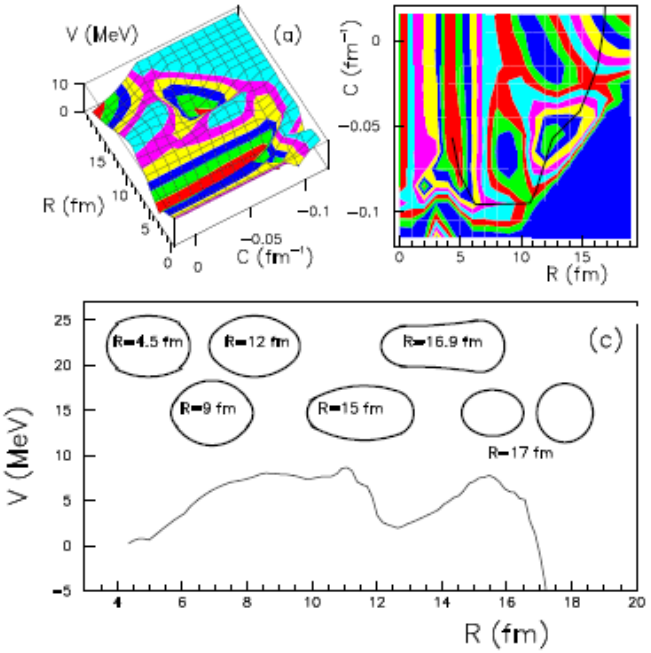

Figure 2. *(a) Minimal values of the deformation energy in MeV as function of the necking coordinate C and the elongation R for ^{236}Np. (b) Contours of the deformation energy in step of 1 MeV. The least action trajectory is superimposed. (c) Potential barrier. Some shapes obtained during the fission process together with the values of the elongation R are inserted.*

Plots of the minimal deformation energy surface as function of the necking coordinate C and the elongation R are displayed in figures 2 (a) and (b). The resulting ^{236}Np fission barrier is plotted on figure 2 (c) as function of the distance between the centres of the nascent fragments. From the exit point of the barrier, the potential energy becomes positive and the parent nucleus is able to collapses into two separated fragments. So it is possible to

appreciate the tip distance between the two fragments by making difference between the elongation in the exit point of the barrier and the dimensions of the two formed nuclei. The value obtained in this way is 3 fm and it is considered as an upper limit of the tip distance. In figure 1 (a) it is observed that the n-n correlation strength has the maximum for r_0=1.88 fm and for r_0 = 2 fm is 17.5. A significant difference between maximum value for n-n correlation function for prompt scission neutrons and for post-fission neutrons is obtained. This difference can be exploited to separate the scission and post-scission neutrons.

Estimation of the C_{nn} strength for post-scission neutrons

The correlation function $C_{nn}(q,p)$ for neutrons emitted from fully accelerated FF where the Fermi statistics contribution is dominant was determined using equations (17) and (21) of Ref. [12]. The root mean square radius was calculated for each light and heavy FF considered. For the fissioning nucleus ^{236}Np the r^{rms} for light fragment (Zr-101) is 2.91 fm and r^{rms} for heavy fragment (I-135) is 3.21fm. The FF masses were chosen considering the most probable fragmentation method and using experimental data [14-16]. The correlation strength for post-scission neutrons is ≤ 2. In figure 1 (b) the correlation strength $C_{nn}(q,p)$ in the case of neutron emission from the neck, at the scission point, exceeds by far the value corresponding to post-scission evaporation neutrons. Due to this difference in $C_{nn}(q,p)$ the two mechanisms involved could be separated, scission neutrons from the neck and post-scission neutrons emission from fully accelerated FF. We stress that the n-n correlation function strength for neutron emitted from halo Borromean nuclei is around 10, while for neutrons resulting from the fission neck, in the final state of the fission process, the correlation strength is around 20, as we expected. This value is significantly higher than the one obtained in the case of neutrons emitted from fully accelerated FF which is 2. This difference is mainly caused by the strong correlations that characterize the few scission neutrons. On the contrary, for the large number of post-fission evaporation neutrons the correlation is practically absent. Another favourable argument for the n-n correlation function measurement is the following: the prompt neutrons emitted from the neck between the FF in the last stage of the fission process require a duration of emission to the order of 10^{-22} s, while the emitted neutrons from the excited FF require much longer time of order of 10^{-19} s. [22]. This time difference can be measured within the $C_{nn}(q,p)$ method and cause modifications in the correlation intensity. Thus, the two processes can be very well distinguished when they are compared through the n-n correlation function strength as in the case of halo nuclei.

Average prompt neutron emission

In this subsection, the prompt neutron spectrum and the average prompt neutron multiplicity are calculated for proton incident energy range between 0.1-20 MeV, exploiting the LA model. The evaluation has been done considering the proton induced fission on three uranium isotopes ^{233,235,238}U, taking into account the most probable fragmentation and the average values of the input parameters of the model. The required values for the model calculation of the average prompt neutron multiplicities and the fission neutron spectra for the reactions studied in the present work are presented in table 1.

Fission Reaction	Average Light Fragment	Average Heavy Fragment	B_p (MeV)	$\langle E_r \rangle$ (MeV)	<TKE> MeV)	$\langle S_n \rangle$ (MeV)	$\langle E_\gamma \rangle$ (MeV)
^{233}U(p,xnf)	^{99}Zr	^{135}I	4.25	201.51	174.31	6.21	4.34
^{235}U(p,xnf)	^{101}Zr	^{135}I	4.83	200.61	173.82	6.41	4.48
^{238}U(p,xnf)	^{103}Zr	^{136}I	5.28	197.18	173.11	4.97	3.48

Table 1. *Average values of the parameters used for calculating the prompt fission neutron spectra and average prompt neutron multiplicities for the p+^{233,235,238}U reactions*

The average energy release $\langle E_r \rangle$ was determined by using the mass excess for the entire FF range. The values of the proton separation energy B_p and also the average neutron separation energy $\langle S_n \rangle$ were calculated with Audi-Wapstra experimental mass table [23]. For the average total kinetic energy we used formula (2) from Ref. [24]. The average prompt

gamma energy <E_γ> was calculated using the approach E_γ = 0.7 <Sn> [25]. The energy dependent CN cross section for representative average central light and heavy fragments corresponding to each CN was obtained using Becchetti-Greenless optical potential [26].

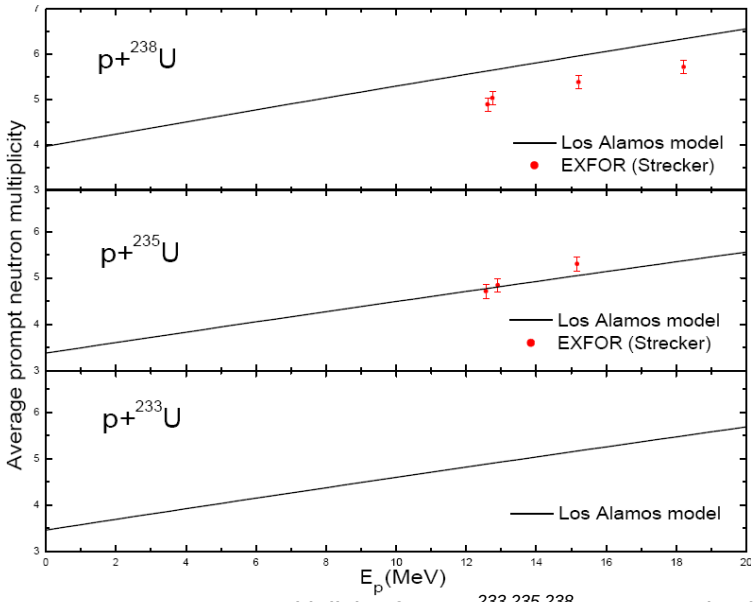

Figure 3. *Average prompt neutron multiplicity for p+ ^{233,235,238}U versus the incident proton energy compared with experimental data*

Calculated average neutron multiplicities as function of the proton incident energies for ^{234,236,239}Np are displayed in figure 3 together with experimental data [14,25]. A good agreement between experimental data for the p+^{235}U reaction and the evaluation is evidenced in the considered energy range. Similar behaviours of the average multiplicity energy dependence are also obtained for p+^{238}U. Some discrepancies can be caused by the choice of the most probable fragmentation that influences the average values of the model parameters. For the energy range considered in case of p+^{233}U reactions, the experimental data are totally missing; therefore it is not possible to appreciate the agreement of the theoretical predictions.

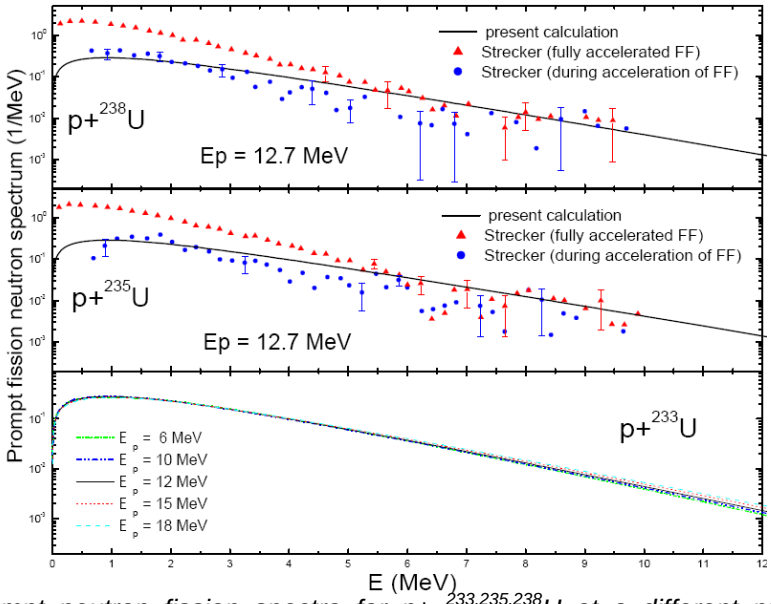

Figure 4. *Prompt neutron fission spectra for p+ ^{233,235,238}U at a different proton incident energies E_p compared with the experimental data.*

In figure 4, the prompt neutron fission spectra of ^{234,236,239}Np isotopes at different incident energies E_p = 6, 10, 12.7, 15, 18 MeV are represented. The evaluated data of p+ ^{235,238}U are

in agreement with the sole available experimental data at E_p=12.7 MeV. The experimental data were obtained by digitizing the experimental points of Ref. [25] with cartographic accuracy. For p+^{233}U the experimental data are completely missing. A systematic analysis of average prompt neutron multiplicity and spectrum will be presented in a forthcoming paper.
Recently a VME data acquisition system used with the array neutron detector mentioned previously has been installed at the Bucharest Tandem accelerator and was tested using the proton induced fission reaction on ^{235}U target. The array neutron detector, with 81 scintillator cells was built in IFIN-HH and tested at the RIKEN-RIPS separator within radioactive beams. It has been successfully used in the investigation of the pair neutron pre-emission from 11Li halo nuclei and has been adapted for Tandem conditions [27]. The work is in progress.

Conclusions

The strength of correlation n-n functions $C_{nn}(q,p)$ for scission and post-scission neutrons are calculated. The strength of the $C_{nn}(q,p)$ at small relative momenta has very large values in the case of scission neutrons. The model used takes into account the final state interaction dominant the case of scission neutrons and the Fermi statistic contribution important in the case of post-scission neutrons. A significant difference between the n-n correlation function intensity obtained for prompt scission neutrons and for post-fission neutrons was evidenced. Due to this difference, the scission and post-scission neutrons could be precisely separated. The LA model was used to evaluate average fission neutron multiplicities and spectra in proton induced fission reactions.

Acknowledgements
This work is dedicated to the memory of Prof. Dr. Marius Petrascu (1929-2007), personality devoted to nuclear physics research. We are grateful to A. Pop, A. Tudora and A. Constantinescu for fruitful discussions. Work supported by CNCSIS IDEI 535 Contract and 1044 DANTE contract

References

[1] H. R. Bowman et al., Phys.Rev. 126, (1962) 2120
[2] G. V. Danilyan et al., Phys. At. Nuclei. 69, (2006) 1158
[3] G. A. Petrov et al., Physics of Atomic Nuclei 71, (2008) 1137
[4] A. S. Vorobyev et al. Nucl. Inst. Method A 598, (2009) 795-801
[5] M. Petrascu, Book of Abs. Int. Conf. 'Nucleus 2007', June 25-29, Voronezh, Russia, (2007) 59
[6] M. Petrascu et al. and RIKEN collaboration, Phys. Rev. C 69, (2004) 011602
[7] M. Petrascu et al., Phys. At. Nucl. 69, (2004) 1261
[8] M. Petrascu et al., Nucl. Phys. A790, (2007) 235c
[9] D. H. Boal, C. K. Gelbke, B. K. Jennings, Rev. Mod. Phys. 62, (1990) 553
[10] G. I. Kopylov and M. I. Podgoretsky, Sov. J. Nucl. Phys. 15, (1972) 219
[11] G. I. Kopylov, Phys. Lett. 50B, (1974) 472
[12] R. Lednicky, V. L. Lyuboshitz, Sov. J. Nucl. Phys. vol.35 (1982) 770
[13] V. L. Lyuboshitz and V. V. Lyuboshitz, Phys. Atom. Nuclei vol 71, (2008) 454
[14] http://www-nds.iaea.org/EXFOR
[15] T. Ohtsuki et al., Phys. Rev. C 44, (1991) 1405
[16] T. Ohtsuki et al., Phys. Rev. C 40, (1989) 2144
[17] D. Madland & R. Nix, Nucl. Sci. Engineering 81, (1982) 213
[18] H. Naik et al., Nucl. Phys. A781, (2007) 1
[19] D. G. Madland, Nucl. Phys. A 772, (2006) 113-137
[20] G. Vladuca, A. Tudora, Comput. Phys. Commun.125, (2000) 221
[21] I. Companis, M. Mirea and A. Isbasescu, Rom. J. Phys., in press
[22] Yu. D. Katarzhnov et al., Physics of Atomic Nuclei 64, (2001) 177
[23] G. Audi, A. H. Wapstra & C. Thibault, Nucl. Phys. A729 (2003), 337
[24] Y. Nagame et al, Rom. Report in Phys. Vol. 59, (2007), 547
[25] M. Strecker et al, Phys. Rev, vol. 41, (1990), 2172
[26] O. Bersillon, SCAT2 optical model code, OECD-NEA-DB-CPS 0829/03, (1991)
[27] H. Petrascu et al., Rom. Journal of Phys., in press

Microscopic description of the fission process with the Gogny force

N. Dubray*, H. Goutte† and J.-F. Berger*

*CEA, DAM, DIF, F-91297 Arpajon, France
†GANIL, Bd Henri Becquerel, BP 55027 - 14076 CAEN Cedex 05, France

Abstract. The fission process is described in a fully microscopic two-steps approach. First, potential energy surfaces are calculated in the elongation-asymmetry plane, with nuclear shapes ranging from sphericity to very large deformations, using the Hartree-Fock-Bogoliubov method and the Gogny nucleon-nucleon effective interaction (parameterization D1S). Fragment properties (fragment deformations, deformation energies, energy partitioning, neutron binding energies at scission, charge polarization, total fragment kinetic energies and neutron emission multiplicities...) are extracted from the scission configurations, following a criterion based on the nuclear density. Then a time-dependent Generator Coordinate Method with a Gaussian Overlap Approximation is performed on these surfaces, leading to exit points probabilities. Some static properties of the fissioning systems ^{226}Th and ^{256,258,260}Fm, and a dynamical calculation of ^{238}U are presented.

Keywords: Hartree-Fock-Bogoliubov, Gogny Force, Fission, Scission, Fission Fragments
PACS: 21.10.Dr, 21.10.Ft, 21.60.Jz, 24.75.+i

INTRODUCTION

The theoretical description of the fission process is a very rich study, which involves nuclear configurations in highly unusual states, very far from equilibrium. In this study, we use Hartree-Fock-Bogoliubov calculations with the nucleon-nucleon effective interaction Gogny D1S, using constraints on quadrupole and octupole moments, ranging from the spherical shape up to very large deformations, and a Time-Dependent Generator Coordinate Method with Gaussian Overlap Approximation. After a short study of the way a compound nucleus splits into two fragments when increasing the constraint placed on its elongation, we find a criterion based on the nuclear matter density to discriminate between pre- and post-scission configurations. Using this criterion, we calculate many fission fragments properties from the very last pre-scission configurations before scission, here called scission configurations, and compare them with experimental results when available[1]. We then present how the fragment mass distribution for ^{238}U can be obtained with our dynamical calculations.

THEORETICAL FRAMEWORK

For the static production of the potential energy surfaces, we use the Hartree-Fock-Bogoliubov (HFB) method [2] with the Gogny effective nucleon-nucleon interaction. This finite range and density dependent interaction allows the simultaneous treatment of the nuclear and pairing mean fields. We have used the D1S set of parameters [3, 4],

which is known for its good reproduction of nuclear properties [5, 6]. In order to obtain a total energy landscape of the nuclear system in the (elongation, asymmetry) coordinates, we put in the main HFB equation additional terms called *constraints*, leading to the constrained HFB equation:

$$\delta\langle\varphi|\hat{H}-\lambda_N\hat{N}-\lambda_Z\hat{Z}-\lambda_{10}\hat{Q}_{10}-\lambda_{20}\hat{Q}_{20}-\lambda_{30}\hat{Q}_{30}|\varphi\rangle=0. \quad (1)$$

The purpose of these constraints is to fix the mean values of the numbers of neutrons and protons of the nuclear system as well as those for the usual multipole operators $\hat{Q}_{10}$, $\hat{Q}_{20}$ and $\hat{Q}_{30}$, namely

$$\begin{aligned}
\langle\varphi|\hat{N}|\varphi\rangle &= N, & (2)\\
\langle\varphi|\hat{Z}|\varphi\rangle &= Z, & (3)\\
\langle\varphi|\hat{Q}_{10}|\varphi\rangle &= 0, & (4)\\
\langle\varphi|\hat{Q}_{20}|\varphi\rangle &= q_{20}, & (5)\\
\langle\varphi|\hat{Q}_{30}|\varphi\rangle &= q_{30}. & (6)
\end{aligned}$$

By using the constraint on the dipole moment $\hat{Q}_{10}$, we ensure that the center of mass of the system is fixed to the origin of axes. We let the constraints values q_{20} and q_{30} take regularly spaced values, and build the total energy map of the system in the (q_{20}, q_{30}) plane.

For each set of constraints, eq. (1) is solved by expanding the quasi-particle operators onto axially-symmetric two-centers harmonic oscillator bases. In these calculations, the conservation of the z-axis symmetry of the system is enforced. For each calculation, the parameters describing the bases are optimized, i.e. they are chosen in order to minimize the total binding energy of the system.

For the dynamical wave-packet propagation on the previous potential energy surfaces, we use the time-dependent generator coordinate method with gaussian overlap approximation. The general time-dependent GCM state with N degrees of freedom $\{q_1,\ldots,q_N\}$ is

$$|\psi(t)\rangle\equiv\left(\prod_i^N\int dq_i\right)f(q_1,\ldots,q_N,t)|\phi(q_1,\ldots,q_N)\rangle. \quad (7)$$

The variational principle is expressed as

$$\frac{\partial}{\partial f^*}\int_{t_1}^{t_2}\langle\psi(t)|\left(\hat{H}-i\hbar\frac{\partial}{\partial t}\right)|\psi(t)\rangle=0. \quad (8)$$

After using the Gaussian Overlap Approximation, we obtain a Schrödinger-like equation

$$\hat{H}_{\rm coll} = -\frac{\hbar^2}{2}\sum_{i,j}^N\frac{\partial}{\partial q_i}B^{ij}\frac{\partial}{\partial q_j}+\hat{V} \quad (9)$$

with

$$g(\{q_i'\},t) = \left(\prod_i^N\int dq_i\right)f(\{q_i\},t)I^{1/2}(\{q_i'\},\{q_i\}) \quad (10)$$

$$I(\{q_i'\},\{q_i\}) \;=\; \langle\phi(\{q_i'\})|\phi(\{q_i\})\rangle \tag{11}$$

and B^{ij} being the components of the inverted inertia tensor[10].

SCISSION CRITERION

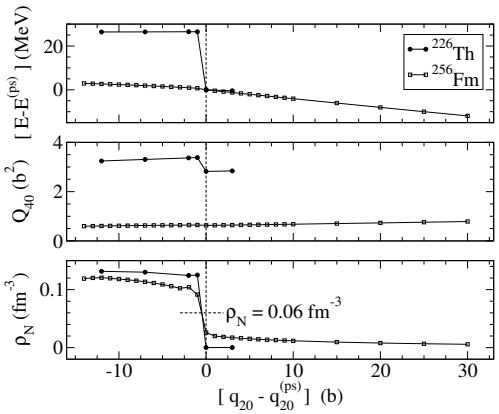

FIGURE 1. Example of very different symmetric scission transitions. $q_{20}^{(ps)}$ and $E^{(ps)}$ represent the quadrupole moment and the HFB energy of the first post-scission point for each fissioning system.

Scission corresponds to a transition from the fission valley, where the fragments still share some nucleons, to the fusion valley, where the fragments are separated. In the (q_{20}, q_{30}) deformation space, this transition most of the time corresponds to a discontinuity in several nuclear observables. Since we want to calculate fission fragment properties at some points that have to be continuously connected to the ground state of the fissioning system, we have to calculate these properties at the very last points before scission occurs (here called scission points). In order to define such scission points, we use the following definition: if a point from the fission valley (compound system with a neck between the fragments) leads to a point in the fusion valley (system splitted into two separated fragments) by a small increase of one deformation parameter, this point is called a *scission point*. To achieve a numerical identification of all the scission points of a given potential energy surface, we need to find a robust and reliable criterion on the nuclear observables.

In Fig. 1, the evolutions of the binding energy (E), the hexadecapole moment (q_{40}) and the density in the neck (ρ_{N}) are plotted in the vicinity of the symmetric scission transitions of ^{226}Th and ^{256}Fm. One clearly sees that the scission transition can be either smooth (^{256}Fm) or sudden (^{226}Th), and that a criterion based on the matter density in the neck is a good way to distinguish pre-scission ($\rho > \rho_c$) from post-scission ($\rho < \rho_{\mathrm{N}}$) configurations. In this study, we use the value $\rho_{\mathrm{N}} = 0.06\mathrm{fm}^{-3}$. Since we are working in a 2-dimensional deformation space (q_{20}, q_{30}), the set of considered scission points forms a line, which we call the *scission line*.

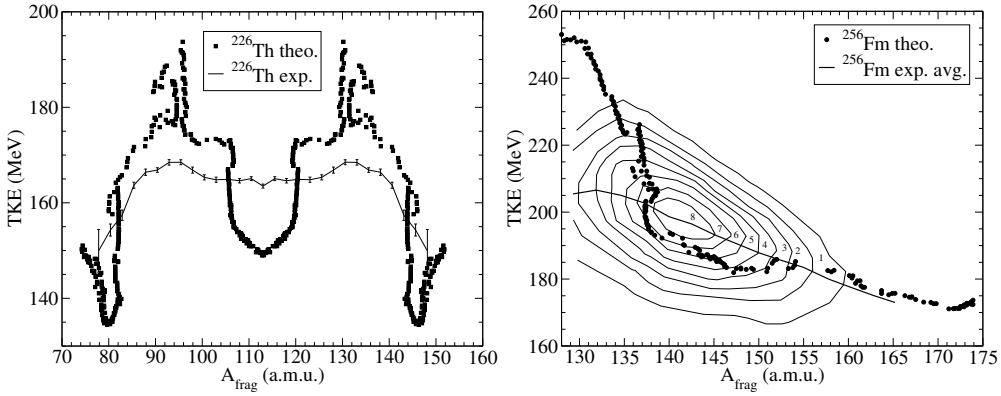

FIGURE 2. Total fragment kinetic energies in ^{256}Fm and ^{226}Th. The average experimental value for each fragmentation has been drawn with a solid line.

STATIC RESULTS

The total kinetic energies of the fragments have been plotted for ^{226}Th and ^{256}Fm (Fig. 2), using the following simple approximation:

$$E_{\mathrm{T}KE} = \frac{e^2 Z_{\mathrm{H}} Z_{\mathrm{L}}}{d_{\mathrm{C}h}}, \tag{12}$$

where e is the electron charge, Z_{H} (Z_{L}) the charge of the heavy (light) fragment, and $d_{\mathrm{C}h}$ the distance between fragment centers of charge at scission. These quantities are in rather good agreement with experimental data [7, 8]. The neutron emission multiplicities for ^{256}Fm, calculated as

$$\nu_{\mathrm{f}rag} = \frac{E_{\mathrm{d}ef}}{\langle E_k \rangle + B^*_{\mathrm{n}}}, \tag{13}$$

where B^*_n is the one-neutron binding energy in nascent fragment, $E_{\mathrm{d}ef}$ is the deformation energy of the fragment, and $\langle E_k \rangle$ the mean energy of the emitted neutron, reproduce the general structure of the sawtooth experimental data[9], even if there seems to be a slightly underestimation of the theoretical values.

DYNAMIC RESULTS

The Time-Dependent Generator Coordinate Method with Gaussian Overlap Approximation has been used for the description of the fragment mass distribution in the ^{238}U fissioning system. The Potential Energy Surface can be seen on Fig. 4. The initial state has been taken as an eigenstate of an artificially extended first well, see [10] for details. The fragment masses have been calculated at scission, by integrating over the left and right "parts" of the fissioning system. The boundary plane between twose parts is orthogonal to the symmetry axis of the system and contains the "neck point", corresponding to the minimum of the density along the symmetry axis of the system. The probability

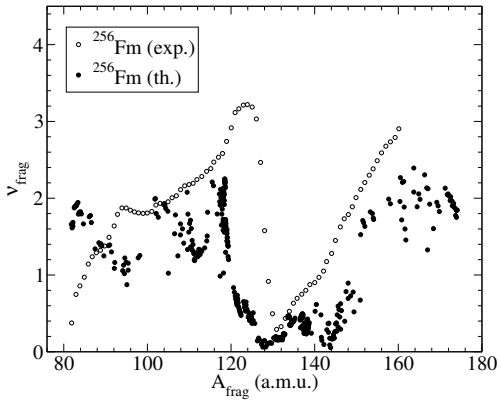

FIGURE 3. Neutron emission multiplicity in ^{256}Fm.

associated with each possible fragmentation has been calculated by time-integrating the flux of the wave function $\vec{J}(q_{20}, q_{30}, t)$ through the scission line :

$$Y(A) = \int_0^T dt \vec{J}(q_{20}, q_{30}, t).\vec{n}ds \tag{14}$$

The resulting mass distribution is shown of Fig. 5. We compare it to a static estimation of

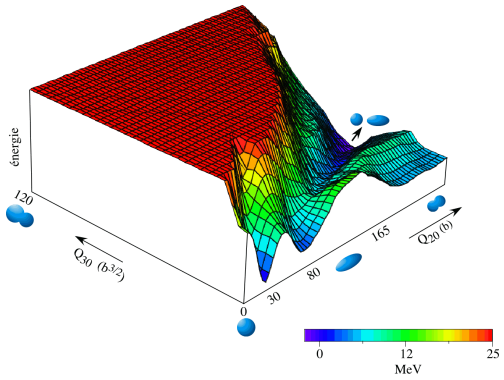

FIGURE 4. Potential Energy Surface for the ^{238}U system in the elongation-asymmetry plane.

the fission fragment mass distribution obtained by considering a Boltzman distribution built on the binding energy of the system along the scission line. We also show the experimental mass distribution given by the Wahl evaluation[11]. One can see that the static estimation reproduces the most probable fragmentation, but fails at reproducing the width of the two bumps of the distribution. The symmetric fragmentation is also highly under-estimated. The dynamic calculation results are much more convincing. They reproduce the most probable fragmentation, the width of the two bumps of the distribution, and the ratio symmetric yield /asymmetric yield seems to be rather close from the experimental one.

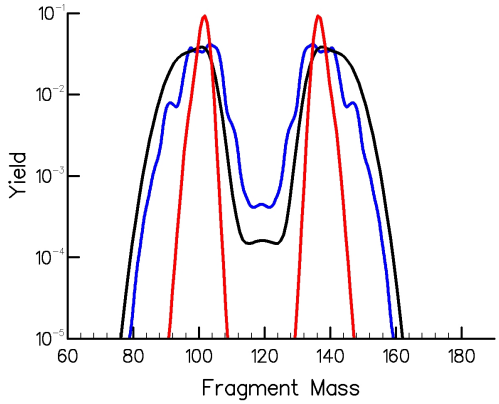

FIGURE 5. Fission fragment mass distribution for the ^{238}U system. Static calculation is plotted in red, dynamic calculation is plotted in blue, Wahl evaluation is plotted in black.

CONCLUSION

The static results here presented for Th and Fm nuclei show that our fully microscopic approach is able to provide a quantitative account of scission properties of actinide nuclei, whithout using any adjustable parameter. Several fragment properties have been computed for many different scission configurations, and are found to be in a qualitative agreement with experimental data. The description of time-dependent fission dynamics and of fragment mass distributions for the ^{238}U fissioning system [10] will be extended in a near future to other nuclei, and will allow us to ponderate the fission fragment properties by the probability of the associated fragmentation. Finally, extensions of the present calculations to a three-dimensional mesh (q_{20}, q_{30}, q_{40}), to non-axial nuclear shapes, to other actinides, and to intrinsic excited configurations are under consideration.

REFERENCES

1. N. Dubray, H. Goutte and J.-P. Delaroche, *Phys. Rev.* **C77**, 014310 (2008).
2. P. Ring and P. Schuck, *The Nuclear Many Body Problem* (Springer-Verlag, New York, 1980), p. 267.
3. J. Dechargé and D. Gogny, *Phys. Rev.* **C21**, 1568 (1980).
4. J.-F. Berger, M. Girod and D. Gogny, *Comp. Phys. Comm.* **63**, 365 (1991).
5. G. Bertsch, M. Girod, S. Hilaire, J.-P. Delaroche, H. Goutte and S. Péru, *Phys. Rev. Lett.* **99**, 032502 (2007).
6. J.-P. Delaroche, M. Girod, H. Goutte and J. Libert, *Nucl. Phys.* **A771**, 103 (2006).
7. K.-H. Schmidt, J. Benlliure and A.R. Junghaus, *Nucl. Phys.* **A693**, 169 (2001).
8. D.C. Hoffman, G.P. Ford, J.P. Balagna and L.R. Veeser, *Phys. Rev.* **C21**, 637 (1980).
9. J.E. Gindler, *Phys. Rev.* **C19**, 1806 (1979).
10. H. Goutte, P. Casoli, J-F. Berger and D. Gogny, *Phys. Rev.* **C71**, 024316 (2005).
11. A.C. Wahl, Los Alamos National Laboratory Report No. LA- 13928, 2002 (unpublished).

Binary and ternary fission models

R. A. Gherghescu[1], N. Carjan[1], D. N. Poenaru[1]

1) Horia Hulubei National Institute of Physics and Nuclear Engineering, P.O. Box MG-6, RO-077125 Bucharest-Magurele, Romania
radu@radu.nipne.ro

Abstract: Deformed two and three center shell models are developed in order to obtain the single-particle energies for binary and ternary fission configurations. The two center shell model is used to calculate the level scheme transition from the superheavy parent nucleus to the emitted cluster plus the daughter nucleus. The three center shell model is also employed to compute the transition toward eventual three equal fragment partition from the superheavy nuclei. The levels are used to compute the shell corrections within the Strutinsky method. The liquid drop part is calculated using the Yukawa-plus-exponential model. The total deformation energy is then minimized over a multidimensional space of deformation. In order to perform a dynamic study of the process, the Werner-Wheeler tensor is calculated, and cluster emission paths for binary and ternary splitting are obtained for Z=120 isotopes.

The two center shell model

The two-center shell model developed in this work is based on the initial version pioneered by the Frankfurt school [1]. The deformation space includes the semiaxis ratios of the parent nucleus and of the two emitted fragments, the neck parameter and the distance between centers. The basic two-center potential is formed from two spheroidally deformed oscillators crossing eachother, linked by a necking potential:

$$V_{DTCSM}(\rho,z)=\begin{cases} V_1(\rho,z) & ,v_1 \\ V_{g1}(\rho,z) & ,v_{g1} \\ V_{g2}(\rho,z) & ,v_{g2} \\ V_2(\rho,z) & ,v_2 \end{cases} \tag{1}$$

where V_1 and V_2 are the two spheroidally deformed potentials and V_{g1} and V_{g2} are the necking microscopic parts

$$\begin{aligned} V_1(\rho,z) &= \tfrac{1}{2}m_o\omega_{\rho_1}^2\rho^2+\tfrac{1}{2}m_o\omega_{z1}^2(z+z_1)^2 \\ V_{g1}(\rho,z) &= 2V_0-[\tfrac{1}{2}m_o\omega_g^2(\rho-\rho_3)^2+\tfrac{1}{2}m_o\omega_g^2(z-z_3)^2] \\ V_{g2}(\rho,z) &= V_0 \\ V_2(\rho,z) &= \tfrac{1}{2}m_o\omega_{\rho_2}^2\rho^2+\tfrac{1}{2}m_o\omega_{z2}^2(z-z_2)^2 \end{aligned} \tag{2}$$

The spin-orbit terms are added following the calculation procedure developed in [2].

The energy levels are input data for the Strutinsky method in order to calculate the shell corrections.

$$\frac{}{3}\rho_e \int_{z_{min}}^{z_{max}} dz \int_{z_{min}}^{z_{max}} dz\prime F_C(z,z') \tag{3}$$

and a similar expression for the nuclear surface Yukawa type energy.

The binary character for the macroscopic part is given by the third term in the total sum of each of the terms:

$$E_C = \frac{2\pi}{3}(\rho_{e1}^2 F_{C1} + \rho_{e2}^2 F_{C2} + 2\rho_{e1}\rho_{e2}F_{C12}) \tag{4}$$

where F_i are shape-dependent integrals and

$$E_Y = \frac{1}{4\pi r_0^2}[c_{s1}F_{EY1} + c_{s2}F_{EY2} + 2(c_{s1}c_{s2})^{1/2}F_{EY12}] \tag{5}$$

where F_j are again shape dependent integrals. The last terms provide the interaction between the emitted cluster and the heavy daughter.

The three center shell model

The same type of calculation is performed to obtain the macroscopic part for the ternary fission process. One uses the three center potential:

$$V_{3osc}(\rho,z) = V(\rho) + V(z) \tag{6}$$

where:

$$V(\rho) = \frac{1}{2}m_0\omega_\rho^2\rho^2 \tag{7}$$

and

$$V(z) = \begin{cases} \frac{1}{2}m_o\omega_z^2(z-z_1)^2 & ,z > z_{01} \\ \frac{1}{2}m_o\omega_z^2 z^2 & ,-z_{01} < z < z_{01} \\ \frac{1}{2}m_o\omega_z^2(z+z_1)^2 & ,z < -z_{01} \end{cases} \tag{8}$$

Every of the three fragment potentials on the symmetry axis is centered in the middle of the corresponding emerging sphere. The initial moment is marked by z_{01}=0, when all three centers coincide. The total Hamiltonian H is written as:

$$H = H_{3osc} + V_{\hat{l}\hat{s}} + V_{\hat{l}^2} \tag{9}$$

where

$$H_{3osc} = -\frac{\hbar^2}{2m_0}\left[\frac{\partial^2}{\partial\rho^2} + \frac{1}{\rho}\frac{\partial}{\partial\rho} + \frac{1}{\rho^2}\frac{\partial^2}{\partial\phi^2} + \frac{\partial^2}{\partial z^2}\right] + V(\rho) + V(z) \tag{10}$$

The calculus of the macroscopic part is similar to the two-center case, but instead of the neck, one has the middle fragment. Finally the shell corrections and the liquid drop part are summed to obtain the total deformation energy for ternary fission configuration.

Results

The Werner-Wheeler irrotational flow method provides the tensor of inertia components which accounts for the dynamical couplings between different deformation degrees of freedom. At the end, the action integral is calculated and penetrabilities are obtained within the WKB semiclassical approximation [4]. The first superheavy nucleus under scrutiny is ^{282}120. Three main valleys are discernable on the potential energy surface after the multidimensional minimization, corresponding to three fission channels: two almost symmetric ones ^{138}Ce+144Sm , ^{118}Sn+^{164}Yb and one corresponding to the cluster emission: ^{58}Ni+^{224}U. The barriers obtained for these channels are displayed in figure 1.

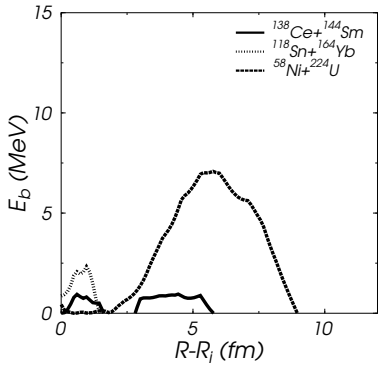

Figure 1: The dynamical barriers for the main fission channels along deformation valleys from ^{282}120.

One can observe that the most favorable channels are the quasi-symmetric ones. The cluster emission from ^{282}120 is higly improbable as compared to the fission channels, as can be seen from the huge difference in barrier height and width.

The second system under study is ^{288}120. The barriers are displayed in figure 2, for the two main fission valleys obtained in the quasi-symmetry mass region: ^{144}Nd+^{144}Nd , ^{128}Sn+^{160}Yb and the cluster type emission valley ^{40}Ca+^{248}Fm. Sn accompanied fission channel is obviously the most favored decay mode, followed by the most symmetric one composed of two Nd nuclei. Again the cluster emission, though being favored by the double-magicity of ^{40}Ca, has a much higher and wider barrier, which yields a very low penetrability value.

The last superheavy nucleus under study is ^{294}120. The corresponding fission barriers are displayed in figure 3.

Once again the most favorable decay channels are the fission type quasi-symmetric ones: ^{146}Nd+^{148}Nd and ^{122}Sn+^{172}Yb. The barrier for the cluster emission of ^{60}Ni is much higher and stretches on a much longer distance between centers to be competitive.

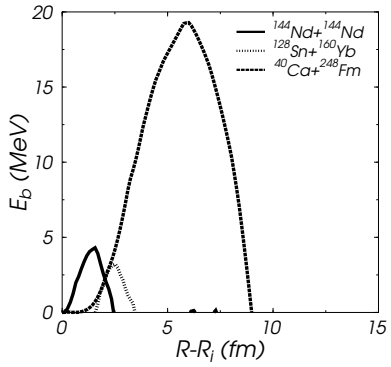

Figure 2: The dynamical barriers for the main fission channels along deformation valleys from ^{288}120.

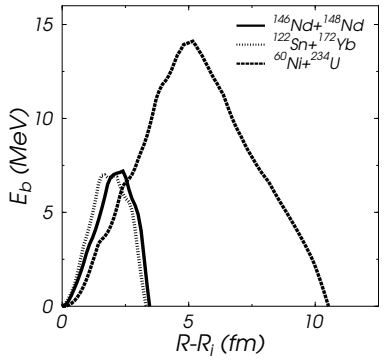

Figure 3: The dynamical barriers for the main fission channels along deformation valleys from ^{294}120.

The ternary fission from the same superheavy nuclei is also calculated and the results are displayed in figure 4 as the dynamical barriers resulted from minimization of the action integral.

All three barriers are extremely large and one can conclude that ternary fission from these superheavy nuclei is highly improbable.

Acknowledgements

The present research was partly supported by the Ministry of Education and Research, Bucharest within the IDEI programme, contract Idei-124.

References

[1] J. Maruhn and W. Greiner, Z. Phys. 251, 431 (1972).

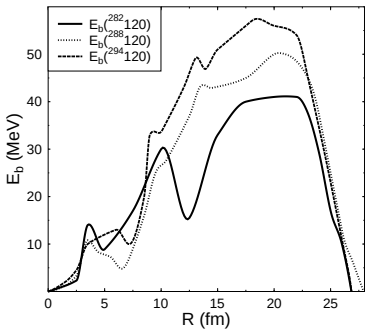

Figure 4: The dynamical barriers for ternary fission channels along deformation valleys from Z=120 isotopes.

[2] R. A. Gherghescu, Phys. Rev. C67, 014309 (2003).

[3] H. J. Krappe, J. R. Nix and A. J. Sierk, Phys. Rev. C20, 992 (1979).

[4] R. A. Gherghescu, J. Skalski, Z. Patyk and A. Sobiczewski, Nucl. Phys. A651, 237 (1999).

Resonance neutron induced fission of ^{239}Pu

F.-J. Hambsch[1)], I. Ruskov[1,2)], L. Dematté[3)]

1) European Commission, Joint Research Centre, Institute for Reference Materials and Measurements, Retieseweg 111, 2440 Geel, Belgium
2) Bulgarian Academy of Sciences, Institute for Nuclear Research and Nuclear Energy, Tzarigradsko chaussee 72, 1784 Sofia, Bulgaria
3) CINECA, I-40033 Casalecchio di Remo, Italy
Franz-josef.hambsch@ec.europa.eu

Abstract: A measurement of the resonance neutron induced ^{239}Pu(n, f) fission fragment kinetic energy and mass distributions has been performed using the twin Frisch grid ionization chamber technique at the GELINA white spectrum pulsed neutron source. Special emphasis was devoted to cope with the strong α-activity of the ^{239}Pu target, taking advantage of an improved pulse pile-up rejection system. For incident neutron energies up to about 200eV all resonances could be resolved and fission fragment mass and total kinetic energy distributions deduced. Compared to a similar experiment on ^{235}U(n,f), in the same resonance region, less pronounced fluctuations of the fission fragment mass and total kinetic energy have been observed in the case of ^{239}Pu(n,f). From a physical point of view such fluctuations have been expected, because the only possible low-energy spin states ($J^{\pi} = 0^{+}$, 1^{+}) belong to well separated (about 1.25MeV) compound system transition state bands. A small spin dependence of about 70keV has been found for the fission fragment mean total kinetic energy in the neutron energy range above 1eV. This means that viscosity effects could take place during the fission of ^{240}Pu. A recently developed theoretical approach has given a possible explanation of the absence of pronounced fluctuations of ^{239}Pu(n,f) fission properties. The experimental two-dimensional mass-total kinetic energy distributions have been interpreted within the theoretical multi-modal fission model of Brosa et al.

Introduction

The investigation of the neutron induced fission of ^{239}Pu is still of primary interest both from fundamental and applied physics point of view. The capture of a s-wave neutron (spin $1/2^{+}$) with thermal or resonance energy by ^{239}Pu ($I^{\pi} = 1/2^{+}$) forms the ^{240}Pu compound nucleus (CN) mainly in 2 states [1] with spins $J^{\pi} = 1^{+}$ and $J^{\pi} = 0^{+}$. They belong to two well separated (~ 1.25MeV) transition state bands with $K^{\pi} = 1^{+}$ and $K^{\pi} = 0^{+}$ [2]. If the coupling between the collective and single-particle degrees of freedom is weak (the system is adiabatic, not viscous) then the energy difference between the bands should appear after scission in the mean total kinetic energy <TKE> of the primary (before neutron emission) fission fragments (FF) from resonances of both spin groups [3].
In case of resonance neutron induced fission of ^{235}U [4, 5] quite pronounced fluctuations of the FF mass (A) and total kinetic energy (TKE) from resonance-to-resonance were observed. They were interpreted within the frame of the multi-modal random-neck-rupture (MM-RNR) model of fission [6]. The transition state spectrum in a ^{236}U CN above the fission barrier results from the mixing of $J^{\pi}= 3^{-}$ and 4^{-} for $K^{\pi}=1^{-}$ and $K^{\pi}=2^{-}$ bands.
Experimental data on ^{239}Pu(n,f) are very important for the design of nuclear facilities and in view of nuclear waste management. Knowledge about the average prompt neutron emission $<\nu_p>$ from this reaction becomes important since ^{239}Pu is used in mixed oxide (MOX) fuel elements. In the resonance neutron energy region quite large fluctuations of $<\nu_p>$ have been observed [7]. These fluctuations have a significant impact on the reactivity coefficient of advanced water reactors [8], but their origin still is not quite clear. Are they correlated with Y(A, TKE)-distribution fluctuations, as it was found for ^{235}U(n,f) [4], or are they a result of the competition of the direct fission ^{239}Pu(n,f) with ^{239}Pu(n, γf)-reaction [9]?. The influence of the (n, γf)-reaction has been observed in the neutron $<\nu_p>$ and gamma $<\nu_\gamma>$ multiplicities, as well as in the average gamma energy $<E_\gamma>$ [10-12] and in the FF independent yields [13]. Results of two measurements of FF characteristics at neutron resonance energies have been reported in the past [3, 14] with apparently controversial outcome.

Therefore, new measurements of ^{239}Pu(n,f) FF Y(A,TKE)-distributions in the resolved resonance region have been performed at Geel Electron LINear Accelerator (GELINA) "white" spectrum neutron source time-of-flight (TOF) spectrometer of IRMM in Geel, Belgium.

Data acquisition, analysis and discussion

The experimental setup and some preliminary results have already been published elsewhere [15-17]. A twin ionization chamber (IC) with Frisch grids was used as charged particle (α, FF) spectrometer. As detecting gas pure CH_4 was used at a pressure of $\approx 1.1 \times 10^5$Pa (electron drift velocity ~10cm/μs) in a continuous gas flow rate of about 0.1 l/min, securing nearly constant FF pulse amplitudes during the duration of the experiment. The electron collecting time was ~300ns. The main characteristics of the target are summarized in Table 1. The IC was installed at a distance of $\approx$9.4m from the GELINA neutron producing target. This way all the resonances were measured simultaneously in the same experimental conditions.

Table 1. *^{239}Pu sample characteristics*

Support		
Backing	Material	Polyimide
	Thickness	$\approx$ 36 μg/cm^2
Coating	Material	Au
	Prep. method	Evaporation
	Thickness	$\approx$ 79 μg/cm^2
Pu target		
Chemical form		PuF_3
Enrichment, ^{239}Pu		99.9774 $\pm$ 0.0027 %
Preparation method		Evaporation
Layer	Diameter	$\approx$ 45 mm
	Thickness	$\approx$ 32 μg/cm^2
Total mass of Pu		$\approx$ 514 μg
Specific α-activity		$\approx$ 1 MBq

Five parameters were recorded in list-mode (event-by-event): the neutron TOF, 2 anode amplitudes containing FF kinetic energy information and 2 cathode-grid electron drift times, from which the FF emission angles were determined. The latter were used also for calculating the energy losses of FF in the sample and backing [4, 15-19].

The data acquisition was performed with two different GELINA parameter sets, corresponding to two different neutron energy ranges (Table 2).

Table 2. *GELINA set of parameters*

f [Hz]	100	800
$\langle I_e \rangle$ [μA]	$\approx$ 40	$\approx$ 75
L [m]	$\approx$ 9.4	$\approx$ 9.4
Δt [ns]	$\approx$ 2000	$\approx$ 1
E_n [eV]	$\geq$ 0.01	$\geq$ 0.3
δE_n (E_n=10eV)	$\approx$ 0.02	$\approx$ 0.006
fission events	~ 4.10^6	~ 5.10^6
In-beam filter	Cd	BC_4
ΔEn, eV	0.008–1	0.3–200

Because of strong pile-up between the pulses from α-particles and FF, a special pile-up rejection system [16] was applied leaving only ~25% of all collected fission events for the analysis. The angular cone of accepted events was restricted to $\cos(\theta) \geq 0.3$ to avoid events with too much degraded kinetic energies.

For 27 incident neutron kinetic energy intervals from 0.008eV up to 1eV, 22 single isolated resonances with $J^\pi=1^+$ and 9 resonances with $J^\pi=0^+$ from 1eV up to 200eV, as well as for 6 intervals between the resonances, two-dimensional $Y_{L,H}$(A,KE) distributions for light (L) and heavy (H) fragments were obtained for the first time. Because primary Y(A,TKE)-distributions, after applying all the corrections, should be symmetrical with respect to mass A=120, only heavy fragment (HF) Y(A,TKE)-distributions were used in the further analysis, particularly when a model was fitted to them.

The calculated ^{239}Pu(n_{th},f) FF $\langle A \rangle_{th}$ and $\langle TKE \rangle_{th}$ and their standard deviations were in agreement with the available literature data in the limits of their experimental uncertainties [16, 20, 21-25].

^{239}Pu(n_{th},f) reaction data, obtained at 100Hz, served as a reference for the TOF-spectra calibration and for comparison to the $J^\pi=1^+$ and 0^+ resonance FF mass-energy distributions. One should keep in mind that to the thermal neutron induced FF yield contribute a broad resonance at $E_n<0$ with $J^\pi=0^+$ [26] (~63%) and resonances at $E_n>0$ (mainly $J^\pi=1^+$ resonance at $E_n<0.296$eV) (~37%) [27, 28].

Comparison of fission fragment mass yields

In order to reveal possible deviation of the experimentally obtained resonance neutron FF mass-yields $Y_{res}(A)$ from the thermal neutron induced fission mass-yields $Y_{th}(A)$, the differences $\Delta Y_{res}(A)=Y_{res}(A)-Y_{th}(A)$ and ratios $R_{res}(A)=Y_{ires}(A)/Y_{th}(A)$ between them were calculated.

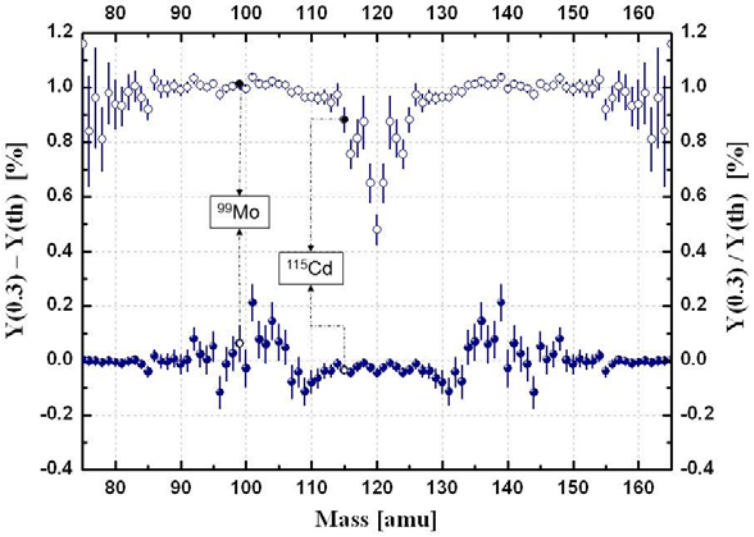

Figure 1. *Y(0.3) mass yields relative to thermal Y(th) ones.*

The results for 0.296eV (in short 0.3eV) 1^+ resonance are shown in Figure 1, the ratio at the top of the difference. There is a pattern structure seen in the asymmetric part relative to the $Y_{th}(A)$ distribution. A definite decrease in the symmetric yield for the 0.296eV resonance compared to thermal is visible, which reaches about 30%. In an early radiochemical experiment [29] the ratio of the yield of ^{99}Mo to that of ^{115}Cd from the 0.296eV resonance neutron induced fission $R(99/115)^{0.3eV}$ was found to be 3 times larger than that from fission with thermal neutrons, $R(99/115)_{th}$. The value $R(99/115)^{0.3eV}{}_{th}$= 3.00±0.28 from Ref. [29] is ~2.5 times higher than the value of $R(99/115)^{0.3eV}{}_{th}$=1.15±0.06, which can be deduced from Figure 1. This significant difference is due, probably, to the different experimental techniques which have been adopted.

A similar pattern as observed in Figure 1 is seen in the difference between the yield from all $J^{\pi}=1^+$ resonances $Y_{1+}(A)$ relative to $Y_{th}(A)$. Here $R(99/115)^{1+}{}_{th}$=1.19±0.07, which is of the same order of magnitude as that for the 0.296eV resonance, which can be expected, since this resonance has the same $J^{\pi}=1$.

The fluctuations of the ratio and the difference between the mass yield $Y_0{}^+(A)$ from the sum of all resonances with $J^{\pi}=0^+$, compared to thermal neutron FF yield $Y_{th}(A)$, are small and here $R(99/115)^{0+}{}_{th}$=1.00±0.11 (it can be coincidence!). It can be explained if the assumption of the authors of Ref. [30], that ^{239}Pu(n_{th},f) reaction is characterized as following the $(J^{\pi},K)=(0^+,0)$ state at the saddle point in the limit of FF mass formation, is correct.

The ratio and the difference between the mass-yields from the resonances of both spin groups $J^{\pi}=1^+$ and 0^+ show similar patterns in mass-yield difference, as those in Figure 1, but here the fluctuations of the individual mass-yields are stronger.

Because of $R(99/115)^{0+}{}_{th}$=1.00±0.11, one can expect the mass-yield ratio $R(99/115)^{1+}{}_{0}{}^{+}$ =1.19±0.11 not to differ from that of $R(99/115)^{1+}{}_{th}$ in their experimental uncertainty limits.

The resonances from both spin groups are forming the FF mass-yield distributions at the neutron energy ranges between them, $Y_{ir}(A)$. The thermal neutron induced FF mass-distribution originate, also from mixed 1^+ and 0^+ states, so, significant differences between $Y_{ir}(A)$ and $Y_{th}(A)$ were neither expected nor found.

The thermal mass distribution peak-to-valley (P/V) value has been determined to be $(P/V)_{th}$ = 76 ± 4. It is less than the value of $(P/V)_{th}$ = 114 ± 2, reported in [21]. The difference is coming from different characteristics of the sample and experimental setup used, and, probably, from not fully suppressed pile-up between the FF and α pulses. The relative value of the 0.296eV resonance $(P/V)_{0.3}$ to thermal was found to be $(P/V)_{0.3}/(P/V)_{th}$=1.74 ± 0.11. Despite of the relatively large errors bars, P/V-ratio changes, as was suggested by Wheeler [31], in the case of resonance neutron induced fission of ^{239}Pu, fluctuate up to a factor of 2-3 for certain resonances. Such a behavior is completely different from that of the fast neutron induced fission, where the P/V-value and <TKE> decrease with increasing E_n.

Variation of fission fragment <TKE> with incident neutron kinetic energy

The energy interval below 1eV was divided into 27 E_n-bins (ΔE_n). Relative to $<TKE>_{th}$, the <TKE> in the intervals was increasing towards the 0.296eV resonance. A similar increase in <TKE> was found by Walsh *et al.* [3].

From the obtained $^{exp}<TKE>_{th}$ = 177.83 ± 0.02MeV and $^{exp}<TKE>_{0.3eV}$ = 177.96 ± 0.01MeV, the difference between the experimental <TKE> of the FF from thermal and 0.296eV resonance neutron induced fission was found to be $\Delta^{exp}<TKE>_{0.3eV-th}$ =130 ± 22keV. This value is of the same order of magnitude as the measure value of $\Delta^{exp}<TKE>_{0.3eV-0.03eV}$ = 185 ± 75keV [3] and the calculated value of $\Delta^{cal}<TKE>_{0.3eV-th}$ = 160 ± 80 keV [32].

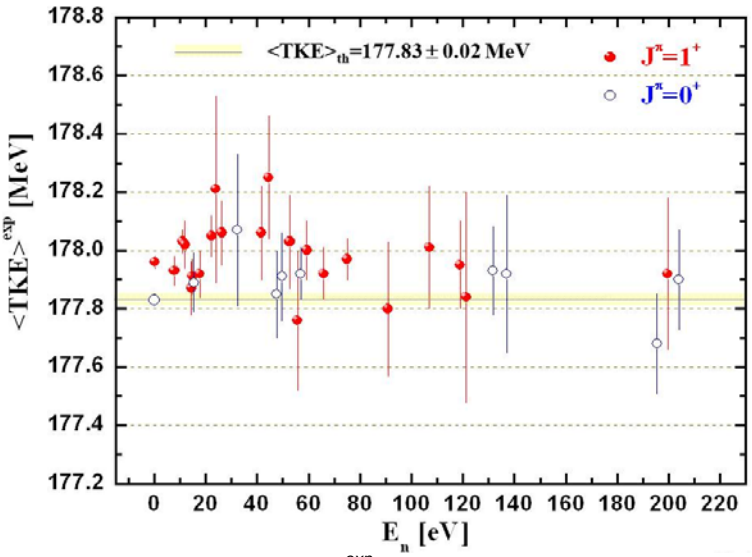

Figure 2. *Variation of <TKE>^{exp} at neutron resonance energies.*

One can see, from Figure 2, that the fluctuations of FF <TKE> for $J^{\pi}=1^+$ resonances are stronger around the E_n~15eV and 40eV resonance clusters. For $J^{\pi}=0^+$ resonances the variation of <TKE> is around the thermal value $<TKE>_{th}$ = 177.83 ± 0.02MeV and in the range of their experimental uncertainties. This behavior of <TKE> is similar to the one observed in the resonance neutron-induced fission of ^{235}U [4] at E_n ~15, 35, 55eV, etc., but less pronounced.

The difference $\Delta<<TKE>>_{1-0}$ between $<TKE>_{1+}$ and $<TKE>_{0+}$ for different resonance intervals were found to be $\Delta<<TKE>>_{1-0}$ (E_n =7-85eV) = 78 ± 27keV and $\Delta<<TKE>>_{1-0}$ (E_n =7-200eV) = 68 ± 54keV. These values are of the same magnitude as the difference $\Delta<<TKE>>_{1-0}$ (E_n =7-85eV) = 50 ± 90keV of Ref. [14]. The maximum value of the difference $<TKE>_{res}-<TKE>_{th}$ is of the order of ~300-400keV, which is of the same order of magnitude as for resonance neutron induced fission of ^{235}U. On the other side, it is only about 30-40% of the ($E_{1+}^*-E_{0+}^*$) ~ 1.25MeV, available at the 1st saddle point of the CN. This means [3] that either ^{240}Pu is a quite viscous system or somewhere along the fission path some mixing between $K^{\pi}=0^+$ and $K^{\pi}=1^+$ fission channels takes place.

Influence of the modes of fission

A quantitative description of the fission process became possible in the frame of the theoretical approach of Brosa et al. [6], combining the multi-modal fission [33] with the random neck-rupture (MM-RNR) model [34].

Because ^{239}Pu(n,f) pre-neutron Y(A,TKE)-distributions and their projections Y(A) and Y(TKE) are near identical for the light and heavy fragment peaks, the model was fitted only to the heavy fragment Y(A,TKE)-distributions. The three most important modes were considered - two asymmetric (standard I-S1, standard II-S2) and one symmetric (super-long, SL). Plots of the model parameters as a function of the resonance energy E_n showed that their values from resonance-to-resonance fluctuate slightly and do not differ very much from those of the thermal neutron Y(A,TKE)-distribution. That is why all the distributions were fitted once more, but with all the parameters, except the fission yields, fixed to the thermal values.

Not only Y(A) and TKE(A) distributions were compared, but also higher moments, namely, the dispersion σ(TKE) and the skewness (dissymmetry) of TKE distributions as a function of A.

The model $<TKE>_{fit}(E_n)$ values show fluctuations similar to those of the experimental ones $<TKE>_{exp}(E_n)$. From the two main asymmetric mode areas (probabilities), the "absolute" branching ratio $R_{res}=(W_1/W_2)_{res}$ as a function of resonance energy was obtained. The R-values of all the measured resonances relative to the thermal $R_{th}=(W_1/W_2)_{th}$ branching ratio show fluctuation similar to those of $<TKE>_{fit}(E_n)$. Both, R and <TKE>-fluctuations, amount to about ~10% with some kind of bump-like structure at E_n~30-40eV like in Figure 2.

The level of dependence between the obtained FF mass-energy characteristics was determined by calculating Pearson's product moment coefficient |r|.

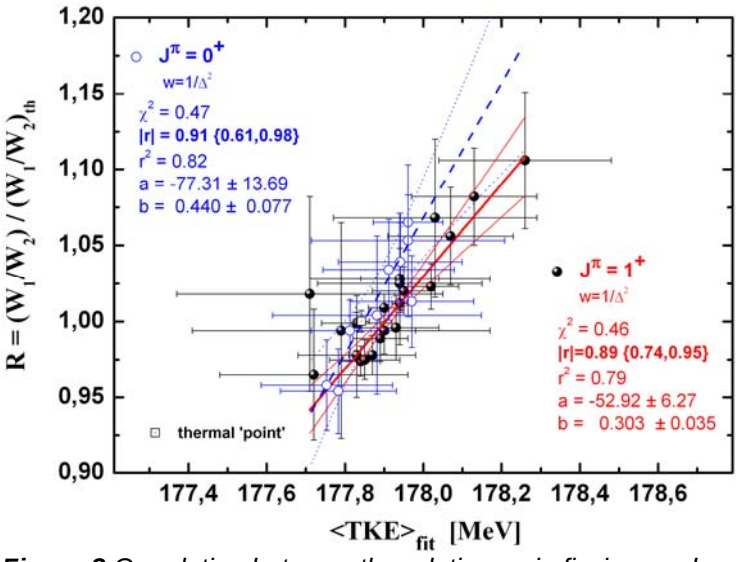

Figure 3.*Correlation between the relative main fission mode branching ratios and FF <TKE>$_{fit}$.*

From the similarity between the changes in <TKE> and R from resonance-to-resonance, one can expect that changes in R will invoke corresponding changes in the <TKE>. The correlation plot is given in Figure 3. The correlation coefficient is high and the correlation is significant. It means that ~70-80% of the fluctuations in <TKE> are due to fluctuations in the branching ratio R. A change in the relative branching ratio dR~10-15% leads to a change in the mean total kinetic energy d<TKE>~0.4-0.5MeV.

Influence of the (n,γf)-reaction

Predicted by Lynn [9] the (n,γf)-reaction, as a possible concurrent of the direct fission, was found in the 1^+ resonance neutron induced fission of ^{239}Pu and investigated in detail [10-12]. When it occurs it will cool-down the CN and as a result the mean prompt neutron emission from FF <ν_p> decreases while the γ-ray yield and its multiplicity should, not so remarkable, increases.

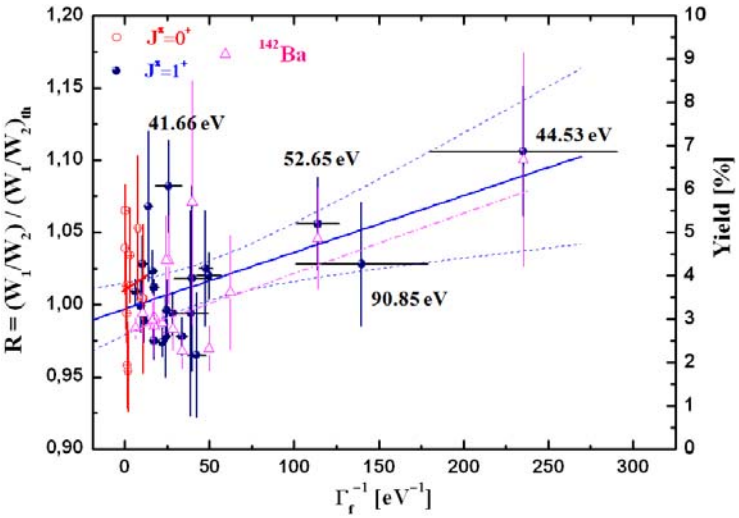

Figure 4.*Correlation between the relative main fission mode branching ratios and resonance reverse fission widths.*

The existence of a strong linear dependence of the <ν_p> on $1/\Gamma_f$ is used as a 'test' for the possible existing of the (n, γf)-reaction. An anti-correlation between these two quantities was found to be moderate and significant. The correlations between (<TKE> and $1/\Gamma_f$) and (P/V-ratio and $1/\Gamma_f$) were found to be moderate, but insignificant, because of the small number of resonances with relatively small fission widths in this neutron energy region. The same holds for the correlation between the branching ratios R for resonances with $J^\pi=1^+$ and $1/\Gamma_f$. It can be seen in Figure 4, where the relative branching ratio R is plotted together with the independent yields of ^{142}Ba [13, 35]. According the authors of these papers such a behaviour can results from the occurrence of the (n,γf)-reaction. For resonances with $J^\pi=0^+$ there no significant correlation was observed.

Conclusions

In comparison to the resonance neutron induced fission of ^{235}U [4], less pronounced fluctuations in <A> and <TKE> distributions for the ^{239}Pu(n,f) reaction were observed. A possible explanation could be, that in the case of resonance neutron induced fission of ^{239}Pu, for each spin state J^{π} of the ^{240}Pu CN, only one possible K-channel above the outer barrier is open, whereas for fission of the ^{236}U CN, a mixture of two to three K-channels can take place [36]. If the quantum number K is considered to be a "good" quantum number, i.e. if it is conserved from second saddle to scission, the scission configuration should have the same K. This way, the fission fragment properties, for a given fission mode and K quantum number should be "fixed". Hence, the superposition of different transition states with different K-quantum number and thus, different fission fragment property distributions can result in fluctuations from resonance-to-resonance. In case of ^{240}Pu CN, with only one single transition state, such fluctuations should be absent or be less pronounced, as it was observed.

The influence of Bohr's channel spin ($J^{\pi}=1^{+}$ and $J^{\pi}=0^{+}$) on <TKE> was found to be small: Δ<TKE> = $<TKE>_{1+} - <TKE>_{0+}$ = 0.068 $\pm$ 0.054MeV, which is of the same order of magnitude as given in Ref. [14].

The correlation of <TKE> and R with $1/\Gamma_f$ and anti-correlation with $<\nu_p>$ were found to be moderate or low, but insignificant, because they are based on 2-3 resonances with relatively small fission widths and large experimental uncertainties.

By the occurrence of an (n,γf)-reaction in the 1st minimum of the fission barrier one can explain the relatively small fluctuations in the primary FF characteristics from resonances with $J^{\pi}=1^{+}$ and absence of pronounced fluctuations for $J^{\pi}=0^{+}$.

The existence of a β-vibration state [30] at ~3MeV below the outer saddle, as well as the decaying of the shape isomer through a ($J^{\pi}K=0^{+}0$) fission channel, pick-up the question about the existence of the (n, γf)-reaction in the IInd well of the double-humped fission barrier, too. Such a hypothesis can be indirectly supported by the existence of two energy groups of γ-rays accompanying the resonance neutron induced fission of ^{239}Pu [10,11].

Despite of not so significant correlations, the understanding of the fluctuations in the FF characteristics from the resonance neutron induced fission of ^{239}Pu are of great importance for evaluations, especially those of the prompt neutron multiplicity $<\nu_p>$ and/or the delayed neutron (DN) yields [37]. The latter is supposed to fluctuate from resonance-to-resonance, because the precursors of the DN are lying in the range where some interplay between fission modes can take place.

Acknowledgements

One of us (I.R.) would like to express his gratitude to the European Commission for the fellowship and the IRMM for the excellent working conditions and the pleasant working atmosphere.

References

[1] A. Bohr, Proc. Int. Conf. on Peaceful Use of Atomic Energy, Geneva, 1955 (UN, New York, 1956), Vol. II, p.151.
[2] J.J. Griffin, Proc. Symp. on Phys. and Chem. of Fission, Salzburg (IAEA, Vienna, 1965), Vol.I, p.23.
[3] R.L. Walsh, and J. W. Boldeman, Nucl. Phys. **A451** (1986) 113; R.L. Walsh, J.W. Boldeman and M.E. Elcombe, Proc. IV IAEA Symp. on Physics and Chemistry of Fission, Jülich, 1979, vol. II, (1980) 129 and ensuing discussion.
[4] F.-J. Hambsch, H.-H. Knitter, C. Budtz-Jørgensen, J.P. Theobald, Nucl. Phys. **A491** (1989) 56.
[5] Sh.S. Zeinalov, M. Florek, W.I. Furman, V.A. Kriatchkov, Yu.S. Zamyatnin, Proc. VII Int. Seminar on Interaction of Neutrons with Nuclei (ISINN-7), Dubna, Russia, May 25-28, (1999) 258.
[6] U. Brosa, S. Grossmann, A. Müller, Phys. Reports **197** (1990) 167.
[7] J. Fréhaut, D. Shackleton, in Proc.III IAEA Symp. on Physics and Chemistry of Fission, vol. II, (1974) 201.
[8] E. Fort, J. Fréhaut, H. Tellier and P. Long, Nucl. Sci. Eng. **99** (1988) 375.
[9] Lynn J. E., Phys. Lett. **18** (1965) 31.
[10] O. Scherbakov, Sov. J. Part. Nucl. **21** (1990) 177.
[11] Trochon J., Etude des proprietes de la fission dans les resonances de ^{239}Pu induites par neutrons lents: *These de Doctorat*, Paris, 1978.

[12] Trochon J., La reaction (n,γf) dans les resonances induites par neutrons lents dans ^{239}Pu, ^{235}U et ^{241}Pu, Proc. Symp. on Physics and Chemistry of Fission", Jülich, 14-18 May 1979, IAEA, Vienna, (1980) 87.
[13] A.A. Bogdzel, N.A. Gundorin, U. Gohs, A. Duka-Zolyomi, J. Kliman, V. Polgorski, A.B. Popov, Dao Anh Minh, Proc. Int. Conf. Nucl. Data for Sci. Tech., Jülich, 13-17 May, (1991) 150.
[14] C.M.C.Wagemans, G. Wegener-Penning, H. Weigmann, R. Barthelemy, Proc. IV IAEA Symp. on Physics and Chemistry of Fission, vol. II, (1980) 143.
[15] L. Demattè, F.-J. Hambsch, H. Bax in: C. Wagemans , O. Serôt, P. D'Hondt(Eds), Seminar on Fission "Pont D'Oye IV", October 6-9, 1999, Habay-la-Neuve. World Scientific, Singapore, (2000)135.
[16] L. Demattè, F.-J. Hambsch, H. Bax, Nucl. Instr. Meth. A480 (2002) 706.
[17] F.-J. Hambsch, L. Demattè, H. Bax, and I. Ruskov, J. Nucl. Sci. Technol. **2** (2002) 307.
[18] C. Budtz-Jørgensen, H.-H. Knitter, Ch. Straede, F.-J. Hambsch and R. Vogt, Nucl. Instr. Meth. A258 (1987) 209.
[19] F.-J. Hambsch, J. van Aarle, R. Vogt, Nucl. Instr. Meth. A361 (1995) 257.
[20] H. Schmitt, J. Neiler, F. Walter, Phys. Rev. 141 (1966) 1146.
[21] L. Demattè, C. Wagemans, R. Barthélémy, P. D'hondt, A. Deruytter, Nucl. Phys. A617 (1997) 331.
[22] P. Schillebeeckx, C. Wagemans, A. J. Deruytter, R. Barthélémy, Nucl. Phys. A545 (1992) 623.
[23] C.Wagemans, E. Allaert, A. Deruytter, R. Barthélémy, P. Schillebeeckx, Phys. Rev. C30 (1984) 218.
[24] G. Simon, Ph.D. Thesis, Orsay, Nr. 3593 (1990).
[25] P. Geltenbort, F. Gönnenwein, A. Oed, Proc. Int. Conf. on nuclear data for basic and applied science, Santa Fé, USA (Gordon and Breach, New York, 1986), vol. I, p. 393.
[26] E. Vogt, Phys. Rev. 118 (1960) 724.
[27] H. Derrien, G. de Saussure, and R.B. Perez, Nucl. Sci. Eng. 106 (1990) 434; H. Derrien, J. Nucl. Sci. Technol. 30 (1993) 845 ; C.W. Reich and M.S. Moore, Phys. Rev. 111 (1958) 929.
[28] S.F. Mughabghab and D.I. Garber, BNL 325, 3rd ed., vol. I, Resonance parameters (1973).
[29] R.B. Regier, W.H. Burgus, R.L. Tromp, and B.H. Soronsen, Phys. Rev. 119 (1960) 2017.
[30] K. Nishio, H. Ikezoe, Y. Nagame, S. Mitsuoka, I. Nishinaka, L. Duan, K. Satou, S.Goto, M. Asai, H. Haba, K. Tsukada, N. Shinohara, S. Ichikawa, and T. Ohsawa, Phys. Rev. C67 (2003) 014604-1.
[31] J.A . Wheeler, Physica 22 (1956) 1103.
[32] U. Gohs, Proc. Int. Workshop on Dynamical Aspects of Nuclear Fission, Smolenice castle, ČSSR, (1993).
[33] A. Turkevich, and J. Niday, Phys. Rev. 84 (1951) 52.
[34] U. Brosa, H.-H. Knitter, Proc. of the XVIIIth Int. Symp. on Nuclear Physics, Physics and Chemistry of Fission, Gaussig, GDR, 1988, eds. H. Märten and D. Seeliger, ZfK-732, 145 (1988).
[35] V. Polhorský, J. Kliman, J. Ktrištiak, A.A. Bogdzel, N.A. Gundorin, A.B. Popov, U. Gohs, Proc. Int. Workshop on Dynamical Aspects of Nuclear Fission", Smolenice castle, ČSSR, (1993) 258.
[36] W. Furman, Proc. FJ/OH Spring Session 99, May 17-21, 1999, Geel, Belgium, 124.
[37] T. Ohsawa, and F.-J. Hambsch, Proc. Int. Conf. on New Frontiers of Nuclear Technology (PHYSOR2002), Seoul Korea, Oct. 7-10, 2002.

Fission fragment total kinetic energy calculation for prompt neutron emission evaluation purposes

V. Manea, A. Tudora

University of Bucharest, Faculty of Physics, Bucharest-Magurele, POB MG-11, R-76900, Romania
vladimir.manea@yahoo.com

Abstract: An approach for the calculation of the fission fragment total kinetic energy TKE(A) is presented, taking into consideration the fragment deformation and the existence of a neck between the two fragments in the pre-scission configuration. The approach offers results in good agreement with the experimental data for multiple fissioning systems, thus representing a solution for nuclear data evaluation purposes in the case of fissioning systems without experimental fission fragment distributions. Applications in the frame of the Point by Point model of prompt neutron emission are presented.

Introduction

The fission fragment total kinetic energy as a function of the fragment mass, TKE(A), is an important input parameter in prompt neutron emission models, such as the Point by Point (PbP) model [1-3]. The exclusive use of experimental TKE(A) input data limits the prompt neutron emission calculations to fissioning systems with experimental fission fragment distributions.

In this work we present a simple method for the TKE(A) calculation, which can be used for nuclear data evaluation purposes in the case of fissioning systems without experimental TKE(A) distributions. TKE is calculated as the electrostatic repulsion energy of two fission pre-fragments, joined by a neck in the pre-scission configuration. The method takes into consideration the deformation of the pre-fragments, as well as the fact that a part of the nucleons (and of the charge) are contained in the pre-scission neck, being incorporated in the two nascent fission fragments after the moment of scission.

Calculations of TKE(A) have been recently reported in the literature by Vogt et al. [4], using a simple Coulomb potential and taking into consideration the fragment deformation, but with a distance between the fragments obtained by fitting the experimental TKE(A) data, thus lacking the required prediction power for fissioning systems without experimental fission fragment distributions.

In the present approach, the length of the neck joining the two pre-fragments is not a freely adjustable parameter. With a simple independent parameterization of the neck length, the calculated TKE(A) values describe very well the experimental data of multiple fissioning systems, such as ^{235}U(n_{th},f), ^{239}Pu(n_{th},f) and ^{237}Np(n,f). Corrections to the simple neck length parameterization, aiming to improve the agreement with the experimental data in the symmetric fission mass region, can be brought by taking into account the multi-modal fission concept, according to Brosa et al. [5] (see also [6-9]).

The results of the presented TKE(A) calculation approach are used as input parameters for the PbP model of prompt neutron emission. Some sensitive output quantities of the model (such as the prompt neutron spectrum, multiplicity and sawtooth ν(A) distribution) are obtained close to the ones calculated using experimental TKE(A) values.

Description of the TKE(A) calculation approach

In the present approach, TKE(A) is calculated as the energy of electrostatic repulsion between the two fission fragments (FF) in the pre-scission configuration. In this configuration, the fissioning nucleus consists of two deformed pre-fragments, joined by a neck, containing a part of the nucleons which will be later incorporated in the two nascent FF. Considering that the axial symmetry of the fissioning system is preserved along the scission path, we can take the two pre-fragments as rotation ellipsoids, described by:

$$R(\theta,\varphi) = r_0 A^{1/3}\,(1+\beta_2 Y_{2,0}(\theta,\varphi)) = R_0\,(1+c\beta_2\,P_2(\cos\theta))\,, \qquad (1)$$

with the reduced radius obtained from volume conservation and $c = \sqrt{5/4\pi}$.

The fraction of the FF nucleons (and of the charge) contained in the pre-scission neck can be calculated as the ratio between the neck and FF volumes:

$$f_{L,H} = \frac{V_{L,H}^{neck}}{V_{L,H}^{frag}}. \tag{2}$$

In Fig. 1 is presented the pre-scission configuration, with the two parts of the neck taken, for simplicity, with spherical shape. The dashed lines join the elements that will form together the two FF after the moment of scission.

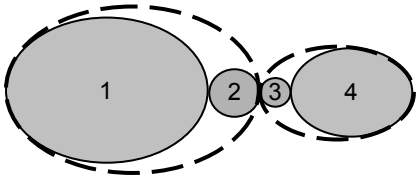

Figure 1. *Schematic representation of the considered pre-scission configuration*

In this configuration, TKE is calculated as the sum of four electrostatic interaction terms: a term of interaction between the two pre-scission deformed fragments (1 and 4), two terms of interaction between one pre-fragment and the part of the neck connected to the other pre-fragment (1 and 3 and, respectively, 4 and 2) and a term of interaction between the two parts of the neck (2 and 3):

$$TKE = \frac{e^2}{4\pi\varepsilon_0}\sum Z_i Z_j \frac{1}{V_i V_j}\int_{V_i}\int_{V_j}\frac{d^3\mathbf{r}_i d^3\mathbf{r}_j}{l(\mathbf{r}_i,\mathbf{r}_j;D_{ij})},\ i=1,2,\ j=3,4\,, \tag{3}$$

where V_i and V_j are the volumes over which the 6-D integral is calculated and $l(\mathbf{r}_i,\mathbf{r}_j;D_{ij})$ is the distance between two points of coordinates $\mathbf{r}_i$ and $\mathbf{r}_j$ (with respect to the centres of the two volumes, separated by the distance D_{ij}).
The integral (divided by the volume product) gives the departure from the pure Coulombian interaction and in the case *ij* = 2,3 is equal to 1. For the other three cases it can be calculated numerically. The charges *Z* are calculated taking into consideration the fractions of nucleons contained in the two parts of the neck.

The radii of the two neck spheres are taken proportional to the FF major semi-axis $a_{H,L}^0$:

$$R_{L,H}^{neck} = \frac{1}{2}x a_{L,H}^0, \quad x = \frac{L}{a_H^0 + a_L^0}\,, \tag{4}$$

where *L* is the neck length and the superscript 0 indicates that the parameters refer to the FF (and not to the corresponding pre-fragments). Substituted in Eq (2), this leads to:

$$f_{L,H} = \frac{x^3}{8}\left(\frac{1+c\beta_{L,H}^0}{1-\frac{c}{2}\beta_{L,H}^0}\right)^2. \tag{5}$$

Parameter calculation and simplified approach

For a certain fissioning system, the FF range is taken as in the Point by Point approach (see [1] and the references therein). The entire mass pair range is considered with a step of one mass unit. For each fragment mass pair {A_L, A_H}, two or four charge numbers *Z* are taken as the nearest integer values above and below the most probable charge obtained from the "unchanged charge distribution" Z_{UCD} corrected with the possible charge polarization ΔZ. TKE(A) is obtained by averaging the two or four values over the charge distribution. Because the charge distribution is a narrow Gaussian [10], the choice of four *Z* values doesn't significantly change the result.

The β_2 deformation parameters of Möller, Nix et al. [11, 12] were used for the calculation. Well known, the FF are generally excited nuclei, while the parameters of [11, 12] refer to the ground state deformations. The deformation data for excited nuclei are however scarce and refer to much lower excitation energies than those of the fission fragments, so we will consider the ground state deformation parameters as good estimators for the general trend of the FF deformations. This can be illustrated by applying Eq. (5) for the calculation of TKE(A) in the case of the ^{235}U(n$_{th}$,f) fissioning system, with the β_2 values of [11, 12] and a neck length taken for simplicity as the average of the equivalent spherical radii of the FF. The ^{235}U(n$_{th}$,f) system was chosen for the first calculation because of the available experimental charge polarization data (taken from [10]).
The results are plotted in Fig. 2 with star symbols, in comparison with the available experimental data from the EXFOR library [13]. As it can be seen, the results are in overall good agreement with the experimental TKE(A) data, but with a significant overestimation in the mass region corresponding to symmetric fission. This can be explained by the simplicity of the neck length parameterization, which does not account for the more complicated neck length variation with the FF mass. This variation can be put into connection with the Multi-Modal Random Neck Rupture model of Brosa et al. [5-9] which predicts a greater neck length in the symmetric fission region, in which the SL (super long) fission mode predominates. Consequently, the neck length was increased in the symmetric fission region, according to [5-9].

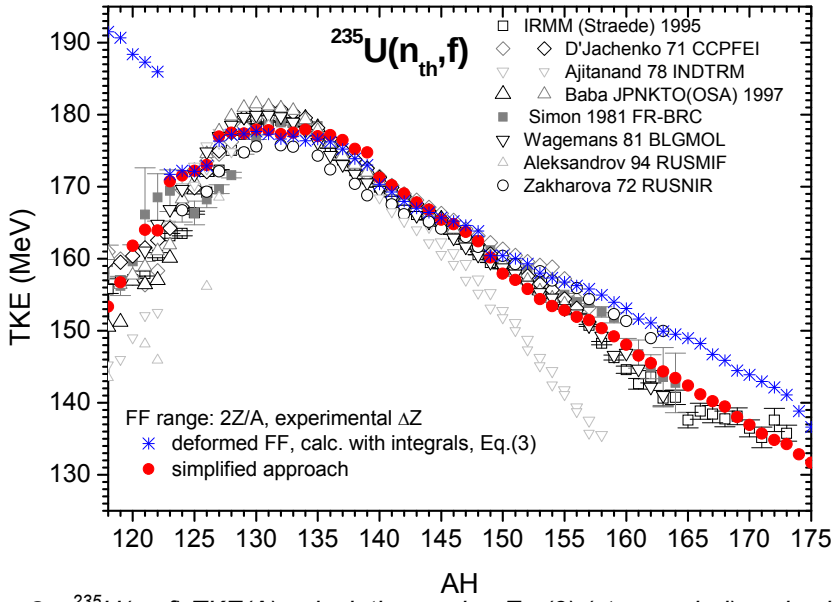

Figure 2. *^{235}U(n$_{th}$,f) TKE(A) calculations using Eq.(3) (star symbol) and using the simplified approach (full circle), in comparison with experimental data taken from EXFOR*

Also, for reducing the amount of calculation, an equivalent spherical shape can be considered for the pre-scission HF, with the radius equal to the pre-fragment semiaxis a_H, concomitantly with an equivalent spherical pre-scission LF shape, with the radius obtained from volume conservation. This reduces the four terms of Eq. (3) to pure Coulombian terms:

$$TKE = \frac{e^2}{4\pi\varepsilon}\left(\frac{(1-f_H)Z_H\,(1-f_L)Z_L}{a_H + R_L^{eqv} + L} + \frac{f_L Z_L (1-f_H)Z_H}{a_H + 2R_{neck}^H + R_{neck}^L} + \right.$$

$$\left. + \frac{f_H Z_H (1-f_L)Z_L}{R_L^{eqv} + 2R_{neck}^L + R_{neck}^H} + \frac{f_L Z_L\, f_H Z_H}{R_{neck}^L + R_{neck}^H}\right), \qquad (6)$$

where we have explicitly mentioned this time the manner in which the charge of each body in Fig. 1 is calculated. The results of the simplified approach are plotted in Fig. 2 with full circles. The improved agreement with the experimental data in the far asymmetric region suggests that the simplified pre-scission scheme can emulate better the neck length variation with the FF mass.

Results of the simplified approach

In the following, we give few examples of the TKE(A) approach results in comparison with the available experimental TKE(A) data. In Fig. 3, the calculated TKE(A) values are presented in comparison with the experimental data [9] for $^{237}Np(n,f)$. The FF range was chosen as in the case of ^{235}U, A_H from 118 to 168, with 2*Z* values per *A*, but without considering any charge polarization. The calculated values are obtained in good agreement with the experimental data. It is worth mentioning that the experimental data do not exhibit a significant dependence of the TKE(A) values on the incident neutron kinetic energy. This supports the independence of the present approach for the TKE(A) calculation on the excitation energy of the fissioning system.
A similar calculation is presented in Fig. 4 for the case of $^{239}Pu(n_{th},f)$, with the FF range from 120 to 175, 2 *Z* values per *A* and no charge polarization. In this case, as in the previous ones, the calculated values are in good agreement with experimental data from the EXFOR library.

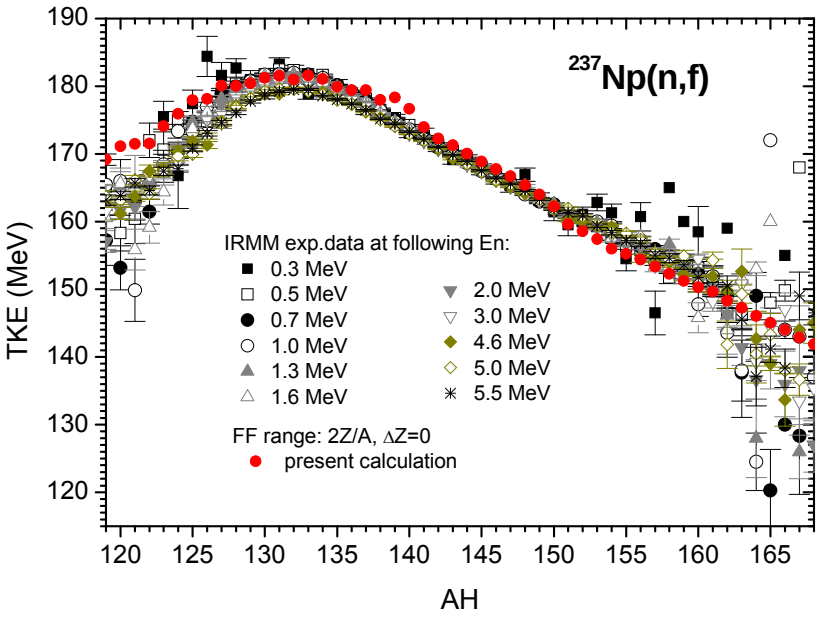

Figure 3. *$^{237}Np(n,f)$ TKE(A) calculation in comparison with experimental data of* [9]

The TKE(A) distribution, as input model parameter, plays an important role in the PbP model calculations of prompt neutron emission. In the following, we give two examples of PbP model calculations of prompt neutron emission quantities, each performed in two cases: a) by using experimental TKE(A) distributions and b) by using the present calculation results of TKE(A), the other input parameters and PbP features being kept the same.
The PbP calculation of the prompt neutron multiplicity sawtooth distribution, *ν(A)*, is presented in Fig. 5 for the case of $^{239}Pu(n_{th},f)$, in comparison with the available experimental data from the EXFOR library [14]. The result obtained using the experimental TKE(A) data of Wagemans [13] is plotted with full circles, while the result obtained using the present TKE(A) calculation is plotted with star symbol. As it can be seen, the two results are close to each other and in good agreement with the experimental data [14].
In Fig. 6 is presented the calculated prompt neutron emission spectrum for $^{239}Pu(n_{th},f)$, as ratio to the Maxwellian spectrum of temperature 1.42 MeV in comparison with the experimental data from EXFOR [14]. The dashed line represents the spectrum calculated using the experimental TKE(A) data of Wagemans [13], while the solid line represents the spectrum calculated using the TKE(A) values of the present approach.
As it can be seen in Fig. 6, the two spectra are close to each other and in very good agreement with the experimental data. The total average prompt neutron multiplicity values obtained in the two cases are also close to each other, as it can be seen in Fig. 6: the multiplicity obtained using the calculated TKE(A) differs with 3.2% from the one calculated

with the experimental TKE(A) of Wagemans [13] and with 3.3% versus the ENDF/B-VII evaluation [15].

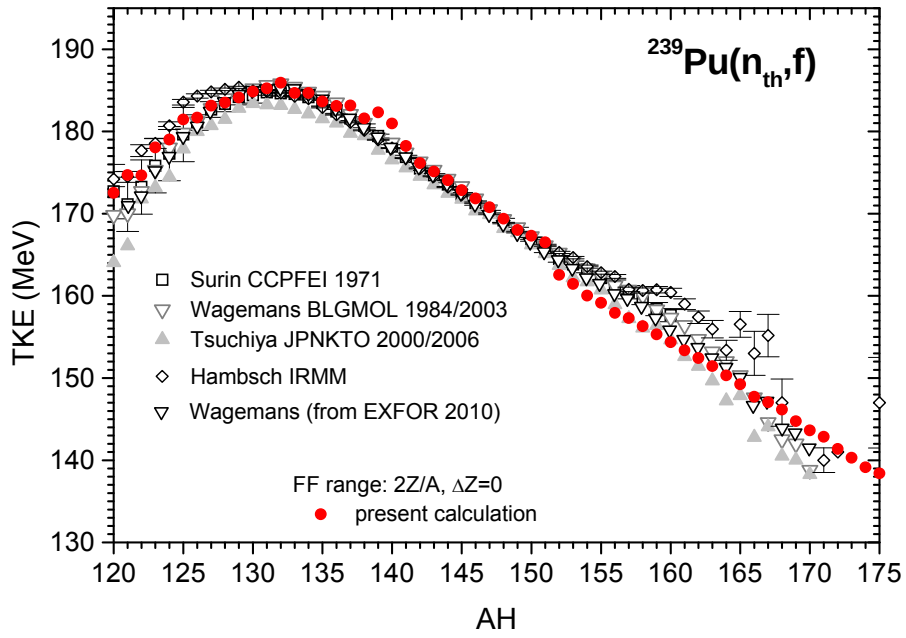

Figure 4. *^{239}Pu(n_{th},f) TKE(A) calculation (full circles) in comparison with experimental data taken from EXFOR (plotted with different black and gray symbols)*

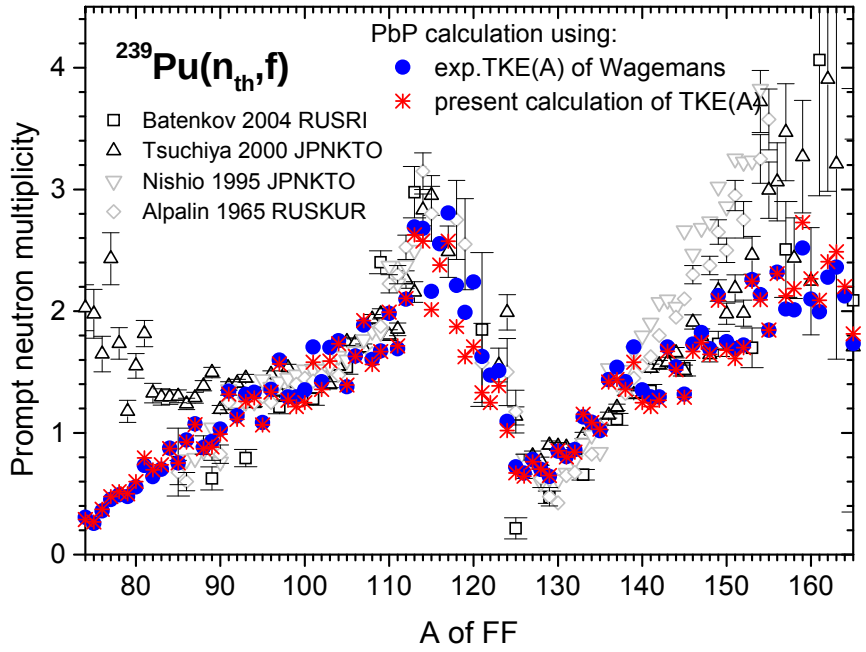

Figure 5. *^{239}Pu(n_{th},f) PbP calculation of the sawtooth ν(A) by using experimental TKE(A) (full circles) and calculated TKE(A) (star symbol) in comparison with experimental data from EXFOR*

Conclusions

In the present paper, a simple approach for the TKE(A) calculation was presented, giving results in very good agreement with the experimental TKE(A) data for multiple fissioning systems, only with minor adjustments of the neck length (according to the multi-modal fission concept).

Consequently, the presented approach can provide the values of the TKE(A) distribution for nuclear data evaluation purposes, in the case of fissioning systems without experimental fission fragment distributions. By means of this approach, the possibility of using the PbP model of prompt neutron emission is extended to such systems.

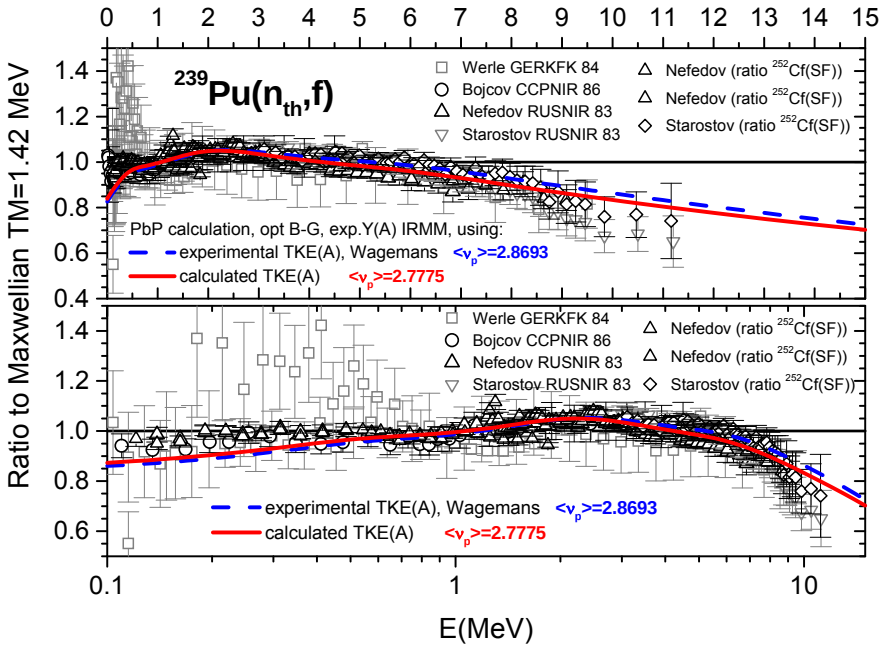

Figure 6. *PbP calculations of prompt neutron spectrum for $^{239}Pu(n_{th},f)$ as ratios to the Maxwellian with T_M=1.42 MeV, compared to experimental data from EXFOR: calculation using the experimental TKE(A) (dashed line) and using the present TKE(A) (solid line).*

References

[1] A. Tudora, Ann. Nucl. Energy 35, 1-10 (2008).
[2] A. Tudora, Ann. Nucl. Energy 37, 43-51 (2010).
[3] A. Tudora, F.-J. Hambsch, Ann. Nucl. Energy 37, 771-777 (2010).
[4] R. Vogt, J. Randrup, J. Pruet, W. Younes, Phys.Rev.C 80, 044611 (2009).
[5] U. Brosa, S. Grossmann, A. Muller, Phys. Rep. (Rev. Sect. of Phys. Lett.) 197, 167-262 (1990).
[6] P. Schillebeckx, C. Wagemans, A.J. Deruytter, R. Barthelemy, Nucl. Phys. A 545, 623-645 (1992).
[7] P. Siegler, F.-J. Hambsch, S. Oberstedt, J. P. Theobald, Nucl. Phys. A 594, 45-56 (1995).
[8] S. Oberstedt, F.-J. Hambsch, F. Vivès, Nucl. Phys. A 644, 289-305 (1998).
[9] F.-J. Hambsch, F. Vivès, P. Siegler, S. Oberstedt, Nucl. Phys. A 679, 3-24 (2000).
[10] C. Wagemans, The Nuclear Fission Process, CRC Press, Boca Raton, Chapter 8, p.392-423 (1991).
[11] RIPL2, 2006. T. Belgya, O. Bersillon, R. Capote, T. Fukahori, G. Zhigang, S. Goriely, M. Herman, A.V. Ignatiuk, S. Kailas, A. Koning, P. Oblozhinsky, V. Plujko, P. G. Young, Handbook for calculations of nuclear reaction data: Reference Input Parameter Library IAEA-TECDOC-1506/2006. Deformations. Electronic files available from http://www-nds.iaea.org/RIPL2
[12] RIPL1, 1998. Reference Input Parameter Library, IAEA, Handbook IAEA-TECDOC-1034. Electronic files: Segment 1 “Deformations”. Electronic files available from http://www-nds.iaea.org/RIPL1
[13] EXFOR Experimental Nuclear Reaction Data Base (2010). <http://www-nds.iaea.org/EXFOR>, targets 235U, 239Pu, reaction (n,f), quantity E.
[14] EXFOR Experimental Nuclear Reaction Data Base (2010). <http://www-nds.iaea.org/EXFOR>, target 239Pu, reaction (n, f), quantities MFQ and DE.
[15] Evaluated Nuclear Data Library ENDF/B-VII, file ZA94239, MF=1, MT=456, available at http://www-nds.iaea.org/ENDF.

Potential energy surfaces in 3-dimensional Langevin calculations

K. Mazurek[1,2], J.P. Wieleczko[1], P. N. Nadtochy[3], C. Schmitt[1]

1) Grand Accélérateur National d'Ions Lourds, CEA/DSM-CNRS/IN2P3, Caen, France
2) Institute of Nuclear Physics PAN, ul. Radzikowskiego 152, 31-342 Kraków, Poland
3) Omsk State University, Department of Theoretical Physics, Mira Prospect 55-A, RU-644077 Omsk, Russia

mazurek@ganil.fr

Abstract: In this work we use a 3-dimensional Langevin approach to explore the influence of the potential energy surface on the fission characteristics. Two macroscopic models were used: the Finite Range Liquid Drop Model (FRLDM) and the Lublin-Strasbourg Drop (LSD) model which reproduce correctly fission barriers on a large range of mass. While both models gives similar characteristics for fission of heavy and super heavy nuclei we observe spectacular differences in the charge distributions and the total kinetic energy spectra of the fragments produced in the fission of medium mass nuclei. This allows to define the experimental conditions to better constrain the potential energy surface used in the dynamical description of the fission phenomenon.

Method

The description of the dynamics of the fission process starts in the beginning of XX century and one of the first works formulating it mathematically was done by Kramers [1]. He treated this process like a Brownian motion in a potential well. The latter studies were based on the solution of the stochastic equation of the Fokker – Planck type. The introduction of the differential form of the stochastic equation of the Langevin type by Abe, Gregoire and Delagrange [2] was a great step forward toward to perform Monte Carlo simulations for the trajectory of the system along one collective coordinate. This approach was recently extended to three dimensions by few groups [3,4,5].
In this work we will use the state of art of such three-dimensional Langevin calculations [5] for investigating the influence of the potential energy surfaces on various observables in the fission process at finite excitation energy. The description of the nuclear shape is based on collective coordinates coming from the Funny-Hill parametrisation of the nuclear shape [6]. In cylindrical coordinates the surface of the nucleus is defined by the radial distance with respect to the surface:

$$\rho_s^2(z) = \begin{cases} (c^2 - z^2)(A_s + Bz^2/c^2 + \frac{\alpha z}{c}), & B \geq 0 \\ (c^2 - z^2)(A_s + \frac{\alpha z}{c})exp(Bzc^2), & B \leq 0 \end{cases}$$

z is the coordinate along the symmetry axis and B, A_s is determined by the Funny-Hill parameters $\{ c, h, \square \}$ as follows:

$$B = 2h + \frac{c-1}{2}$$
$$A_s = \begin{cases} c^{-3} - \frac{B}{5}, & B \geq 0; \\ -\frac{4}{3}\frac{B}{exp(Bc^3)+(1+\frac{1}{2Bc^3})\sqrt{-\pi Bc^3}erf(\sqrt{-Bc^3})}, & B < 0 \end{cases}$$

The parameter *c* corresponds to the elongation of the nucleus, h is the neck (mass asymmetry) parameter respectively. The collective coordinates used in the Langevin equations are chosen to be:

$$q_1 = c$$
$$q_2 = \frac{h+3/2}{\frac{5}{2c^3}+\frac{1-c}{4}+3/2}$$
$$q_3 = \begin{cases} \alpha/(A_s+B), & B \geq 0 \\ \alpha/A_s, & B < 0 \end{cases}$$

This collective parameters (q_1, q_2, q_3) compose the vector ***q*** which is used to solve the Langevin equations:

$$\frac{dq_i}{dt} = \mu_{ij} p_j,$$
$$\frac{dp_i}{dt} = -\frac{1}{2} p_j p_k \frac{\partial \mu_{jk}}{\partial q_i} - \frac{\partial F}{\partial q_i} - \gamma_{ij}\mu_{jk} p_k + \theta_{ij}\xi_j(t),$$

with ***p*** is the vector of conjugate momenta and $F(q_i) = V(q_i) + a(q_i)T^2$ is the Helmholtz free energy, *V(**q**)* corresponds to the potential energy for given coordinates, $m_{ij}(q_i)$ the tensor of inertia and γ_{ij} is the friction tensor. The white noise is taken like the normalized random variable ξ_j and the strength of the random force θ_{ij} is given by the relation $\sum \theta_{ik}\theta_{kj} = T\gamma_{ij}$, where the temperature of the "heat bath" *T* is determined by the Fermi – gas model formula $T = \sqrt{E_{intr}/a(q)}$.

The energy conservation law is the constrain during the random walk along the Langevin trajectory. The total excitation energy of the system is the sum of the kinetic energy of the collective degrees of freedom, the internal excitation energy (E_{intr}) and the potential energy for the given deformation (*V(**q**)).* In many works the potential energy surfaces had the form of a macroscopic model with finite range of the nuclear forces such as the Finite Range Liquid Drop Model (FRLDM) [7].

In the present work we would like to compare the results obtained within this framework with the recently developed macroscopic model called Lublin-Strasbourg Drop (LSD) [8]. The main difference between LSD and the previously used potential formulation is the implementation of the additional curvature term in the liquid drop formula. This term can play a major role in the region where the neck is pronounced (a nucleus for two different deformations can have identical surfaces but various curvatures and different potential energies) like at the scission stage or for intermediate mass region for which the shape at the saddle point looks like a scission configuration. To illustrate the differences between the Potential Energy Surfaces (PES) calculated with the FRLDM method and LSD model we perform calculations for a nucleus of intermediate mass (Barium) and superheavy one (Rutherfordium).

Potential energy surfaces

The potential energy is evaluated on the three-dimensional deformation space (q_1, q_2,, q_3) within the FRLDM and the LSD models.

The main differences between potential energy surfaces obtained with FRLDM and LSD models are visible in Fig. 1. - the FRLDM predicts much flat surfaces as compared to the LSD formula. For deformations close to a sphere the energy in both cases are similar but starting from the elongation q_1=2.0 the differences exceed 30 MeV.

Fig. 1 – 3 shows the maps of the energy for spins: 0, 40, 70 $\hbar$ in the (q_1, q_2,) plane for α=0.0, i. e. symmetric fission. In both cases of PES (comparing Fig.1 and Fig. 3) the energy landscape is not changing and the rotational energy does not depend strongly on the collective coordinates in the present range of deformations.

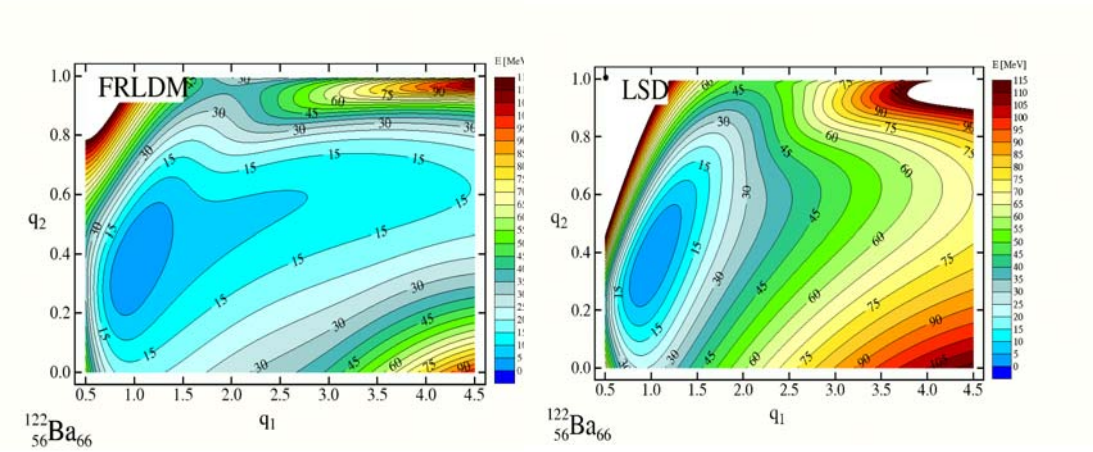

Figure 1. The potential energy surfaces for ^{122}Ba for the spin L=0 $\hbar$ in the (q_1, q_2) plane for α=0.0 as obtained with the Finite Range Liquid Drop Model (FRLDM) (left) and Lublin-Strasbourg Drop (LSD) model (right).

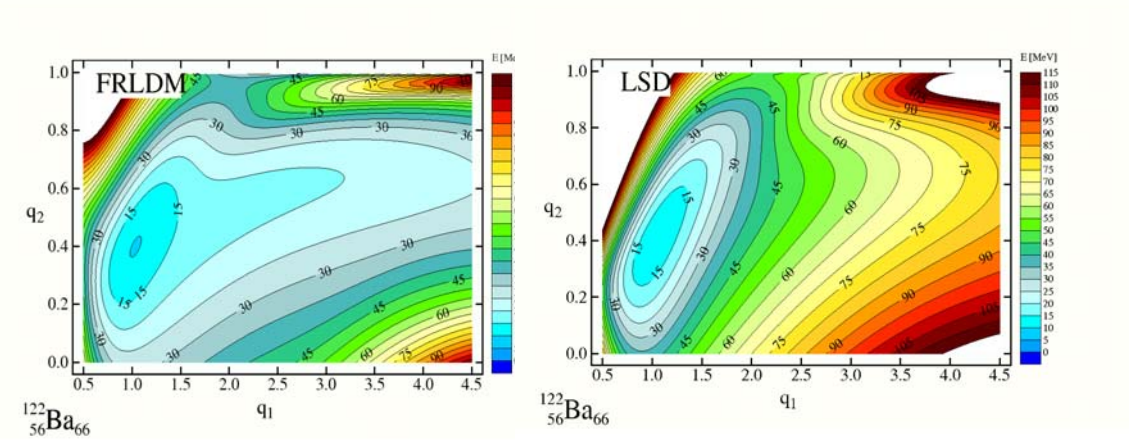

Figure 2. *Same as Fig. 1 for the spin L=40 $\hbar$.*

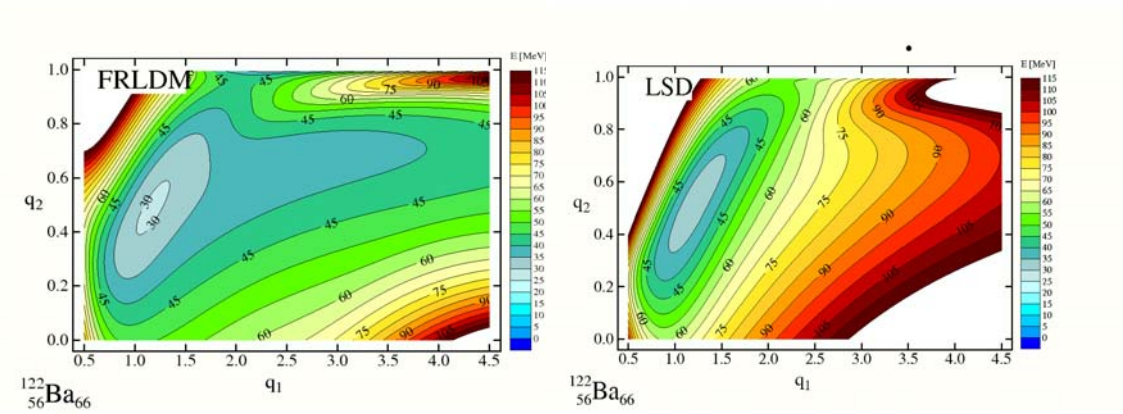

Figure 3. *Identical to Fig. 1 for the spin L=70 $\hbar$.*

Similar trends are observed in Fig. 4, 5 where the potential surfaces maps are shown in the (q_1,q_3) plane for spins L=0;70 $\hbar$. The potential energy is less sensitive for the changing q_3 parameter than for q_2 . Again the FRLDM landscape is seen to be more flat than the LSD one, in this plane as well.

The q_3 coordinate is connected directly with the Funny-Hill parameter α which is responsible for the mass asymmetry of the nucleus. Comparing both maps of Fig. 4 we can notice that for the FRLDM calculation the fission barrier (~20 MeV) is reached at q_3 = 0.6 while the barrier for the LSD model is still around 40 MeV . For the mass symmetric shapes barriers are higher then for asymmetric ones: ~35 MeV for the FRLDM and ~45 MeV for the LSD. In the case of fast rotating nucleus (Fig. 5) the landscape of potential energy is similar but the barriers are smaller.

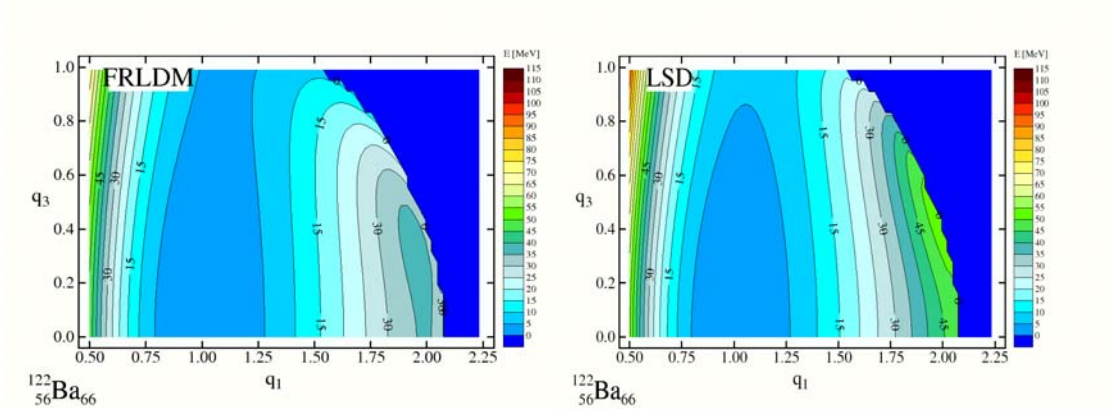

Figure 4. *The potential energy surfaces for ^{122}Ba for the spin L=0 ħ and the collective coordinates (q_1, q_3) with h=0.0 with the finite Range Liquid Drop Model (FRLDM) (left) and Lublin-Strasbourg Drop (LSD) model(right).*

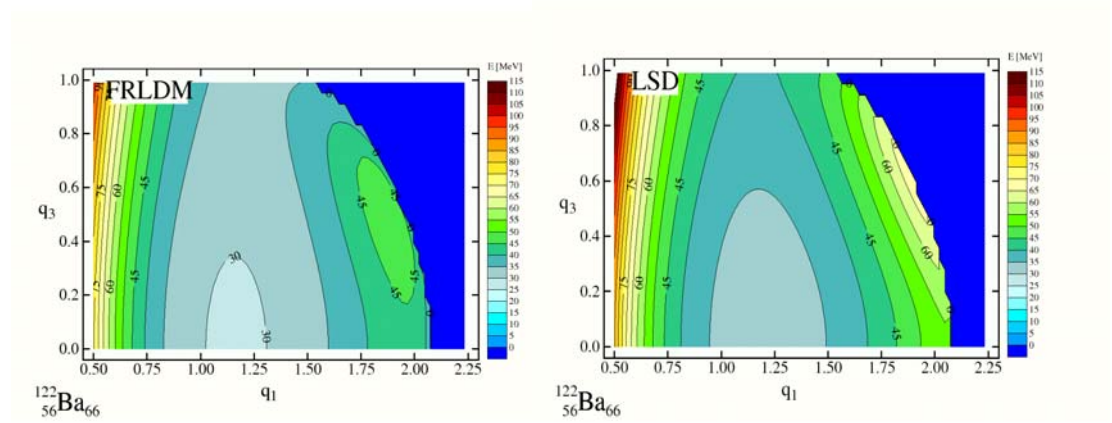

Figure 5. *Identical to Fig.4 for the spin L=70 ħ.*

Dynamical observables

There are many observables which can be calculated within the present 3D dynamical calculations such as: the distribution of the spin of the compound nucleus; the charge and mass distribution of the fission fragments or evaporation residues ; the light charge particles spectra; , the shape of the fissioning nucleus at the scission point and many others. For example, many experimental works have shown that the total fission cross-sections together with the width of the mass distribution of the fission fragments provide important constraints on the strength of nuclear viscosity and on the collective degrees of freedom driving the fission process. This work contains only few of them such as the spin of the compound

nucleus (Fig. 6), Z distribution of the fission fragments (Fig.7) and the kinetic energy of the fragments (Fig. 8).
The calculations have been performed for the heavy nucleus ^{260}Rf and also for few isotopes of Barium. Our results show that the properties of the fragments produced in the fission ^{260}Rf are not so sensitive to the shape of potential energy surfaces, while for light compound nuclei like Barium, the characteristics of the fragments have been found to strongly depend on the model used for the PES. This is illustrated in Fig. 6 – 8.
For investigating the influence of the potential energy surface on dynamical observables we used a viscosity coefficient k_s=0.2 [5], and a constant level density parameter a(**q**)=A/8, where A is the mass number of the fissioning system. Other calculations performed for different viscosity parameters k_s=0.2, 0.5, 0.7 and 1.0 does not give significantly different results. Sensitivity on the level density parameter choice are under investigation.
The compound nucleus spin distribution shown in the Fig. 6 was obtained from the Langevin calculation assuming the FRLDM or LSD potential energy. A sharp cut off approximation is assumed for the maximum angular momentum in the nucleus. The low spins of the compound nucleus drive the evaporation residues while the high spin part leads to the fission. Comparing the results for two different PES, one observe two different spin limits for the evaporation residue channel: for the calculation with the FRLDM model the spin is around 45 $\hbar$ whereas for the LSD case this limit is shifted to 52 $\hbar$.

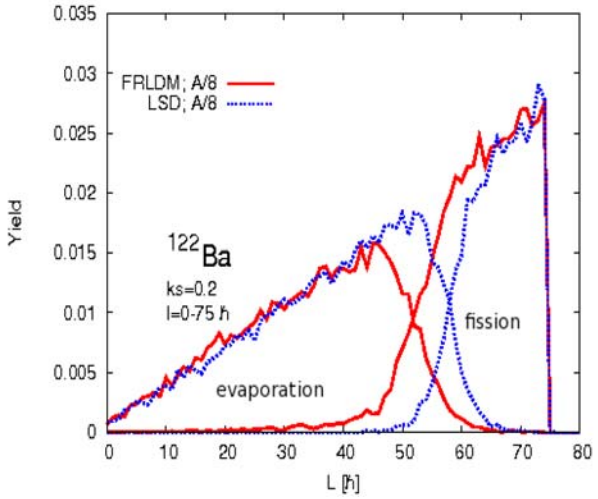

Figure 6. *The initial spin distribution of the compound nucleus ^{122}Ba for events leading either to evaporation residues or to fission, obtained with the FRLDM (red) and LSD (blue) potential energy surfaces.*

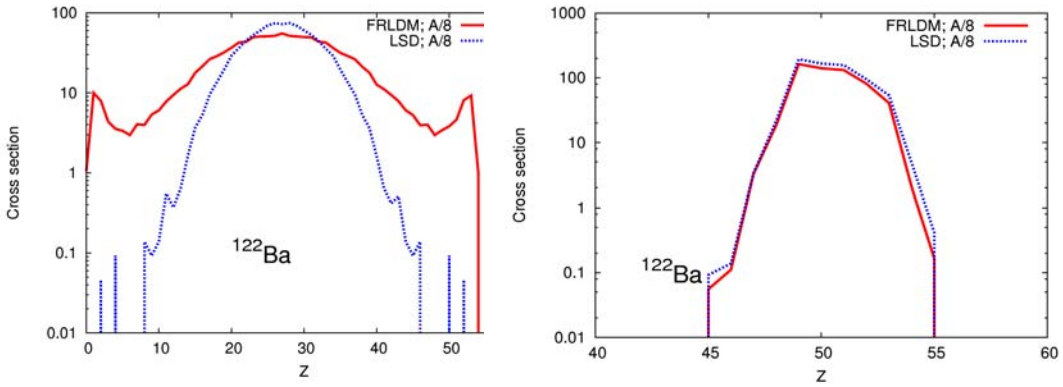

Figure 7. *The charge distribution for ^{122}Ba for the fission (left) and evaporation (right) channels calculated with the FRLDM (red) and LSD (blue).*

The choice of the PES has a negligible influence on the charge (or mass) distribution of the evaporation residues (Fig.7 right) whereas it is crucial for the fission fragment Z distribution.
The evaluation of the spin limits for the evaporation channel could depends of the choice of the PES but the effect modify only slightly light charge particle emission and thus the Z distribution of the evaporation residues are similar.
The shape of the fission fragment charge distribution reflects the shape of the PES: the flatter energy surfaces of FRLDM lead to wider Z distribution as compared to the LSD (Fig.7 left).

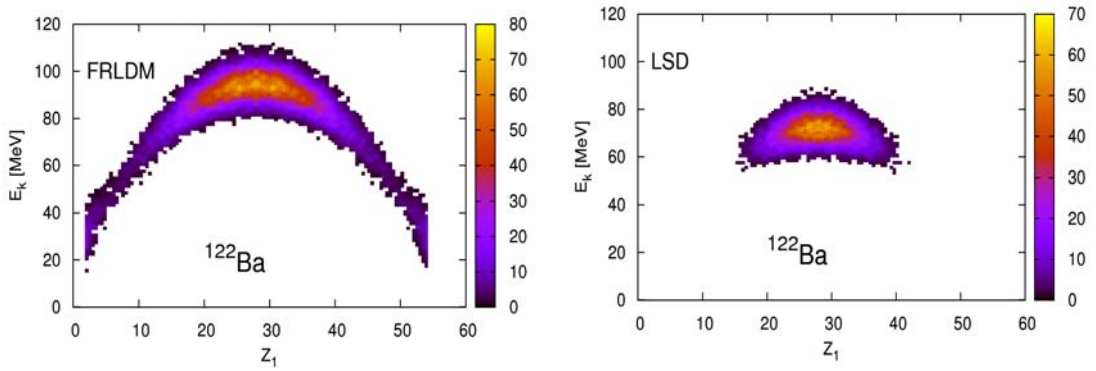

Figure 8. The kinetic energy distribution for ^{122}Ba for the fission (left) and evaporation (right) channel calculated with the FRLDM (left) and LSD (right) potential energy surfaces.

Similar behaviour is also observed for the kinetic energy distribution of the fission fragments (Fig. 8) as a function of the atomic number Z. In the LSD case the distribution is focused around mass-symmetric fragments whereas the FRLDM gives also asymmetric fission events.
The location of the maximal yield of the kinetic energy of the fission fragments for the symmetric fission for the FRLDM model is around 86 MeV while for the LSD PES it is around 71 MeV. Moreover, the average width of the kinetic energy spectra is 15 MeV for the FRLDM and only 5 MeV in the LSD PES. These dramatic differences in the kinetic energy distribution reflect the differences in the landscape around the symmetric fission valley.

Summary

Based on the solution of a 3-dimensional Langevin equation, the present contribution shows the importance of the potential energy surface in the modelling of the fission process at high excitation energy. Dynamical calculations were performed for two macroscopic models as the driving force in the equations: the FRLDM and the LSD model. The properties of the fragments formed in the fission of Barium compound nuclei are found to be very sensitive to the parametrization used for the potential energy. Excited medium – mass nuclei are thus a relevant probe, complementary to customarily used heavy systems, for studying the various ingredients entering into the modelling of the fission dynamics.

Acknowledgements
This work is supported by the ANR PROVA and COPIN 09-136.

References

[1] H. A. Kramers, Physica 7, 284 (1940).
[2] Y. Abe, C. Gregoire, H. Delagrange, J. Phys. (Paris) 47, C4-329 (1986).
[3] A. V. Karpov, P. N. Nadtochy et al. Phys. Rev. C 63, 054610 (2001).
[4] G. D. Adeev et al. Phys. Part. Nucl. 36, 378 (2005).
[5] P. N. Nadtochy et al. Phys. Lett. B 685, 258 (2010)
[6] M. Brack et al. Rev. Mod. Phys. 44, 320 (1972).
[7] A. J. Sierk, Phys. Rev. C 33, 2039 (1986);
K. T. R. Davies et al.Phys. Rev. C 13, 2385 (1976).
[8] K. Pomorski, J. Dudek, Phys. Rev. C67, 044316 (2003);
J. Dudek, K. Pomorski, N. Schunck, N. Dubray, European Phys. J. A20, 165 (2004).

Odd-even effect in cold fission

M. Mirea

Horia-Hulubei National Institute for Physics and Nuclear Engineering, O.O. Box MG-6, Bucharest-Magurele, Romania
mirea@ifin.nipne.ro

Abstract: A new set of time-dependent coupled channel equations for pair breaking are deduced from the variational principle. The odd-even effect in the charge and mass distribution of cold fission is investigated within the model. The essential idea is that the seniority one and the seniority two configuration mixing is managed under the action of some inherent low lying time dependent excitations produced in the avoided crossing regions due to the Landau-Zener promotion mechanism. It must be mentioned that the odd-even effect in cold fission is a strange phenomenon. The odd even fragmentation dominates at very low excitation energy while the even-even partitions are dominant for excitations above 4-6 MeV. The problem is that in cold processes the nuclear system doesn't possess enough energy to break a pair. This phenomenon is explained within our equations.

Introduction

In the thermal neutron induced fission, the mass and charge distributions of fragments evidence a fine structure that show a preference for an even number of protons and neutrons in both products. It can be expected that this phenomenon will be more evident in the case of cold fission, where the excitation of the fragments is so small that no neutrons are emitted. This is not true. There are some strange experimental evidences in cold fission. As remarked in Refs. [1-4], in cold fission, at very low excitation energy of the fragments, the odd-odd yields are always larger than the even-even ones. The even-even fragmentation dominates at larger excitation of the fragments, above 4-6 MeV. This behavior cannot be easily explained because in cold processes the system doesn't posses enough energy to break a pair and because the penetrability through the barrier is hindered for odd-systems due to the specialization energies associated to the unpaired nucleons. The odd-even structure in fission is explained usually within statistical arguments [5]. Up to now, the statistical explanation of this phenomenon involved some modifications of the level densities for odd-even and even-even partitions [6] by according them within the deformations of the fragments as function of the excitations energies and the shell effects. In the following, this phenomenon will be alternatively explained by solving a coupled-channel system of time-dependent pair breaking equations [7].

Equations of motion

In order to obtain the equations of motion, we shall start as in Ref. [6] from the variational principle taking the following energy functional

$$L = \left\langle \Psi \left| H - i\hbar \frac{\partial}{\partial t} + H' - \lambda N \right| \Psi \right\rangle \qquad (1)$$

where

$$H(t) = \sum_{k>0} \varepsilon_k (a_k^+ a_k + a_{\bar{k}}^+ a_{\bar{k}}) - G \sum_{k,i>0} a_k^+ a_{\bar{k}}^+ a_i a_{\bar{i}} \qquad (2)$$

is a many-body Hamiltonian with pairing residual interactions. This Hamiltonian depends on some time-dependent collective parameters $q(t)=\{q_i(t)\}$ (i=1,...n), such as the internuclear distances between atoms or nuclei. ε_k are single-particle energies of the molecular potential, a_k^+ and a_k denote operators for creating and destroying a particle in the state k, respectively. The state characterised by a bar signifies the time-reversed partner of a pair. The pairing

correlation arises from the short range interaction G between fermions moving in time-reversed orbits. Using quasiparticle creation $\alpha_{k(\gamma)}^{+}$ and annihilation operators $\alpha_{k(\gamma)}$ a term able to break a Cooper pair when the system traverses an avoided crossing region is constructed:

$$H' = \sum_{t,\, j\neq i}^{n} h_{ij}(t)\left[\alpha_{i(0)}\alpha_{\bar{j}(0)}\prod_{k\neq i,\, j}\alpha_{k(0)}\alpha_{k(ij)}^{+} + \alpha_{i(0)}^{+}\alpha_{\bar{j}(0)}^{+}\prod_{k\neq i,\, j}\alpha_{k(ij)}\alpha_{k(0)}^{+}\right] \qquad (3)$$

When an operator of the type $\alpha_{i(0)}\alpha_{j(0)}$ acts on a seniority zero Bogoliubov wave function, a pair is broken and a seniority two Bogoliubov wave function is obtained. On another hand, the term of the type $\alpha_{i(0)}^{+}\alpha_{j(0)}^{+}$ creates a pair when it acts on a seniority two wave function. The trial many-body wave function is expanded as superposition of time dependent BCS seniority-zero and seniority-two adiabatic wave functions

$$\left|\Psi\right\rangle = \left[c_0\prod_{k}(u_{k(0)} + v_{k(0)}a_k^{+}a_{\bar{k}}^{+}) + \sum_{j,l\neq j} c_{jl}a_j^{+}a_{\bar{l}}^{+}\prod_{k\neq j,l}\left(u_{k(jl)} + v_{k(jl)}a_k^{+}a_{\bar{k}}^{+}\right)\right]\left|0\right\rangle \qquad (4)$$

where c_0 and c_{jl} are amplitudes of the two kind of configurations, seniority zero and seniority two, respectively. The seniority zero configuration means that the system is completely paired while the seniority two one implies that one pair is broken. The functional (1) is minimised in a way analogue to that described in Refs. [8,9]. In these references, the form of the corrections produced due to the inherent interaction in the avoided crossing regions were postulated. Eventually, eight coupled-channel equations are obtained:

$$\begin{aligned}
i\hbar\dot{\rho}_{k(0)} &= \kappa_{k(0)}\Delta_0^{*} - \kappa_{k(0)}^{*}\Delta_0 \\
i\hbar\dot{\rho}_{k(\gamma)} &= \kappa_{k(\gamma)}\Delta_\gamma^{*} - \kappa_{k(\gamma)}^{*}\Delta_\gamma \\
i\hbar\dot{\kappa}_{k(0)} &= (2\rho_{k(0)} - 1)\Delta_0 + 2\kappa_{k(0)}(\varepsilon_k - \lambda_0) - 2G\rho_{k(0)}\kappa_{k(0)} \\
i\hbar\dot{\kappa}_{k(\gamma)} &= (2\rho_{k(\gamma)} - 1)\Delta_\gamma + 2\kappa_{k(\gamma)}(\varepsilon_k - \lambda_\gamma) - 2G\rho_{k(\gamma)}\kappa_{k(\gamma)} \\
i\hbar\dot{P}_0 &= \sum_{\gamma} h_\gamma(S_{0\gamma}^{*} - S_{0\gamma}) \\
i\hbar\dot{P}_\gamma &= h_\gamma(S_{0\gamma} - S_{0\gamma}^{*}) \qquad (5) \\
i\hbar\dot{S}_{0\gamma} &= S_{0\gamma}(E_0 - N\lambda_0 - E_\gamma + N\lambda_\gamma) + S_{0\gamma}\left(\sum_{k\neq\gamma}T_{k(\gamma)} - \sum_{k}T_{k(0)}\right) \\
&\quad + \sum_{\beta} h_\beta S_{\beta\gamma} + h_\gamma(P_\gamma - P_0) \\
i\hbar\dot{S}_{\beta\gamma} &= S_{\beta\gamma}(E_\beta - N\lambda_\beta - E_\gamma + N\lambda_\gamma) + S_{\beta\gamma}\left(\sum_{k\neq\beta}T_{k(\beta)} - \sum_{k\neq\gamma}T_{k(\gamma)}\right) \\
&\quad + h_\beta S_{0\gamma} - h_\gamma S_{0\beta}^{*}
\end{aligned}$$

where the partial derivatives with respect the time are denoted by a dot. The first four equations are similar to the time dependent Hartree-Fock-Bogoliubov equations [10,11] for seniority zero and seniority two configuration. If the configurations $\gamma=(j,l)$ and $\beta=(m,n)$, then the sums are restricted by the conditions $j\neq l$, $m\neq n$, $m\neq j$, and $n\neq l$. E_γ are exactly the expected values of the Hamiltonian (2) for the seniority-zero or seniority-two configurations:

$$E_0 = 2\sum_k \rho_{k(0)}\varepsilon_k - \frac{|\Delta_0|^2}{G} - G\sum_k \rho_{k(0)}^2 \qquad (6)$$

$$E_{jl} = 2\sum_{k\neq j,l} \rho_{k(jl)}\varepsilon_k - \frac{|\Delta_{jl}|^2}{G} - G\sum_{k\neq j,l} \rho_{k(jl)}^2 + \varepsilon_j + \varepsilon_l$$

and $T_{k(\gamma)}$ are energy terms associated to single-particle states:

$$T_{k(\gamma)} = 2\rho_{k(\gamma)}(\varepsilon_k - \lambda_\gamma) - 2G\rho_{k(\gamma)}^2 + \frac{\kappa_{k(\gamma)}\Delta_\gamma^* + \kappa_{k(\gamma)}^*\Delta_\gamma}{2}\left(\frac{\rho_{k(\gamma)}^2}{|\kappa_{k(\gamma)}|^2} - 1\right)$$

The following notations are used in Eqs. (5):

$$\Delta_0 = G\sum_k \kappa_{k(0)}$$

$$\Delta_{jl} = G\sum_{k\neq j,l} \kappa_{k(jl)}$$

$$\kappa_{k(\gamma)} = u_{k(\gamma)}v_{k(\gamma)}$$

$$\rho_{k(\gamma)} = |v_{k(\gamma)}|^2$$

$$P_\gamma = |c_\gamma|^2$$

$$S_{\gamma\beta} = c_\gamma c_\beta^*$$

where $\rho_{k(\gamma)}$ are single-particle densities and $\kappa_{k(\gamma)}$ are pairing moment components. P_γ denote the probabilities to find the system in the configurations γ. $S_{\gamma\gamma'}$ are moment components between two configurations γ and γ' and have the property $|S_{\gamma\gamma'}|^2=P_\gamma P_{\gamma'}$. Δ_γ is the gap parameter that takes into account the blocking effect. The values of $\rho_{k(\gamma)}$ and P_γ are reals. The particle number conservation conditions $2\sum_k \rho_{k(0)}=2N$, $2\sum_{k\neq j,l}\rho_{k(jl)}=2N-2$ and $P_0+\sum_{j,l\neq j}P_{jl}=1$ are fulfilled by Eqs. (5). N denotes the number of particles in the active pairing space. The ingredients needed to solve the system (5) are the single particle levels, the interactions in the avoiding level crossing regions and the velocity of deformation. The first two ingredients will be calculated within the macroscopic-microscopic model while the velocity is taken as variable parameter.

Results

In the following, our calculations address the cold fission of ^{234}U.

In order to determine the energy diagram of the process and the interactions in the avoided level crossings, the macroscopic-microscopic model is used. In such a treatment, the whole nuclear system is characterised by some collective variables associated to some degrees of freedom that determine approximately the shape of the nucleus. The generalized coordinates vary in time leading to a split of the nuclear system. The behaviour of many intrinsic variables are managed by the shape of the nuclear system. Therefore, the basic ingredient is a nuclear shape parametrization. Our nuclear shape parametrization is given by two ellipsoids smoothly joined with a third surface obtained by rotating a circle around the axis of symmetry, as described in Ref. [8]. This nuclear shape parametrization takes into consideration the most important degrees of freedom encountered in fission: elongation (given by the distance between the two spheroids R); necking (given by the curvature of the median surface C); the mass-asymmetry (given by the ration of the major semi-axis of the fragments) and the deformations of the fragments (given by the eccentricities of the spheroids). Within this nuclear shape configuration it is possible to characterise swollen shapes that address the

ground state and necked ones that are available in the hyper-deformation region of the exit point from the barrier. One fragment and two separate fragments are allowed configurations.

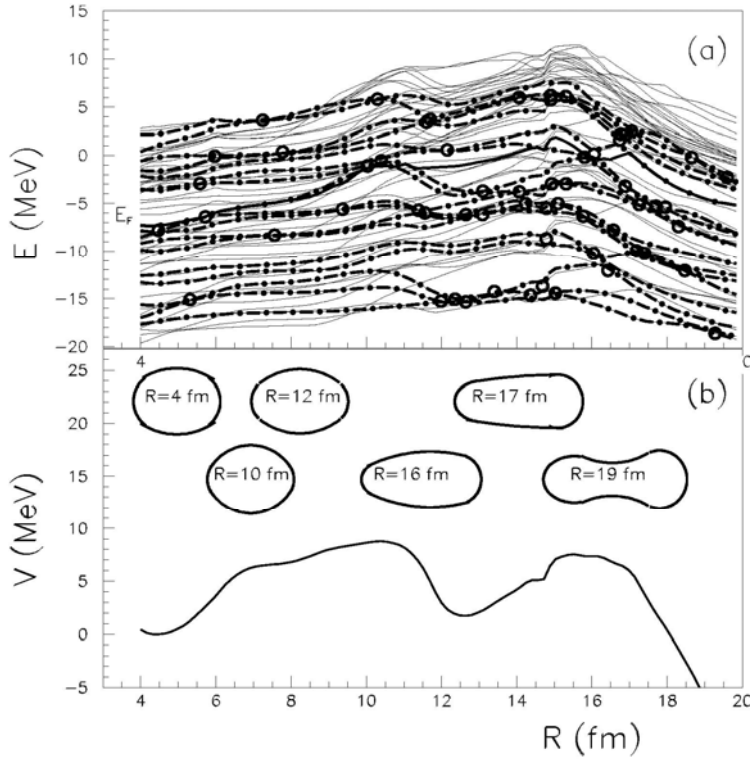

Figure 1. *(a) Proton level scheme as function of the elongation along the minimal action path. Only the active level space is plotted. The Fermi energy is plotted with a thick curve and the selected Ω=1/2 levels are plotted with a dot dashed thick line. The identified avoided crossing regions are marked with circles. (b) The fission barrier along the minimal action trajectory. Several shapes are inserted in the plot..*

In order to simulate the rearrangement of the intrinsic single-particle states, the first problem is to perform a full calculation of the trajectory in the configuration space spanned by our five degrees of freedom. A dependence between all generalized coordinates is obtained by minimizing numerically the WKB functional between the ground state of the parent and the exit point from the barrier, as realised in Refs. [12,13]. Two quantities intervene in the WKB integral: the deformation energy and the inertia. The deformation energy is a sum between a liquid drop part and the shell corrections. The macroscopic part is obtained in the framework of the Yukawa plus exponential model extended for binary systems with different charge densities [14]. The Strutinsky prescriptions were computed on the basis of the Woods-Saxon two center shell model. The Woods-Saxon two-center shell model uses the analytic eigenvector basis of the semi-symmetric harmonic potential to diagonalize a Woods-Saxon well corrected within spin-orbit and Coulomb terms. It is the sole model able to determine single particle level schemes for superasymmetric fission processes as cluster- and alpha-decay [15-17]. Due to its ability to characterise the configuration given by two separated fragments, this model was already used in fission studies or for superheavy element synthesis [18,19]. The quantities needed to evaluate the inertia are computed within the cranking model [20]. A numerical procedure is used to determine the least action trajectory in our five dimensional configuration space. The fission barrier obtained in this context is plotted in Fig. 1(b).

Now, it is possible to calculate the single-particle diagram along the optimal fission path. The diagram is displayed in Fig. 1(a). This level scheme supply the main quantities needed to solve our system of channel equations (5). Therefore, the excitation energy and the probabilities to find the nuclear system in a seniority one or in a seniority two state will be obtained.

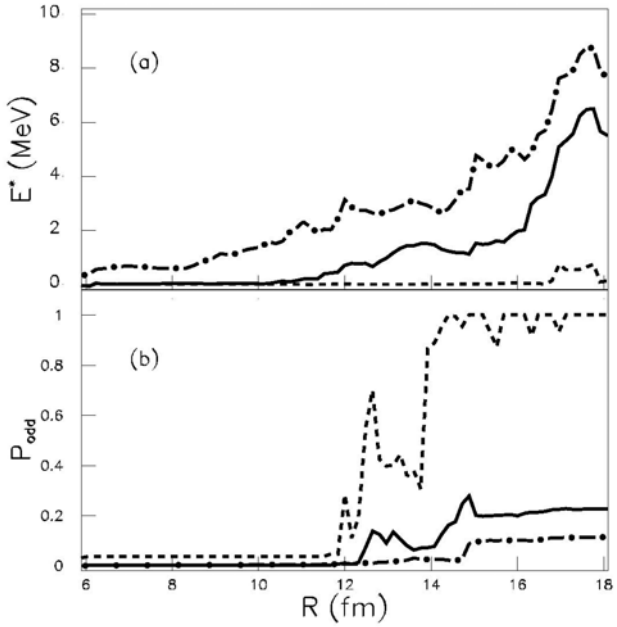

Figure 2. *(a) The average excitation energy E^* as function of the elongation R. The inter-nuclear velocities R are 10^4 , 10^5 and 10^6 m/s for the dashed, full and dot- dashed lines, respectively. (b) The probability P_{odd} of a seniority-two state with respect to the elongation R. The same line types and inter-nuclear velocities as in to determine dynamically the mixing between seniority-zero and panel (a) are used.*

Different constant values of the inter-nuclear velocity R ranging from 10^4 to 10^6 m/s were tested. These values can be translated in a time to penetrate the barrier ranging in the interval [$1.4x10^{-18}$, $1.4x10^{-20}$] s. The values of the excitation energy E^* and of the seniority two probability P_{odd} are plotted in Figs. 2(a) and 2(b) as function of the elongation for some inter-nuclear velocities $\partial R/\partial t$.

In Fig. 3, the dependencies of the seniority zero probability P_0 and of the seniority two probability P_{odd} versus E^* are displayed in the selected velocity domain. This values corresponds to an elongation R=20 fm, that is, in the vicinity of the exit point from the fission barrier. The theoretical results exhibit a clear decrease of P_{odd} as function of E^*. It is interesting to note that at zero excitation energy, the probability to find the system in a seniority-two state is practically one. In cold fission, at very low excitation energies of the fragments, the odd-even yields are always larger than the even-even ones. These theoretical results exhibit the main trends as exhibited by the experimental data evidenced above.

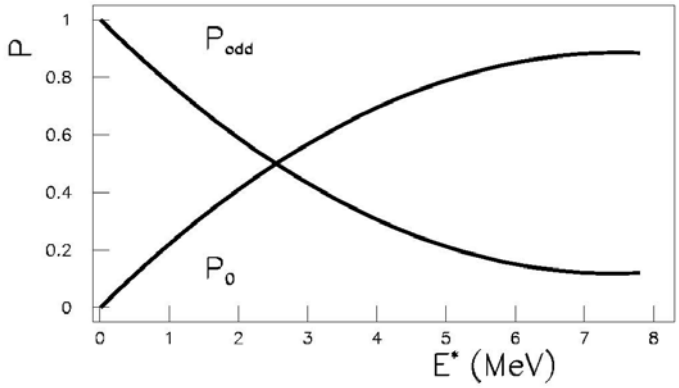

Figure 3. *The probabilities to obtain a seniority-zero state P_0 and a seniority-two state P_{odd} as function of the excitation energy E^* of the fragments at the elongation R=20 fm.).*

Conclusions

In conclusion, a new set of time-dependent coupled channel equations derived from the variational principle is proposed to determine dynamically the mixing between seniority-zero and seniority-two configurations. The essential idea is that the configuration mixing is managed under the action of some inherent low lying time dependent excitations produced in the avoided crossing regions. These equations were used to explain the odd-even effect in cold fission processes. Only the radial coupling was used in the analysis, but it is possible to extend the equations to take into account even the Coriolis coupling, as in Ref. [15]. The main trends concerning the dependence of the odd-even effect in fragments yields versus the fragments excitation energy were reproduced.

Acknowledgements
Work performed in the frame of the CNCSIS IDEI 512 contract of the Romanian Ministry of Education and Research..

References

[1] H.-G. Clerc, in Heavy Elements and Related New Phenomena, edited by W. Greiner and R.K. Gupta, World Scientific, Singapore, 1999, pp. 451.
[2] W. Schwab, H.-G. Clerc, M. Mutterer, J.P. Theobald, and H. Faust, Nucl. Phys. A 577, 674 (1994).
[3] F.-J. Hambsch, H.-H. Knitter, and C. Budtz-Jorgensen, Nucl. Phys. A 554 209 (1993).
[4] H.-H. Knitter, F.-J. Hambsch, and C. Budtz-Jorgensen, Nucl. Phys. A 536 221 (1992).
[5] F. Rejmund, A.V. Ignatyuk, A.R. Junghans, and K.-H. Schmidt, Nucl. Phys. A 678, 215 (2000).
[6] V. Avrigeanu, A. Florescu, A. Sandulescu, and W. Greiner, Phys. Rev. C 52, R1755 (1995).
[7] M. Mirea, Phys. Lett. B 680, 316 (2009).
[8] M. Mirea, Phys. Rev. C 78, 044618 (2008).
[9] M. Mirea, Mod. Phys. Lett. A 18, 1809 (2003).
[10] J. Blocki and H. Flocard, Nucl. Phys. A 273, 45 (1976).
[11] S.E. Koonin and J.R. Nix, Phys. Rev. C 13, 209 (1976).
[12] M. Mirea, L. Tassan-Got, C. Stephan, C.O. Bacri, and R.C. Bobulescu, Phys. Rev. C 76, 064608 (2007).
[13] M. Mirea, D.S. Delion, and A. Sandulescu, Phys. Rev. C 81, 044317 (2010).
[14] M. Mirea, O. Bajeat, F. Clapier, F. Ibrahim, A.C. Mueller, N. Pauwels and J. Proust, Eur. Phys. J. A 11, 59 (2001).
[15] M. Mirea, Phys. Rev. C 63, 034603 (2001).
[16] M. Mirea, Phys. Rev. C 57, 2484 (1998).
[17] M. Mirea, Eur. Phys. J. A 4, 335 (1999).
[18] M. Mirea, D.S. Delion and A. Sandulescu, EPL 85, 12001 (2009).
[19] M. Mirea, and L. Tassan-Got, Cent. Eur. J. Phys. In print.
[20] M. Mirea, and R.C. Bobulescu, J. Phys. G 37, 055106 (2010).

Correlation measurements with neutrons and γ-rays in binary and ternary fission of ^{252}Cf

M. Mutterer [1,2)]

1) Institute of Nuclear Physics, University of Technology, Schlossgartenstrasse 9, 64289 Darmstadt, Germany, and
2) GSI Helmholtz Centre for Heavy Ion Research GmbH, Planckstrasse 1, 64291 Darmstadt,Germany
mutterer@email.de

Abstract: The present contribution briefly reviews a series of correlation measurements in binary and ternary spontaneous fission of ^{252}Cf with placing emphasis on the emission of neutrons and γ-rays with fission fragments (FF), and light-charged-particles (LCP) in ternary fission (TF). Traditional TF studied were restricted to measurements of energy distributions and fractional yields of the LCPs, or the angular and energy correlation between LCPs and fission fragments.
In a first experiment to be discussed here, prompt γ-ray and neutron emission in binary and ternary spontaneous fission of ^{252}Cf were investigated with the aid of the 4π Darmstadt-Heidelberg NaI(Tl) Crystal Ball spectrometer. Analysing γ-ray spectra in both fission modes permitted to assess the so-called "high-energy component" in the γ yield, in the energy interval from 3.5 to 8 MeV and near mass asymmetry, to the statistical γ decay of fragments around the doubly magic ^{132}Sn. Furthermore, population of excited states in LCPs was ascertained for the first time. A particular structure observed in the γ yield associated with Be emission proved the occurrence of ternary ^{10}Be nuclei in a rather high excited state at 3.37 MeV. On the other hand, the measured anisotropy of γ-ray emission for various particle-accompanied fission modes tells, contrary to previous experimental studies, that the emission of ternary particles at scission does not influence the alignment of fragment spins, although it takes away some fragment spin. As for prompt neutron emission, measured angular correlations between neutrons and LCPs have permitted identification of the formation of the neutron-unstable nuclei ^{5}He, ^{7}He and ^{8}Li* as short-lived intermediate LCPs. Furthermore, the neutron multiplicity numbers <ν(A)> and distributions of fragment masses A, measured for the ternary fission modes with various LCP isotopes, give a valuable hint of the role played by nuclear shell structure in the fission process near scission.
In another experiment, the angular correlation of prompt γ-rays in binary and ternary ^{252}Cf (sf) was measured with two super-clover germanium (VEGA) detectors as position-sensitive γ-ray spectrometers. Here, the main interest has been to study, on the one hand, the γ decay from individual FFs and, on the other hand, the population of lower-lying excited states in the LCPs.

Introduction

The main part of the energy set free in the nuclear fission process is released in the form of kinetic energies of the fragments. Besides, a relatively large amount of energy (35 MeV on average in the case of ^{252}Cf) still remains confined just after scission as excitation of the fragments being stored mainly in two forms: (a) fragment deformation or collective rotations and vibrations, and (b) internal heat due to dissipation processes from saddle to scission. This energy is released by evaporation of neutrons and emission of γ rays, predominantly after the fragments had been fully accelerated. The study of prompt neutron and γ-ray emission is thus of great interest. The γ rays, allow us to determine fragment excitation energy after neutron evaporation, fragment spin distributions and the level structure of fission fragments [1]. As for the ternary fission (TF) mode, a light charged particle (LCP) is formed right at scission and ejected at about right angle with respect to the fission fragment direction (see reviews [2, 3]). The study of TF, although being rather rare (~ 1/260 relative to binary fission, for ^{252}Cf) and consequently difficult to measure, provides another valuable means to the experimentalist to explore the fissioning system, mainly at the short instant of rupture [4]. In the last two decades, a number of elaborate correlation experiments on TF which include the registration of either prompt neutrons or γ-rays with LCPs and FFs were able to considerably enlarge our knowledge on TF and fission dynamics

near scission. Ternary-particle emission in fission gives several possibilities for further investigating the characteristics of γ-ray emission. First, the emission of a third particle changes the mass and charge of both fragments, thus resulting in the formation of correlated fragment pairs which essentially differ from the binary ones at the scission point. This fact helps us to identify whether special components in the prompt fission γ spectrum, such as the so-called "high-energy γ-ray component" (see below), are correlated with the de-excitation of fragments from either of the light and heavy group, or rather with collective vibrations of the composite system at scission. Second, the emission of particles in fission approximately orthogonal to the fragments provides an additional spatial vector, allowing us to analyze the angular distribution of γ rays with respect to a plane built-up by the momenta of the two fragments and the ternary particle. And third, heavier ternary particles may also be created in excited states which can decay by γ-ray emission [5], what can be observed experimentally.
In the following, a brief survey of the most prominent features of these experimental studies is presented.

Experiment with the Darmstadt-Heidelberg crystal-ball spectrometer

In the first experiment presented here, a highly efficient angular sensitive detection system, i.e. the Darmstadt-Heidelberg 4π NaI(Tl) Crystal Ball (CB) spectrometer [6], was applied for the first time for measuring γ-ray emission and, at the same time, neutron evaporation in the rare ternary fission modes in ^{252}Cf (sf) accompanied by a variety of ternary particles. The experiment was performed at the MPI Heidelberg [7].

(a) (b)

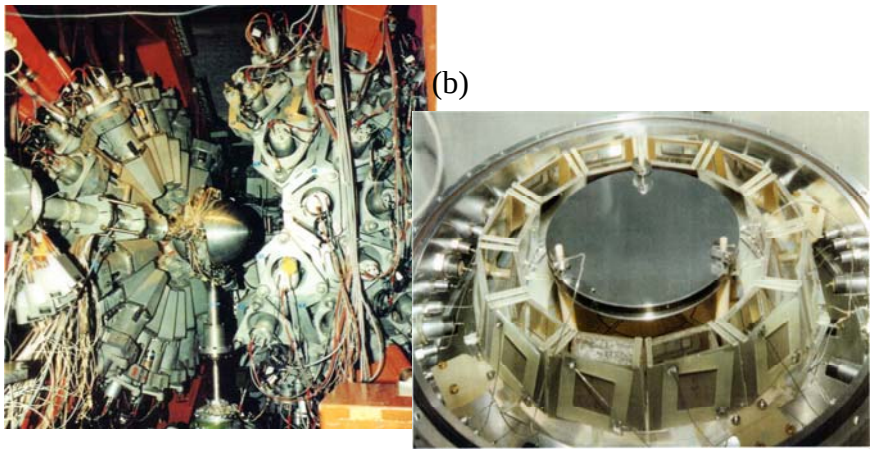

Figure 1.(a) *The Darmstadt-Heidelberg 4π NaI(Tl) Crystal Ball (CB) spectrometer, shown with its two halves moved apart to have access to the CODIS chamber placed it its centre. (b) Components of the detector system "CODIS" for fission fragments and LCPs.*

This instrument (see Fig. 1 a) is a segmented 4π detection system (162 NaI(Tl) crystals) of high detection efficiency (> 90% for γ rays and approx. 60% for fission neutrons). Gamma rays and neutrons are separated by their time of flight. The ^{252}Cf sample on thin backing and the assembly of detectors "CODIS" for fission fragments and light particles were mounted inside the hollow sphere of 50 cm diameter at the centre of the crystal ball. CODIS is displayed in Fig. 1b, with one side of the chamber housing removed. A Frisch-gridded 4π twin ionization chamber measures the FFs. As a specific feature of the CODIS FF chamber the cathode is segmented into 8 sectors which permits measuring not only the energies of both FFs but also their polar and azimuth angles of emission relative to the chamber axis. LCPs were identified by a ring of 12 ΔE-E telescopes composed of ΔE ICs and silicon PIN diodes, with a solid angle of about 0.4 π.
The set of measured parameters has allowed to determine, for each fission event, the following quantities and their mutual correlations:
-- fragment masses and kinetic energies;
-- multiplicity and angular distribution of fission neutrons;
-- multiplicity, energy and angular distributions of fission γ-rays;
-- energy, nuclear charge (mass) and emission angle of the LCP from ternary fission.

High-energy gamma-ray component.
Let us deal first, as particular result of the γ-ray measurement, with the study of the so-called "high-energy γ-ray component", i.e. the enhancement over exponential shape of the γ yield in the energy region between 3.5 and 8 MeV observed for fission events near mass symmetry. This component was first observed in 1989 [8] and thought to be a sign of a collective excitation near the scission point [9]. The phenomenon was studied quite extensively during the following years. In Ref. [10] different fission reactions were studied for several compound systems, and in a recent CB experiment on ^{252}Cf binary fission [11] the mass assignment of the surplus of high-energy γ rays was achieved by a Doppler analysis, permitting to determine the mean velocity vector of the emitting source.
In the present experiment, γ-ray spectra, in the energy range from 50 keV to 10 MeV, were measured both, in binary and ternary fission [12]. Fragment masses were deduced from the ratio of measured fragment kinetic energies considering prompt neutron evaporation. In applying this procedure for the ternary fission events, the ternary particle recoil momentum was taken also into account, using the measured particle energies, masses and emission angles. The high-energy γ-ray component was found to be equally pronounced in binary and α-accompanied fission (see Fig.2a). Figure 2b depicts mean γ-ray multiplicity in the energy interval between 4 and 8 MeV, as a function of fragment mass. In the α-accompanied fission mode, unlike in the binary case, the observed peak around A=132 is clearly resolved from its counterpart located at the complementary light mass, since the sum of fragment mass numbers is reduced by 4 units compared to binary fission. The peak at the heavy masses remains at the same position (A = 131.2 (0.2) units) in the binary and in ternary case. Thus, the comparison of the spectra for both fission modes proves that the spectral enhancement is not around mass symmetry but due to the reduced level density of fragments in the vicinity of the double-magic shell closure N = 82 (Z = 50) [11].

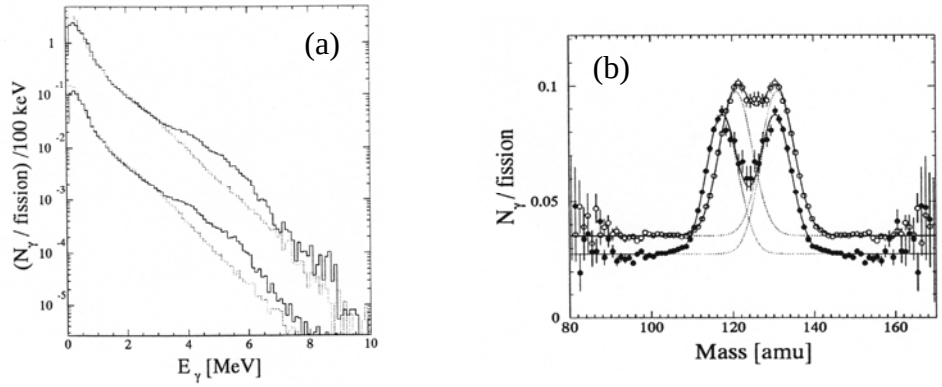

Figure 2. (*a) γ-ray spectra for binary (upper curves) and α ternary fission (lower curves), for near symmetric (full lines) and asymmetric (dashed lines) mass splits. (b) Yield of γ-rays, for energies from 4 to 8 MeV, vs. fragment mass, for binary (open symbols) and α ternary fission (full symbols) (data from [12].)*

Fragment spins and spin alignment in ternary fission.
From the measurement of neutron multiplicity distributions as well as of fragment total excitation energies TXE it was concluded that fragment deformation in ternary fission is considerably less than in binary fission (e.g. by 7.4 MeV in TXE for the emission of α particles [13]). One might expect hence, that the average spin of fragments should change also. An indication for some decrease of average fragment spin is that the total γ-ray multiplicity in the ternary case was measured to be less by at least 10 %. An even stronger evidence comes from the ternary-to-binary inter-comparison of γ-ray multiplicities for various γ-energy regions [7]. While the multiplicity in the region of discrete γ rays tells us about the values of fragment spins, the analysis of γ-ray angular distributions gives an information about spin orientation, which may help us to understand the origin of fragment spins. Our current understanding is that fragment spins are basically due to the collective motion of nuclear matter at scission, known as bending modes [14] although a minor contribution may come from the Coulomb repulsion of the deformed fragments at close distances after scission [15]. In spontaneous binary fission of an even-even nucleus with ground state spin *0* (like ^{252}Cf), the orbital angular

momentum and the spins of the two fragments emitted must couple to zero. Fragment spins are aligned in the plane orthogonal to the fission axis. Since the emission of ternary particles occurs close to the instant of scission, one might expect some correlation between the emission of LCPs and the direction of fragment spins. Assuming, that the emission of ternary particles occurs due to bending modes at scission, it was suspected [16] that the alignment of fragment spins in ternary fission must be even stronger than in binary. Experimentally, the information on the degree of fragment spin alignment can be obtained from a γ-ray anisotropy measurement. In the case of spin alignment, one should expect an angular distribution in the form $W(\theta) = 1 + A_2 P_2(\cos\theta)$, ($P_j(\cos\theta)$ being the Legendre polynomials) when streched E2 cascades dominate. In binary fission, this dependence was consistently found in various experiments [17,18]. In the ternary case, only two measurements are known. In Ref. [19] the ratio of anisotropy $W(0^0)/W(90^0)$ was measured. For the binary case, a value was obtained close to that from literature but, in ternary fission, the result was equal to unity, within about 2 % of stated experimental error. The interpretation was that the emission of the α particle fully destroys the alignment. In Ref. [20] the angular distribution of γ rays was measured over full angles. While in the binary case again results consistent with literature were obtained, an angular anisotropy in α-accompanied fission was observed, with the maximum intensity shifted away from the fission axis. This effect was explained by a displacement of the alignment due to the influence of the recoil momentum when the α particles are emitted at a certain distance from the fission axis.

In the experiment with the CB, the full angular distribution of γ-ray emission with respect to the fission axis was deduced, both for binary and LCP-accompanied fission. The results for the distributions averaged over fragment pairs in binary and α ternary fission [21] are depicted in Fig. 3. The total amount of 1.2×10^6 measured ternary events results in a previously not achieved statistical accuracy, so that the total errors are dominated by systematic uncertainties, such as cross-talk between neighbouring crystals. The relative error between the ternary and binary results is very small since both data sets were accumulated simultaneously under the same experimental conditions. The value for binary fission is very close to that obtained in [14] while the present result for ternary fission is in obvious contradiction to the results of Refs. [19,20].

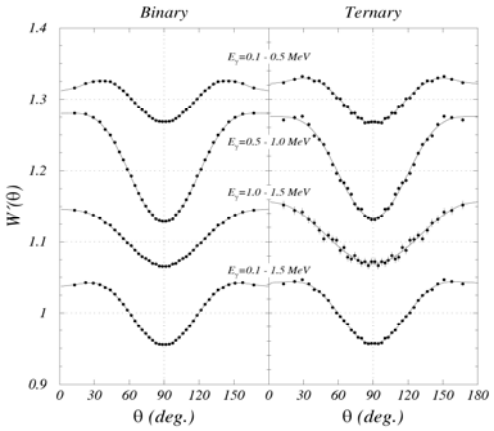

Figure 3. *Symmetrised angular distribution of γ-ray emission with respect to fragment motion for binary and α ternary fission, for different energy intervals. (data from [21]).*

It can safely be stated, that the difference in γ-ray anisotropy between ternary and binary fission is very small, if any. This means that the emission of ternary particles does not influence, or even destroy, the alignment of fragment spins, although ternary particles seems to take away some spin. The analysis of the γ-ray anisotropy for other LCPs (tritons, ^{6}He, and Li and Be nuclei), which was possible for the first time from the data, confirm the result obtained for the a particles. Furthermore, the projection of the γ-ray distribution onto the plane perpendicular to the (light) fragment direction were analyzed, i.e. the plane which is close to the emission direction of the α's. Gamma emission in this plane was found to be isotropic within 1% of error, indicating also no correlation of fragment spins with the emission direction of the ternary particles [21].

Gamma-ray emission from light charged particles.
High-efficiency γ-ray registration with the CB provided clear evidence for ternary fission proceeding with the emission of Be nuclei in an excited level which decays by γ-ray emission. Figure 4 shows the γ-energy spectrum for Be-accompanied fission, in comparison with the spectra for binary, α- and Li-accompanied fission, respectively. There is a significant enhancement at energies around 3.37 MeV, which corresponds to the energy of the first excited level in ^{10}Be, this isotope making about 80% of the Be element yield but is down in probability by two orders of magnitude compared to ternary α-particles [22]. No other ternary particles show structures in the γ spectra which are considered to be statistically significant. Besides, the peak structure in Be remains present (although it changes slightly its shape) when setting constraints on different fragment mass regions. This may exclude a possible emission of these γ rays from fission fragments.
At the time, from seemingly absence of Doppler broadening within the limited resolution of NaI(Tl), there have been suggestions that these γ quanta might be emitted from a resting Be source [7]. This idea has been tested by using data of γ-γ-γ coincidences obtained at an experiment with high-resolution γ-ray spectroscopy with the Gammasphere [23]. The data supported the NaI(Tl) result, but with limited statistics and no direct LCPs identification. The possibility that the ^{10}Be nucleus may stay between two fission fragments for a long time ~10^{-13} s to create a so-called triple nuclear molecule was discussed in Ref. [24]. Re-measurements on Gammasphere [25,26] with LCPs identification could confirm the existence of the 3.37 MeV γ line from ternary ^{10}Be, and finally assess, by Doppler shift analysis, γ-ray emission by ternary ^{10}Be nuclei in flight, so denying any existence of a triple nuclear molecule.

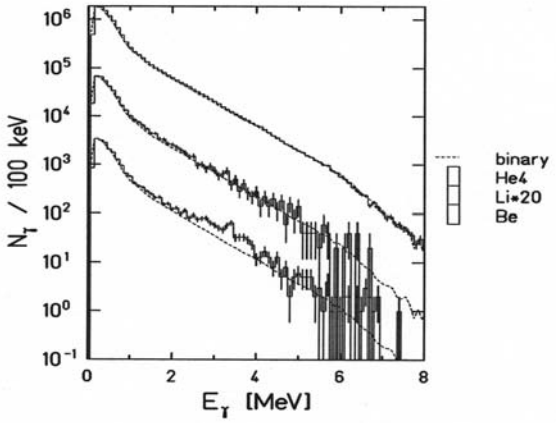

Figure 4. *γ-Ray spectra for α– particle, Li and Be accompanied fission (top to bottom). Dashed lines represent the shape of the spectrum from binary fission.*

Correlation measurements with prompt neutrons.
(a) From the kinematical data and the multiplicity of emitted neutrons the fragment total excitation energies TXE could be deduced, for the first time for various ternary fission modes with LCPs up to carbon. It turns out that LCP emission proceeds in expense of a considerable amount of TXE (35 MeV, on average, for binary Cf fission), with the required energy for particle emission increasing with LCP mass and energy. As an example, the average TXE decreases from 27 MeV to 15 MeV when instead of an α-particle a ternary C isotope is emitted. In a sense, TF with emission of heavier LCPs features a rather cold large-scale rearrangement of nuclear matter. The neutron multiplicity numbers <ν(A)> and distributions of fragment masses A, measured for the ternary fission modes with various LCP isotopes, from α-TF to C-TF (Fig.5 shows data from α-TF to Be-TF) give a clear evidence for a pronounced preformation of the FFs right at scission dominated by the well-known double-magic shells, mainly Z = 50 and N = 82. At scission, the biggest amount of TXE is obviously stored in the deformation due to neck formation. In TF, part of this TXE is consumed by LCP emission [4, 27]

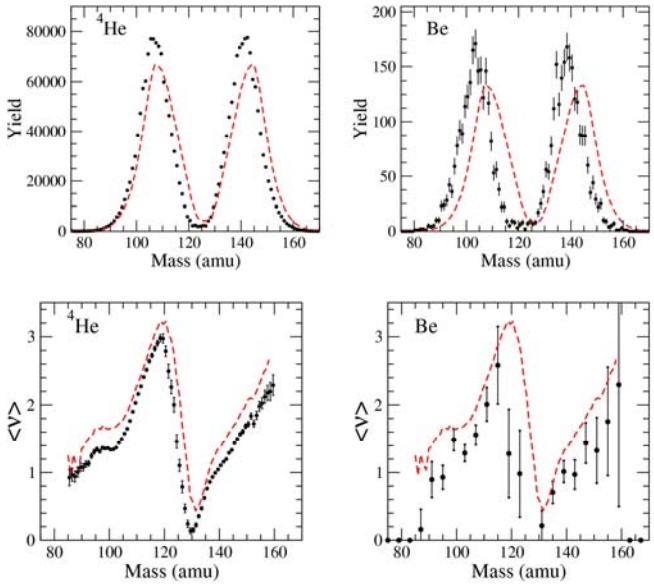

Figure 5. *(top) Fragment mass distributions in ternary fission of ^{252}Cf(sf) with ^{4}He and Be as the light particle. Binary mass distributions are shown as dash lines. (bottom) Neutron multiplicity vs. fragment mass for the same reactions. Dashed line is neutron multiplicity in binary fission.*

(b) In the same experiment, the neutron-unstable odd-N isotopes ^{5}He, ^{7}He and ^{8}Li* (in its excited state of E = 2.26 MeV) were identified to show up as intermediate LCPs in TF [28]. The emergence of the ternary ^{5}He and ^{7}He particles (lifetimes: 1 x 10^{-21}s, and 4 x 10^{-21}s, respectively) was disclosed from the measured angular distributions of their decay neutrons focused by the emission in flight towards the direction of motion of ^{4}He and ^{6}He particles (Fig. 5).

Previously, only ternary ^{5}He emission was observed by analyzing relative neutron intensities measured at forward and backward angles with respect to the α particles [29,30]. In the present work, neutrons were observed to be peaked also around Li-particle motion, which is attributed to the decay of the second excited state at E* = 2.26 MeV (lifetime: 2 x 10^{-20} s) of ^{8}Li. The population of ^{8}Li* was deduced to be 0.06(2), relative to Li ternary fission, and 0.33(20) relative to the yield of particle stable ^{8}Li. The fractional yields of the ^{5}He and ^{7}He TF modes relative to "true" ^{4}He and ^{6}He TF, respectively, were determined to be 0.21(5) for both cases. The mean energy of the ^{4}He residues resulting from the ^{5}He decay was determined to be 12.4(3) MeV, compared to 15.7(2) MeV for all ternary α-particles registered, and to 16.4(3) MeV for the true ternary α-particles. We note that ^{5}He in Cf fission has the second highest yield among all LCPs, being only superseded (by a factor of ~5) by ^{4}He emission, but downgrading ^{3}H (by a factor of ~2) to the third most-abundant LCP. The surprisingly high yields for these exotic clusters indicate that they are formed as the stable species inside the parent nuclei [28]. However, established theoretical yield estimations [31,32,33] when applied to the particle-unstable LCP species, predict about a factor of 4 lower ^{5}He and ^{7}He yields as were actually measured. This inconsistency is removed when besides the energetics at scission also the spins of the LCPs are considered in calculating LCP yields. In a systematic statistical approach, theoretical yields should be multiplied with the statistical weight factor, $(2I_i + 1)$, with I_i being the spin of the LCPs in states I [5]. With this ansatz, theoretical yield ratios ^{5}He/^{4}He, and ^{7}He/^{6}He will increase by a factor of 4 due to the 3/2^{-} spin of the ^{5,7}He ground states as compared to the 0^{+} spin of ^{4,6}He. It is worthwhile to note that ternary fission with the emission of neutron-unstable LCPs provides a source of neutrons that are emitted at about right angles to the fission axis, the dominant part coming from ^{5}He, with about one neutron in every 1500 binary fission events. This source of neutrons thus may mimic the search for so-called scission neutrons [34] thought to be related to the binary fission process.

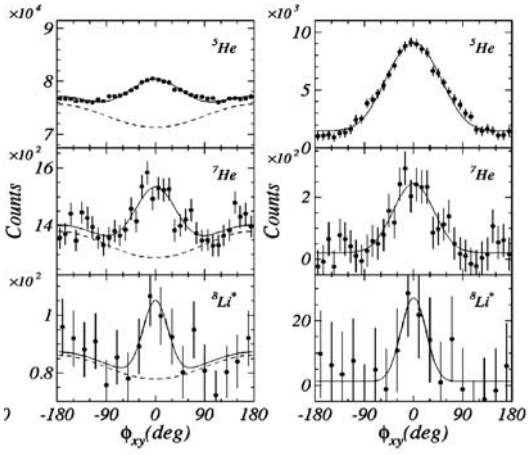

Figure 6. *Measured neutron angular distributions from the decay of intermediate LCPs ^{5}He, ^{7}He and ^{8}Li* of ^{252}Cf(sf), compared to a simulation (solid line). Shown are spectra with (left) and without (right) the background of neutron emitted by the fission fragments.(from Ref. [28])*

Experiment with super-clover germanium (VEGA) detectors

In another experiment to be briefly mentioned, the angular correlation of prompt γ-rays in binary and ternary ^{252}Cf was measured with two super-clover germanium (VEGA) detectors as position-sensitive γ-ray spectrometers [35]. Here, the main interest is to study, on the one hand, the γ-decay from individual FFs and, on the other hand, the population of lower-lying excited states in the LCPs. The FFs were again detected by an energy and angle sensitive 4π twin ionization chamber CODIS2 while the LCPs were intercepted by a number of 24 improved ΔE-E_{rest} telescopes, permitting to deduce isotopic yield up to Be LCPs [22,36]. For the γ-ray angular correlation study, the intensities of individual γ-transitions were measured relative to the fission fragment axis. First results indicate a surprisingly large γ-ray anisotropy, which seems in agreement with a complete alignment of the initial fragment spins with respect to the fission axis [37]. Careful data evaluation of this complicated study is quite laborious and final results come slowly.

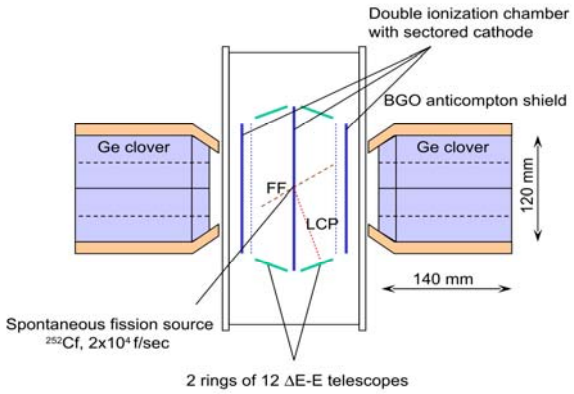

Figure 7. Experimental setup for measuring γ-ray angular correlation with binary and ternary fission of ^{252}Cf. The detector system CODIS2 measures fission fragments and LCPs. γ-ray are intercepted with two super-clover germanium (VEGA) detectors.

Summary and Conclusions

The present experiments on the prompt neutron and γ-ray emission in the spontaneous fission of ^{252}Cf has yielded new experimental data. Measuring γ-ray spectra associated with TF could clear up the origin of the high-energy component and discover population of excited

states in LCPs. The precise measurement of γ-ray anisotropy has told us that ternary particle emission does not influence the alignment of fragment spins. As for prompt neutron emission, measured neutron multiplicities and angular correlations between neutrons and LCPs have permitted probing excitation energy at scission, and identification of the neutron-unstable nuclei ^{5}He, ^{7}He and ^{8}Li* as short-lived intermediate LCPs. We finally mention two more recent series of experiments aiming at probing nuclear fission dynamics by quite different methods [38,39]

References

[1] J.H. Hamilton et al., Prog. Part. Nucl. Phys. 35 (1995) 635.
[2] C. Wagemans, in The Nuclear Fission Process, edt. C. Wagemans, CRC Press, Boca Raton, Fl. USA, 1991, Chap. 12.
[3] M. Mutterer, and J. Theobald, in Nuclear Decay Modes, edt. D.N. Poenaru, IOP, Bristol, UK, 1996, Chap. 12.
[4] F. Gönnenwein, M. Mutterer, and Yu. Kopatch, Europhysics News 36/1 (2005) 11.
[5] G. Valskii, Sov. J. Nucl. Phys. 24 (1976) 140.
[6] V. Metag et al., Lecture Notes in Physics, 178 (1983) 163.
[7] P. Singer et al., Proc. DANF96, Casta Papiernicka, Slovakia, 1996, (JINR, Dubna, 1996), p. 262; P. Singer, Ph.D. Thesis, TU Darmstadt (1997).
[8] P. Glässel et al., Nucl. Phys. A502 (1989) 315c.
[9] M. Zielinska-Pfab and K. Dietrich, Phys. Lett. 49B (1974) 123.
[10] J.B. Fitzgerald et al., Z. Phys. A355 (1996) 401.
[11] A. Hotzel et al., Z. Phys. A356 (1996) 299.
[12] P. Singer et al., Z. Phys. A359 (1997) 41.
[13] M. Mutterer et al., Proc. DANF96, Casta Papiernicka, Slovakia, 1996, (JINR, Dubna, 1996), p. 250;
[14] K. Skarsvag, Phys. Rev. C22 (1980) 638.
[15] J.O. Rasmussen et al., Proc. DANF96, Casta Papiernicka, Slovakia, 1996, (JINR, Dubna, 1996), p. 289;
[16] A.L. Barabanov, Phys. Atom. Nucl. 57 (1994) 1157.
[17] J.B. Wilhelmy et al., Phys. Rev. C5 (1972) 2041.
[18] A. Wolf, and E. Cheifetz, Phys. Rev. C13 (1976) 1952.
[19] O.I. Ivanov, Sov. J. Nucl. Phys. 15 (1972) 620.
[20] W. Pilz and W. Neubert, Z. Phys. A338 (1991) 75.
[21] Yu.N. Kopatch et al., Phys. Rev. Lett. 82 (1999) 303.
[22] Yu.N. Kopatch et al., AIP Conf. Proc. 798 (2005) 115.
[23] A.V. Ramayya et al, Phys. Rev. Lett., 81 (1998) 81.
[24] W. Greiner, Acta Physica Slovakia 49 (1999) 9.
[25] M. Jandel et al., Proc. DANF01, Casta Papiernicka, Slovakia, 2001, (World Scientific, Singapore, 2002), p. 350.
[26] A.V. Daniel et al., Proc. Int. Workshop New Applications of Nuclear Fission, Bucharest, Romania, 2003, (World Scientific, Singapore, 2004), p.41.
[27] M. Mutterer et al., Nucl. Phys. A 738 (2004) 122.
[28] Yu.N. Kopatch et al., Phys. Rev. C 65 (2002) 044614.
[29] E. Cheifetz et al., Phys. Rev. Lett. 29 (1972) 805.
[30] A.P. Graevskii, and G.E. Solyakin, Sov. J. Nucl. Phys. 18 (1974) 369.
[31] I. Halpern, Annu. Rev. Nucl. Sci. 21 (1971) 245.
[32] V.A. Rubchenya, and S.G. Yavshits, Z. Phys. A 329 (1988) 217.
[33] A. Pik-Pichak, Phys. Atom. Nucl. 57 (1994) 906.
[34] H.H. Knitter, et al., in The Nuclear Fission Process, edt. C. Wagemans, CRC Press, Boca Raton, FL., USA, 1991, Chap. 11.
[35] Yu.N. Kopatch et al., Acta Physica Hungarica, New Series - Heavy Ion Physics 18, 399 (2003).
[36] V. Tishchenko et al., Proc. ISINN-13, Dubna, Russia, 2005, (JINR, Dubna, 2006), p. .
[37] P. Adrich et al., Proc. 3rd. Int. Conf. Fission and Neutron-Rich Nuclei, Sanibel Island Fl. USA, 2002, (World Scientific, Singapore, 2003), p..
[38] F. Gönnenwein et al., Phys. Lett. B 652 (2007) 13.
[39] L. Stuttgé et al., Proc. Seminar on Fission VII, Gent, Belgium, 2010, (World Scientific, Singapore), in press.

Fission dynamics in heavy ion collisions on ^{238}U

K. Nishio

Japan Atomic Energy Agency, Tokai, Ibaraki 319-1195, Japan
nishio.katsuhisa@jaea.go.jp

Abstract: Fragment mass distributions for fission after full momentum transfer (FMT) were measured for the ^{30}Si,^{31}P,^{34,36}S,^{40}Ar + ^{238}U reactions at bombarding energies around the Coulomb barrier. The experiment was carried out at the JAEA tandem accelerator facility. We observed strong variation of the mass distribution on beam energy and projectile nucleus. In the reaction of ^{36}S +^{238}U we observed a transition from symmetry to asymmetry mass distributions when the beam energies were decreased from the above-barrier to sub-barrier values. The mass asymmetry was A_L /A_H = 74 /200, which corresponds to the fission valley leading to the doubly closed-shell nuclei ^{78}Ni /^{208}Pb. The fission channel is populated by quasifission, which is the disintegration without forming the compound nucleus. The incident-energy dependence is strongly correlated with the prolate deformation of ^{238}U and the orientation at the initial impact. The results indicate that the reaction starting at the polar collisions on ^{238}U has larger quasifission probability. The mass distributions are nicely reproduced by a model calculation using Langevin equation. The ^{40}Ar + ^{238}U reaction also has the similar mass asymmetry (A_L /A_H ≈ 78 /200) in quasifission. In the reactions of ^{31}P + ^{238}U and ^{30}Si + ^{238}U, mass asymmetries are A_L /A_H ≈ 81 /188 and 90/178, respectively. The results suggest that the system populated by the reaction using lighter projectile approaches closer to the shape of the compound nucleus even when quasifission occurs.

Introduction

Experimental challenges to produce superheavy nuclei (SHN) have been carried out by using heavy ion fusion reactions [1-3]. Development of a theoretical model to predict cross sections for nuclei located at the extreme end of heavy elements is important for the proper selection of target and projectile as well as the bombarding energy to produce these nuclei. The reaction is considered to proceed in three steps; (1) penetration of the Coulomb barrier between two colliding nuclei, (2) formation of a compound nucleus after the system is captured inside the Coulomb barrier and (3) survival of the exited compound nucleus to produce evaporation residue (ER) against fission (fusion-fission).

The first step, penetrating the Coulomb barrier, is relatively well understood. Enhancing of the capture cross section σ_{cap} relative to the one-dimensional barrier penetration model has been observed at the sub-barrier energy. For the actinide-based reactions, the enhancement is explained by the lowering of the Coulomb barrier when projectile hits the polar sides of the prolately deformed nucleus. The second process, forming a compound nucleus (fusion probability), is not well understood. A theoretical model must treat the dynamic evolution of a system from the initial touching configuration up to the compound nucleus state. In a reaction using a heavy target and projectile, quasifission competes against fusion. Once the fusion cross section is calculated, it is multiplied by the survival probability, which can be determined by a statistical model, to calculate the cross section to produce SHN.

Measurement of the ER cross sections gives information on the fusion probability. However, because of the low production rate for SHN, available data with high statistical accuracy are limited. When a model can treat fusion-fission and quasifission in a consistent framework, such as the unified theory [4], the measurement of fission properties can be another benchmark for testing the model, as fusion-fission and quasifission would have different decay properties.

Fusion reactions using actinide target nuclei are extensively used to investigate SHN. The reasons are ; (1) a relatively neutron rich SHN than the cold fusion reactions are produced, thus the decay properties of these nuclei have information on the structure in the vicinity of the spherically closed-shell at N=184, (2) nuclei having a relatively long half-lives allows a study for the chemical property, and (3) the cross sections maintain values of a few picobarn even for the production of the heaviest elements [1,5]. The relatively large cross sections for SHN produced using a ^{48}Ca beam are explained by a high survival probability of the

compound nuclei in competition with fission owing to large fission barriers of nuclei in the vicinity of the N=184 shell closure. Another reason could be a higher fusion probability in reactions using actinide targets. Since actinide nuclei are prolately deformed, there exists a configuration at which the projectiles hit the equatorial region of the deformed target nuclei. In this case a compact configuration is achieved and the system may have a larger fusion probability than the reactions using spherical target nuclei such as lead or bismuth.

We have investigated the effects of nuclear orientation on fusion and/or quasifission by measuring the fission fragment mass distributions and the ER cross sections in the reactions using ^{238}U target nuclei to obtain information on fusion probability. The evolution of the nuclear shape from the contact point is largely influenced by the structure of the potential energy and the initial touching point as shown in Figure 1. At the equatorial collisions, the system has a larger probability to form the compound nucleus, whereas the polar collisions would give higher probability to disintegrate as quasifission. The quasifission is expected to fission through the mass-asymmetric channel.

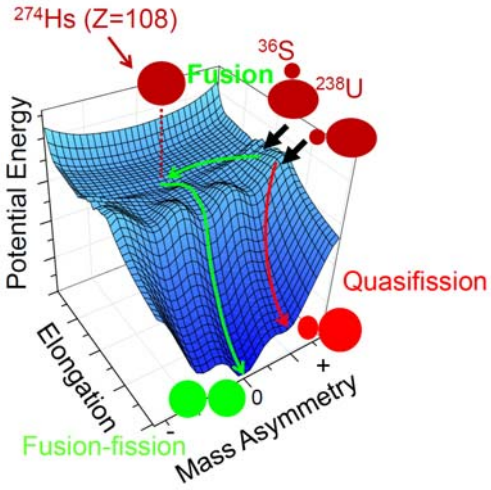

Figure 1. *Potential energy for ^{274}Hs produced in the fusion reaction of ^{36}S+ ^{238}U.*

We also made a theoretical calculation based on a dynamical model using Langevin equation to interpret the measured mass distributions, where fusion-fission and quasifission fragments are separately determined. With the model calculation, fusion corss sections are determined. The results are compared with those determined from the ER cross sections produced in ^{30}Si,^{34}S +^{238}U. The production of ER and the measurement of their cross sections were carried out at GSI using linear accelerator UNILAC and the velocity filter SHIP [2].

Experimental details

In-beam fission measurement

The mass distributions and cross sections of fission fragments in the reactions of ^{30}Si,^{31}P, ^{34,36}S,^{40}Ar + ^{238}U were measured using beams supplied by the tandem accelerator of the Japan Atomic Energy Agency (JAEA) in Tokai. The experimental set-up and the analysis method were described in [6]. The beam energies were changed from above-barrier to sub-barrier values to measure the energy dependence of the mass distribution as well as the fission cross section. The beam intensities were typically from 0.1 to 1.0 *particle*-nA.

The ^{238}U target was prepared by electrodeposition of UO_2 on a 90 μg/cm^2 thick nickel backing. Both fission fragments (FFs) were detected in coincidence by position-sensitive multiwire proportional counters (MWPCs). The detectors were located on both sides of the target each at a distance of 211 mm and at angles of θ_1 = - 61.0^o for MWPC1 and θ_2 = + 90.0^o for MWPC2 in the reactions of ^{30}Si, ^{34,36}S, ^{31}P + ^{238}U. The angles of θ_1 = -72.0^o and θ_2= +72.0^o were chosen for the ^{40}Ar + ^{238}U reaction. The MWPCs covered the emission angles of ± 25.0^o around the detector center. We also determined the our-of-plane angles of both

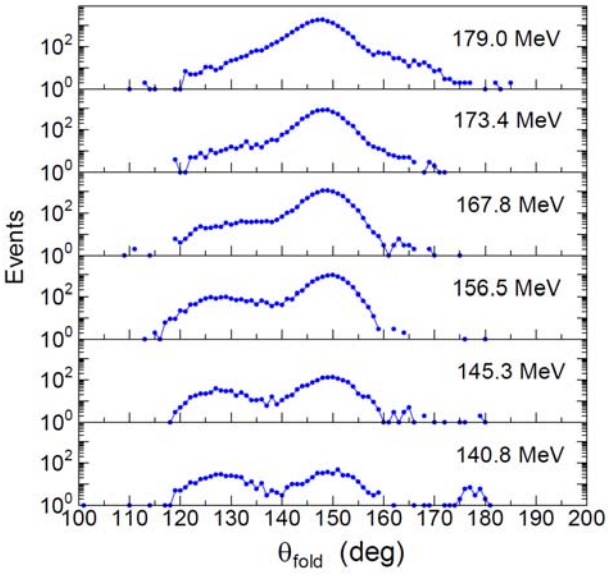

Figure 2. *Distribution for folding angle of fission fragments produced in the ^{30}Si +^{238}U reaction. The beam energy in the laboratory frame is indicated.*

fragments Φ_1 and Φ_2. The time difference, ΔT, between the signals from MWPC1 and MWPC2 was measured. The charges induced in both MWPCs contain information on the energy deposition ΔE_1 and ΔE_2 of particles traversing the detectors and were recorded. In the two dimensional spectrum of ΔT versus $\Delta E_1+\Delta E_2$, fission events were well separated from elastically scattered projectile-target events.
Fission events occurring after complete transfer of the projectile momentum to the composite system (full momentum transfer (FMT) fission) are separated from those fission events following nuclear transfer. These latter events occur when fissile targets like ^{238}U are irradiated. Figure 2 shows the folding angle distributions for fission fragments produced in the ^{30}Si +^{238}U reaction. The FMT fissions are located around θ_{fold} =148^o at the incident energy of E_{lab} =179.0 MeV and around θ_{fold} = 150^o at the lowest energy 140.8 MeV. Fission following nucleon transfer has a larger folding angle than the FMT fission in the high energy region of E_{lab}= 179.0 MeV, as seen in the tail on the spectra which extends over θ_{fold} =160^o. In the low energy region, nucleon transfer fission is observed with a smaller folding angle of θ_{fold} =120^o - 140^o than the FMT fission. These trends are explained by the angular dependence of the transfer reactions, which preferentially occur at grazing angles. The FMT fission fragments were separated from the nuclear transfer fission on the (θ_{fold}, Φ_{sum}) plane, and used for the analysis.

Evaporation residue measurement
Measurements of ER cross sections were carried out in the reactions of ^{30}Si +^{238}U and ^{34}S +^{238}U. The experiments were performed at the linear accelerator UNILAC and the velocity filter SHIP at GSI in Darmstadt. The SHIP set-up was essentially the same as described in [2]. The ^{30}Si beam was extracted from a 14 GHz ECR ion source using isotopically enriched material, ^{30}SiO (99.5% isotopic enrichment). A $^{34}SO_2$ gas with a 99 % isotopic enrichment was used to extract the ^{34}S beam. Average beam intensities at the target position were typically 0.7-1.0 *particle*-μA for ^{30}Si and 2.0 - 2.5 *particle*-μA for ^{34}S. The beam had a pulse structure of 5.0 ms width at 50 Hz repetition frequency. Details of the experiments are described in [7,8].
For the ^{30}Si +^{238}U run, the uranium targets were prepared by evaporation of isotopically depleted $^{238}UF_4$ and condensation on a carbon backing. In the experiment of ^{34}S+^{238}U, the targets were prepared by sputtering the depleted ^{238}U metal on a carbon backing.
The efficiency of SHIP was determined using a Monte Carlo calculation. We obtained a value of 11% and 15% for ^{30}Si+^{238}U and ^{34}S+^{238}U, respectively.
In the focal plane of the SHIP, ERs and their subsequent α decay and/or spontaneous fission (sf) were detected by a position sensitive 16-strip Si PIPS detector (stop detector). The energy resolution for fully stopped α's was typically 25 - 26 keV (FWHM). Escaping α particles or a complementary fission fragments were detected by a 'box detector' which covered 85% of the area of the backward hemisphere. Timing detectors were located in front of the silicon detector array to distinguish signals from implanted ERs or background particles from radioactive decays in the stop detector. The correlated events is identified primarily based on a coincidence of the positions of implanted ER, subsequent α decays and/or sf.

Experimental results

In-beam fission measurement
The cross sections for the FMT fissions (σ_{fiss}) of ^{30}Si +^{238}U are shown in Figure 3 (a) as a function of the center-of-mass energy, $E_{c.m.}$, as well as an excitation energy of the compound nucleus, E^*. The cross section was obtained by fitting the fragment angular distribution in the center-of-mass angle to a function described in [9] and integrating the fitted curve over the solid angle. The fission cross section is almost equal to the capture cross section (σ_{cap}).
In order to see the effects of nuclear properties on the capture cross sections, we show in Figure 3 (a) the calculation using the coupled-channels code, CCDEGEN [10]. The dotted curve is the result without considering any collective properties or deformation of the target and projectile (one-dimensional barrier penetration model). The dashed curve is the result which takes into account the prolate deformation of ^{238}U with (β_2, β_4) = (0.275, 0.050) [11]. The calculation reproduces within the error the experimental data down to $E_{c.m.}$ = 129.0 MeV. The solid curve is the result additionally taking into account the coupling to the 3$^-$ state at 0.73 MeV in ^{238}U [12] (β_3 = 0.086 [13]), which reproduces the data at the lowest incident energy of 125.0 MeV. Low Coulomb barrier for the polar collisions, as marked in the upper part of

Figure 3, is the main reason for the enhancement of the capture cross section at the sub-barrier energies relative to the one-dimensional barrier penetration model.
The fission cross sections for $^{34}S + ^{238}U$ are shown in Figure 4 (a). The data are compared with the coupled-channels calculations. The assumptions given to draw the dotted and

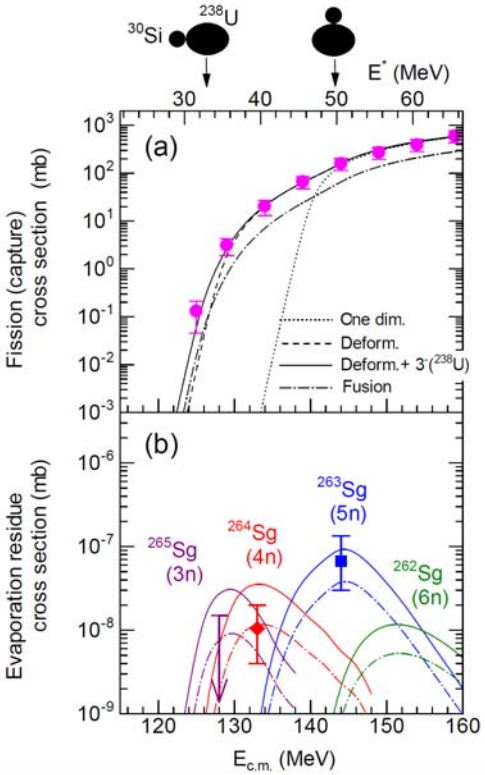

Figure 3. *(a) Cross sections for FMT fission and (b) evaporation residue cross sections for $^{30}Si+^{238}U$. Curves are the model calculations (see text).*

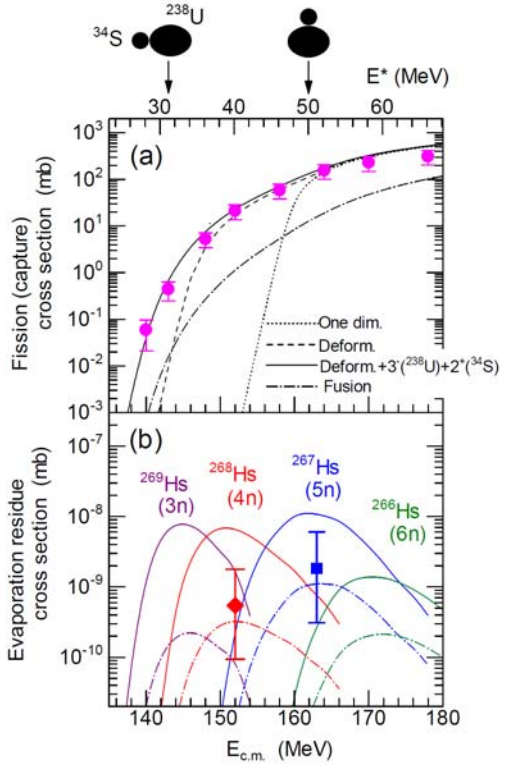

Figure 4. (*a) Cross sections for FMT fission and (b) evaporation residue cross sections for $^{34}S+^{238}U$. Curves are the model calculations (see text).*

dashed curves are the same as in Figure 3 (a). To reproduce the lowest data point at $E_{c.m.}$ =140.0 MeV, couplings to 3^- state (0.73 MeV) in ^{238}U and to the 2^+ state (2.13 MeV [12]) in ^{34}S (β_2 = 0.25 [14]) are taken into account (solid curve).
Figure 5 (a) shows the mass distributions for the FMT fissions in the $^{30}Si + ^{238}U$ reaction [15]. To draw the mass distribution, we assumed that the mass distributions do not depend on $\theta_{c.m.}$ The distributions are Gaussian with mass symmetry in the energy range from $E_{c.m.}$ =139.0 MeV to 154.0 MeV. The shape of the distributions, however, are different for the sub-barrier energies at $E_{c.m.}$=134.0 and 129.0 MeV. They have asymmetric component around A_L/A_H = 90 /178. The difference of the mass distribution at the lowest energy data is characterized also by the standard deviation σ_m as indicated in each panel of Figure 5 (a). The value increases from 28.1±1.0 u (139.0 MeV) to 37.5±1.0 u (134.0 MeV). Considering the measured ER cross sections Figure 3 (b), as discussed in the following, we conclude that the asymmetric fission channel originates from quasifission.
The mass distributions in the $^{34}S + ^{238}U$ reaction are shown in Figure 5 (b). At the highest energy of 170.0 MeV, the distribution is Gaussian with mass symmetry. The σ_m value of the spectrum, however, is far larger than the one for $^{30}Si + ^{238}U$. Toward the low incident energy, the asymmetric fission yield increases sharply around the mass asymmetry A_L= 68 and A_H= 204. The mass asymmetry corresponds to the fragments near the double-closed shell nuclei, ^{78}Ni and ^{132}Sn (see Figure 1).
A similar observation was made in the study of the reaction $^{36}S+^{238}U\rightarrow\ ^{274}Hs^*$ [6]. The phenomenon was interpreted by the effects of nuclear orientation on fusion and/or quasifission. At the sub-barrier energy, projectiles collide on the polar sides of the ^{238}U nucleus. In this case the reaction starts from a distant contact point with a large charge-center distance, which results in a larger quasifission probability than the reactions starting from the equatorial collisions (see Figure 1).

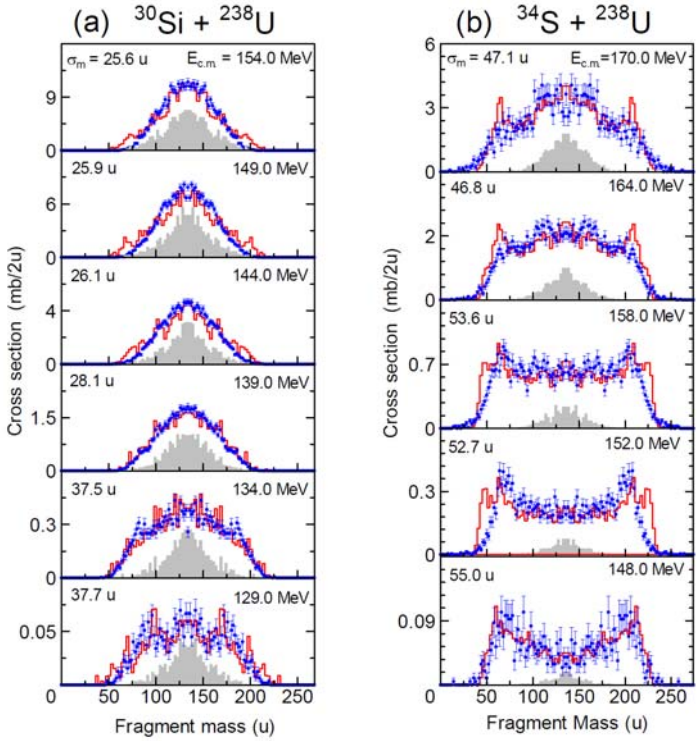

Figure 5. *Fragment mass distributions for FMT fissions of the reactions (a) ^{30}Si+ ^{238}U and (b) ^{34}S + ^{238}U. Histograms shows a model calculation. The calculated fusion-fission spectrum is shown by the filled area. Reaction energy in the center-of-mass system and the standard deviation σ_m of the measured spectrum are shown.*

Figure 6 shows the mass distributions in the reactions using different projectiles of ^{30}Si, ^{31}P, ^{36}S and ^{40}Ar. The excitation energy of a compound nucleus is shown in each section of the figure. For a fixed excitation energy, a yield for an asymmetric fission channel increases with projectile charge, showing that quasifission probability increases due to the larger Coulomb repulsive force in the reaction process. The enhanced quasifission yield toward the low incident energy are observed for all the reactions owing to the orientation effects.

In the reactions of ^{34}S+^{238}U (Figure 5 (b)), ^{36}S+^{238}U (Figure 6) and ^{40}Ar +^{238}U (Figure 6), the quasifission mass asymmetries are nearly the same, and centered around $A_L/A_H \approx 68/204$, 74 /200 and 76 /202, respectively. According to the mass asymmetry parameter $\alpha = (A_H - A_L) / (A_H + A_L)$ defined by the light (L) and heavy (H) fragment masses, they corresponds to 0.50, 0.46 and 0.45. These mass asymmetry are closely correlated to the fission channel formed by the shells near the double-closed shell nuclei, ^{78}Ni and ^{208}Pb (see Figure 1). This channel is the same as observed in reactions using heavier projectiles bombarded to actinide target nuclei [16], where the reactions of ^{48}Ca + ^{238}U,^{244}Pu,^{248}Cm produce asymmetric fission centered at $A_H \approx 210$ ($\alpha = 0.42 \sim 0.46$).

The observed mass asymmetry in the quasifission for ^{30}Si + ^{238}U is $\alpha = 0.33$ ($A_L/A_H \approx 90/178$). The value is significantly smaller than those obtained for ^{34}S,^{36}S, ^{40}Ar + ^{238}U. The asymmetric fission channel in the ^{31}P + ^{238}U reaction, $\alpha = 0.40$ ($A_L/A_H \approx 81/188$), also does not fit the shells of ^{78}Ni / ^{208}Pb. The potential energy landscape of ^{268}Sg produced by ^{30}Si + ^{238}U has almost the same structure as ^{274}Hs produced by ^{36}S + ^{238}U (see Figure 4 in [6]). The observation of the different mass asymmetry indicates the difference in the evolution of nuclear shape in quasifission.

Evaporation residue measurement

The measurement of ER cross sections in the fusion of ^{30}Si + ^{238}U was carried out from April 8 to May 1, 2006. We used three different beam energies of $E_{c.m.}$ = 144.0, 133.0 and 128.0 MeV, which correspond to the anticipated maximum cross sections of 5*n*-, 4*n*-, and 3*n*-evaporation channels. Details of the experimental results are described in [7].

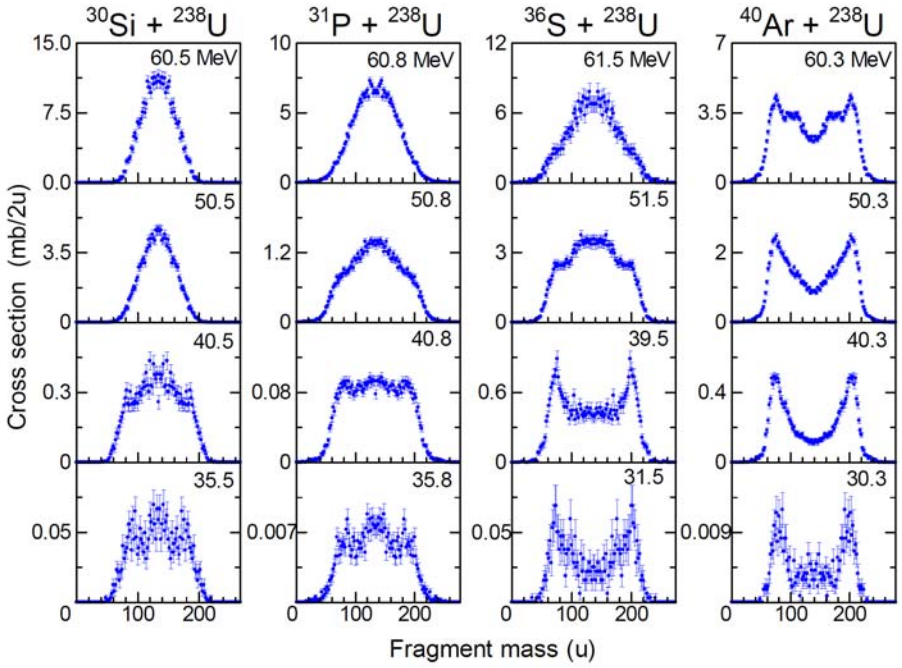

Figure 6. Fission fragment mass distributions in the reactions of ^{30}Si, ^{31}P, ^{36}S, ^{40}Ar + ^{238}U. The excitation energy E* of a compound nucleus is shown in each spectrum.

At 144.0 MeV, a beam dose of 1.8×10^{18} was accumulated. We observed three α-decay chains starting from ^{263}Sg (5*n*). We obtained the cross section of 67 ($^{+67}_{-37}$) pb. At the sub-barrier energy of $E_{c.m.}$=133.0 MeV, we observed four spontaneous fission events with a beam dose of 4.0×10^{18}. The lifetime of three sf events is similar and relatively short. The half-life was determined to be 120 ($^{+126}_{-44}$) ms from three sf events. The nucleus was assigned to the spontaneously fissioning isotope ^{264}Sg (4*n*). The cross section for the three ^{264}Sg sf events was 10($^{+10}_{-6}$) pb. At the lowest beam energy of 145.5 MeV, no decay events were measured with a beam dose of 1.7×10^{18}. An upper cross section limit was determined to be 15 pb at 68 % confidence level (one event would have had a cross section of 8.2 pb). Measured cross sections and/or the cross section limit are shown in Figure 3 (b).

Production of hassium isotopes in the fusion of ^{34}S+^{238}U was carried out from January 1 to February 8, 2009. Two different beam energies of $E_{c.m.}$ = 163.0 and 152.0 MeV were chosen, corresponding to the maximum 5*n*- and 4*n*-evaporation cross sections. Details of the experimental results are described in [8].

At $E_{c.m.}$= 163.0 MeV, a beam dose of 4.8×10^{18} was accumulated. We observed one decay chain, which we assign to the production of ^{267}Hs as shown in Figure 7. The cross section for ^{267}Hs was determined to be 1.8($^{+4.2}_{-1.5}$) pb as plotted in Figure 3 (b). The value agrees with 2.5 pb measured in [17] . At the sub-barrier energy of $E_{c.m.}$ =152.0 MeV, a beam dose of 1.2×10^{19} was accumulated. In this irradiation, one decay chain was identified, as shown in Figure 7. We assigned the decay chain starting from the new isotope ^{268}Hs. The 9749-keV α-decay was followed by the sf of ^{264}Sg which was produced directly in the 4*n*-evaporation in fusion of ^{30}Si +^{238}U [7]. The obtained cross section 0.54 ($^{+1.3}_{-0.45}$) pb is shown in Figure 4 (b).

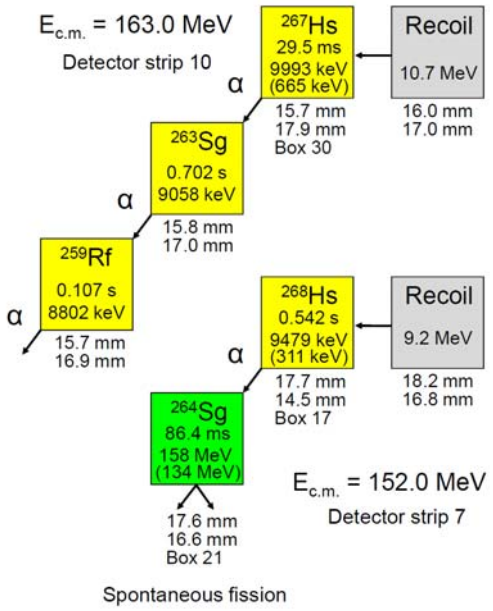

Figure 7. *Decay chains observed in the ^{34}S + ^{238}U reaction.*

Discussions

For a quantitative analysis of the mass distributions, we performed a model calculation combining the coupled channels method and a dynamical description of the reaction based on the three-dimensional Langevin equation [18]. The dynamical calculation based on the Monte Carlo method was used for describing the reaction paths in the potential energy landscape. The two-center shell model was used to calculated the potential energy of a nucleus whose shape is defined by z (charge center distance), δ (deformation) and α (mass asymmetry). The deformation of the reaction partners and their orientation in the reaction plane was considered. The coupled channels method was first used to compute the penetration probability of the Coulomb barrier for a fixed orientation angle. The dynamical calculation was then started from the shape at contact configuration for each orientation. Fusion is defined as the case when the trajectory enters inside the local energy minimum corresponding to the compound nucleus, whereas quasifission is defined as disintegration without reaching the minimum.

The calculated distributions of FMT fragments for ^{30}Si +^{238}U are represented by the histograms in Figure 5 (a). The model reproduces the general shape of the distribution as well as the feature of the appearance of the asymmetric fission channel and increase of the standard deviation σ_m at the sub-barrier energies. The calculated fusion-fission events in this model are shown by the filled areas in Figure 5 (a). It is Gaussian with mass symmetry, and the standard deviation of the spectrum σ_m is nearly constant with 21 ~25 u in the entire energy rage. The value is significantly smaller than 37 ~38 u for the measured distributions at the sub-barrier energies of 129.0 and 134.0 MeV. Furthermore the calculated fusion-fission spectrum does not show any asymmetric fission channels. The results support the observed asymmetric fission to be quasifission. In the calculation, we can determine the fusion probability P_{fus} as the ratio of fusion-fission events to the FMT fission events. By multiplying the P_{fus} to capture cross section (σ_{cap}), a fusion cross sectionσ_{fus} is obtained. The results for ^{30}Si +^{238}U are shown by the dash-dotted curve in Figure 3 (a).

The same calculation was made in the ^{34}S +^{238}U reaction as shown in Figure 5 (b). The results reproduce the measured distribution, especially transition from symmetric to asymmetric mass distributions with different incident energy is well reproduced. The σ_m value in the calculated fusion-fission spectrum is 16 ~ 20 u, which is nearly the same as the ^{30}Si + ^{238}U reaction.

The value is about factor two less than those for the measured distribution. A remarkable difference between ^{30}Si +^{238}U and ^{34}S +^{238}U reactions is the fusion-fission yield among the FMT fissions. Even in the symmetric mass region, the yield drops significantly in the case of ^{34}S projectile. The fusion cross sections σ_{fus} for ^{34}S +^{238}U are shown in Figure 4 (a) by the dash-dotted curve.

To see if the above model is appropriate to estimate the fusion probability, P_{fus}, a statistical model code HIVAP [19] was used to calculate the ER cross sections by inputting the fusion cross sections for ^{30}Si +^{238}U (dash-dotted curve in Figure 3 (a)), and the results are compared them the experimental data. The calculation reproduces the cross sections for ^{263,264}Sg within errors as well as the cross section limit for ^{265}Sg. Similarly, the model can account for the cross sections for ^{267,268}Hs produced in the fusion of ^{34}S +^{238}U as shown in Figure 4 (b). If we assume all the fragments were arising from the compound nucleus fission, the ER cross sections would have values shown by the solid curves in Figure 3 (b) or Figure 4 (b). Apparently, this assumption contradicts the cross sections of ^{264,265}Sg and ^{267,268}Hs.

It is shown in the calculated ER cross sections for ^{34}S+ ^{238}U in Figure 4 (b) that the probability for quasifission after the capture process becomes larger toward the low bombarding energy, demonstrating the orientation effects. It is consistent with the experimental data of ^{268}Hs and ^{267}Hs.

In spite of the reduced fusion probability to produce SHN using heavier projectiles, ^{34}S, our cross section calculations reveal a considerable yield for producing relatively neutron rich nuclei at energies below the Bass barrier, when targets of deformed actinide nuclei are used. Figure 4 (b) shows the cross sections for the 3*n* evaporation channel, ^{269}Hs. The cross section is expected to be comparable to the one for the 4*n* evaporation residue, ^{268}Hs. By applying fusion reaction at the energy below the Bass barrier, the new isotopes $^{274\text{-}277}$Ds (N=164 -167) could be produced in the reactions ^{34,36}S + ^{244}Pu in 3*n* - 4*n* evaporation channels or $^{278\text{-}281}$Cn (N =166 -169) in ^{34,36}S + ^{248}Cm reactions also in 3*n* - 4*n* channels. Alpha decay from these nuclei would populate isotopes of hassium and seaborgium, from which the isotopes ^{272,273}Hs (N =164 and 165) and ^{268,269}Sg (N =162 and 163) are not yet known.

Similarly, isotopes of odd elements could be produced in reactions with ^{34,36}S beams and a ^{243}Am target. The ERs and their daughter nuclei includes new isotopes of ^{273,275,276}Rg (N =162, 164 and 165) and ^{269,271,272}Mt (N =160, 162 and 163).

Conclusions

The mass distributions for FMT fission fragments in the reactions of ^{30}Si,^{31}P,^{34,36}S,^{40}Ar +^{238}U were measured at bombarding energies around the Coulomb barrier. The probability of asymmetric fission increases at the sub-barrier energy. The phenomenon is interpreted as the enhanced quasifission probability, which represents orientation effects on fusion and/or quasifission. The ER cross sections were measured in the reactions of ^{30}Si + ^{238}U and ^{34}S + ^{238}U to obtain information on fusion probability P_{fus}. The P_{fus} decreased significantly for the latter reaction, thus showing the enhanced quasifission probability. The conclusion was consistent with the theoretical model calculation which is based on the Langevin equation and takes into account the orientation of the deformed nucleus ^{238}U, in which fusion-fission and quasifission are separately determined. In spite of the significantly low fusion probability at the sub-barrier energy, there are fusion probabilities large enough to produce 3*n*- and 4*n*-evaporation residues. In the combination between ^{34,36}S projectile and several actinide target nuclei, totally 18 new isotopes could be produced as ER or α-decay descendants. They are located in the region of elements from seaborgium to copernicium with neutron numbers N >162 so that the gap between the known nuclei produced in cold and hot fusion reactions could be filled.

Acknowledgements
The investigations were accomplished with the collaborators of H. Ikezoe, S. Mitsuoka, Y. Nagame, I. Nishinaka, K. Tsukada, K. Tsuruta (JAEA), S.Hofmann, D. Ackermann, V.F. Comas, Ch.E. Düllmann, S. Heinz, J.A. Heredia, F.P. Hessberger, J. Khuyagbaatar, B. Kindler, I. Kojouharov, P. Kuusiniemi, B. Lommel, R. Mann, M. Mazzocco, M. Schädel, H.J. Schött, B.~Sulignano (GSI), Y. Aritomo (JAEA,FLNR), K. Hagino, K. Hirose, T. Ohtsuki (Tohoku University), A.G. Popeko, A. Svirikhin, A.V. Yeremin(FLNR), S. Antalic, S. Saro (Comenius University), A. Gorshkov, R. Graeger, A. Türler, A. Yakushev (TU München),
Y. Watanabe (KEK), Z.Gan (IMP). We are grateful to W. Hartmann, J. Steiner, H.G. Burkhard, and J. Maurer of GSI.
We would like to thank the UNILAC staff and the crew of the JAEA tandem accelerator facility for preparation and operation of the beams. This work was supported by a Grant-in-Aid for Scientific Research of the Japan Society for the Promotion of Science.

References

[1] Yu.Ts. Oganessian, J. Phys. G 34, R165 (2007).
[2] S. Hofmann and G. Münzenberg, Rev. Mod. Phys. 72, 733 (2000).
[3] K. Morita et al., J. Phys. Soc. Jpn. 73, 1738 (2004).
[4] V. Zagrebaev and W. Greiner, J. Phys. G, 31, 825 (2005).
[5] S. Hofmann et al., Eur. Phys. J. A 32, 251 (2007).
[6] K. Nishio et al., Phys. Rev. C 77, 064607 (2008).
[7] K. Nishio et al., Eur. Phys. J. A 29, 281 (2006).
[8] K. Nishio et al., Phys. Rev. C, 82 024611 (2010).
[9] R. Vandenbosch and J.R. Huizenga, Nuclear Fission (Academic Press, New York, 1973).
[10] Modified version of the CCFULL code, K. Hagino et al., Computer Phys. Comm. 123, 143 (1999)
[11] K. Nishio et al., Phys. Rev. Lett. 93, 162701 (2004).
[12] R.B. Firestone et al., Table of Isotopes Eighth Edition (JohnWiley & Sons, Inc.)
[13] R.H. Spear et al., At. Data Nucl. Data Tables, 42, 55 (1989).
[14] S. Raman et al., At. Data Nucl. Data Tables, 36, 1 (1987).
[15] K. Nishio et al., Phys. Rev. C 82, 044604 (2010).
[16] M.G. Itkis et al., Nucl. Phys. A787, 150c (2007).
[17] Yu.A. Lazarev et al., Phys. Rev. Lett. 75, 1903 (1995).
[18] Calculation is based on a model in Y.Aritomo, Phys. Rev. C, 80, 064604 (2009), but effects of nuclear orientaion was taken into account.
[19] W. Reisdorf and M. Schädel, Z. Phys. A 343, 47 (1992).

Fission γ-ray data measurements – a challenging endeavour

S. Oberstedt[1)], T. Belgya[2)], R. Billnert[1,3,4)], R. Borcea[1)], A. Göök[4,5)], F.-J. Hambsch[1)], J. Karlsson[4)], Z. Kis[2)], X. Ledoux[6)], J.-G. Marmouget[6)], T. Martinez[7)], A. Oberstedt[3,4)], L. Szentmiklosi[2)], K. Takács[2)]

1) European Commission, Joint Research Centre, Institute for Reference Materials and Measurements, Retieseweg 111, 2440 Geel, Belgium
2) Institute of Isotopes, Hungarian Academy of Sciences, H-1525 Budapest
3) Fundamental Fysik - Chalmers Tekniska Högskola, S-41296 Göteborg
4) Akademin för Naturvetenskap och Teknik, Örebro Universitet, S-70182 Örebro
5) Institut für Kernphysik, Technische Universität Darmstadt, D-64289 Darmstadt
6) CEA/DAM Ile de France, F-91297 Arpajon
7) Innovation Group Department of Energy, CIEMAT, E-28040 Madrid

stephan.oberstedt@ec.europa.eu

Abstract: The successful modelling of the fission process strongly depends on a good understanding of the particular mechanism of scission, the mass fragmentation and partition of excitation energy. Experimental observables are fission-fragment properties like mass- and energy-distributions, as well as prompt neutron and γ-ray multiplicities and emission spectra. Prompt fission neutrons and γ-rays represent very powerful probes of the nuclear fission process near the scission point. They can be used to study the configurations of fission fragments very close to the scission point and to better understand how the total excitation energy available in the fissioning system gets transferred to intrinsic excitation in the fragments. Average observables as e.g. the average prompt fission-neutron and γ-ray spectra or their corresponding multiplicities are not sufficient to provide clear answers to remaining open fundamental questions about the fission process. Those quantities should preferably be known as a function of fission-fragment mass and excitation energy. This paper aims at discussing today's and future activities on measurements of γ-ray data with a particular emphasis on the recent implementation of state-of-the art fission-fragment and γ-ray detectors.

Introduction (the past)

In nuclear fission pairs of fission fragments with different mass and kinetic energy are produced [1]. This process is accompanied by prompt neutrons and γ-rays, emitted from the highly excited fission fragments (FF). Experimental observables are FF properties like mass- and energy-distributions, as well as prompt neutron and γ-ray multiplicities and emission spectra. Prompt fission neutrons and γ-rays represent very powerful probes of the nuclear fission process near scission. They can be used to study the configuration of fission fragments very close to the scission point and may help to better understand how the total excitation energy available in the fissioning system gets transferred into intrinsic excitation in the fragments. Average observables as e.g. the average prompt fission-neutron and γ-ray spectra or their corresponding multiplicities are not sufficient to provide clear answers to remaining open fundamental questions about the fission process. Those quantities, however, are needed in attempts to fully describe the fission process and should, therefore, be known as a function of fission-fragment mass and excitation energy as well.

About ten percent of the total energy release in the core of a standard nuclear reactor is accounted for by the γ-ray energy released in fission, of which 40% or 8 MeV result from the prompt γ-decay of fission products [2]. Although the characteristics of the γ-ray emission, e. g. multiplicity, total energy and energy distribution, is fairly well known for neutron capture and inelastic neutron scattering, fission γ-rays are the major source of uncertainty in the modelling of γ-heating. Since four out of six nuclear systems identified by the Generation-IV international forum are fast reactors, a very innovative core design is required in order to respond to the high performance expected of those future systems. One particular challenge in modelling new

generation reactor neutron kinetics is to calculate the γ-heat deposition in e. g. steel and ceramics reflectors without UO_2 blankets. According to Ref. [3] those modern designs require γ-heating to be known with an uncertainty as low as 7.5% (1σ). The comparison of various benchmark experiments with calculated γ-heating shows a systematic underestimate ranging from 10 to 28% for the main fuel isotopes ^{235}U and ^{239}Pu. This is attributed to deficiencies in γ-ray production data in evaluated nuclear data files [4].
Relevant data found in modern nuclear-data libraries all date back to experiments performed in the early 1970's [5-7] and, experimental γ-ray data correlated with fission-fragment mass and kinetic energy were obtained in the 1960s and 1970s for ^{235}U(n_{th}, f) [8,9] and ^{252}Cf(SF) [10-12] and are reviewed in Ref. [13]. In a recent modelling exercise of neutron emission from fission fragments by means of a Monte-Carlo approach [14] the authors achieved a reasonably good description of the average γ-energy released in fission, but they were unable to reproduce the experimentally obtained dependence as a function of the fission fragment mass.
In all those experiments NaI scintillation detectors were used as γ-ray spectrometers with an ionization chamber as fission trigger. However, NaI detectors are today proven to be inferior with respect to energy and timing resolution as well as to efficiency. Therefore, requests for new measurements on prompt γ-ray emission in the reactions ^{235}U(n, f) and ^{239}Pu(n, f) have been formulated and included in the Nuclear Data High Priority Request List of the Nuclear Energy Agency (NEA, Req. ID: H3, H4) [15,16].
In the following we report on on-going experimental activities within our collaboration.

Feasibility study on fission γ-ray measurements (the present)

In order to take up the challenge and to arrive at new and precise correlated γ-ray emission data, the problem of efficient neutron/γ-ray separation has to be solved. This is usually achieved by means of the time-of-flight and the pulse-shape discrimination techniques, which requires excellent timing resolution of the measurement system. Additionally, the measurement requires an instrument with high detection efficiency to assess correlations with fission-fragment masses and total kinetic energies. A promising step towards better data might be achieved by using the recently developed cerium-doped lanthanum-chloride ($LaCl_3$:Ce) crystal scintillation detectors, which have shown to provide a timing resolution better than 500 ps [17,18] together with a more than 40% better energy resolution compared to NaI, i.e. less than 4% (FWHM) compared to 6.5% at 662 keV (^{137}Cs) [17,19].
Below we present the results of the characterisation of a coaxial 1.5" × 1.5" (38 mm in diameter and 38 mm in thickness) $LaCl_3$:Ce detector in terms of energy calibration and resolution, linearity, intrinsic efficiency, timing resolution and intrinsic radioactivity. Then, we show results from a first in-situ spectral measurement of prompt fission γ-rays with this detector and discuss the discrimination of prompt fission γ-rays from prompt neutrons.

Detector characterisation

The three $LaCl_3$:Ce detectors were produced by the company SCIONIX [20]. Details about the detectors and their characterisation may be found elsewhere [19]. Here, we present only the essential results, i.e. energy resolution, intrinsic peak efficiency and intrinsic timing resolution, and recall details of the set-up where necessary for understanding the present work.
In the left part of Fig. 1 the energy resolution (FWHM in %) of detector SEB 347 is shown for the energy range from 80 keV to 7000 keV. As indicated by the straight line, the resolution follows the expected $E^{-1/2}$ dependence. A comparison with a NaI(Tl) detector of same size shows a 40% better energy resolution. At the same time the intrinsic peak efficiency for a $LaCl_3$:Ce detector turned out to be 52% larger [19].

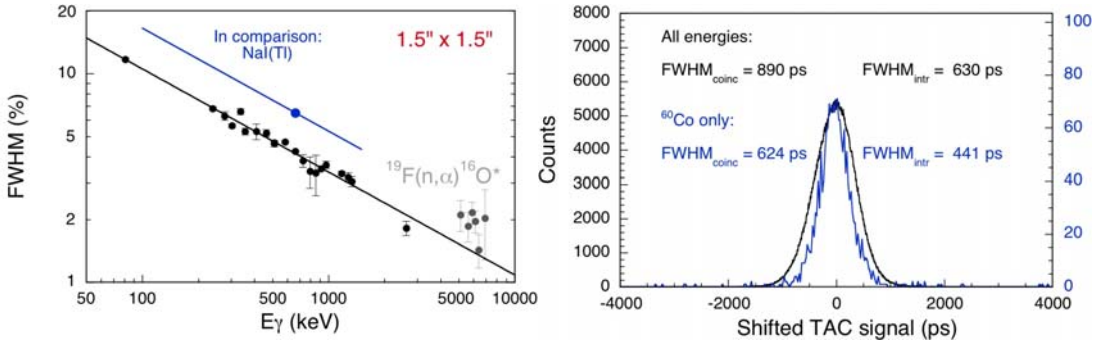

Figure 1. *Left: Energy resolution as a function of γ-ray energy as FWHM in % for the $LaCl_3$:Ce detector SEB347 (black dots) compared to the resolution of a NaI(Tl) of same size (blue dot) [19]. The lines indicate the expected $E^{-1/2}$ dependence. Right: Coincidence timing resolution for two similar $LaCl_3$:Ce detectors (SEB 345 and 347) for γ-rays of all energies (black) and with a threshold set just below 1173 keV.*

In the right part of Fig. 1 the coincidence timing spectra of two identical $LaCl_3$:Ce detectors are shown. In one case the spectrum was taken over the whole γ-energy range (black line, left scale). In the other case an energy threshold was set just below the ^{60}Co full peak energy at 1173 keV leading to an intrinsic timing resolution of 441 ps. The overall intrinsic timing resolution of 630 ps leads to an improvement of at least a factor of 5 compared to the NaI(Tl) detectors employed in the past. From References [21,22] we may expect that $LaBr_3$:Ce detectors possess an even better timing resolution by about 50%. Also the energy resolution of $LaBr_3$:Ce detectors is better by 25% [23]. A characterisation of those detectors is on-going, but below a first application to spectral prompt fission γ-ray measurements will be reported about.

For supplying the fission trigger in our experimental set-up artificial diamond material was chosen. Detectors made from diamond are known to be radiation resistant and to have an intrinsic timing resolution below 50 ps for relativistic heavy ions [24,25]. As depicted in the left part of Fig. 2, a fission-fragment time-of-flight distribution from the spontaneous fission of ^{252}Cf is shown, obtained with two identical artificial diamond detectors used for the start and stop signals. From a Monte-Carlo simulation, with the coincidence timing resolution as free parameter, the intrinsic timing resolution for fission-fragments was inferred to be better than 150 ps. Details about the characterisation of the diamond detectors may be found in Ref. [26]. It is evident that diamond-based fission fragment detectors are well suited for our contemplated fission γ-ray measurements, because they match the excellent timing resolution of our lanthanum-chloride detectors.

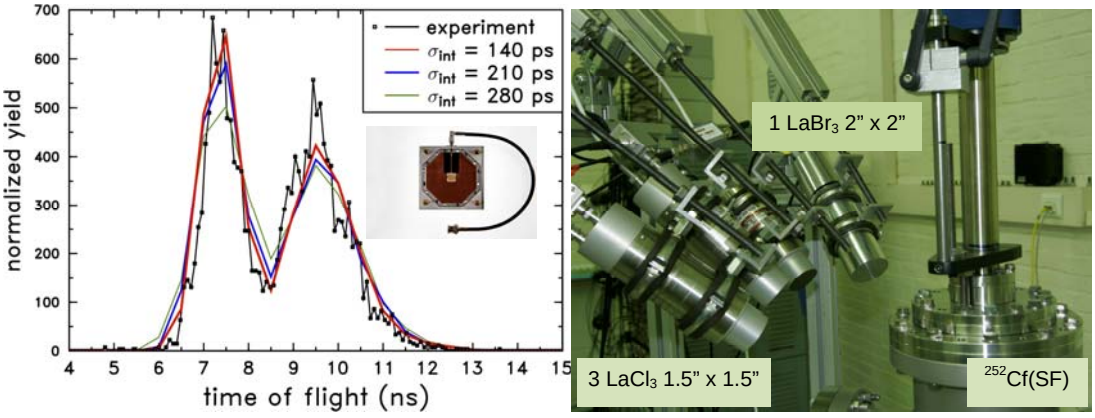

Figure 2. *Left: Time-of-flight spectrum of fission fragments taken with two identical detectors made from artificial poly-crystalline diamonds (dots) [26]; the lines represent Monte-Carlo simulations assuming different intrinsic timing resolutions, σ_{int}. Right: detector configuration as used for the first spectral fission γ-ray measurements; the detectors are placed 30 cm away from the fission source.*

Since poly-crystalline diamond detectors are used in the single (v, E) version of the VERDI fission-fragment spectrometer [26], we coupled a series of lanthanum-halide detectors to it at a distance of 30 cm from the fission source. A photo of such an experimental set-up is shown in the right part of Fig. 2.

First in-situ test measurements

We conducted a first test measurement with ^{235}U as target nucleus with the cold neutron beam of the Budapest Research Reactor, where we employed different lanthanum halide detectors. The experiment was performed in parallel with a feasibility study of the fission-fragment spectrometer VERDI. A ^{235}U sample of 113 μg/cm^2 was placed on top of a 1 cm^2 large poly-crystalline artificial diamond detector at the centre position of VERDI. The scintillation detectors were placed as shown in the right part of Fig. 2, but one of the 1.5" ×1.5" $LaCl_3$ detectors was replaced by a 3" × 3" $LaCl_3$ detector, which was produced by Saint Gobain [27]. In the following part of the report we focus on presenting data taken with this large detector. Due to the very high detection efficiency of this detector and the enhanced intrinsic activity from the radioactive isotope ^{138}La, which is proportional to the crystal volume, we had to apply a low-energy threshold around 400 keV as visible in Fig. 3.

In a two-dimensional matrix (time-of-flight versus γ-energy) three different time-of-flight (TOF) regions may be distinguished. An example, applied to another measurement, is given further below. The first TOF region closest to the instant of fission contains prompt fission γ-rays as well as random coincidences due to the intrinsic activity and thermal-neutron induced background reactions. This spectrum is quasi-continuous and shows almost no structure. The second, adjacent region shows single γ-lines corresponding to the decay of spin isomers in the fission fragments with half-lives of $T_{1/2} = \mathcal{O}(1\text{ ns})$ and from inelastic scattering reactions of prompt fission neutrons in the detector or in the construction materials. The third region, finally, contains only random coincidences with natural radioactivity and the intrinsic activity of the detector.

From an energy calibration, performed directly after the measurement campaign, we are able to identify activation products, here ^{56}Mn from the ^{56}Fe(n, p) reaction, induced by fission neutrons. Those peaks appear also in the third region of the TOF spectrum, which allows an efficient correction of the prompt fission γ-ray spectrum. In the left part of Fig. 3 we show a calibration spectrum taken after irradiation, which shows, beside the calibration sources ^{60}Co and ^{207}Bi, the decay of the activation product ^{56}Mn. In the right part of Fig. 3, which corresponds to a cut in the third region of the TOF spectrum, the same lines of the ^{56}Mn decay may be identified. More details about the measurement and the analysis of the γ-ray spectra are given in Ref. [28].

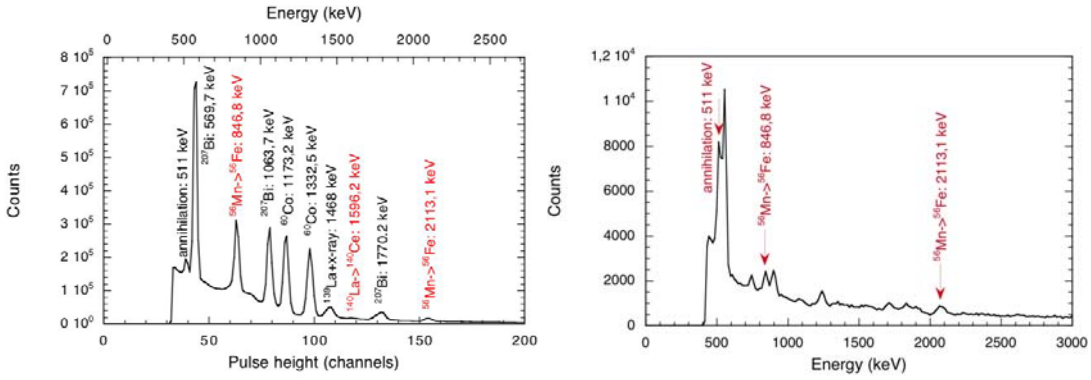

Figure 3. *Left: Calibration spectrum taken after the spectral measurement of prompt fission γ-rays (see text); right: γ-ray spectrum for a time-of-flight region that corresponds to region 3 as defined in the text. Note that the γ-peak from the decay of the fast-neutron activation product ^{56}Mn appears in both spectra.*

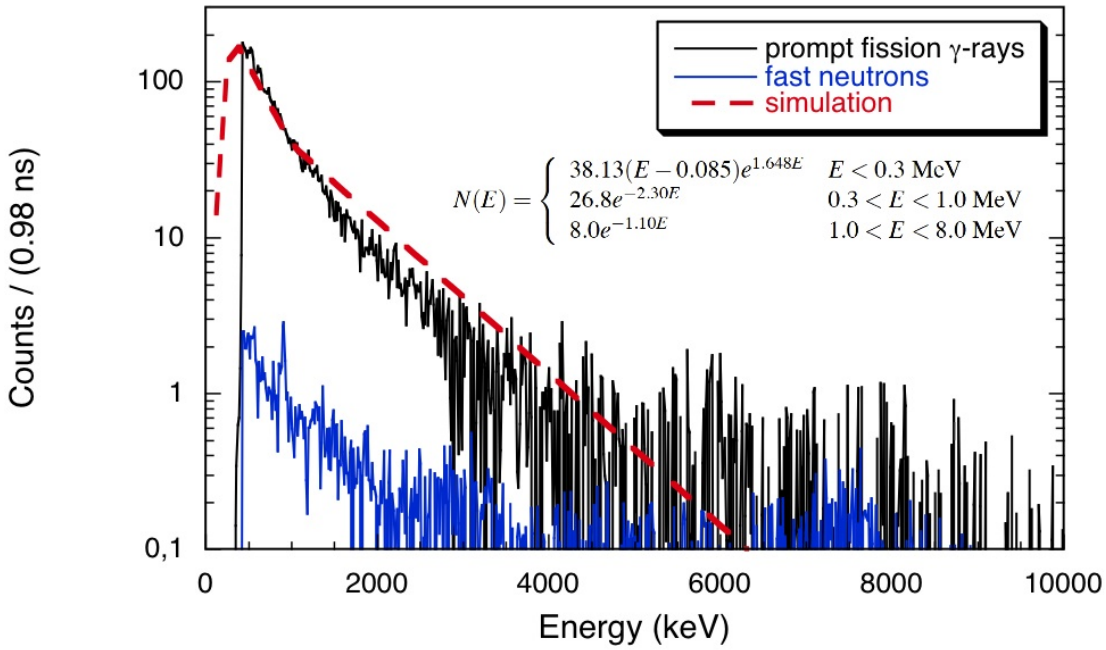

Figure 4. *Normalized prompt fission γ-ray spectrum for a 3" x 3" $LaCl_3$:Ce detector taken from the reaction $^{235}U(n_{th}, f)$ (black line) and γ-rays produced in fast-neutron reaction in construction materials (blue line). All spectra are background corrected, but no response function was applied yet. The dashed line corresponds to systematics established by Verbeke et al. [29], based on earlier experimental data [30], and serves to guide the eye.*

Already in this application the choice of lanthanum-halide detectors turned out to be successful. Firstly, the very good timing resolution permits clean distinction of the different reactions taking place as a function of time after the occurrence of fission. Secondly, the good energy resolution leads to a reasonable identification of individual reactions induced by the different neutron source, at the same time allowing online monitoring of the instrument stability.

With these tools at hand we corrected the γ-spectra taken for the first two TOF regions for possible contributions from background reactions. The resulting net spectra are shown in Fig. 4. The blue spectrum contains only events from fast-neutron induced reactions and isomeric decay of fission fragments. Prompt fission γ-rays are indicated by the black histogram reaching up to 10 MeV in energy. However, we have to underline, that the shown spectra are not yet corrected for the energy dependent response of the detector. Still, we compare the results from our measurements with a systematic trend established by Verbeke et al. [29] on the basis of earlier experimental data [30], indicated by the dashed line together with the mathematical description in Fig. 4. The comparison between our data and the systematic trend, albeit preliminary, indicates already the positive features of the new measurement set-up and demonstrates the capability of lanthanum-halide detectors for prompt fission γ-ray measurements.

In a following campaign we measured γ-rays from the reaction $^{252}Cf(SF)$ with a 2"× 2" $LaBr_3$:Ce detector. In the left part of Fig. 5 we show the prompt fission γ-ray spectrum (black), together with the spectrum from fast-neutron induced reactions (blue), which both may be compared with those in Fig. 4. The green spectrum represents the background, where the intrinsic activity appears mainly around 800 and 1460 keV as well as between 1800 and 2600 keV, which is typical for lanthanum-halide detectors [22]. An even more interesting feature is visible in the right part of Fig. 5. In a two-dimensional presentation of time-of-flight vs. pulse height many (vertical) γ-lines are observed. Since their time distributions all have in common that they start right after the detection of prompt fission γ-rays, i.e. below the dashed line, their origin may be attributed to inelastic neutron scattering in the detector or in structural materials of the measurement cabin. Moreover, depending on neutron energy, the time distribution for a given de-excitation ends, where the corresponding time-of-flight of a neutron is in accordance with its kinetic energy. This is indicated by the dotted line in the right part of Fig. 5, where also two examples are given for the γ-decay of the first excited state of ^{81}Br (276 keV) and ^{56}Fe (847 keV),

respectively. It reflects the fact that the minimum kinetic energy of the neutron necessary for a certain excitation is equal to the excitation energy.

We observe, that due to the excellent timing resolution neutrons with energies up to 18 MeV may easily being separated from prompt fission γ-rays and that neutron spectrometric data may be obtained as well. This leaves neutrons as observables during fission γ-ray measurements rather than as an unwanted background.

Conclusions (the future)

In this paper we have presented a new set-up for measuring fission γ-rays, which will allow assessing their emission characteristics as a function of fission fragment mass and kinetic energy. The new lanthanum-halide scintillation detectors fulfil the requirements set out for measuring prompt fission γ-rays with respect to energy resolution, intrinsic peak efficiency and timing resolution. The by 40% improved energy resolution enables the distinction of the origin of a detected γ-ray, as it may be from fission fragment de-excitation, inelastic prompt fission-neutron scattering as well as neutron capture. The excellent timing resolution, in conjunction with fission detectors based on artificial diamond, allows almost perfect separation of prompt fission neutrons from γ-rays already at short flight paths. The influence of the, in some cases, considerable intrinsic radioactivity of the detector crystals is manageable, when a coincidence condition is applied. The analysis of the time distribution of each γ-line produced in (n, n') reactions leaves prompt fission neutrons as a valuable observable rather than as unwanted background. This feature of lanthanum-halide detectors will be subject of future investigations.
We expect further improvement from the experimentalist's point of view when single-crystal diamonds will be available at reasonable size (total area of the order of 1 cm^2). Then fission-fragment spectrometry will become possible with reasonable mass resolution, i.e. comparable to the one obtainable with ionization chambers. The expected compact geometry will then allow measuring correlations between spectral shape and multiplicity of prompt fission γ-rays and fission-fragment excitation energy within reasonable measurement times. We plan first correlation measurements in the second half of 2011.

Acknowledgements
This work was supported by the EFNUDAT programme of the European Commission (agreement number 31027) and NAP VENEUS05 (agreement number OMFB 00184/2006).

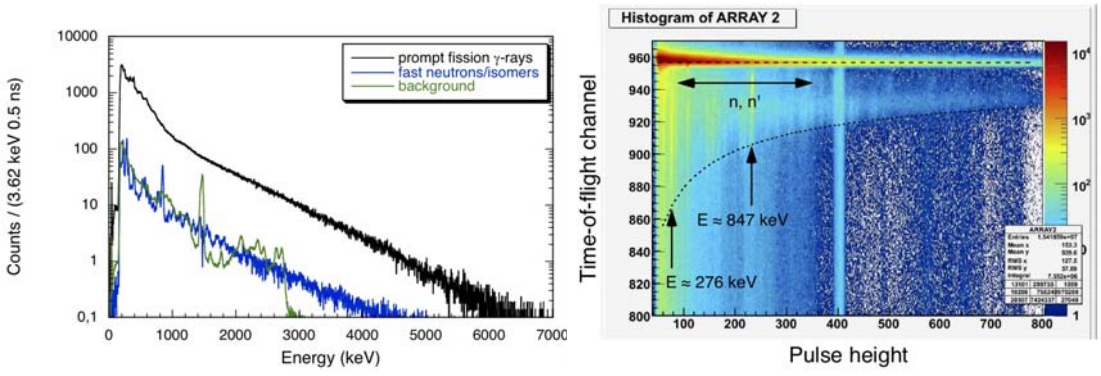

Figure 5. Left: Normalized prompt fission γ-ray spectrum taken from the reaction ^{252}Cf(SF) (black line), γ-rays produced in fast-neutron reactions in construction materials (blue line) and background spectrum (green line); the first two spectra are background corrected, but no response function was applied yet. Right: Distribution of time-of-flight (TOF) vs. pulse height. The fission γ-rays are represented by a horizontal area around TOF channel 960 (dashed line), while the vertical lines represent γ-rays from reactions induced by prompt fission neutrons. The dotted line connects the points of neutron TOF versus energy, which indicates the minimum energy γ-ray that can be induced by inelastic scattering of a neutron of a certain energy (see text for details).

References

[1] The Nuclear Fission Process, editor C. Wagemans, CRC Press, ISBN 0-8493-5434-X (1991)
[2] K. S. Krane, Introductory Nuclear Physics, John Wiley & Sons, ISBN 0-471-80553-X (1987)
[3] G. Rimpault, A. Courcelle and D. Blanchet, Comment to the HPRL: ID H.3 and H.4
[4] G. Rimpault, Proc. Workshop on Nuclear Data Needs for Generation IV, April 2005 (Editor: P. Rullhusen) Antwerp, Belgium, World Scientific, ISBN 981-256-830-1 (2006) 46
[5] R. W. Peelle and F. C. Maienschein, Phys. Rev. C3 (1971) 373
[6] F. Pleasonton, R. L. Ferguson and H. W. Schmitt, Phys. Rev. C6 (1972) 1023
[7] V. V. Verbinski, H. Weber and R. E. Sund, Phys. Rev. C7 (1973) 1173
[8] H. Albinssona and L. Lindow, Internal Rep. AE-398 (1971)
[9] H. Albinsson, Internal Rep. AE-417 (1971)
[10] S. A. E. Johansson, Nucl. Phys. 60 (1964) 378
[11] W. John, J. J. Wesolowski, F. Guy, Phys. Lett. 30B (1969) 340
[12] H. Nifenecker, C. Signarbieux, M. Ribrag, J. Poitou, J. Matuszek, Nucl. Phys. A189 (1972) 285
[13] H. Nifenecker, IAEA-SM-174/207 (1973)
[14] S. Lemaire, P. Talou, T. Kawano, M. B. Chadwick, and D. G. Madland, Phys. Rev. C72, 024601 (2005)
[15] http://www.nea.fr/html/dbdata/hprl/hprlview.pl?ID=421
[16] http://www.nea.fr/html/dbdata/hprl/hprlview.pl?ID=422
[17] K. S. Shah, J. Glodo, M. Klugerman, L. Cirignano, W. W. Moses, S. E. Derenzo, M. J. Weber, Nucl. Instr. Meth. A 505 (2003) 76
[18] A. Iltis, M. R. Mayhugh, P. Menge, C. M. Rozsa, O. Selles, V. Solovyev, Nucl. Instr. Meth. A 563 (2006) 359
[19] A. Oberstedt, R. Billnert, J. Karlsson, S. Oberstedt,W. Geerts, and F.-J. Hambsch, in: A. Chatillon, H. Faust, G. Fioni, D. Goutte, and H. Goutte (Eds.), Fourth Int. Workshop on Nuclear Fission and Fission-Product Spectroscopy, AIP Conf. Proc., vol. 1175 (2009) 257
[20] SCIONIX Holland bv, P.O. Box 143, 3980 CC Bunnik, The Netherlands
[21] R. Nicolini, F. Camera, N. Blasi, S. Brambilla, R. Bassini, C. Boiano, A. Bracco, F.C.L. Crespi, O. Wieland, G. Benzoni, S. Leoni, B. Million, D. Montanari, A. Zalite, Nucl. Inst. Meth. A582 (2007) 554
[22] G. Anuil Kumar, I. Mazumdar, D. A. Gothe, Nucl. Inst. Meth. A610 (2009)
[23] B. D. Milbrath, B. J. Choate, J. E. Fast, W. K. Hensley, R. T. Kouzes, J. E. Schweppe, Nucl. Instr. Meth. A 572 (2007) 774
[24] E. Berdermann, K. Blasche, P. Moritz, H. Stelzer, B. Voss, Diamond and Related Materials 10 (2001) 1770-1777.
[25] M. Marinelli, E. Milani, A. Paoletti, A. Tucciarone, G. Verona Rinati, M. Angelone, M. Pillon, Nucl. Inst. Meth. A 476 (2002) 701-705.
[26] S. Oberstedt, R. Borcea, F.-J. Hambsch, Sh. Zeynalov, A. Oberstedt, A. Göök, T. Belgya, Z. Kis, L. Szentmiklosi, K. Takács, T. Martinez-Perez, Seminar on Fission, Het Pand, Gent, Belgium, Ed. C. Wagemenas, J. Wagemans, P. D'hondt, World ScientificISBN-13 978-981-4322-73-7 (2010) 207-213
[27] Saint Gobain, http://www.detectors.saint-gobain.com/
[28] A. Oberstedt, R. Billnert, A. Göök, J. Karlsson, S. Oberstedt, F.–J. Hambsch, R. Borcea, T. Martinez Perez, D. Cano-Ott, T. Belgya, Z. Kis, L. Szentmiklosi, and K. Takács, Final Scientific EFNUDAT Workshop, 30 August 2010 - 02 September 2010, CERN
[29] J. M. Verbeke, C. Hagmann, D. Wright, UCRL-AR-228518, Lawrence Livermore National Laboratory (2009).
[30] F. C. Maienschein, R. W. Peelle, T. A. Love, Neutron Phys. Ann. Prog. Rep. for Sept. 1, 1958, ORNL-2609, Oak Ridge National Laboratory (1958)

Assessments in the computation of fission prompt neutron multiplicity by statistical decay of fragments

S. Perez-Martin[1)], S. Hilaire[2)] and E. Bauge[2)]

1) CIEMAT, Nuclear Innovation Unit, Department of Energy, Avda. Complutense, 22. 28040 Madrid, Spain
2) CEA, DAM, DIF, F-91297 Arpajon, France
sara.perez@ciemat.es

Abstract: We present a methodology to assess fission prompt neutron multiplicity for neutron induced fission reactions. This methodology is based on the statistical decay of fission fragments where the neutron/γ emission competition is taken into account. We have evaluated the predictive power resulting from the equal nuclear temperature approximation concerning the partitioning of the Total Excitation Energy among heavy and light fragments at scission. The γ-ray strength function and the level density used in the decay of fragments are other relevant parameters that have also been studied.
Neutron-induced fission on ^{235}U has been calculated over a large range of neutron incident energies (0.01-30 MeV). The neutron multiplicity probability distribution P(ν) as well as the average prompt neutron energy has also been computed and compared with other estimations and experimental data.

Introduction

New nuclear systems such as those proposed for Gen-IV and ADS reactors require new and improved nuclear data in order to better develop them with uncertainties as low as possible; for example the minor actinides cross section for their transmutation. Specifically the knowledge of fission prompt neutron multiplicity and spectrum is a key-point in the design of nuclear applications. Consequently, the implementation of a systematic analysis that provides an evaluation of both data as accurately as possible is of great interest.
In our description of neutron-induced fission reactions, the decay of the excited fission fragments is modeled and computed by TALYS code (Ref. 1). This code is used to follow the statistical decay of the fission fragments in order to collect all neutrons emitted. This is done by looking at the neutron production cross section. TALYS is based on the optical, pre-equilibrium and Hauser-Feshbach models. It calculates partial and total fission cross sections, γ-ray and neutron production cross sections, total exclusive (n,γ), (n,n'), (n,2n), (n,3n), ... cross sections and their corresponding emission spectra, among other quantities. This code does not only model nuclear reactions, but also describes the decay of an initial populated nucleus, which will be the main utility of TALYS for this study. An important advantage of our procedure compared to other models is that we explicitly account for the γ/neutron emission competition in the fission fragment decay.

Methodology

We present here the main points of the systematic analysis carried out in this study. The first point is the accurate description of the neutron-induced fission reaction in terms of the fission cross section. For this task we used TALYS code. It provides us with the total fission cross section, as well as with all the partial and exclusive fission cross sections (n,f), (n,nf), (n,pf), (n,2nf), (n,npf), (n,df), …. These exclusive fission cross sections are needed when the incident neutron energy is large enough to open the corresponding decay channels. This means that second, third, etc fission chance channels are open and the neutron multiplicity should account not only for neutrons emitted by fragments, but also for those emitted before fission.
Once the fissioning nuclei are known, the next point is the fission fragment yields. In the present work, fission mass distributions have been taken from Wahl's evaluation (Ref. 2) in which the latter are given in terms of the specific incident neutron energy. The multi-fission chance is also treated for higher incident energies.

After the selection of fragment pairs, the energy release in fission for each fission possibility is nothing but the difference in mass of the fission fragments and the compound nucleus. For the first fission chance, the excited energy of the compound nucleus ^{236}U is thus:

$$E^*\left(^{236}U\right) = M\left(^{235}U\right)c^2 - M\left(^{236}U\right)c^2 + E_n^{inc.} + B_n(^{236}U)$$

where M is the mass, E^{inc} is the incident neutron energy and B_n is the neutron binding energy. The above expression is generalized for the subsequent fissioning nuclei:

$$E^*\left(^{235}U\right) = E_n^{inc.} - \left\langle \epsilon_n^{(n,nf)} \right\rangle$$

$$E^*\left(^{234}U\right) = M(^{235}U) + E_n^{inc.} + B_n(^{236}U) - 2\left\langle \epsilon_n^{(n,2nf)} \right\rangle - B_{2n}(^{236}U)$$

where $\langle\varepsilon_n^{(n,nf)}\rangle$ is the average energy of the evaporated neutron prior to fission.

The energy Q released by the first fission chance is then:

$$Q_{fiss}^{236U} = M(^{235}U)c^2 + E_n^{inc.} + B_n(^{236}U) - M(FF_1)c^2 - M(FF_2)c^2$$

Concerning the Total Kinetic Energy Distribution (TKE), no phenomenological deduction has been used. On the contrary experimental data has been utilized to parameterize such a distribution as a Gaussian where both the mean value $\overline{TKE}$ and the width σ depend on the fragment mass. For the thermal neutron induced fission on ^{235}U, Ref. **Error! Reference source not found.** to **Error! Reference source not found.** were the experimental data used, so that :

$$P(TKE\,(A)) = \frac{1}{\sigma\sqrt{2\pi}} e^{-\frac{(TKE(A)-\bar{TKE}(A))^2}{2\sigma^2}}$$

Since TKE is assumed to be a Gaussian, on the right-hand side of Gaussian tail, the TKE can be larger than Q. We then neglect such cases applying the energy conservation condition.

If it is easy to see that the Total Excitation Energy is the difference between Q and TKE, it is not so easy to divide the total energy among light and heavy fragment. In fact a hypothesis must be adopted to share the remaining excitation energy between both fragments. As a first approximation, we have adopted the equal nuclear temperature approximation, and thanks to the nuclear equation of state $U=aT^2$ supposed to be valid for each individual fragment with excitation energy U, this leads to the expression:

$$E_L^* = TXE\frac{1}{1+\frac{a_H}{a_L}}$$

where a_H and a_L are the level density parameters of the heavy and light fragments, respectively. Once this approximation is adopted, the initial population of every fragment is available and TALYS can then compute the decay by statistical emission of prompt neutrons in competition with other open channels. In Figure 1, the energy released in fission Q and the Total Kinetic Energy TKE (obtained using the previously described procedure) are plotted as a function of the fission fragment mass for 0.01 MeV incident neutron fission.

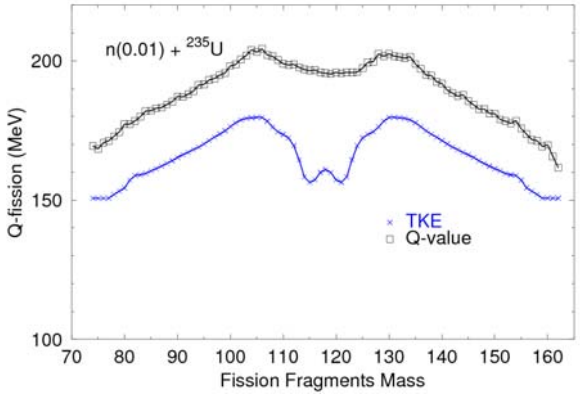

Figure 1. *Fission Q-value and TKE as a function of the Fission Fragment Mass*

The way of estimating any particle multiplicity in this work is through the emission cross section. The ratio between the neutron production cross section and the initial population of the fissionning fragment gives us the number of neutrons that have been emitted in the decay process.

Once we know the contribution of each fragment, we sum all them up, and then we take into account the contribution of all the fissionning nuclei provided not only the first fission chance is open. The weighting factor for the fragments summation is the fission yield y_{FF}. For the fissioning nuclei summation the weighting factor is the ratio of the individual fission cross section and the total fission cross section $\sigma_{FN}^{fiss} / \sigma_{TOTAL}^{fiss}$. In addition to the neutron emission coming from the decay of fragments, another source of fission neutrons (those emitted prior to fission) has to be accounted for. This is done thanks to multiple chances fission cross sections provided by TALYS (more details can be found in Ref. **Error! Reference source not found.** and **Error! Reference source not found.** regarding this point), so that finally:

$$\bar{\nu}_n = \sum_{FN=1}^{N} \frac{\sigma_{FN}^{fiss}}{\sigma_{TOTAL}^{fiss}} \left(\sum_{FF} y_{FF} \sigma_{n\,prod.}^{FN-FF} + n_{FN}^{n} \right)$$

where y_{FF} is the fission fragment yield, n^n_{FN} is the number of pre-fission neutrons associated to the fissioning nucleus FN.

The multiplicity distribution P(v) is computed as the sum of exclusive reactions which generate v prompt neutrons. For P(0) we add all exclusive reaction with no neutron emission, that is p, d, t, 2p, 2d, …; P(1) would be made by all contributions with one and only one neutron emission, that would be, n, np, nd, n2p, etc. and so on according to the multiplicity.

$$P_{ave}^{FN}(0) = \sum_{FF} y_{FF} \left(\sigma_{\gamma}^{FN-FF} + \sigma_{p}^{FN-FF} + \sigma_{d}^{FN-FF} + ... \right)$$

$$P_{ave}^{FN}(1) = \sum_{FF} y_{FF} \left(\sigma_{n}^{FN-FF} + \sigma_{pn}^{FN-FF} + \sigma_{dn}^{FN-FF} + ... \right)$$

In the above formulae, $\sigma_x^{FN\text{-}FF}$ is the exclusive reaction cross section for the channel x, where x can be gamma, neutron, proton, etc.

The global multiplicity distribution should be an average of all the fission fragments in all the fission chances ways. Moreover the neutrons emitted before fission n_{NF}^n should be included in the description by offsetting the corresponding multiplicity distribution by n_{NF}^n units. Therefore the global multiplicity distribution is:

$$P(\nu) = \sum_{FN} \frac{\sigma_{FN}^{fiss}}{\sigma_{TOTAL}^{fiss}} P^{FN}(\nu)$$

where

$$P^{FN}(0) = 0$$

$$P^{FN}(n_{NF}^{n}) = \frac{\sigma_{fiss}^{FN-FF}}{\sigma_{fiss}^{TOTAL}} P_{FF_{ave}}^{FN}(0) * P_{FF_{ave}}^{FN}(0)$$

$$P^{FN}(n_{FN}^{n}+1) = \frac{\sigma_{fiss}^{FN-FF}}{\sigma_{fiss}^{TOTAL}} \left(P_{FF_{ave}}^{FN}(0) * P_{FF_{ave}}^{FN}(1) + P_{FF_{ave}}^{FN}(1) * P_{FF_{ave}}^{FN}(0) \right)$$

The average prompt neutron energy of a given fission fragment is estimated using the centre of mass (C.O.M) emission spectra provided by TALYS, which is averaged over all energy bins:

$$\bar{\varepsilon}_n^{FN-FF} = \frac{\sum_{bin} E_{bin} \left[\left(\frac{\Delta \sigma_{n\,prod}^{FN-FF}}{\Delta E} \right)_{bin} \Delta E_{bin} \right]}{\sum_{bin} \left[\left(\frac{\Delta \sigma_{n\,prod}^{FN-FF}}{\Delta E} \right)_{bin} \Delta E_{bin} \right]}$$

where $\left(\frac{\Delta\sigma_{n.prod}^{FN-FF}}{\Delta E}\right)$ is the energy spectrum and $\sum_{bin}\left[\left(\frac{\Delta\sigma_{n.prod}^{FN-FF}}{\Delta E}\right)_{bin}\Delta E_{bin}\right]$ is nothing but the neutron production cross section.

For the average pre-fission neutron energy $\varepsilon_n^{(n,nf)}$, we employ the same procedure, using the neutron spectrum of the (n,nf), (n,npf), (n,2nf), etc reactions. Actually such pre-fission neutron energy is also needed to estimate the excitation energy of the residual fissionning nucleus in second and successive fission chances.

Finally the global prompt neutron energy for the neutron induced reaction is an average over all fission fragments and pre-fission neutron sources (v_{PF}^{FN})

$$\bar{\epsilon}_n = \frac{\sum_{FN}\frac{\sigma_{FN}^{fiss}}{\sigma_{TOTAL}^{fiss}}\left(\nu_n^{\bar{F}N}\bar{\epsilon}_n^{FN}+\nu_{PF}^{\bar{F}N}\bar{\epsilon}_{PF}^{FN}\right)}{\sum_{FN}\frac{\sigma_{FN}^{fiss}}{\sigma_{TOTAL}^{fiss}}\left(\nu_n^{\bar{F}N}+\nu_{PF}^{\bar{F}N}\right)}$$

where $\bar{\varepsilon}_{PF}^{-FN}$ is the average kinetic energy of evaporated neutrons prior to fission.

Results

We have performed calculations with neutron energies ranging from 0.01 to 30 MeV for n+^{235}U reaction. Since TALYS contains many options and parameters for driving its statistical model module, we have studied the influence of level density parameters and γ-ray strength functions on prompt neutron emission. Therefore we have computed two sets of calculations, one with the Fermi gas phenomenological level density model and a Kopecky-Uhl generalized Lorentzian for the γ-ray strength function (what will be called TALYS-ph) and the other with microscopic level densities and Hartree-Fock-Bogoliubov γ-ray strength functions (called TALYS-mic).

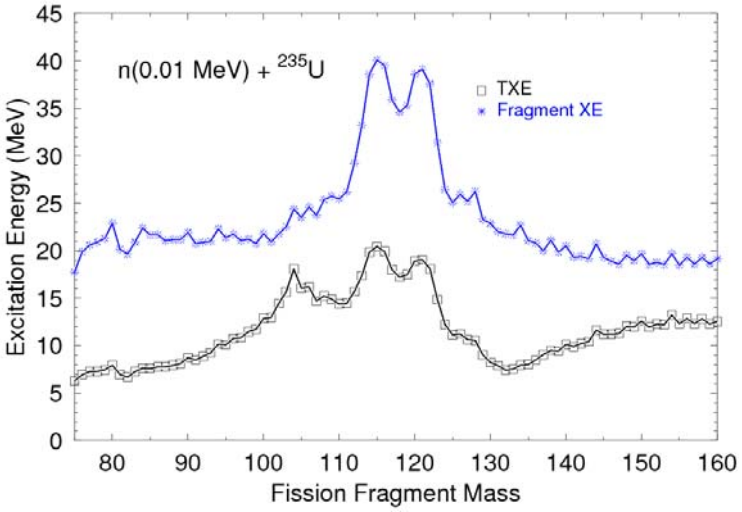

Figure 2. *Total Excitation Energy and Fragment Excitation Energy*

In Figure 2, the mean value of the total excitation energy available for both fragments as a function of the fragments mass for a 0.01 MeV ^{235}U neutron induced fission is shown (squares) as well as the excitation energy of each fragment (crosses). The effect of the energy partition approximation can be observed. The sharp drop in the A=120-130 region is due to the difference between the energy released in fission and the total kinetic energy as shown in Figure 1, where the Q-value is almost constant while the TKE increases.

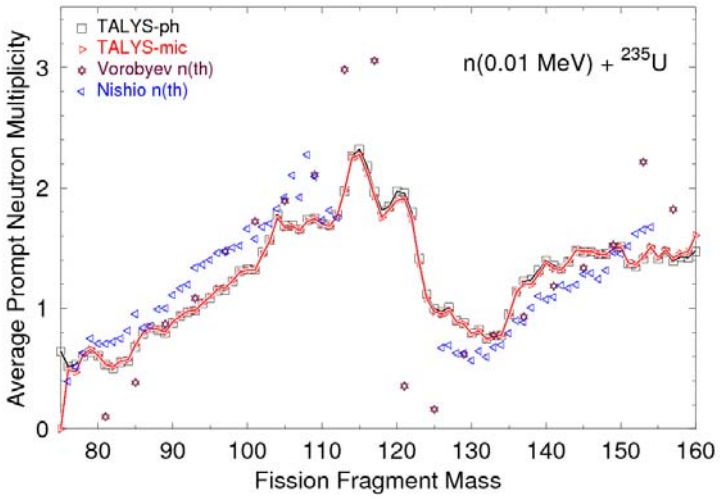

Figure 3. Average Prompt Neutron Multiplicity for n(0.01 MeV) + ^{235}U

In Figure 3, the average prompt neutron multiplicity as a function of the fission fragment mass obtained for 0.01 MeV incident neutrons on ^{235}U is plotted. We compare our results with experimental data (Ref. **Error! Reference source not found.** and 9). The general trend of the data (the sawtooth shape) is accounted for by our results, both TALY-ph and TALYS-mic which are practically the same. There are, however, sizable differences between our results and experimental data. The largest disagreement occur in the symmetric fission mass region where the yield is low, thus limiting the effect of such a mismatch. There are also some differences in the region of the light and heavy asymmetric fission, but they are smaller and of opposite directions. This fact has to do with the partition approximation which is analyzed in the following figure.

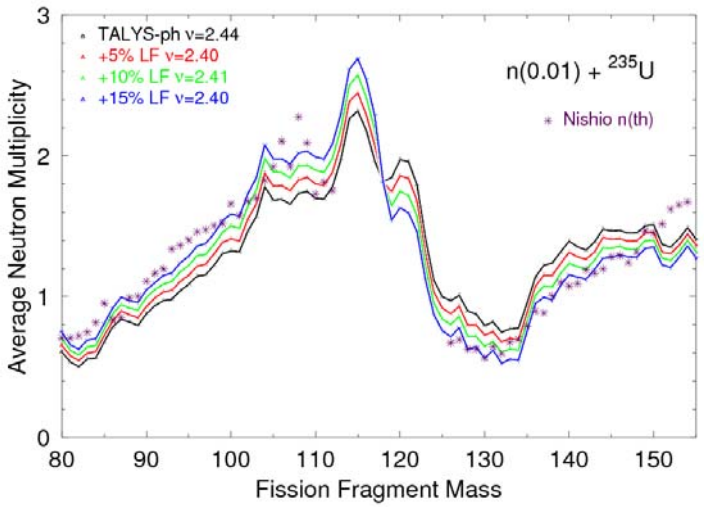

Figure 4. *Average Neutron Multiplicity for n(0.01 MeV) + ^{235}U with different Energy Partitions*

We have made some sensitivity analysis with respect to the partition of the energy. Starting from the equal nuclear temperature approximation, we have indeed increased the light fragment energy 5, 10 and 15% to study the effect on the fragment multiplicity. The impact on both light and heavy mass zone is shown in Figure 4. Comparing with Nishio data, we can see that the set of results that are closer are those with an increase of 15% in the light fragment energy. We can conclude that, in our systematic, the partition energy approximation results in an overestimation of the neutron multiplicity for the heavy asymmetric fission region and underestimates in the light fragment region.

The prompt neutron multiplicity distribution is shown in Figure 5. In the panel on the left, we compare our results with the experimental data of Diven et al. (Ref. **Error! Reference source not found.**) for 0.01 MeV incident neutron. Notwithstanding the difference of $\bar{\nu}$, both distributions look similar, and the maximum value of the neutron multiplicity distribution is

located at the same value v=2. In the right-panel, results for 0.53 MeV incident neutron energy are shown. Here our results are compared with those coming from Monte Carlo simulation (Ref. **Error! Reference source not found.**). Large differences are observed between them. For example, our multiplicity distribution peaks at v=2 while Lemaire's peaks at v=3. Moreover, our calculation (TALYS-ph) produces an average prompt neutron multiplicity value of $\bar{\nu} = 2.45$ whereas the Monte Carlo model estimate reaches $\bar{\nu} = 2.73$ using the same equal temperature energy partition hypothesis. The experimental result (Ref. **Error! Reference source not found.**) gives $\bar{\nu} = 2.46$ and is thus in closer agreement with our predictions.
The effect of phenomenological or microscopic parameters in the TALYS calculation results in slight differences for fragments near A=91 and 143. These changes seem quite small and produce a change of $\bar{\nu}$ from 2.40 for the TALYS-ph calculation to 2.39 for TALYS-mic.

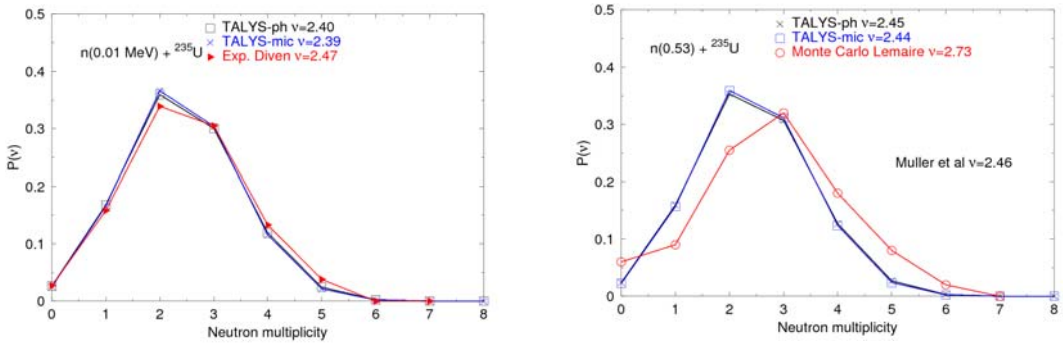

Figure 5. *Neutron Multiplicity Distribution P(nu) for 0.01 and 0.53 MeV Incident Neutron energy*

The average prompt neutron multiplicity as a function of the incident neutron energy is shown in Figure 6. Our results are compared with the ENDF-B VII.0 evaluation library as well as with experimental data (Ref. 12). For low incident energy a good agreement is obtained, whereas for higher incident energy (from 10 MeV on), larger differences are obtained. This fact shows us that our treatment of various open fission channels should be improved.

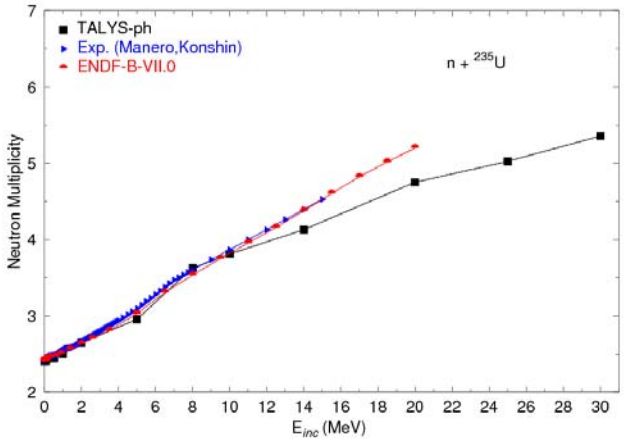

Figure 6. *Neutron Multiplicities in terms of the Incident Neutron Energy*

The average prompt neutron energy is shown in Table 1. Our results are smaller than those of Los Alamos (Ref. **Error! Reference source not found.**) and Monte Carlo code (Ref. 11). As it stands now, our model produces less neutrons which are on average less energetic than the other models. Figure 7 shows the average prompt neutron energy as a function of the fission fragment mass. Our results lay below experimental data and point by point results (Ref. 14). From A=115 until A=130, TALYS-ph and TALYS-mic give considerable differences in the average energy, the microscopic fragment decay providing in particular larger average neutron energy. The modification obtained by increasing by 15% the excitation energy of light fragments produces as a consequence higher neutron energy of light fragments and lower neutron energy of heavy fragments, as expected.

Table 1. *Average Prompt Fission Neutron Multiplicity and Energy*

n(0.53MeV)+^{235}U	ν	ε_{COM}(MeV)
TALYS-ph	2.45	1.04
TALYS-mic	2.44	1.09
Monte Carlo (Ref. **Error! Reference source not found.**)	2.73	1.241
Experimental	2.46 (ref. **Error! Reference source not found.**)	1.269 (ref. **Error! Reference source not found.**)

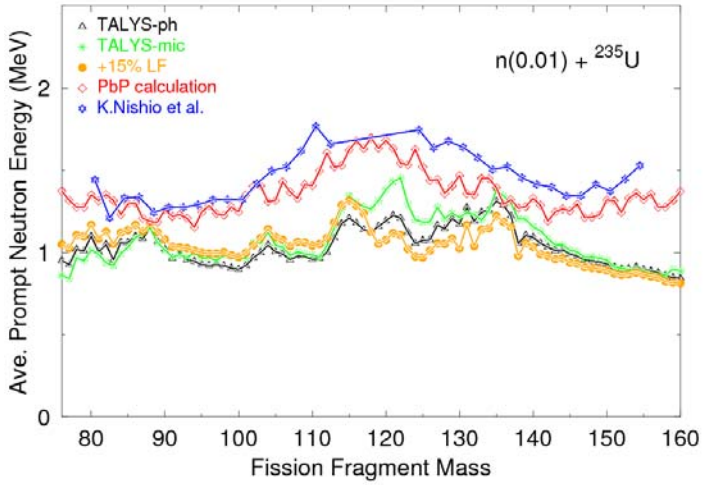

Figure 7. *Average Neutron Emission Energy*

Conclusions and Projects

In this study we have presented a method to compute prompt neutron multiplicity which accounts for the competition between neutron and γ emission. The computational tool is the TALYS code, which describes the fission fragment decay within the statistical model framework. We simultaneously collect the various emitted neutron spectra, and process them to produce the usual average prompt neutron multiplicity, multiplicity distribution, and average energy. Our calculations of these quantities have been compared with available experimental data as well as with results from other models.

The equal nuclear temperature approximation has been used for the partition of the Total Excitation Energy, and since the obtained results do not match experimental data very well, we have made afterwards some modifications by increasing the light fragment energy (and correspondingly decreasing the heavy fragment energy) by an amount of 5%, 10 and 15%. The 15% growth results appear to be quite close to the experimental results. This means that the partition approximation we use underestimates the light fragment energy and overestimates the heavy fragment energy.

We have also investigated the influence of various parameters driving the statistical decay such as the level densities and γ-ray strength functions. Moving from phenomenological to microscopic parameters induces differences that are not negligible and worth further investigations.

In general, although general trends seem to be well described by our model, we do not reach the level of precision needed for applications. The main reason for this mismatch is most

likely the hypothesis used for populating the initial fission fragment distribution. Our next task will be to implement more realistic initial fragment populations in our model and investigate their influence on prompt neutron distributions.

References

[1] http://www.talys.eu/ TALYS-1.2 A nuclear reaction program A.J. Koning, S. Hilaire and M. Duijvestijn (2009)
[2] A. C. Wahl, At. Data Nucl. Data Tables, 39 (1988)
[3] Schmitt H. W., Neiler J. H., and Walter F. J., Phys. Rev. 141, 1146 (1966)
[2] Meadows J. W. Phys. Rev. 177, 1817 - 1825 (1969)
[5] Müller R., Naqvi A. A., Käppeler F., and Dickmann F. Phys. Rev. C 29, 885 - 905 (1984)
[6] Perez-Martin S, Hilaire S. and Bauge E. Seminar on Fission VI. World Scientific 2008 p.147-158
[7] Perez-Martin S, Hilaire S. and Bauge E. AIP Conference Proceedings of 4th International Workshop on Nuclear Fission and Fission Product Spectroscopy. May 2009
[8] Nishio K., Nakagome Y., Yamamoto H., and Kimura I. Nucl. Phys. A632, 540 (1998)
[9] Batenkov O.A., et al. AIP Conf. Proc. May 2005 Vol. 769, 1003
[30] Diven B. C., Martin H. C., Taschek R. F. and Terrell J. Phys. Rev. 101, 1012 (1956)
[41] Lemaire S., Talou P., Kawano T., Chadwick M. B., and Madland D. G. Phys. Rev. C 72, (2005) 024601
[52] Manero F., Konshin V.A. Atomic Energy Review, IAEA; Vol.10, p.637 (1972)
[63] Madland D. G. and Nix J. R. Nucl. Sci. Eng. 81, 213 (1982)
[74] Tudora A. Private Communication.

Extension of nuclear fission theory to the Coulomb explosion of metallic clusters

D. N. Poenaru[1,2)], R. A. Gherghescu[1,2)], W. Greiner[2)]

1) Horia Hulubei National Institute of Physics and Nuclear Engineering, P.O. Box MG-6, RO-077125 Bucharest-Magurele, Romania
2) Frankfurt Institute for Advanced Studies, J. W. Goethe University, Ruth-Moufang-Str. 1, D-60438 Frankfurt am Main, Germany
poenaru@nipne.ro

Abstract: The nuclear liquid drop model and the the shell correction method, have been adapted for neutral and charged atomic clusters. We used the macroscopic-microscopic method to investigate neutral hemispheroidal atomic clusters deposited on a surface. Compared to nuclei, in which the electric charge of protons is assumed to be homogeneously distributed in the volume, in metallic atomic clusters the excess charge of electrons produced by ionization is concentrated on the surface. The most important yield in fission of charged metallic clusters is usually obtained when the light fragment is a singly charged trimer (the analog of an α-particle with magic number of delocalized electrons $n_e = 2$). In this case both the shell corrections and the LDM deformation energy have minima at the same mass asymmetry which corresponds to the trimer emission. Charged metallic clusters are ideally emitters of α-clusters.

Introduction

The density functional theory [1] is successfully employed in the field of atomic cluster physics. Alternatively, with less computational effort, one can use some simple models [2] replacing the many-body effects by an effective single-particle potential, since to a good approximation the delocalized conduction electrons of neutral small metallic clusters form a Fermi liquid like the atomic nucleus [3]. The liquid drop model (LDM) dominated for many decades the theory of nuclear fission, starting with the first explanation of the induced fission process. We have used the LDM to develop the analytical superasymmetric fission model [4] allowing to predict in 1980 heavy particle radioactivity [5, 6]. For the ground state properties of neutral clusters or the fission of charged clusters, the LDM expresses the smooth part of the total energy to which the shell corrections [7, 8] may be added.
The nanostructured coating of surfaces by cluster deposition is at present a rapidly growing field. By analyzing some shapes of cluster deposited on a surface obtained by using scanning probe microscopy [9, 10], one can see that a semi-spheroid with the z axis of cylindrical symmetry oriented perpendicularly on the surface plane may be a good approximation. Since 2007 we adapted the macroscopic-microscopic method to semi-spheroidal atomic clusters deposited on a planar surface [11-16] . The interdisciplinary character of our research work was particulary stressed in several publications [17-20] including those on trimer emission from charged metallic clusters.
According to the macroscopic-microscopic method, the deformation energy is given by

$$E = E_{LD} + \delta E = E_{LD} + \delta U + \delta P \tag{1}$$

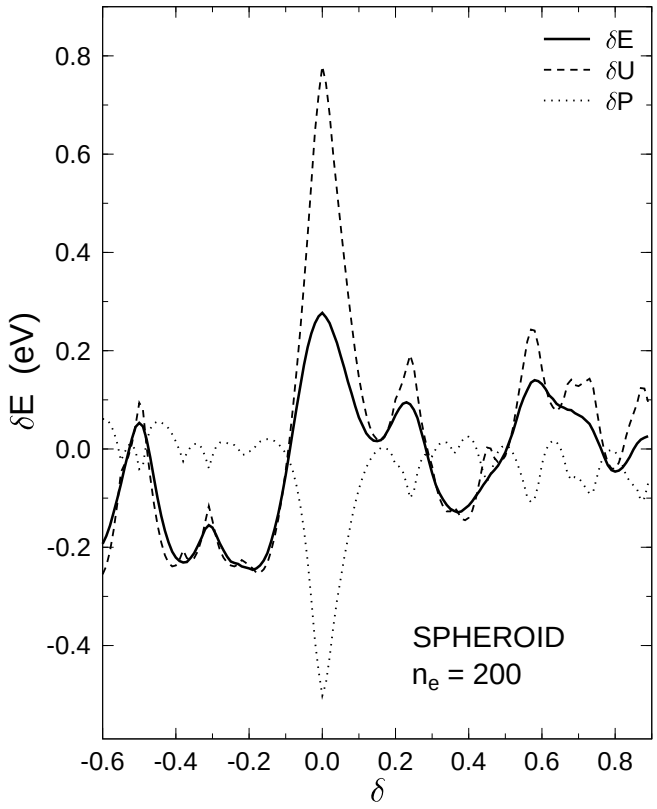

Figure 1: Shell and pairing corrections vs. deformation δ for a spheroidal Na_{210}^{10+} cluster.

in which E_{LD} is the liquid-drop term, δU is the shell correction, δP is the pairing correction and $\delta E = \delta U + \delta P$. An example is given in figure 1 for a spheroidal Na_{210}^{10+} cluster. The amplitudes of shell and pairing corrections are as low as few fractions of an eV. Spherical magic numbers: 2, 8, 40, 58, 92,136, 198, 264, 344, 442, 554, 680, 800, 970, 1120, 1310, 1500, ...

Fission of a charged metallic cluster

A neutral cluster with N atoms of a metal with valence $v = 1$ will have $n_e = N$ delocalized electrons. The number of delocalized electrons left after ionization or electron attachment are $n_e = N - z$ for a cation and $n_e = N + z$ for an anion, where z is called the excess charge and N the size of the cluster. In the most frequently studied fission ("Coulomb explosion") process

$$\mathbf{M_N^{z+}} \;\rightarrow\; \mathbf{M_{N_1}^{z_1+}} \;+\; \mathbf{M_{N_2}^{z_2+}} \tag{2}$$

we have $n_e = n_{e1} + n_{e2}$ and $z = z_1 + z_2$. The parent is doubly charged ($z = +2$) so that the fragments are single ionized: $z_1 = z_2 = 1$. The numbers of electrons are conserved: $N = N_1 + N_2$; $z = z_1 + z_2$; $n_e = N - z = n_{e1} + n_{e2}$; $n_{ei} = N_i - z_i$. Charged clusters are produced by photoionization with laser beams, or by collision. The ionization energy of metals is generally much lower than the ionization energy of nonmetals hence metals will generally lose electrons to form cations while nonmetals will generally gain electrons to form anions. The fission channel

with the trimer fragment M_3^{+1}, having a magic number of delocalized electrons $n_e = 2$, is very frequently the predominant one, in analogy to α-decay of nuclei (see e.g. fission of K^{2+} NaK^{2+} [21]; of Li^{2+} and K^{2+} [22]; of $Na^{2+\ to\ 7+}$, $K^{2+\ to\ 7+}$, $Rb^{2+\ to\ 7+}$, and $Cs^{2+\ to\ 7+}$ [23], and of Ag^{2+} [24]). Deformation energy

$$E_{LDM} = E - E^0 = (E_s - E_s^0) + (E_C - E_C^0) = E_s^0(B_s - 1) + E_C^0(B_C - 1) \tag{3}$$

For spherical shapes: $E_s^0 = 4\pi R_0^2\sigma = a_s n_e^{2/3} = 4\pi r_s^2 n_e^{2/3}$; $E_{C-metal}^0 = z^2e^2/(2R_0) = z^2e^2/(2r_s n_e^{1/3})$ for a surface distribution of charge. A charged cluster is stable as long as its fissility is smaller than one

$$Fissility \quad X = \frac{E_c^0}{2E_s^0} = \frac{e^2}{16\pi r_s^3\sigma}\frac{z^2}{n_e} < 1\ ; \quad n_e > n_c = \frac{e^2z^2}{16\pi r_s^2\sigma} \tag{4}$$

Very light charged clusters are unstable. One should take into account the special behavior of

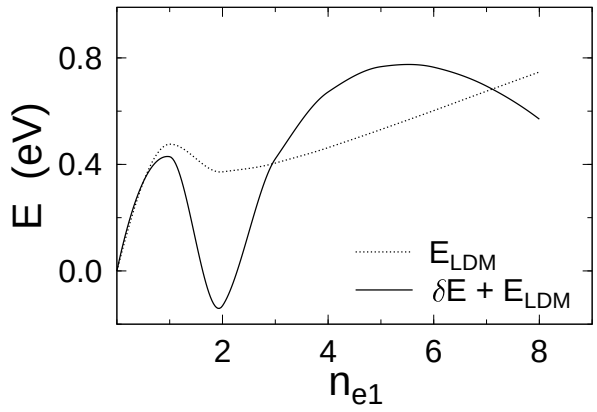

Figure 2: Details of the large asymmetry part of scission point deformation energies E_{LDM} (dotted line) and $E_{LDM} + \delta E$ (full line) for fission of a Cs cluster with 64 atoms and a charge $z = 4$.

a charged metallic cluster when the Coulomb energy is calculated: unlike the bulk distribution of the charge in nuclei, here we have a surface density σ_e [25, 26]. The electrostatic energy of a charge distribution

$$E_C[\sigma_e] = \frac{1}{2}\int\int \frac{\sigma_e(\mathbf{r})\sigma_e(\mathbf{r}_1)d^2\mathbf{S}d^2\mathbf{S_1}}{|\mathbf{r} - \mathbf{r}_1|} \tag{5}$$

The distribution σ_e on the surface is obtained by minimizing the energy under the constraint $Q = ze = \int \sigma_e(\mathbf{r})d^2\mathbf{S}$ i.e. the functional derivative

$$\frac{\delta(E - \lambda Q)}{\delta\sigma_e} = \frac{1}{2}\int \frac{\sigma_e(\mathbf{r}_1)d^2\mathbf{S_1}}{|\mathbf{r} - \mathbf{r}_1|} - \lambda = 0 \tag{6}$$

The polarizabilities of the two fragments has to be taken into account when we calculate the Coulomb interaction. One can use the image charge method [27] or the simpler approach [24]. From the figure 2 one can see that both LDM and shell correction energies are favouring the singly charged trimer emission at $n_{e1} = 2$.

Released energy

Within the liquid drop model (LDM) for charged metallic clusters the dissociation energy (Q-value) for this reaction, assuming spherical shapes [21] may be written as a sum of surface, Coulomb and ionization contributions

$$Q = Q_s + Q_C + Q_{IP} \tag{7}$$

$$Q_s = a_s[n^{2/3} - p^{2/3} - (n-p)^{2/3}] \tag{8}$$

$$Q_C = \frac{e^2}{2r_s}\left[\frac{z^2}{n^{1/3}} - \frac{z_1^2}{p^{1/3}} - \frac{(z-z_1)^2}{(n-p)^{1/3}}\right] \tag{9}$$

$$Q_{IP} = \frac{e^2}{8r_s}\left[\frac{z_1}{p^{1/3}} + \frac{(z-z_1)^2}{(n-p)^{1/3}} - \frac{z}{n^{1/3}}\right] \tag{10}$$

where $n = n_e$, $p = n_{e1}$, $n - p = n_{e2}$, $a_s = 4\pi r_s^2\sigma$ is the surface energy constant proportional

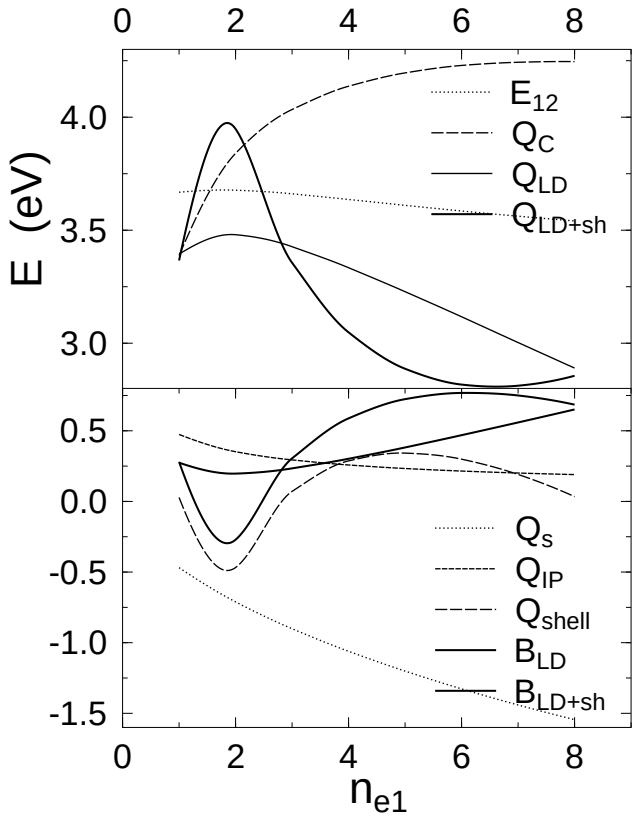

Figure 3: Fission of Cs_{100}^{6+} with singly charged light fragments. Q-values and fission barriers. Minimum barrier height and maximum Q-value reached at a very large mass asymmetry corresponding to $p = n_{e1} = 2$.

to the surface tension σ, $e^2/2 = 7.1998259$ eV·Å. Experimental results are showing minima of the LDM fission barrier $E_{12} - Q$ for $p = 2$, like in figure 2. As suggested by the figure 3, this

may be simply explained within LDM by plotting the derivative dQ/dp vs. p. It vanishes at a value of p very close to $p = 2$. Due to the smooth variation with p of the interaction energy E_{12} between the separated fragments, the barrier is minimum when the Q-value is maximum.

$$\frac{dQ}{dp} = \frac{dQ_s}{dp} + \frac{dQ_C}{dp} + \frac{dQ_{IP}}{dp} \tag{11}$$

$$\frac{dQ_s}{dp} = \frac{2a_s}{3}\left[\frac{1}{(n-p)^{1/3}} - \frac{1}{p^{1/3}}\right] \tag{12}$$

$$\frac{dQ_C}{dp} = \frac{e^2}{6r_s}\left[\frac{z_1^2}{p^{4/3}} - \frac{(z-z_1)^2}{(n-p)^{4/3}}\right] \tag{13}$$

$$\frac{dQ_{IP}}{dp} = \frac{e^2}{24r_s}\left[\frac{z-z_1}{(n-p)^{4/3}} - \frac{z_1}{p^{4/3}}\right] \tag{14}$$

Unlike in nuclear fission, the low n_{e1} channels (in particular the trimer Na_3^+ fragment) are promoted not only by the shell effects but also by the LDM!
According to LDM (collective properties of fermions) in fusion and fission (including cluster radioactivity and α-decay) of nuclei one should only have mass symmetrical processes $\eta = 0$. The experiments are explained only by adding the quantum shell effects (individual properties of nucleons). The fission channel with a light trimer M_3^+, frequently met in experiment, is promoted not only due to shell effects but also due to LDM low fission barrier. *Charged clusters are ideally "alpha" emitters!* By increasing the charge and the ratio a_s/r_s one may obtain large Q-values. They may be used in applications. Deformations and shell effects are usually increasing the Q-values.

Acknowledgements

This work is partially supported by Deutsche Forschungsgemeinschaft, Bonn, and partially within IDEI Programme under contracts 123/01.10.2007 and 124/01.10.2007 with UEFISCSU, Bucharest.

References

[1] R. G. Parr and W. Yang, *Density-Functional Theory of Atoms and Molecules* (Oxford University Press, New York, 1989).

[2] W. A. de Heer, in *Metal Clusters at Surfaces* (Springer, Berlin, 2000), pp. 1–35.

[3] *Nuclear Physics Concepts in the Study of Atomic Cluster Physics*, Lecture Notes in Physics Vol. 404, Eds. R. Schmidt *et al.* (Springer, Berlin, 1992), p. 677.

[4] D. N. Poenaru and W. Greiner, in *Nuclear Decay Modes*, edited by D. N. Poenaru (Institute of Physics Publishing, Bristol, UK, 1996), Chap. 6, pp. 275–336.

[5] A. Săndulescu, D. N. Poenaru, and W. Greiner, Sov. J. Part. Nucl. **11**, 528 (1980).

[6] The New Encyclopaedia Britannica, 15th Edition, 1995, Encyclopaedia Britannica Online http://www.britannica.com/EBchecked/topic/465998/.

[7] V. M. Strutinsky, Nucl. Phys. A **95**, 420 (1967).

[8] C. Yannouleas, U. Landman, and R. N. Barnett, in *Chapter 4 in Metal Clusters*, Ed. W. Ekardt (Wiley, New York, 1999), pp. 145–180.

[9] K. Seeger and R. E. Palmer, Appl. Phys. Lett. **74**, 1627 (1999).

[10] B. Bonanni and S. Cannistraro, J. Nanotechnology Online **1**, 1 (November 2005), doi: 10.2240/azojono0105.

[11] D. N. Poenaru, R. A. Gherghescu, A. V. Solov'yov, and W. Greiner, Europhys. Lett. (EPL) **79**, 63001 (2007).

[12] D. N. Poenaru, R. A. Gherghescu, A. V. Solov'yov, and W. Greiner, Phys. Lett. A **372**, 5448 (2008).

[13] D. N. Poenaru, R. A. Gherghescu, I. H. Plonski, A. V. Solov'yov, W. Greiner, Europ. Phys. J. D **47**, 379 (2008). HIGHLIGHT PAPER

[14] R. A. Gherghescu, D. N. Poenaru, A. V. Solov'yov, and W. Greiner, Int. J. Mod. Phys. B **22**, 4917 (2008).

[15] D. N. Poenaru, R. A. Gherghescu, A. V. Solov'yov, and W. Greiner, EPL **88**, 23002 (2009).

[16] D. N. Poenaru, R. A. Gherghescu, W. Greiner, Int. J. Mod. Phys. B **24**, 3411 (2010).

[17] D. N. Poenaru, R. A. Gherghescu, W. Greiner, J. Phys. G: Nucl. Part. Phys. **36**, 125101 (2009).

[18] D. N. Poenaru and W. Greiner, Nucl. Phys. A **834**, 163c (2010).

[19] D. N. Poenaru, R. A. Gherghescu, W. Greiner, J. Phys. G: Nucl. Part. Phys. **37**, 085101 (2010).

[20] D. N. Poenaru, W. Greiner, in *Clusters in Nuclei. Lecture Notes in Physics Vol. 818*, Ed. C. Beck (Springer, Berlin, 2010), Vol. I, Chap. 1, pp. 1–56.

[21] C. Bréchignac *et al.*, Phys. Rev. B **44**, 11386 (1991).

[22] C. Bréchignac, P. Cahuzac, F. Carlier, M. de Frutos, Phys. Rev. B **49**, 2825 (1994).

[23] U. Näher *et al.*, Z. Phys. D **31**, 191 (1994).

[24] S. Krückeberg *et al.*, Phys. Rev. A **60**, 1251 (1999).

[25] H. J. Krappe, Z. Phys. D **23**, 269 (1992).

[26] H. Koizumi, S. Sugano, and Y. Ishii, Z. Phys. D **28**, 223 (1993).

[27] U. Näher *et al.*, Phys. Rep. **285**, 245 (1997).

Light-Particle Emission from Deformed, Hot and Rotating Nuclei

K. Pomorski [1)] *, B. Nerlo-Pomorska* [1)] *, J. Bartel* [2)]

1) Department of Theoretical Physics, University MCS, Lublin, Poland
2) Institute Pluridisciplinaire Hubert Curien and Université de Strasbourg, France
Krzysztof.Pomorski@umcs.pl

***Abstract*:** The decay process of hot and rotating compound nuclei is studied. In particular the competition between fission and n, p and α–particle emission is discussed. The nuclear fission process is described by a Langevin equation coupled to Master equations for particle evaporation. Light particle emission rates obtained with the Weisskopf theory and the semiclassical Wigner-function approximation are compared.

Introduction

In this paper we are going to present the most important results obtained in our previous works [1-10] as well as the actual status of the research. We study systems with excitation energies of the order of (80–300) MeV. We assume that the particle emission is described by the Weisskopf theory [11] and alternatively by a semiclassical model developed in Ref. [4], and that the nuclear fission is a transport process [12]. The emission of photons is neglected because at these excitation energies the particle evaporation is expected to be dominant.
Grangé and Weidenmüller [13] first to point out the importance of the non–statistical aspects of the fission process. Our model and also the ones of Fröbrich, Abe and Carjan [14,15,16] are based on their work. In the last years one can observe the increasing amount of experimental studies of the evaporation of light particles from excited nuclei and of the concomitant decay by fission [17]. Results of our calculations are presented and compared with experimental work, especially the ones of Ref. [18,19,4]. The present research is in particular correlated with the measurements performed in GANIL.
In our model we assume that the fission process is described by a Langevin equation which is dynamically coupled with a Master type equation for the light-particles evaporation. We take into account the dependence of the evaporation probabilities on the deformation of nucleus, on its excitation and collective rotation. We assume that the transmission coefficient depends on deformation and on the collective rotation of the nucleus. The collective potential of the fissioning nucleus is evaluated within the model of a deformed, hot and rotating liquid drop [21,7]. The effective one–dimensional path to fission is determined in a three–dimensional deformation space. The collective inertia is obtained in the irrotational flow model and the wall formula [26] is used to evaluate the strength of the friction force. The Einstein relation between the friction and diffusion parameters is assumed to hold.

Theoretical model

We consider an ensemble of deformed nuclei with finite excitation energies and rotational angular momenta as given by the initial conditions determined from the entrance channel. The subsequent time evolution of the nucleus is governed in a simplified description by a single collective coordinate $q = R_{12} / R_0$ where R_{12} is the distance between the two centers of mass of the left-right symmetric deformed nucleus and R_0 is the radius of the corresponding spherical nucleus having the same volume. This collective variable is defined in the framework of a Trentalange–Koonin–Sierk (TKS) [20] parametrisation of the surface of the nucleus. The TKS deformation parameters are related to q by means of a minimisation procedure of the collective potential energy defined below [21].
Denoting the conjugate momentum by $p(t)$ we use the following classical equations of motion to describe the time evolution of the fissioning nucleus [3]

$$\begin{cases} \dfrac{dq}{dt} = \dfrac{p}{M(q)} \\ \dfrac{dp}{dt} = \dfrac{1}{2}\left(\dfrac{p}{M(q)}\right)^2 \dfrac{dM(q)}{dq} - \dfrac{dV(q)}{dq} - \dfrac{\gamma(q)}{M(q)}\, p + F_L(t). \end{cases} \tag{1}$$

Here $M(q)$ is the collective mass determined in the incompressible fluid approximation [22] and $\gamma(q)$ the friction coefficient calculated in the wall-and-window friction model [23]. The collective potential V(q) is obtained as the difference of the Helmholtz free energy at deformation q minus the one for the ground-state deformation.

Particle emission before scission is governed by transition rates $\Gamma_\nu^{\alpha\beta}(E^*, L)$ which determine the number of particles of type ν (we take into account neutrons, protons, and α particles) emitted per unit time with an energy e_α and with an angular momentum ℓ_β from a nucleus with average excitation energy E^* and total angular momentum L. In Ref. [3] we have used the well known Weisskopf formula [11] for the partial width $\Gamma_\nu^{\alpha\beta}(E^*, L)$ in terms of densities of states of the emitting and residual nucleus and the transmission coefficient $w_\nu(e, \ell_\beta)$ for the emitted particle ν with given energy e and angular momentum ℓ_β.

In Refs. [2,4] another more microscopic determination of these transition rates was proposed. In this framework the transition rates $\Gamma_\nu^{\alpha\beta}$ are given as

$$\Gamma_\nu^{\alpha\beta} = \frac{d^2 n_\nu}{d\varepsilon_\alpha d\ell_\beta} \Delta\varepsilon\, \Delta\ell, \tag{2}$$

where ε_α and ℓ_β characterise an emission energy and angular momentum lying in the intervals $[\varepsilon_\alpha - \frac{1}{2}\Delta\varepsilon, \varepsilon_\alpha + \frac{1}{2}\Delta\varepsilon]$ and $[\ell_\beta - \frac{1}{2}\Delta\ell, \ell_\beta + \frac{1}{2}\Delta\ell]$, respectively.

The number n_ν of particles of type ν which are emitted per time unit through the surface Σ of the fissioning nucleus is given by [2]

$$n_\nu = \int_\Sigma d\sigma \int d^3p'\, f_\nu(\vec{r}_0, \vec{p})\, v'_\perp(\vec{r}_0)\, w_\nu(v'_\perp(\vec{r}_0)) \tag{3}$$

where $\vec{p}$, $\vec{v}$ are the momentum and velocity in the body-fixed frame. The quantity $v'_\perp$ is the velocity component perpendicular to the emission surface at the surface point $\vec{r}_0$. The $\vec{p} = m\vec{v} + m\vec{\omega}\times\vec{r}$ is the momentum of the particle of mass m in the laboratory reference frame and $\vec{\omega}$ the angular velocity of the nucleus in this frame. Here and henceforward, primed quantities refer to the body-fixed frame.

The classical distribution in phase space reads

$$f_\nu(\vec{r}, \vec{p}) = \frac{2}{h^3} \frac{\theta(\vec{r})}{1 + \exp\left[\frac{1}{T}\left(\frac{p'^2}{2m} + U - \omega\ell' - \mu_\nu\right)\right]}. \tag{4}$$

The θ function is 1 if $\vec{r}$ lies inside the nuclear volume or on its surface Σ and zero otherwise. The quantity μ_ν is the chemical potential and ℓ' the body-fixed angular momentum in the direction perpendicular to the axis of rotational symmetry of the deformed nucleus. The potential U is taken as

$$U(\vec{r}) = -V_0 + V_{Cb}(\vec{r}), \tag{5}$$

where $V_0 > 0$ is chosen as a mean field potential and V_{Cb} is the Coulomb potential experienced at $\vec{r}$ by protons. The quantity $w_\nu(v'_\perp(\vec{r}_0))$ is the classical transmission coefficient for the emission of a particle of type ν. The transmission factor w_ν was chosen to be the one of an inverted harmonic oscillator [3].

The transition rates $\Gamma_{\nu}^{\alpha\beta}$ are used in a simulation algorithm by means of which we determine at each time step $[t,t+\tau]$ along each classical trajectory whether a particle of given type with an energy and angular momentum in given intervals is emitted or not from the compound nucleus. Since the emission algorithm is already described in detail in Ref. [3] we do not repeat it here.

The friction term and the Langevin force $F_L(t)$ in Eq. (1) generate the irreversible production of heat energy and the energy fluctuations respectively which both originate from the coupling of the collective dynamics to the intrinsic degrees of freedom. In practice one defines $F_L(t)=\sqrt{D(q)}\,f_l(t)$, where $D(q)$ is the diffusion coefficient. We assumed that it is related to the friction coefficient $\gamma(q)$ through the Einstein relation $D(q)=\gamma(q)T$, where T is the temperature of the system. The quantity $f_L(\tau)$ can be written in the form $f_L(\tau)=\sqrt{\tau}\,\eta$, where τ is a time step length corresponding to a time interval $[t,t+\tau]$ and η is a Gaussian distributed random number with zero average $<\eta>=0$ and variance $<\eta^2>=2$, where brackets represent ensemble averages.

In order to integrate the classical equations (1) one needs to fix the initial conditions from which the compound system starts and evolves either through a fission channel to its saddle and scission point or stays as a compound system and only emits light particles, i.e. ends up as an evaporation residue. All the experimental systems which are considered here are produced by means of heavy ion collisions. Their initial conditions corresponding to the origin of time are fixed by q_0 and p_0, the initial value of the collective variable and its conjugate momentum and the spin distribution of the system which fixes the relative weight of the angular momentum of the initial compound systems.

The coordinate q_0 is fixed at the value of q, where the collective potential $V(q)$ is minimal and its conjugate momentum is drawn from a normalised Gaussian distribution

$$P(p_0)=(2\pi MT_0)^{1/2}\exp[-p_0^2/(2MT_0)], \tag{6}$$

where $M=M(q_0)$ is the collective mass. The initial temperature T_0 is obtained through $E_0^*=a(q_0)T_0^2$, where E_0^* is the initial excitation energy which can be obtained from the knowledge of the total energy as explained below and $a(q)$ is the single-particle level density (see Ref. [8]).

In the entrance channel, the compound nucleus can be formed with different values of the angular momentum. Such a distribution can be estimated using appropriate Langevin equations [24,25]. Repeating the trajectory calculations leads to the initial spin distribution

$$\left(\frac{d\sigma_F}{dL}\right)_{L_i}=\frac{2\pi}{k^2}L_i\frac{N_i^F}{N_i}, \tag{7}$$

where L_i is the considered angular momentum, N_i^F is the number of trajectories which lead to fusion and N_i is the total number of trajectories. The quantity k is the wave–number of the relative motion of the incident nuclei.

Finally, in order to describe the evolution of the excited compound system one needs to follow the evolution of the average excitation energy along the trajectory. This is achieved by the requirement of energy conservation. At the initial point of a trajectory the total available energy can be written as

$$E_{\rm tot}=E_{\rm coll}+E_{\rm rot}+E_0^*=\frac{p_0^2}{2M(q_0)}+V(q_0)+\frac{L_0^2}{2J(q_0)}+E_0^*. \tag{8}$$

Here, $J(q_0)$ is the moment of inertia of the compound system taken as a rigid deformed rotator and E_0^* is the initial intrinsic excitation energy of the compound nucleus. At any later time *t* this excitation energy $E^*(t)$ can be determined from the energy balance

$$E_{\text{tot}} = E_{\text{coll}} + E_{\text{rot}} + E_0^* + B_\nu + e_\alpha + E_{\text{recoil}}, \quad (9)$$

where B_ν is the binding energy of the emitted particle (different from zero only for α-particles), e_α is the kinetic energy of the emitted particle and E_{recoil} is the recoil energy of the nucleus after the particle.

For each choice of the initial conditions one generates a separate trajectory. Emitted particles are counted with their energy and angular momentum. If the system overcomes the fission barrier this trajectory contributes to the final fission cross section

$$\sigma_{\text{fiss}} = \sum_i \frac{d\sigma_{\text{fiss}}}{dL_i} = \sum_i \left(\frac{d\sigma_F}{dL_i} \right)_{L_i} \cdot \frac{N_i^{\text{fiss}}}{N_i^F}, \quad (10)$$

where N_i^{fiss} is the number of trajectories which lead to fission, and N_i^F – the number of fused trajectories at a given angular momentum L_i. The sum runs over all angular momentum bins and $d\sigma_F / dL$ is the fusion cross section given by Eq. (7).

The numbers of prefission particles obtained for each angular momentum of the compound nucleus (M_ν) are weighed with the differential fission cross section in order to obtain the measured number of particles emitted in coincidence with fission:

$$< M_\nu >= \frac{\sum_i \frac{d\sigma_{\text{fiss}}}{dL_i} \cdot M_\nu(L_i)}{\sigma_{\text{fiss}}}. \quad (11)$$

Results

We have studied the decay of the compound nuclei at various excitation energies ranging from 80 MeV to 300 MeV and from different mass regions. Our special interest was to investigate the influence of deformation and fast rotation on the emission of n, p and α–particles from excited states of these nuclei.

Let us begin with the decay of ^{160}Yb in order to show in details how our model works. We have selected this nucleus because a careful experimental investigation of its decays is available [18] and because it has a large ground state deformation. The deformation dependent emission width for n, p and α is shown in Fig. 1 for two different isotopes of both $_{64}$Gd and $_{70}$Yb. These 4 nuclei were chosen in order to illustrate how the deformation dependence of the emission widths for n, p, and α varies with the neutron and proton number of the emitting nucleus.

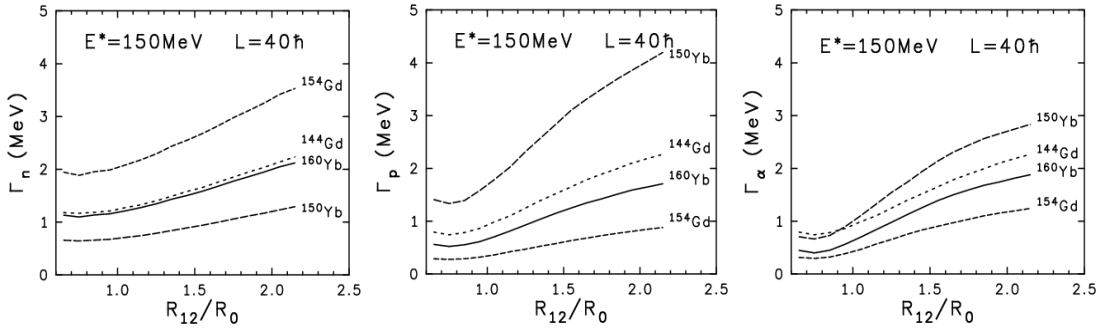

Figure 1. *Decay rates for emission of neutrons, protons and α –particles evaluated for different compound nuclei as functions of the elongation of nucleus.*

All the emission rates grow as a function of increasing deformation. This trend can be easily understood since for increasing deformation the transmission occurs through a larger surface. The effect has already been observed for all three types of particles [27]. We have noticed, however, that the emission width for p and α–particle increases more steeply than the one for n. This is due to the fact that, as the nucleus is elongated, the barrier height for charged

particles is reduced in the section of the surface which is further away from the nuclear center and increased in the section which is closer to the center. Consequently, the emission rate for charged particles increases faster than the one for neutrons.
The dependence of the number of decays of a given type on the time which elapses starting from the formation of the compound nucleus is unfortunately not measurable. Nevertheless, it is interesting to study this dependence theoretically in order to illustrate the time scale of this process. In Fig. 2 we show the number of fission events as function of time *t* on a logarithmic scale.

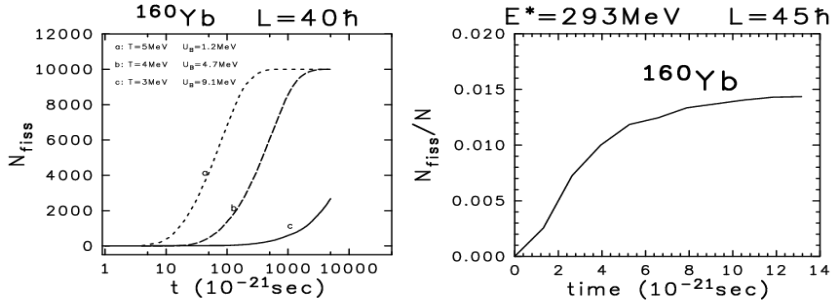

Figure 2. *Time evolution of the fission events without taking into account particle evaporation (l.h.s. plot) and with particle emission (r.h.s. plot).*

This result was obtained with the light-particle evaporation channels turned off. The initial compound nucleus is $^{160}_{70}$Yb with an initial angular momentum $L = 40\,\hbar$. The three curves on the l.h.s. of Fig. 2 correspond to 3 different initial temperatures resulting in 3 different initial fission barrier heights U_B. It is seen that the transient time increases with decreasing excitation energy, as one expects. Please note that the transient time interval is seen to be totally different from the one in the Kramers [12] regime. The Kramers limit is only valid in the cases when the fission barrier is much higher than the temperature of the fissioning nucleus. On the r.h.s. of Fig. 2 the fraction $N_{\rm fiss}/N$ of nuclei undergoing fission is shown for the initial compound nucleus $^{160}_{70}$Yb as a function of time. Contrary to the results presented in the l.h.s. of Fig. 2, the emission of light particles is now taken into account. This implies that the fission barrier rises as a function of time, since, at each particle emission, the excitation energy and (on the average) the angular momentum of the emitting nucleus decrease. Consequently, the time scale of the fission process is stretched. The initial excitation energy of the nucleus is $E^{å} = 293$ MeV ($T \approx 5$ MeV) and an initial angular momentum $L = 45\,\hbar$ is assumed.
The theoretical estimates of the prefission particle multiplicities, averaged over all angular momenta of the compound nucleus, are compared in Table 1 with the experimental data taken from Ref. [18].

Table 1. *Comparison of the theoretical predictions with the experimental data.*

	E*=251 MeV		E=293 MeV	
ν	model	exp.	model	exp.
n	5.98	6.10± 1.5	7.80	8.50± 1.6
p	0.94	0.51±0.0.7	1.19	0.70± 0.08
α	0.58	0.48±0.07	0.66	0.75±0.08

All parameters of the model are standard and given in Ref. [21]. We have chosen a preformation factor $f_\alpha = 0.2$, that reproduces on average the experimental number of α–particles in different excitation energies and mass regions. This goes into the right direction since our calculations show that α–particle emission is strongly enhanced by rotation and deformation effects. One of the most important further improvements of the theory consists in the evaluation of this preformation factor within the temperature–dependent semiclassical (Thomas–Fermi) approximation which underlies our theory [5]. At low temperature, the

Thomas-Fermi approximation is expected to yield too low values of the preformation factor. Additional effects like the pairing correlations will then increase the value of the preformation factor at low excitation energies (T $\leq$ 1 MeV).

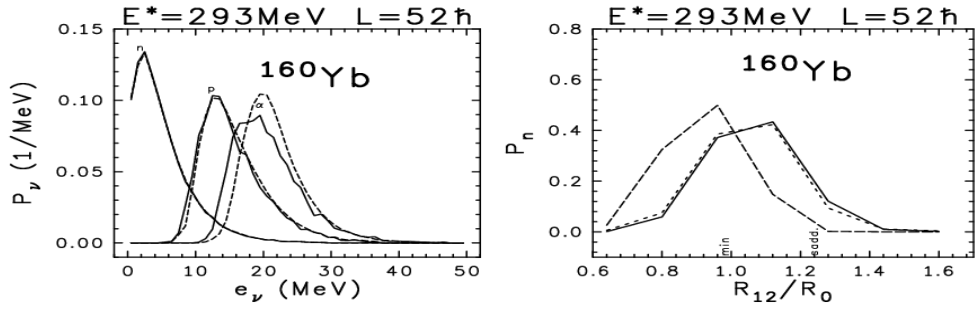

Figure 3. *Energy spectra of neutrons (n), protons (p) and α –particles emitted by fissioning nuclei (solid lines) and by the fission residua (dashed lines) (l.h.s. plot) and the deformation distribution of the neutron emitters (r.h.s. plot).*

In the l.h.s. of Fig. 3, we present the energy spectra of neutrons (n), protons (p) and α – particles emitted by fissioning nuclei (solid lines) and by the fission residua (dashed lines). The spectral distribution for α –particles emitted in coincidence with fission is shifted by about 2 MeV towards smaller energies as compared to the distribution obtained when measured in anti-coincidence with fission, while for neutrons the both distributions are very close to each other. This is due to the fact that charged particles are preferentially emitted from the pole tips around the long half axis. The larger deformation then implies a smaller gain of kinetic energy from the repulsive Coulomb field.

Our model was also applied to lighter elements. As a good example of the decay of such compound nuclei can serve ^{126}Ba* in which the prefission neutrons multiplicities were studied in two types of reactions [19,4]:

- ^{28}Si + ^{98}Mo at E_{lab} = 142.*, 165.8, 187.2 and 204 MeV,
- ^{19}F + ^{107}Ag at E_{lab} = 128.0 and 147.8 MeV

at four different excitation energies E^* = 84.1, 101.5, 118.5 and 131.7 MeV. The spin distribution differs in each case since it depends on the energy and on the way in which the compound nucleus was produced. Similarly as in the case of ^{160}Yb we have estimated the fusion cross section using the model described in [28,24]. The maximal angular momentum of the fused system varies from about 60$\hbar$ up to 100$\hbar$ depending on the way in which ^{126}Ba is produced.

Table 2. *Experimental prefission neutron multiplicities and their theoretical estimates for ^{126}Ba* formed in different reactions. Last two columns give the prediction for the prefission proton and α -particle multiplicities [4].*

Reaction	E_{lab}	E^*	M_n^{exp}	δM_n^{exp}	M_n	M_p	M_α	S_n	S_p	S_α
	MeV	MeV	-	-	-	-	-	-	-	-
	204.0	131.7	2.52	0.12	2.29	0.03	0.79	2.30	0.11	4.11
^{28}Si + ^{98}Mo	187.2	118.5	2.01	0.13	1.71	0.00	0.09	2.19	0.09	3.71
	165.8	101.4	1.32	0.09	1.83	0.00	0.04	2.13	0.05	3.20
	142.8	84.1	-	-	0.27	0.04	0.88	2.23	0.02	2.56
^{19}F + ^{107}Ag	147.8	118.5	1.85	0.11	1.99	0.00	0.16	2.13	0.09	3.84
	128.0	101.5	1.31	0.17	1.80	0.01	0.06	2.11	0.05	3.30

The initial temperatures of the compound nucleus ^{126}Ba are rather low since the total excitation energy of the system is not very high and a large fraction of the excitation energy is stored in the form of rotational and deformation energy. It is seen that for angular momenta $L \geq 80\ \hbar$, which contribute mostly to fission of ^{126}Ba, and the lowest excitation energy

E^* =84.1MeV the initial temperature reaches a value $T \approx$ 0.5 MeV. At such a low temperature our model (transport equation for fission without superfluidity coupled with the Master equation for particle evaporation) is poorly justified. So one should consider the estimates of the prefission particles we obtained for this energy as only a rough estimate.
Theoretical estimates of the multiplicities of neutron, proton and α–particles are given in Table 2. The thermal excitation energies of ^{126}Ba are rather low, so we have assumed here the preformation factor for α–particles f_α =1 as for cold nuclei. Just for comparison we have presented also the multiplicities of these particles (S_i, $i = n, p, \alpha$) connected with the evaporation residua. One can see from the table that a rather large number ($\approx$ 4) of α–particles is emitted by the residua. This is due to the fact that the nucleus ^{126}Ba has a rather small Coulomb barrier for of α–particles. Furthermore, the large average orbital momentum of the mother nucleus favours the emission of α–particle. Due to these two effects even the emission of α–particles with very low kinetic energy becomes possible. As a consequence the α emission competes significantly with neutron emission and becomes even larger for the evaporation residua.
If the particles are emitted in coincidence with fission they are emitted at very large deformation ($R_{12} \approx 2$), whereas if they are emitted in coincidence with evaporation residua the emission occurs at smaller deformation ($R_{12} \approx$ 1.2). This effect could be observed in the angular distribution of the emitted neutrons: more particles should be emitted in the direction perpendicular to the reaction plane as compared to the reaction plane. This effect will not be so visible for α–particles because the reduction of the Coulomb barrier is largest at the tips of the highly deformed nucleus and at the same time the collective centrifugal force acting on the α–particle is largest in this direction what favours emission in the reaction plane.

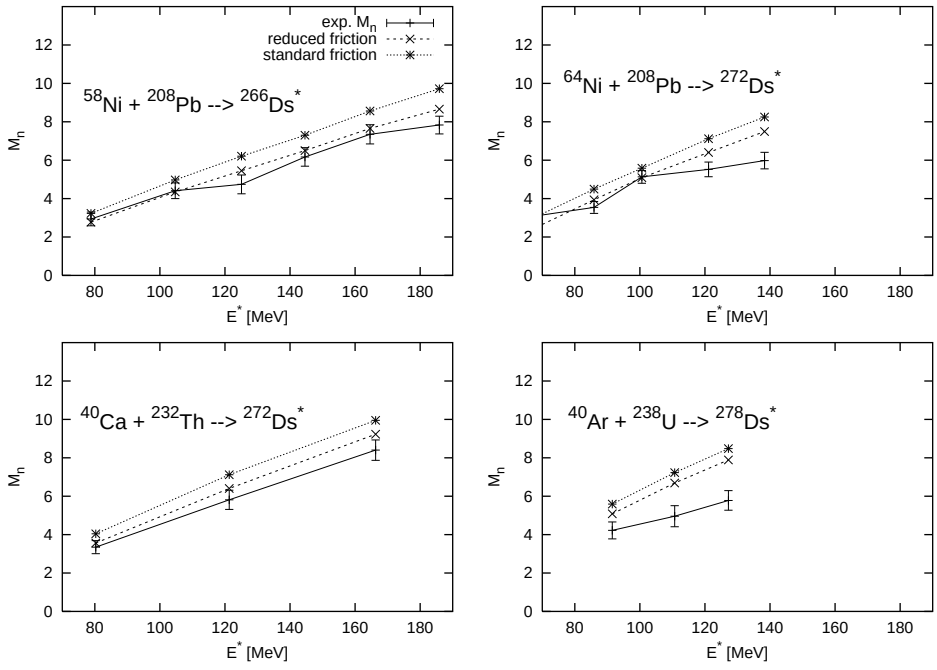

Figure 4. *Prescission neutrons multiplicities for ^{266,272,278} Ds* as function of the excitation energy of the compound nucleus [4].*

*

Our model was also applied to describe the decay of superheavy compound nuclei formed in hot fusion reactions [4]. In Fig. 4 the estimated prefission neutron multiplicities are compared with the experimental data obtained with different excitation energies. The theoretical values obtained with a reduced (by 50%) wall friction (dotted lines) agree better with the measured values.

Summary

Our results clearly show the influence of the nuclear deformation and of the collective rotation on the evaporation of light particles from excited nuclei. The dependence on the deformation plays an important role also for the competition between fission and particle emission and might modify the limits which were determined for the nuclear friction force [1] from the experimental data on evaporation and fission.
Due to the strong dependence of the fission probability on the initial angular momentum, it is very important to obtain a precise information on the angular momentum distribution of the initial ensemble of compound nuclei. The outcome of the competition between light particle emission and fission depends strongly on the initial angular momenta. The reason is that the rotational angular momentum of the nucleus has a very noticeable influence on the height of the fission barrier which decreases as a function of increasing angular momentum. Thus, at high angular momentum, nuclear fission can compete more effectively with evaporation.
We expect that the angular distribution of emitted particles, especially of neutrons, depends on the deformation of the emitting nuclei in a sufficiently sensitive way, so as to determine the nuclear deformation from such measurements. The experimental data on the angular distribution of emitted neutrons, protons, and α–particles from aligned rotating deformed nuclei would be of great interest for these studies.

References

[1] E. Strumberger, K. Dietrich,K. Pomorski, Nucl. Phys. A529 (1991) 522.
[2] K. Dietrich, K. Pomorski and J. Richert, Z. Phys. A351 (1995) 397.
[3] K. Pomorski, J. Bartel, J. Richert, K. Dietrich, Nucl. Phys A605 (1996) 87.
[4] K. Pomorski, B. Nerlo-Pomorska, A. Surowiec, M. Kowal, J. Bartel, K. Dietrich, J. Richert, C. Schmitt, B. Benoit, E. de Goes Brennand, L. Donadille, C. Badimon, Nucl. Phys. A679 (2000) 25.
[5] A. Surowiec, K. Pomorski, C. Schmitt, J. Bartel, Acta Phys. Polonica B33 (2002) 479.
[6] C. Schmitt, J. Bartel, K. Pomorski, A. Surowiec, Acta Phys. Polonica B34 (2003) 1651.
[7] K. Pomorski, J. Dudek, Phys. Rev. C67 (2003) 044316.
[8] B. Nerlo-Pomorska, K. Pomorski, J. Bartel, Phys. Rev. C74 (2006) 034327.
[9] A. Dobrowolski, K. Pomorski, J. Bartel, Phys. Rev. C75 (2007) 024613.
[10] F. Ivanyuk, K. Pomorski, Phys. Rev. C79 (2009) 054327.
[11] V. Weisskopf, Phys. Rev. 52 (1937) 295.
[12] H. Kramers, Physica 7 (1940) 284.
[13] P. Grangé, H.C. Pauli, H.A. Weidenmüller, Phys. Lett. B88 (1979) 9; Zeit. Phys. A296 (1980) 107.
[14] P. Fröbrich, Nucl. Phys. A545(1992) 87c.
[15] G.R. Tillack, R. Reif, A. Schülke, P. Fröbrich, H.J. Krappe, H.G. Reusch, Phys. Lett. B296 (1992) 296.
[16] Y. Abe, N. Carjan, M. Ohta, T. Wada, Proc. IN2P3–RIKEN Symp. on Heavy–Ion Collisions, Obernai, 1990, France
[17] D. Hilscher, H. Rossner, Ann. Phys. Fr. 17 (1992) 471
[18] M. Gonin, L. Cooke, K. Hagel, Y. Lou, J.B. Natowitz, R.P. Schmitt, S. Shlomo, B. Srivastava, W. Turmel, H. Ustunomiya, R. Wada, G. Nardelli, G. Nebbia, G. Viesti, R. Zanon, B. Fornal, G. Prete, K. Niita, S. Hannuschke, P. Gonthier, B. Wilkins, Phys. Rev. C42 (1990) 2125.
[19] L. Donadille et al., Nucl. Phys. A656 (1999) 259.
[20] S. Trentalange, S.E. Koonin, A.J. Sierk, Phys. Rev. C22 (1980) 1159.
[21] J. Bartel, K. Mahboub, J. Richert, K. Pomorski, Z. Phys. A354 (1996) 59.
[22] K.T.R. Davies, A.J. Sierk, J.R. Nix, Phys. Rev. 13C (1976) 2385.
[23] J. Blocki, J. Randrup and W. J. Swiatecki, Ann. Phys. 105 (1977) 427.
[24] K. Pomorski, W. Przystupa, J. Richert, Acta Phys. Pol. 25B (1994) 751.
[25] K. Pomorski, W. Przystupa, J. Bartel, J. Richert, Acta Phys. Pol. 30B (1999) 809.
[26] J. Błocki, H. Feldmeier, W.J. Swiatecki, Nucl. Phys. A459 (1986) 145.
[27] M. Blann, Phys. Rev. C21 (1980) 1770.
[28] W. Przystupa, K. Pomorski, Nucl. Phys. A572 (1994) 153.

Event-by-Event Fission with FREYA

J. Randrup [1] *and R. Vogt* [2,3]

1) Lawrence Berkeley National Laboratory, Berkeley, California 94720, USA
2) Lawrence Livermore National Laboratory, Livermore, California 94551, USA
3) University of California at Davis, Davis, CA 95616, USA

Abstract: The recently developed code *FREYA* (Fission Reaction Event Yield Algorithm) generates large samples of complete f ssion events, consisting of two receding product nuclei as well as a number of neutrons and photons, all with complete kinematic information. Thus it is possible to calculate arbitrary correlation observables whose behavior may provide unique insight into the f ssion process. The presentation f rst discusses the present status of *FREYA*, which has now been extended up to energies where pre-equilibrium emission becomes signif cant and one or more neutrons may be emitted prior to f ssion. Concentrating on ^{239}Pu(n,f), we discuss the neutron multiplicity correlations, the dependence of the neutron energy spectrum on the neutron multiplicity, and the relationship between the fragment kinetic energy and the number of neutrons and their energies. We also brief y suggest novel f ssion observables that could be measured with modern detectors.

Introduction

Nuclear f ssion presents an interesting and challenging physics problem which is still, about seventy years after its discovery, relatively poorly understood. Although much of the key physics involved is understood qualitatively, a quantitative description is still not in sight, despite vigorous efforts by many researchers. Because of its inherent complexity, f ssion provides an important testing ground for both static and dynamical nuclear theories. Furthermore, f ssion is also important to society at large because of its many practical applications, including energy production and counter proliferation, topics of current urgency.

Whereas the more traditional treatments of f ssion have sought to describe only fairly integral f ssion properties (see in particular Ref. [1]), such as the average energy release and the average differential neutron yield, many modern applications require more exclusive quantities, such as f uctuations in certain observables (e.g. neutron multiplicity) and correlations between different observables (e.g. neutrons and photons). There is thus a need for developing models that include the treatment of f uctuations and correlations.

Simulation models offer a powerful means for meeting this challenge because they generate large samples of complete f ssion events and subsequent event-by-event analysis can then provide any specif c correlation observable of interest. Furthermore, due to the more detailed quantities that can be addresses, such models may provide valuable guidance with regard to which observables are most crucial for further progress in the understanding of f ssion.

We have developed a calculational framework within which large samples of complete f ssion events can be generated, starting from a f ssionable nucleus at a specif ed excitation energy [2]. The associated computer code is named *FREYA* (Fission Reaction Event Yield Algorithm). We present here the model in a fairly basic form which, though quite simplistic in many regards, is already capable of producing interesting results. *FREYA* was employed in a recent study of sequential neutron emission following neutron-induced f ssion of ^{240}Pu [3] and it has recently been extended to pre-f ssion neutron emission [4].

We give here a brief overview of *FREYA*; more complete discussions may be found in the published literature [2–4]. Since the model is under active development, the results shown here are illustrative only.

Model components

The main components of *FREYA* are described below. The discussion follows the successive temporal stages of the f ssion process, from the agitation by the incident neutron to the deexcitation of the f ssion fragments.

Pre-fission emission

When the initial compound nucleus (^{240}Pu* here) is suff ciently excited, it may emit one or more neutrons before f ssion occurs. We take this into account in a manner similar to the post-f ssion evaporation (see later). At suff ciently high excitations we include pre-equilibrium emission [4]. At each stage, neutron emission competes with f ssion according to a simple model for the energy-dependent branching ratio [5]. Figure 1 (left) shows the resulting multi-chance f ssion probabilities compared to the *GNASH* calculations used in the ENDF-B/VII.0 evaluation [6]. The two calculations give rather similar probabilities. The kinematics, including the recoil momentum of the nucleus, is treated in an exact manner, while angular-momentum effects are ignored.

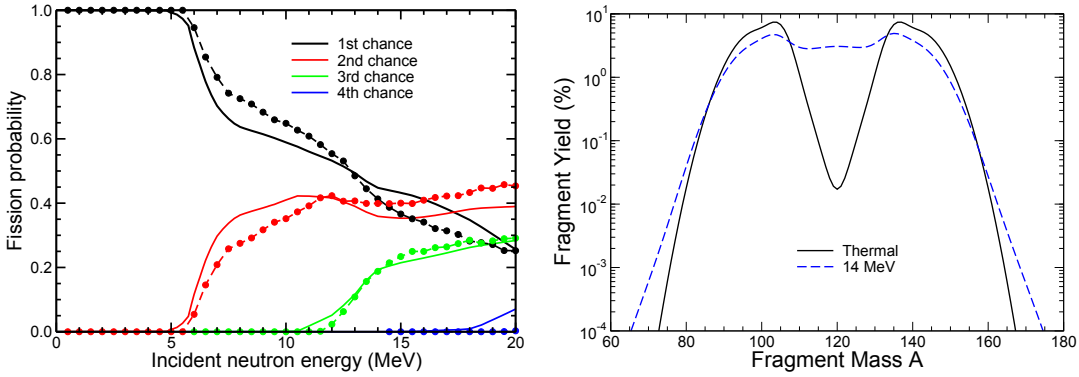

Figure 1: *Left: Probabilities for N^{th}-chance fission as functions of incident neutron energy E_n; the solid curves are GNASH calculations used in the ENDF-B/VII.0 evaluation while the dashed curves with circles are FREYA calculations. Right: Calculated fragment mass yields caused by thermal and 14 MeV neutrons (the latter includes contributions from multi-chance fission).*

Mass and charge partition

At the present stage of development, the fragment mass distribution $P(A_f)$ is based on experimentally observed yields. We employ a f ve-gaussian f t to $P(A_f)$ [7, 8], using energy dependent coeff cients so the distribution evolves from being asymmetric to predominantly symmetric as the energy is raised, as illustrated in Fig. 1 (right). Once the fragment masses, A_L and A_H have been sampled from $P(A_f)$, the fragment charges are sampled from a (truncated) normal distribution having a dispersion of $\sigma_Z = 0.50$ [9]. The Q-value associated with that particular split can then be calculated, $Q_{LH} = M(^{240}\text{Pu}^*) - M_L - M_H$. We use experimental data for the fragment masses where available [10] and supplement with calculated values [11] as needed.

Fragment kinetic energy

The Q-value is divided between the relative fragment kinetic energy *TKE* and internal fragment excitation. Since we do not yet have a suff ciently quantitative model for this division, we seek to match *TKE* to the experimental data [12–14]. A small overall energy-dependent adjustment *dTKE* is made subsequently in order to reproduce the measured average total neutron multiplicity $\bar{\nu}$ (see below), $TKE(A) \rightarrow TKE(A) + dTKE(E_n)$, where $dTKE \approx 1$–2 MeV. Figure 2 shows the resulting mass dependence of the total fragment kinetic energy. The two fragments are assumed to emerge isotropically back-to-back in the reference frame of the f ssioning nucleus and to have been fully acelerated before neutron evaporation commences.

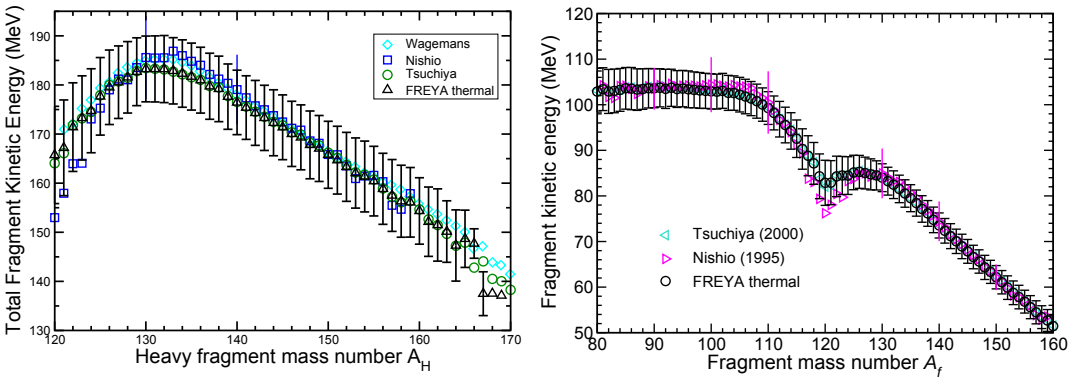

Figure 2: *The measured average TKE as a function of the heavy fragment mass number [12–14] compared to FREYA calculations at thermal energies, shown with the calculated dispersion in TKE for each A_H (left). The average fragment kinetic energy as a function of the fragment mass A_f from Refs. [13, 14] as well as FREYA results, at thermal energies (right).*

Energy partition

We assume that the remaining energy appears as statistical excitation of the two fragments. We first divide this energy between the two fragments in proportion to their respective heat capacities which are proportional to the Fermi-gas level-density parameters a_A for which we use the values calculated in Ref. [15], $\overline{Q}_L : \overline{Q}_H = a_L : a_H$. We then adjust the partioning in favor of the light fragment which tends to become hotter than the heavy one, $\overline{Q}_L \rightarrow x\overline{Q}_L$ (with a balancing decrease of Q_H), where the the global parameter x exceeds unity by 10–20%.

Subsequently we add statistical fluctuations to these mean excitations, assuming that they are given by the associated thermal variances, $\sigma_i^2 = 2\overline{Q}_i T_{LH}$. The fluctuations δQ_i are therefore sampled from normal distributions with variances σ_i^2. The fragment excitations in a given event are then $Q_i = \overline{Q}_i + \delta Q_i$. Energy conservation implies that the distribution of the total kinetic energy K_{LH} is a gaussian (such a form was already assumed in Ref. [16]) with the variance $\sigma_K^2 = \sigma_L^2 + \sigma_H^2$. The resulting fragment excitations are shown in Fig. 3 (left).

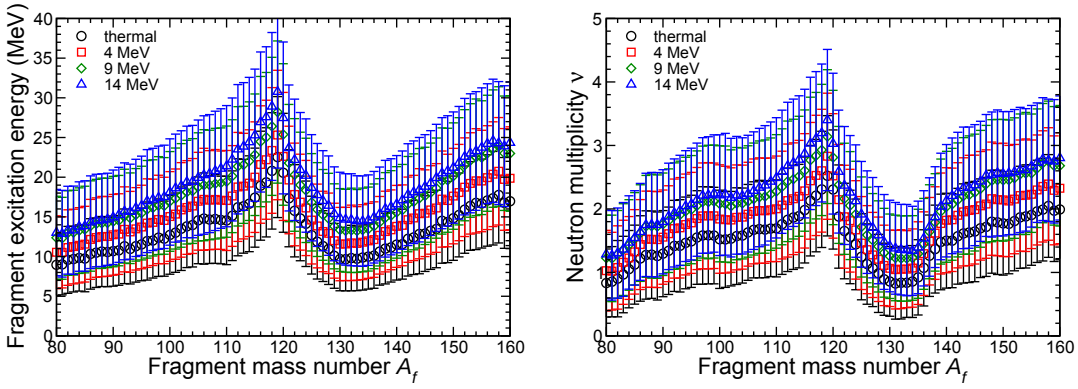

Figure 3: *The pre-evaporation excitation energy of a fully accelerated fission fragment (left) and the total multiplicity of (both pre- and post-fission) neutrons (right), calculated with FREYA for various incident neutron energies E_n. Both are shown as functions of the fragment mass number A_f. The vertical bars indicate the dispersions of the respective distributions.*

Neutron evaporation

We assume that the two excited fragments do not begin to de-excite until after they have been fully accelerated by their mutual Coulomb repulsion and their shapes have reverted to their equilibrium form. Furthermore, we ignore the possibility of charged-particle emission from the f ssion fragments. Each of the fully relaxed and accelerated f ssion fragments typically emits one or more neutrons as well as a (larger) number of photons. We assume that neutron evaporation has been completed before photon emission sets in, thus obviating the need for knowing the ratio of the decay widths, $\Gamma_\gamma/\Gamma_\mathrm{n}$.

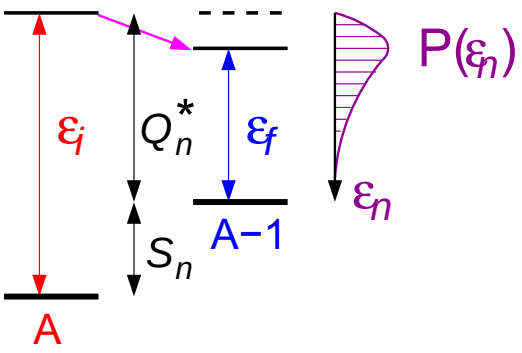

$$Q^*_\mathrm{n} = \varepsilon^*_i - S_\mathrm{n} = \varepsilon_f + \epsilon_\mathrm{n}$$

$$T_f^\mathrm{max} = \sqrt{Q^*_\mathrm{n}/a_A}$$

$$dP(\epsilon_\mathrm{n})/d\epsilon_\mathrm{n} \sim \epsilon_\mathrm{n}\,\mathrm{e}^{-\epsilon_\mathrm{n}/T_f^\mathrm{max}}$$

$$\epsilon_\mathrm{n} = -T_f^\mathrm{max}\ln(\eta_1\eta_2)\,,\quad \eta_i \in (0,1]$$

Figure 4: *The energetics relevant to the evaporation of a neutron from a nucleus with mass number A and excitation ε_i. The resulting neutron kinetic energy ϵ_n peaks at twice the maximum temperature in the daughter nucleus and can be quickly sampled from the associated spectral distribution $P(\epsilon_\mathrm{n})$ by means of standard uniform random numbers η.*

For each f ssion fragment, neutron radiation is treated by iterating a simple treatment of a single neutron evaporation until no further neutron emission is energetically possible, as illustrated in Fig. 4. Once the Q-value is known, it is straightforward to sample the momentum of an evaporated neutron, assuming that it is isotropic in the frame of the emitting nucleus and assuming that the kinetic energy has the distribution $P(\epsilon_\mathrm{n}) \sim \epsilon_\mathrm{n}\exp(-\epsilon_\mathrm{n}/T)$. Relativistic kinematics ensures exact conservation of energy and momentum. The resulting neutron multiplicity ν, shown in Fig. 3 (right), has a mass dependence similar to that of the fragment excitation energy.

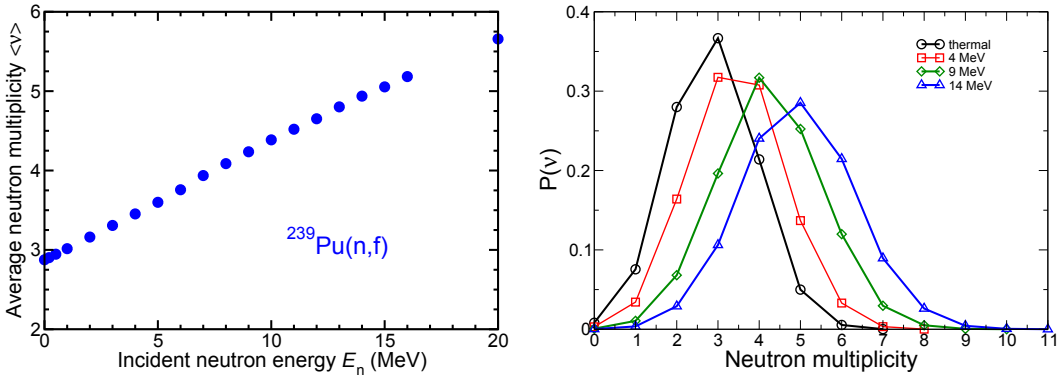

Figure 5: *The average neutron multiplicity as a function of the incident neutron energy E_n (left) and the neutron multiplicity distribution $P(\nu)$ for selected values of E_n (right).*

Above $E_n \approx 0.2$ MeV the expected neutron multiplicity grows steadily with the kinetic energy of the incident neutron, from nearly three for thermal neutrons to almost six for 20 MeV, as shown in Fig. 5 (left). The entire multiplicity distribution $P(\nu)$ is shown in the right panel for several selected energies. An examination of $P(\nu)$ shows that it is signif cantly narrower than the corresponding Poisson distribution. This is presumably because the reduction in excitation energy caused by an emission is dominated by the separation energy $S_n \approx 6.5$ MeV, which is signif cantly larger than the average of the statistical part of the energy reduction, $2T \approx 2$ MeV.

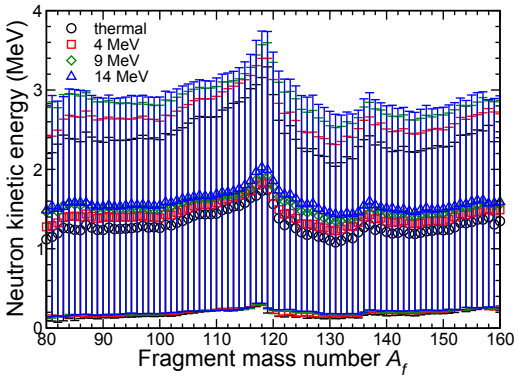

E_n (MeV):	0.5	14	14
ν	1st	1st	N^{th}
1	2.22	2.49	2.62
2	2.21	2.58	2.60
3	2.14	2.58	2.52
4	2.07	2.56	2.45
5	1.99	2.52	2.38
6	1.90	2.49	2.32
7	1.83	2.47	2.28
8		2.44	2.27
all	2.11	2.52	2.37

Figure 6: *The dependence of the neutron kinetic energy on the fragment mass number for various incident energies, with the bars indicating the respective energy dispersions (left) and the mean neutron kinetic energy for various total neutron multiplicities ν for $E_n = 0.5$ MeV and $E_n = 14$ MeV including either only 1st-chance fission or unlimited pre-fission emission (right).*

Generally, the f rst neutron evaporated from a fragment will tend to have a higher energy than the second one, and so on, see Fig. 6 (right). For this reason and due to the f uctuation in mass partition the resulting overall neutron spectral shape will not be of a simple form but have many components. While this complexity is automatically accounted for in event-by-event simulations, the feature cannot be obtained in treatments that consider only averages (e.g. [1]).

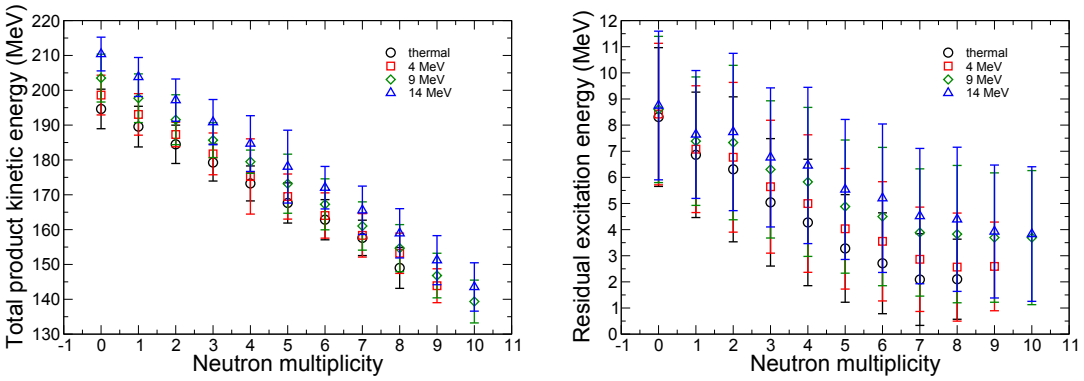

Figure 7: *The neutron-multiplicity dependence of the total kinetic energy of the two fission products (left) and their combined excitation after the neutron evaporation cascade (right), as obtained with FREYA for various incident neutron energies. The bars show the dispersions.*

Events having lower-than-average fragment kinetic energies will, by energy conservation, tend to have higher-than-average initial fragment excitations and, therefore, they will on average produce more neutrons. This expected anti-correlation between the neutron multiplicity and the product kinetic energy is indeed brought out by the *FREYA* results, as illustrated in Fig. 7 (left).

Photon emission

When the neutron evaporation cascades have been completed, the product nuclei are left with some residual excitation which will give rise to subsequent photon radiation. As illustrated in Fig. 7 (right), the degree of residual excitation tends to decrease with the multiplicity of emitted neutrons, as one might have expected on the basis of energy conservation. Consequently, one should also expect that the number of photons emitted will be anti-correlated with the neutron multiplicity.

At the present stage of development, *FREYA* treats the photon emission process only in a very rudimentary manner, considering it as if it were simply evaporation of massless particles. While this approach would certainly not be adequate for calculating the emission rates, it may provide a reasonable approximation for the spectral *shape* which should be primarily governed by phase space. Furthermore, as an elementary analysis will reveal, the ultra-relativistic limit appropriate for massless particles is as easy to simulate as the non-relativistic limit employed for the neutrons, the key feature being $\epsilon_\gamma \sim \ln(\eta_1\eta_2\eta_3)$. Therefore, in this approximate manner, *FREYA* can also treat the photon emission cascades in a numerically very eff cient manner.

Observables

FREYA produces a sample of complete f ssion events, each one being described by the four-vectors of the two product nuclei and of all the individual neutrons and photons emitted in that event. Special effort has been made to make the numerical code fast and, as a result, one million events can be generated within about ten seconds on a standard laptop computer. While such statistics suff ce for calculating most quantities of interest, it should be possible to devise more eff cient calculational strategies for the generation of specif c classes of rare events that might be of special interest.

Because *FREYA* produces complete events, it is straightforward to extract any observable of interest. The above exposition has presented a variety of observables. The special advantage of an event-by-event treatment is that it readily permits the extraction of f uctuations in any observable and the correlations between different observables, quantities that are not accessible in models designed to merely provide the mean behavior. Furthermore, because the elementary physical processes are treated explicitly, *FREYA* also tends to yield improved results for certain average quantities, such as the neutron energy spectrum.

As an example of a readily obtainable correlation observable, we consider here the angular correlation $C(\phi_{12})$ between two emitted neutrons. Fig. 8 shows the result for ^{239}Pu(n_{th},f). The correlation functions shown in the left panel include *all* the neutrons emitted in each event with kinetic energies above specif ed thresholds of 0.5, 1.0 and 1.5 MeV. The extracted $C(\phi_{12})$ is remarkably insensitive to the total neutron multiplicity ν (though it is somewhat stronger for events having very low multiplicity) and the correlations grow slightlystronger as the threshold energy is raised. Its form can readily be understood by considering events that have only two neutrons (with energies above 1 MeV), as shown in Fig. 8 (right): When both neutrons are emitted by the same fragment they exhibit a close angular correlation. It is strongest when the common source is the light fragment, presumably because of its higher speed. Conversely, when the two neutrons come from different fragments they exhibit a strong directional anti-correlation that is enhanced by the relative fragment motion. The combined correlation function for $\nu = 2$, $C_{\nu=2}(\phi_{12})$ is shown in both panels for reference.

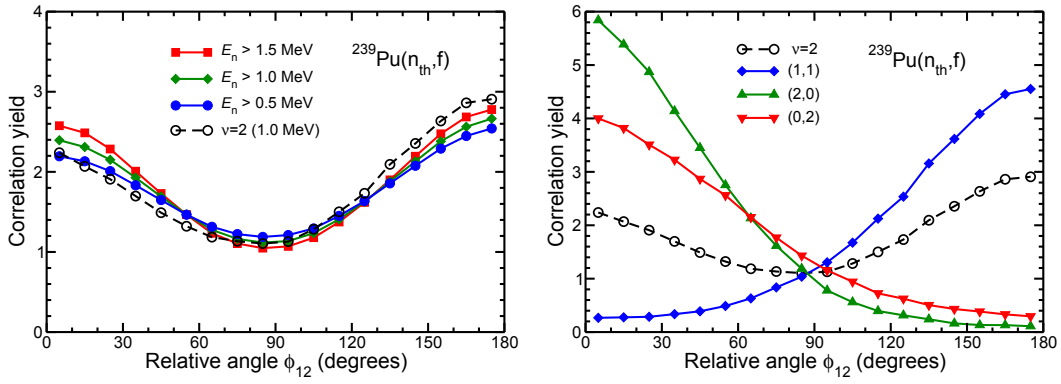

Figure 8: *Neutron angular correlations. Left: The correlation yield C(ϕ_{12}) for neutrons having energies above a specified threshold. Right: C(ϕ_{12}) for events that have a total multiplicity of two (each one with energy above one MeV), $\nu \equiv \nu_L + \nu_H = 2$ (solid black dots), together with the correlation for events where the two neutrons come from different fragments, $(\nu_L, \nu_H) = (1, 1)$ (blue diamonds) and for events where both neutrons come from the same fragment, either the light, $(\nu_L, \nu_H) = (2, 0)$ (green) or the heavy, $(\nu_L, \nu_H) = (0, 2)$ (red).*

A second example is the correlation between the neutron and photon multiplicities. As already mentioned above, a larger-than-average neutron multiplicity tends to yield a lower-than-average product excitation and, therefore, one would expect the neutron and photon multiplicities to be anti-correlated. This is indeed borne out by the *FREYA* calculations. Contrary to the mean neutron multiplicity $\bar{\nu}$, which increases steadily with the incident neutron energy E_n, the calculated average photon multiplicity is fairly independent of E_n. The magnitude of the calculated multiplicity correlation coeff cient (which is thus negative) decreases steadily with E_n. A quantitative discussion requires a more ref ned treatment of the photon emission.

Outlook

Over the past few years, experimental capabilities have improved dramatically while the practical applications of f ssion have broadened signif cantly. As a consequence, there has been an growing need for calculations of increasingly complex observables that are beyond the scope of the traditional f ssion models.

To meet this need, we have developed a new calculational framework, *FREYA*, which can generate large samples of individual f ssion events. From those it is then possible to extract any specif c observable of interest, in particular correlation observables of any complexity, without the need for further approximation. In developing *FREYA*, we have sought to make the numerics suff ciently fast to facilitate use of the code as a practical calculational tool.

Although the current version of *FREYA* is still only preliminary, it has already proven to be quantitatively useful. For example, the combination of the Monte Carlo f ssion model with a statistical likelihood analysis presents a powerful tool for the evaluation of f ssion neutron data which was used to develop an estimate of the f ssion neutron spectrum with uncertainties several times smaller than current experimental uncertainties [3]. *FREYA* has already proven to be capable of making interesting predictions for correlations in variety of contexts and we foresee an increased number of applications.

Acknowledgments
We acknowledge many helpful discussions with D.A. Brown, M.-A. Descalle, D. Gogny, E. Ormand, P. Möller, E.B. Norman, J. Pruet, W.J. Swiatecki, P. Talou and W. Younes. This work was performed under the auspices of the US Department of Energy by the Lawrence Livermore National Laboratory under Contract DE-AC52-07NA27344 (R.V.) and by the Lawrence Berkeley National Laboratory under Contract DE-AC02-05CH11231 (J.R.) and was also supported in part by the National Science Foundation Grant NSF PHY-0555660 (R.V.).

References

[1] D.G. Madland and J.R. Nix, Nucl. Sci. Eng. **81** (1982) 213.
[2] J. Randrup and R. Vogt, Phys. Rev. C **80** (2009) 024601.
[3] R. Vogt, J. Randrup, J. Pruet and W. Younes, Phys. Rev. C **80** (2009) 044611.
[4] R. Vogt, J. Randrup, D.A. Brown and E. Ormand, in preparation (2010).
[5] W.J. Swiatecki, K. Siwek-Wilczynska and J. Wilczynski, Phys. Rev. C **78** (2008) 054604.
[6] M.B. Chadwick *et al.*, Nucl. Data Sheets **107** (2006) 2931.
[7] U. Brosa *et al.*, Phys. Rep. **97** (1990) 1; U. Brosa, Phys. Rev. C **32** (1985) 1438.
[8] F.-J. Hambsch *et al.*, Nucl. Phys. A **491** (1989) 56.
[9] W. Reisdorf, J.P. Unik, H.C. Griff n and L.E. Glendenin, Nucl. Phys. A **177** (1971) 337.
[10] G. Audi and A.H. Wapstra, Nucl. Phys. A **595** (1995) 409.
[11] P. Möller, J.R. Nix, W.D. Myers and W. J. Swiatecki, At. Data Nucl. Data Tab. **59** (1995) 185.
[12] C. Wagemans *et al.*, Phys. Rev. C **30** (1984) 218.
[13] K. Nishio, Y. Nakagome, I. Kanno and I. Kimura, J. Nucl. Sci. Technol. **32** (1995) 404.
[14] C. Tsuchiya *et al.*, J. Nucl. Sci. Technol. **37** (2000) 941.
[15] T. Kawano, S. Chiba and H. Koura, J. Nucl. Sci. Technol. **43** (2006) 1.
[16] S. Lemaire *et al.*, Phys. Rev. C **72** (2005) 024601.
[17] N. Koura, M. Uno, T. Tachibana, and M. Yamada, Nucl. Phys. A **674**, 47 (2000).

Time dependent approach to the transition of the fissioning nucleus from saddle to scission

M. Rizea[1)], N. Carjan[1,2)]

1) Horia Hulubei – National Institute of Physics and Nuclear Engineering, Str.Atomistilor 407, P.O.Box MG-6, RO-077125, Bucharest-Magurele, Romania
2) Centre d'Etudes Nucleaires de Bordeaux-Gradignan, UMR 5797, CNRS/IN2P3 University Bordeaux I, BP 120, 33175 Gradignan Cedex, France
rizea@theory.nipne.ro

Abstract: We investigate the transition of the fissioning nucleus from the saddle to the scission point through the numerical solution of the bi-dimensional time-dependent Schrödinger equation (TDSE) with time-dependent potential. To describe the axially symmetric extremely deformed nuclear shapes involved, we have used modified Cassini ovals. The Hamiltonian in cylindrical coordinates ρ and z is discretized by using finite difference approximations of the derivatives. The initial wave-functions for TDSE are the eigensolutions of the stationary Schrödinger equation whose potential corresponds to the saddle point deformation. The TDSE is solved by a Crank-Nicolson method associated with transparent conditions at numerical boundaries. The time evolution is calculated until the neck connecting the primary fission fragments suddenly breaks. The numerical solutions have been used to evaluate relevant physical quantities in the case of the fissioning nucleus ^{236}U.

Introduction

Our study concerns the influence of the change of the nuclear shape on the nucleonic motion. In particular, we focus our attention to the diabatic fast descent of the fissioning nucleus from the saddle to the scission point. The numerical modelling of this process implies the solution of the time-dependent **Schrödinger** equation (TDSE) with time-dependent potential. Modified **Cassini** ovals were used to describe the nuclear shapes involved. The **Hamiltonian** in cylindrical coordinates is discretized by using adapted finite difference approximations of the derivatives. An algebraic eigenvalue problem is solved to obtain the initial wave functions, while the solution of TDSE is obtained by a **Crank-Nicolson** scheme with transparent boundary conditions. The resulting linear system at each time step is solved by the conjugate gradient method. The numerical solutions have been used to evaluate the number of emitted pre-scission neutrons, the spatial distribution of the emission points and the fragments' excitation energy just-before-scission. The approach has been applied to the nucleus ^{236}U at two mass asymmetries.

The time-dependent Schrödinger equation

The equation that describes the motion of a nucleon in an axially deformed nucleus has the form:

$$I\hbar\, \partial Y(\rho,z,\varphi,t)/\partial t = H(\rho,z,\varphi,t)\, Y(\rho,z,\varphi,t).$$

In cylindrical coordinates, the wave-function has two components, corresponding to spin up and down: $Y(\rho,z,\varphi,t)=f_1(\rho,z,t)e^{i\Lambda_1\varphi}|\uparrow>+f_2(\rho,z,t)e^{i\Lambda_2\varphi}|\downarrow>$, where $\Lambda_1=\Omega-1/2$, $\Lambda_2=\Omega+1/2$ and Ω is the projection of the total angular momentum along the symmetry axis. The **Hamiltonian** has also two components, H_1 and H_2. Due to the axial symmetry, φ is dropped out and we have:

$$H_1Y = O_1f_1 - C\,(S_c f_1 + S_a f_2),\quad H_2Y = O_2f_2 - C\,(S_b f_1 + S_d f_2)$$

where $O_{1,2} = -\hbar^2/(2\mu)(\Delta-\Lambda_{1,2}^2/\rho^2) + V(\rho,z,t)$, $\Delta = (1/\rho)\partial/\partial\rho + \partial^2/\partial\rho^2 + \partial^2/\partial z^2$. Δ is the **Laplacean**, V is the potential, C is a constant and the operators $S_a,\ldots,S_d$ represent the spin-orbit coupling.

The orientation (up and down) is implicitly considered. The nuclear shape is described in terms of modified **Cassini** ovaloids [1]. This representation depends on a set of parameters, allowing a flexible modeling of deformed nuclei. In our case we took only two shape parameters: α(elongation) and α_1(mass asymmetry). By the transformations $g_1 = \rho^{1/2} f_1$, $g_2 = \rho^{1/2} f_2$ (of **Liouville** type), the first derivative from the **Laplacean** is removed, resulting a simplified **Hamiltonian** $\hat{H}$ with the components $\hat{H}_1$, $\hat{H}_2$ and a wave function $\hat{Y}$ with the components g_1, g_2. We have:

$$\hat{H}_1\hat{Y} = L_1 g_1 + P_c g_1 + P_- g_2,\ \hat{H}_2\hat{Y} = L_2 g_2 + P_+ g_1 + P_d g_2,$$

where $L_{1,2} = -\hbar^2/(2\mu)[\partial^2/\partial\rho^2 + \partial^2/\partial z^2 + (1/4 - \Lambda_{1,2}^2)/\rho^2] + V(\rho,z,t)$, $P\pm = Q_1 \pm Q_2$, $Q_1 = C(\Omega/\rho)(\partial V/\partial z)$, $Q_2 = C[(\partial V/\partial\rho)(\partial/\partial z) - (\partial V/\partial z)(\partial/\partial\rho)]$, $P_c = -C(\Lambda_1/\rho)(\partial V/\partial\rho)$, $P_d = C(\Lambda_2/\rho)(\partial V/\partial\rho)$.
The **potential** V contains a **nuclear** term given by $V_N = -V_0[1+\exp(\Theta/a)]^{-1}$, where V_0 is the depth and a the diffuseness. The quantity Θ is an approximation to the distance between a point and the nuclear surface, described by **Cassini** ovals. The **spin-orbit** interaction is taken proportional to the gradient of V_N. The constant C involves the strength of the interaction. For charged particles, the potential contains also a **Coulomb** term [2].

Numerical solution
The **TDSE** is solved by a **Crank-Nicolson** scheme which includes the first derivative of V with respect to t:

$$[1+(i\Delta t)/(2\hbar)\hat{H}+(i\Delta t^2)/(4\hbar)V_t']\hat{Y}(t+\Delta t) = [1-(i\Delta t)/(2\hbar)\hat{H}-(i\Delta t^2)/(4\hbar)V_t']\hat{Y}(t),$$

where Δt is the time step. For numerical solving, the infinite physical domain should be limited to a finite one, [0,R]x[-Z,Z], which is discretized by a grid with the mesh points: $\rho_j = j\,\Delta\rho, 1 \le j \le J$ ($\rho_J = R$), $z_k = k\Delta z$, $-K \le k \le K$ ($z_K = Z$). At each point the partial derivatives in $\hat{H}$ are approximated by finite difference formulas. For the derivatives with respect to z we used standard 3-point formulas, while for the derivatives in ρ, we used adapted formulas with variables coefficients [3], which take into account the accomplished function transformation (of the form: $g = \rho^{1/2} f$). Let us denote g_{jk}^n the approximation of g in the point (ρ_j, z_k) and at time $t_n = n\Delta t$ (g is any of g_1 and g_2). As initial solution (at $t_0 = 0$) we take an eigenfunction of the **stationary Schrödinger equation** whose potential corresponds to the saddle point deformation. We use the same discretization of the Hamiltonian and we arrive to an algebraic eigenvalue problem, which is solved by the package **ARPACK** [4], based on the Implicitly Restarted **Arnoldi** Method. The solution at time t_{n+1}, represented by the values g_{jk}^{n+1}, is obtained in terms of the solution at time t_n, on the basis of the above Crank-Nicolson scheme, which turns into a linear system, after the discretization. It is solved by the **conjugate gradient method** [5].
Special conditions on the boundaries of the computional domain should be imposed to avoid the reflexions which alter the propagated wavefunction. We implemented a variant of **transparent boundary conditions**. The idea is to assume near the boundary r_B the following form of the solution: $g = g_0 \exp(i\, k_r\, r)$, where $g_0, k_r \in \mathbb{C}$ (a 1D notation was used). Linear relations between g_{B+1} and g_B then result, which are used in the finite difference formulas for the derivatives at r_B, when the Crank-Nicolson scheme is applied. In 2D, this algorithm should be used at each point of the grid belonging to boundaries.
We advance the solution during a temporal interval [0,T]. The deformation parameters are changing on this interval. The times 0 and T correspond to the saddle point and to the scission moment (when the neck connecting the primary fission fragments suddenly breaks), respectively. At each time step the potential and its derivative are recalculated.

Application to pre-scission neutrons and pre-scission fragments' excitation energy
Let $|Y^i\rangle$ and $|Y^f\rangle$ be the eigenfunctions corresponding to the saddle point and just-before-scission configurations respectively. The propagated wave functions $|Y^i(t)\rangle$ become wave

packets with few positive-energy components. The probability that a neutron occupying the state $|Y^i>$ at saddle point populates such unbound states gives the probability of this neutron to be emitted before scission:

$$P_{em}^{\ i}=\sum_f |a_{if}|^2,\ a_{if} = <Y^i(T)|\ Y^f> = 2\pi \int\int (g_1^{\ i}(T)\, g_1^{\ f} + g_2^{\ i}(T)\, g_2^{\ f})\, d\rho\, dz.$$

The sum on index f is over the unbound states. From computational point of view it is more convenient to obtain the bound than the continuum states. Therefore, we change the formula to $P_{em}^{\ i}=1-\sum_f |a_{if}|^2$, where the sum is now over the bound states. From this we can obtain

- **the total number of emitted pre-scission neutrons**:

$$v_{ps} = 2\ \sum_i v_i^2\ P_{em}^i.$$

The factor of 2 is due to the spin degeneracy. v_i^2 is the ground-state occupation probability of the state $|Y^i>$. To obtain it one can consider the neutrons either **independent** or **pairing correlated.** In the first case $v_i^2 = 1$ if $1 \le i \le N/2$ (N is the number of neutrons) and 0 otherwise (a step function). In the second case $v_i^2 = \frac{1}{2}\{1-(e_i-\lambda)/[(e_i-\lambda)^2+\Delta^2]^{1/2}\}$ with Δ and λ deduced from the BCS equations. e_i is the eigenenergy of the state $|Y^i>$.
One can also calculate:

- **the fragments' excitation energy just-before-scission**, given by

$$E^*_{ps} = 2\ \sum_f (V_f^2\ - v_f^2)\ e_f \text{ with } V_f^2 = \sum_i v_i^2\ |a_{if}|^2.$$

The sums are over the bound states. V_f^2 is the occupation probability of each final state $|Y^f>$ just-before-scission and e_f is the corresponding eigenenergy;

- **the spatial distribution of the emission points** as a function of ρ and z:

$$S_{em}(\rho,z) = \sum_i v_i^2 |Y^i_{em}(\rho,z)|^2,$$

where $|Y^i_{em}> = |Y^i(T)> - \sum_f a_{if}|Y^f>$ is the part of the initial wave function that has been emitted. The sum is over the bound states. The numerical evaluation of the overlap integrals is performed by the **Simpson** formula. With respect to ρ the formula is adapted as well to the special form of the solutions g_1, g_2. Before calculating the coefficients a_{if}, the eigenfunctions provided by ARPACK are orthonormalized by the **Gram-Schmidt** algorithm.

Numerical experiment
We have applied the above formalism to the nucleus $^{236}U_{92}$. The numerical domain was:
$\rho \in [\Delta\rho,32]$, $z \in [-32,32]$, while $\Delta\rho = \Delta z = 1/8$. The saddle point and the just-before-scission point are characterized by the parameters $\alpha^i = 0.7$ and respectively, $\alpha^f = 0.985$ in the Cassini description of the nuclear shapes. The fission can be symmetric (each fragment has the mass 118) or, more frequently, asymmetric. As illustration we present two cases: $A_L = 86$ and $A_L = 114$, where A_L the light fragment mass. Depending of this mass and of α, one more deformation parameter (α_1) for the modified Cassini ovals is deduced.

In the next Table we present the pre-scission neutron multiplicities (v_{PS}) and excitation energies (E^*_{ps}) in MeV obtained for different durations T of the saddle to scission descent at $A_L = 86$ and 114. We used a time step $\Delta t = 1/256 \times 10^{-22}$ s, while Ω has taken the values 1/2, 3/2,...,11/2. Both types of occupation probabilities have been used. T=0 corresponds to the sudden approximation [6].

Table 1. *Pre-scission neutron multiplicity and excitation energy*

A_L	T (10^{-22} s)	ν_{PS} - IP	ν_{PS} - PC	E^*_{ps} - IP	E^*_{ps} - PC
86	0	40.3257	40.2805	663.209	656.067
86	10	3.36526	3.63580	90.8306	86.9816
86	30	0.39024	0.51667	35.6318	31.8354
-----	-----	-----	-----	-----	-----
114	0	45.5216	45.6982	719.324	709.990
114	10	3.66186	4.26683	85.3434	86.6716
114	20	0.78603	1.28048	39.8740	42.9365
114	30	0.30819	0.83811	29.7251	33.3912
114	40	0.15444	0.54392	25.0595	27.5400
114	50	0.08669	0.44597	21.3422	23.9871
114	100*	0.00600	0.18804	16.3270	17.9709

*extrapolated values

As expected, both ν_{PS} and E^*_{PS} are decreasing with increasing T, a slow descent being adiabatic and the sudden approximation being an upper limit. Due to the limited speed of the available computers, we could not calculate cases with saddle-to-scission times larger than $50*10^{-22}$ sec. For zero dissipation, the Los Alamos Finite Range Macroscopic Model predicts T = $25*10^{-22}$ sec. [7]. More realistic calculations including the "wall and window" one-body dissipation predict T = $300*10^{-22}$ sec. It would be therefore useful to improve the efficiency of our computer codes and repeat the present calculations for larger T values. We are planning to do this in the near future. However, to get an idea of the ν_{PS} and E^*_{PS} values expected at T = 100 we have used an extrapolation (see the last row in Table 1). The very low extrapolated value of ν_{PS} seems to indicate that adiabaticity is already attained at T = 100. The still large value of the excitation energy left at scission (≈ 17 MeV) originates from the single-particle approximation used and not from the interaction with the moving potential wall. In our model the neutrons conserve their Ω-value and they are therefore promoted at each level-crossing to the higher level. This creates an excitation energy even in the adiabatic regime.

In Figures 1-5 the spatial distributions of the emission points for A_L=86 (asymmetric case) and for A_L=114 (nearly symmetric case) are shown for different saddle-to-scission times T. The distributions correspond to the whole set of Ω's between 1/2 and 11/2. The BCS probabilities have been considered. To give an idea of the nuclear shapes involved, we added (dotted) in each figure the equipotential $V_0/2$ lines at the saddle and at the just-before-scission points. For short times (T ≤ 10) the emission points are concentrated in the region between the nascent fragments similar to the case of the sudden transition at scission previously studied [8]. For longer times (T ≥ 30), in addition to the decrease of the integrated value

$$\int S_{em}(\rho,z)\, \rho\, d\rho\, dz = \nu_{PS}$$

already noticed above, there is also a simultaneous spread of the emission points all over the fragments. This effect, that is best observed by comparing Figs.3 and 5, influences both the final (i.e. after taking into account the reabsorption [9]) pre-scission neutron multiplicity and their angular distribution. All the S_{em} functions are represented between their minimum and maximum values in the spatial domain. The maximum decreases with increasing T (about one order of magnitude between T=10 and T=30).

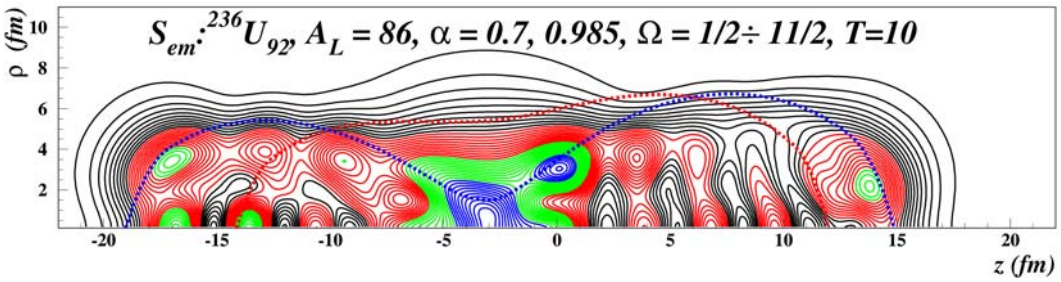

Figure 1. *Distribution of emission points at A_L=86, Ω*=1/2,...,11/2, T=10

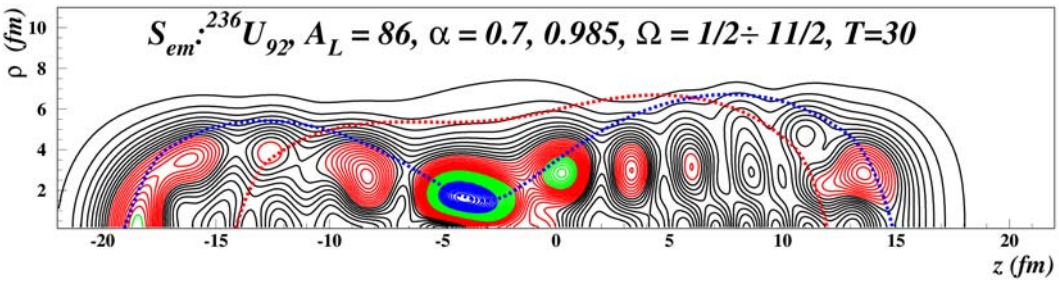

Figure 2. *Distribution of emission points at A_L=86, Ω*=1/2,...,11/2, T=30

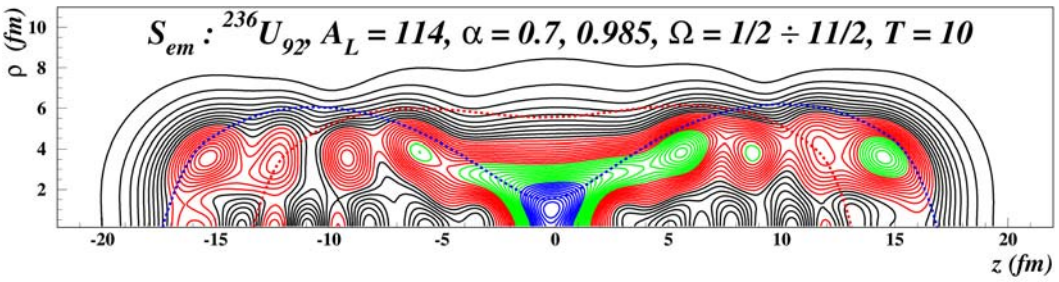

Figure 3. *Distribution of emission points at A_L=114, Ω*=1/2,...,11/2, T=10

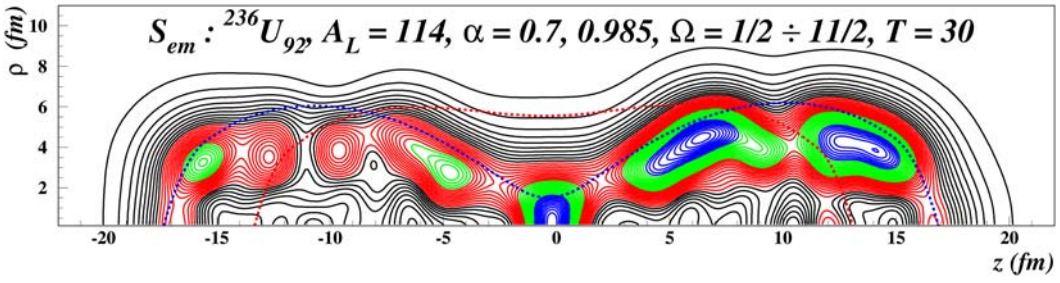

Figure 4. *Distribution of emission points at A_L=114, Ω=1/2,...,11/2, T=30*

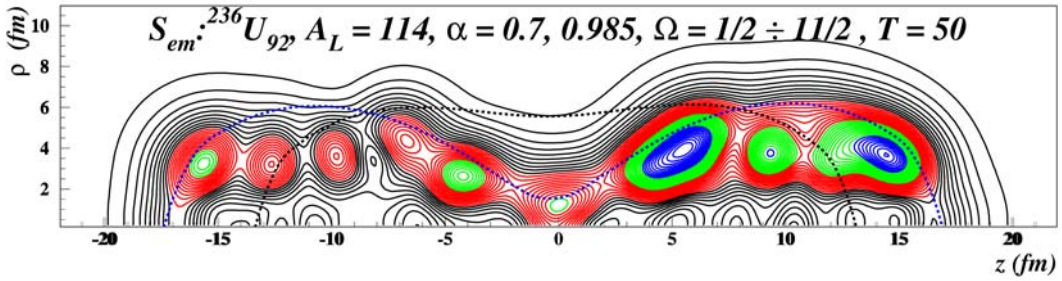

Figure 5. *Distribution of emission points at A_L=114, Ω=1/2,...,11/2, T=50*

Conclusions

In order to numerically describe the transition of the fissioning nucleus from saddle to scission we have used a time-dependent approach. This implies the solution of the TDSE in two spatial coordinates. Applying adequate procedures, which include Liouville transformation and special finite differences adapted to the solution behavior, we were able to determine relevant physical quantities like pre-scission neutron multiplicity and fragments' excitation energy and also to evaluate the spatial distribution of emission points. The neutrons were considered independent as well as pairing correlated. Calculations of this type for a large set of mass asymmetries, for longer, more realistic durations and for different fissioning nuclei can contribute to an improved characterization and understanding of this most important stage of the fission process.

Acknowledgement

Work partially supported by the projects PN09370102 and CNCSIS/IDEAS 119/2007.

References

[1] V.V. Pashkevich, Nucl.Phys. A 169, 275 (1971)
[2] J. Damgaard, H.C.Pauli, V.V. Pashkevich, V.M. Strutinsky, Nucl.Phys. 135, 432 (1969)
[3] M. Rizea, V. Ledoux, M. Van Daele, G. Vanden Berghe, N. Carjan, Comput. Phys. Comm. 179, 466 (2008)
[4] D. Sorensen, R.Lehoucq, Chao Yang, K. Maschhoff: www.caam.rice.edu/software/ARPACK
[5] H.A.vanderVorst,SIAMJ.Sci.Stat.Comput.13,631(1992) www.math.uu.nl/people/vorst/software.html
[6] N. Carjan, P. Talou, O. Serot, Nucl.Phys. A 792, 102 (2007)
[7] N. Carjan, A.J. Sierk, J.R. Nix, A 452, 381 (1986)
[8] N. Carjan, M. Rizea, Phys.Rev. C 82, 014617 (2010)
[9] T. Wada et al., these Proceedings.

Excitation-energy sorting in pre-scission dynamics

K.-H. Schmidt, B. Jurado

CENBG, CNRS/IN2P3, Chemin du Solarium B.P. 120, 33175 Gradignan, France
K.H.Schmidt@gsi.de

Abstract: The thermodynamically driven processes in pre-scission dynamics are investigated. During the shape evolution towards scission, the two nascent fragments develop their individual properties. The fact that the different temperatures of the two fragments do not depend on excitation energy, which is deduced from recently measured level densities, leads to an excitation-energy sorting process, where all intrinsic excitation energy is transferred to the cold fragment. This process has an impact on the emission of prompt neutrons and gamma rays from the two fragments. If the energy-sorting process is completed, before the exchange of protons through the neck becomes inhibited, the hotter fragment is formed with a preferentially even number of protons.
Calculations with a schematic model demonstrate that the proposed scenario accounts for several complex features of prompt neutron emission and of the even-odd effect in fission-fragment yields, which remained unexplained up to now. The importance of nuclear fission as a laboratory for studying the dynamics of non-equilibrium processes between mesoscopic superfluid objects is stressed.

Introduction

Most objects in nature have an approximately constant number of degrees of freedom, and their temperature, defined as the average excitation energy per degree of freedom, increases with increasing total excitation energy E^* of the system. However, nuclei with moderate E^* behave very differently. Experiments on nuclear level densities have shown that at least up to E^* = 6-7 MeV the temperature of nuclei does essentially not change with increasing E^* [1]. Moreover, it was even found recently that for medium-mass nuclei the temperature stays constant up to E^*= 20 MeV [2]. The main reason for this constant-temperature behaviour is that pairing correlations lead to an effective number of degrees of freedom that increases in proportion to E^*. Cooper pairs of neutrons and protons melt in a way that the mean energy per nucleonic excitation and thus the nuclear temperature stays constant. In nature, this behaviour appears in first-order phase transitions (e.g. solid-liquid or liquid-gas). In a mixture of two phases, like ice and water, the temperature of the mixture remains constant when energy is introduced or extracted, as long as both phases are present. Only the fractions of the two phases vary. It is of special interest to study, how two mesoscopic quantum-mechanical objects in such a particular regime of constant temperature behave when they are in thermal contact. The scission configuration in the nuclear-fission process, where two different nuclei can exchange E^* through the neck, offers a unique possibility to investigate this phenomenon.

Energy balance at scission

In fission, the energy difference between the ground-state masses of the initial fissioning system and the final fission fragments, given by the Q value, and the initial excitation energy of the fissioning nucleus E^*_{CN}, end up either in the total excitation energy (*TXE*) or in the total kinetic energy (*TKE*) of the fragments. The *TXE* is available for particle evaporation and gamma emission either before scission or from the separated fragments. In this work, we consider low-energy fission with initial excitation energies E^*_{CN} up to a few MeV where evaporation and gamma emission on the fission path is considered to be weak. The same is true for neck emission of neutrons. Since fission fragments are neutron-rich, evaporation proceeds almost exclusively by neutrons. We assume that already somewhat before the scission configuration the two nascent fragments have acquired their individual properties concerning shell effects [3,4,5] and pairing correlations [6] and can be treated as two well defined nuclei set in thermal contact through the neck. Theoretical investigations of the gradual transition from the mononucleus regime to the di-nuclear system [3,4,5,6,7,8] support this assumption.

We will now consider how the *TXE* is divided between the two nascent fragments. Following the transition-state approach of Bohr and Wheeler [9], all the available *E** above the barrier height is assumed to be thermalised, that means it is, on the average, equally distributed between all available intrinsic and collective degrees of freedom. These are the single-particle excitations and the collective normal modes. On the way to scission, the difference in potential energy between saddle and scission [10] may feed some amount of pre-scission kinetic energy in fission direction, excitations of normal collective modes and additional intrinsic excitations.
We may distinguish three classes of energy, which add up to the final *TXE* of the fission fragments, according to their appearance at scission: (i) Collective excitations stored in normal modes. (ii) Intrinsic excitations by single-particle or quasi-particle excitations. (iii) Deformation energy. The deformation energy ends up as part of the *E** available when the fission fragments recover their ground-state deformations.
The deformation induced in the two nascent fragments can be considered as a superposition of a macroscopic trend, caused by the mutual Coulomb repulsion of the nascent fragments, which favours a large prolate deformation around β = 0.5 [11] and a structural influence due to shell effects. Different fission modes correspond to substantially different deformations at scission and, thus, to different amounts of deformation energy of the individual fragments. Theoretical arguments on the deformation of the fragments at scission can be deduced from shell-model calculations [11,12], while experimental information can be extracted from the saw-tooth-like behaviour of the neutron yields, which is thought to be caused to a great extent by the variation of the contribution of the deformation energy to the *E** of the fragments.
The division of collective excitations among the two fragments is intimately related to the nature of the specific collective mode considered. As an example, the division of *E** stored in angular-momentum-bearing modes is governed by the momenta of inertia of the fragments and the conservation of total angular momentum. If the fissioning nucleus has zero angular momentum, and orbital angular momentum is neglected, both fragments must carry the same amount of angular momentum (in opposite direction), and, thus, the *E** is inversely proportional to their moment of inertia. Thus, for these specific modes, the lighter fragment tends to carry the larger portion of *E**.

Division of intrinsic excitation energy

The division of intrinsic excitations can be derived when thermal equilibrium at scission is assumed among the intrinsic degrees of freedom in each fragment. As said above, the nuclear level density at low *E** is very well described by the constant-temperature formula:

$$\rho(E^*) \propto \exp(E^*/T) \tag{1}$$

In a recent work, Egidy et al. have obtained the following dependence of the nuclear temperature *T* with the nucleus mass number *A* and with shell effects *U* from a fit to available data on nuclear level densities [13] :

$$T = \frac{1}{A^{2/3}}(17.45 - 0.51\,U + 0.051\,U^2) \tag{2}$$

This leads to a very interesting situation for the two nascent fragments at the scission-point configuration: The level density of each fragment is represented by the constant-temperature formula (1) with a specific value of *T* for each fragment. As a consequence, there is no solution for the division of intrinsic *E** with $T_1 = T_2$. As long as some excitation energy remains in the fragment with the higher temperature, its *E** is transferred to the fragment with the lower temperature. That means, a process of *E** sorting takes place where all *E** accumulates in the fragment with the lower temperature, while the other fragment looses its entire *E**. According to formula (2) the heavy fragment generally has the lower *T* and thus attracts all the *E**. Some deviations from the constant-temperature behaviour appear in the range of the first quasi particle excitations [14].
Due to the influence of shell corrections on *T*, see eq. (2), the direction of the energy transfer may be reversed if the heavy fragment is stabilised by a strong shell effect. This may be possible in the standard I (SI) fission channel, which is characterised by the formation of a heavy fragment close to the doubly magic ^{132}Sn.
The flow of excitation energy from the hot fragment to the cold fragment is a way for the entire system made of the two nascent fragments in contact to maximise the number of occupied

states or its entropy. In fact, the entropy S is a linear function of the partitioning of the total excitation energy $E^* = E^*_1 + E^*_2$:

$$S = S_1 + S_2 = \frac{E_1^*}{T_1} + \frac{E_2^*}{T_2} = \frac{E_1^*}{T_1} + \frac{E^* - E_1^*}{T_2} = \frac{E^* T_1 + (T_2 - T_1)\cdot E_1^*}{T_1 \cdot T_2} \tag{3}$$

The number of available states of the light nucleus or closed-shell nucleus is small compared to that of the complementary fragment. Therefore, the situation in which the light nucleus or the closed-shell nucleus has part of the E^* leads to a smaller entropy than the situation in which the entire E^* is transferred to the heavy or the non-closed-shell nucleus which has considerable more available states.

Prompt neutron yields

The number of evaporated neutrons as a function of the fragment mass is directly related to the excitation energy of the fragment and, therefore, should clearly reflect the peculiar situation of the full transfer of the intrinsic excitation energy to the cold fragment. The neutron-induced fission of ^{237}Np has been studied very carefully at two different neutron energies [15]. Fig. 1 shows the average number of evaporated neutrons as a function of the fragment mass. As mentioned above, the well known saw-tooth-like behaviour of this curve is attributed to the deformation energy. The minimum close to A=130 is due to the shell closures N=82, Z=50 that lead to spherical fission fragments. An increase of incident neutron energy translates into an increase of E^* of the compound nucleus. The increase of the emitted neutrons near symmetry for 110<A<130 with incident neutron energy is caused by the increase of the yield of the super long (SL) mode which is related to well deformed fission fragments. For more asymmetric mass splits outside this range, we observe a very peculiar feature: Interestingly, Fig. 1 shows that the increase of E^* leads to an increase of the number of evaporated neutrons for the heavy fragment, only. Since the neutron yield of the fission fragments for a fixed mass fluctuates over several neutrons, the mean value is a very sensitive measure of the fragment excitation energy. If the mean energy available changes, the contribution on one or the other wing of the neutron-multiplicity distribution decreases respectively increases, and, thus, the mean value is shifted. Actually, a quantitative analysis of the data reveals that all of the increased E^* appears in the heavy fragment. This observation is rather general as it was also found for other fissioning systems such as ^{233}U and ^{238}U and other incident particles like protons [16,17,18,19]. However, no clear explanation has yet been found for this effect. The reason is that all the work [20,21,22] done to study the partition of intrinsic excitation energy between fission fragments is based on the formula of Bethe [23].

$$\rho(E^*) \propto \exp(2\sqrt{a E^*}) \tag{4}$$

where a is the level-density parameter which is proportional to the mass number A of the nucleus. The latter formula is based on independent particles in an equidistant single-particle level scheme. Under the assumption of thermal equilibrium at scission, one obtains an intrinsic E^* division in proportion of the mass ratio of the fragments: $E^*_1 / E^*_2 = A_1 / A_2$.

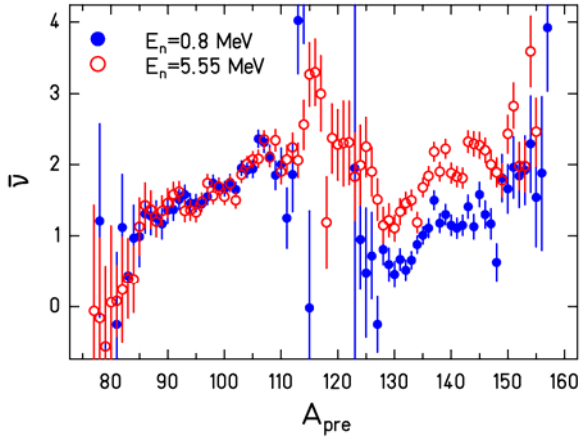

Figure 1. *Average number of prompt neutrons as a function of the primary fragment mass for the neutron-induced fission of ^{237}Np at two incident-neutron energies, data taken from ref. [15].*

The tendency to divide the available excitation energy according to the mass ratio has been confirmed empirically in many binary reactions involving relatively high E^* [24], although also deviations from full equilibration were observed due to insufficient reaction time [25]. However, this expression is not applicable at low E^* and fails to explain the observation presented in Fig. 1 that all the increase in E^* is found in the heavy fragment. Actually, this effect is a direct consequence of the different constant temperatures of the two fragments at scission. According to eq. (2), the temperature of the heavy fragment, in the absence of strong shell effects, is always lower than the temperature of the light fragment. Therefore, the heavy fragment will absorb the entire available intrinsic E^* and evaporate more neutrons.
We would like to stress that our argumentation is based on the same assumptions as other work that investigates the sharing of intrinsic E^* at scission [20,21,22]. That is, we have assumed independent fission fragments and a process of thermal equilibration between the fragments at scission. What is substantially different in our approach is that we use the constant-temperature level density which correctly describes the behaviour of nuclei at moderate E^* and not the commonly used Fermi gas level density of eq. (4) which is only valid at high E^*.

Features of the even-odd effect in fission

Pairing correlations are not only at the origin of the constant-temperature behaviour of the nuclear level density, they manifest themselves also in a number of observables, which are modulated by an even-odd structure [26]. The most prominent manifestation of pairing correlations in nuclear fission is the enhanced production of even-Z elements in low-energy fission of an even-Z compound nucleus. Figure 2 shows the Z distribution observed in the fission of ^{229}Th, which was produced as a secondary beam from 1 A GeV ^{238}U projectiles and which was excited in the Coulomb field of lead target atoms slightly above the fission barrier with a width of about 5 MeV (FWHM) [27]. Due to the inverse kinematics, an excellent Z resolution has been achieved. Moreover, this experiment allowed measuring the even-odd structure continuously over a large range of mass splits. This was not possible in heavier actinides due to the extremely low yields for symmetric splits.

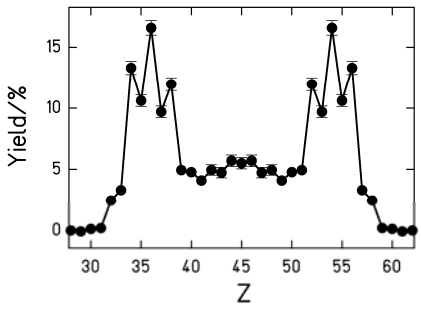

Figure 2. *Element distribution observed in the electromagnetic-induced fission of ^{229}Th [28].*

At present, several systematic features have been established experimentally [29]. The left part of Fig. 3 shows experimental data on the local even-odd effect δ_p, defined as the logarithmic four-point difference [30] as a function of charge asymmetry for different fissioning nuclei measured at ILL Grenoble. Fission was induced by thermal neutrons with the exception of ^{229}Th, where fission was induced by electromagnetic excitations. The experimental data from previous compilations (refs. [28,31,32]) and from figure 3 clearly illustrate several features:
(i) The amplitude δ_p of the even-odd structure decreases with increasing initial excitation energy and with increasing mass of the fissioning system.
(ii) There is a drastic increase of the even-odd structure at large asymmetry.
(iii) Also odd-Z fissioning systems like ^{239}Np and ^{244}Am show an even-odd structure in the Z yields, however, only at large asymmetry. Enhanced production of even-Z nuclei is observed in the light fragment, while the production of odd-Z nuclei is enhanced in the heavy fragment. The magnitude of the even-odd effect observed at large asymmetry is about the same in even-Z and in odd-Z fissioning systems of comparable mass.
The theoretical interpretation of the even-odd effect in fission-fragment yields was inspired for a long time by the observation that the magnitude of the effect is very sensitive to the initial excitation energy of the fissioning system and that no even-odd effect had been observed in odd-Z fissioning systems. Thus, the even-odd effect seemed to be a measure for the survival

of a completely paired proton configuration at scission. Based on statistical concepts, several authors attempted to relate the magnitude of the even-odd structure in the *Z* yields with the intrinsic excitation energy available in the fissioning system in the vicinity of the scission point [26,31]. In this spirit, the lowering of the even-odd effect towards symmetry and the increase towards asymmetry was associated with "hot" symmetric fission and "cold" asymmetric fission [33]. It seems plausible that the amount of intrinsic excitation energy is reduced in very asymmetric fission due to the higher conditional fission barrier, since this interpretation is in line with the reduced yields. However, this explanation is not consistent with the assumption of "hot" symmetric fission, which is also characterised by low yields and a higher barrier in the heavier actinides [34].

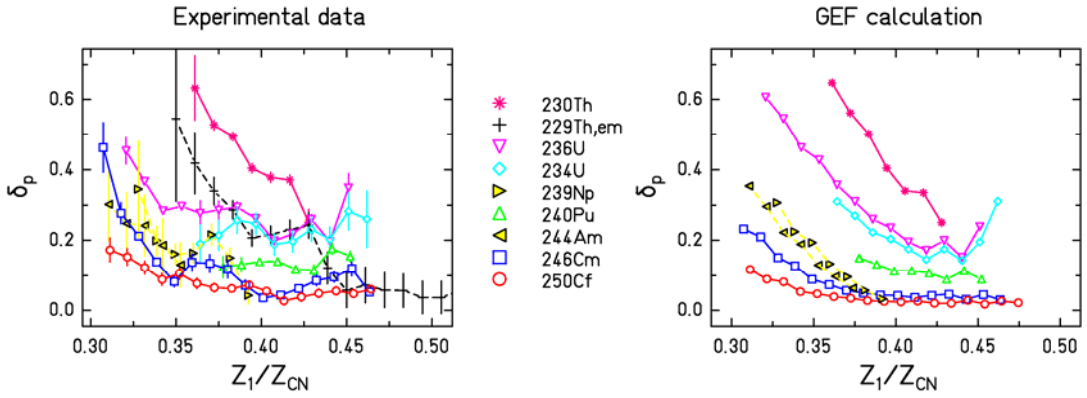

Figure 3. *Left part: Systematics of the measured local even-odd effect as a function of asymmetry, parameterised as the ratio of the Z of the light fragment and the Z of the fissioning nucleus Z_1/Z_{CN}, for thermal-neutron-induced fission of heavy nuclei. The fissioning nucleus is indicated. The data have been taken from ref. [29]. The local even-odd effect of the electromagnetic-induced fission of ^{229}Th [28] (see figure 2) is shown in addition. Right part: Result of a calculation with the GEF code [35].*

Some attempts were made to theoretically study the dynamical process of pair breaking in the fission process [6,31,36,37]. But none of them can explain the drastic increase of the even-odd effect at large asymmetry. Qualitative arguments for this increase were given on the basis of the mass dependence of the pairing gap [38] or the single-particle level density [28,39], but they stayed on a purely statistical level, and the quantitative agreement with the data was not satisfactory.

Even-odd effect in asymmetric fission and energy sorting

In the present work, we apply our considerations on the energy-sorting mechanism in superfluid fission dynamics [40] to propose a dynamical scenario for the asymmetry-associated even-odd effect in fission. Since the temperature of the fragments remains unchanged in spite of the variation of E^*, the light fragment will transfer all its E^* to the heavy one. It seems natural and unavoidable that the complete energy sorting finally also favours the production of even-*Z* (and even-*N*) nuclides in the light fragment, because this leads to a considerable energy gain in the heavy fragment and thus to an increase in entropy of the system. The gain in E^* can be up to four times the pairing gap. Therefore, according to the energy-sorting mechanism, there will be a tendency for the hot (normally the light) fragment to be fully paired.

Let us now consider the dynamics of the energy-sorting process. The time *t* to form a fully paired light fragment is the sum of the time needed for the light fragment to transfer all its E^* to the heavier one, and the time to exchange few nucleons through the neck. The latter time is rather short so that the time *t* is dominated by the time to transfer all the E^*. The latter will increase with the initial excitation energy in the light fragment $E^*_{0,\mathrm{light}}$ since it will take a longer time to transfer all the energy from the light to the heavy nucleus. We consider that the initial excitation energy $E^*_{0,\mathrm{light}}$ is proportional to the available excitation energy at scission E^*_{sci} which is the sum of the excitation energy at saddle E^*_{CN} and the dissipated energy between

saddle and scission $E^*_{sad-sci}$. E^*_{CN} increases with beam energy and $E^*_{sad-sci}$ increases with the Coulomb parameter $Z^2/A^{1/3}$ since the saddle-to-scission path becomes longer [10]. On the other hand, the time t will decrease when the temperature difference $T_1 - T_2$ between the two fragments increases. A higher temperature gradient leads to faster flow of E^* between the two fragments. According to eq. (2). an increase in temperature difference corresponds to an increase in the asymmetry of the mass split. To resume, the time t follows the expression:

$$t \propto \frac{E^*_{sci}}{T_1 - T_2} \tag{5}$$

As a consequence, t will increase with the beam energy and the Coulomb parameter of the fissioning nucleus and will decrease with increasing asymmetry of the mass split. Eq. (5) is reflected by the schematic drawing shown in Fig. 4, which illustrates the variation of the mean E^* in the light fragment as a function of time. Two fissioning nuclei and several mass splits, corresponding to equivalent mass asymmetries in both fissioning systems, are considered. One can see that the drop to E^*=0 (complete energy sorting) occurs faster for the more asymmetric splits. It also shows that the energy-sorting process takes longer for the heavier fissioning nucleus, because the E^* to be transferred is larger.

Let us now assume that there exists a time t_p, above which the exchange of protons through the neck is very much hindered due to the growing Coulomb barrier between the two fragments. If $t > t_p$, no net even-odd effect is induced because protons cannot be transferred to the heavy nucleus. Thus, according to the energy-sorting process the even-odd effect as a function of asymmetry should have a threshold character. The threshold asymmetry where the even-odd effect created by the energy sorting sets in (corresponding to the asymmetry for which $t = t_p$) will increase with the Coulomb parameter of the fissioning nucleus. According to Fig. 4, in ^{236}U the energy sorting is accomplished within the time window t_p for the most asymmetric mass split (156/180) and, thus, the formation of an even-even light fragment is strongly enhanced. For ^{250}Cf, an even larger mass asymmetry than 165/85 is required. For a fixed even-Z fissioning nucleus, the general trend presented by the data in the left part of Fig. 3 is a small and rather constant even-odd effect close to symmetry and a strong increase as we move to more asymmetric fission. The latter feature occurs at an asymmetry value that increases with the mass of the fissioning nucleus, in agreement with what is expected from the energy-sorting process. For ^{230}Th, this change is not shown by the data. However, we presume that this is because the threshold asymmetry for this nucleus is close to symmetry where no data have been measured. The data of the electromagnetic-induced fission of ^{229}Th, which cover the whole mass range, support this assumption.

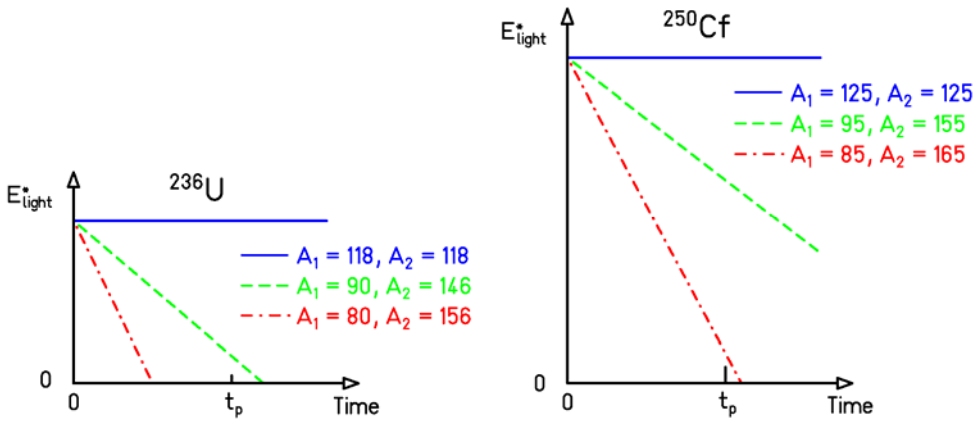

Figure 4. *Schematic drawing representing the mean excitation energy in the light fission fragment as a function of time. Two fissioning nuclei and different mass splits are considered. See text for details.*

For several systems, the data point in Fig. 3 that is closest to symmetry is appreciably higher than expected from the global trend. This effect may be associated to the influence of the Z=50 shell in the complementary fragment, which is known to enhance the yield of tin isotopes and, thus, leads to a local increase of the deduced even-odd effect. In the GEF code

[35] the dependence of the local even-odd effect with asymmetry is modelled in a phenomenological way with a smoothed step function, obtained by a convolution with a Gaussian function. The threshold asymmetry value is the one that fulfils the condition $C\,E^*_{sci}/|T_1-T_2| = t_p$, where C is a constant. t_p/C is adjusted to the data and has the same value for all nuclei. In accordance with the data, the width of the Gauss function is set proportional to $|T_1 - T_2|$. The scaling factor for $|T_1 - T_2|$ is the same for all nuclei and fitted to the experimental data. In the GEF model it is assumed that 50% of the energy release from saddle to scission [10] is dissipated into intrinsic excitations. The intrinsic excitation energy at scission determines also the magnitude of the even-odd effect at symmetry according to the model of ref. [41].
On the right part of Fig. 3, the results of the GEF code for the same fissioning systems are presented. The main tendencies of the experimental data are nicely reproduced by our description. The energy-sorting mechanism also predicts that, for a given fissioning nucleus, the threshold asymmetry should increase with increasing initial excitation energy of the compound nucleus. In addition, since the transfer of neutrons is possible until neck rupture, one expects smaller threshold asymmetries for the even-odd effect in the fission-fragment neutron yields. Unfortunately there are no data to verify these statements.

Summary and outlook

Nuclei at low excitation energy E^* are peculiar systems, since their temperature remains approximately constant with increasing E^*. In this sense, the nuclear superfluid to normal-liquid phase transition seems to behave like a first-order phase transition. The very special feature of this phenomenon in nuclei is that the constant-temperature regime essentially reaches down to zero energy, with only some fluctuations at the thresholds for the first quasi-particle excitations. The scission configuration of the fission process offers the unique possibility to investigate, how two different nuclei in this special regime of constant temperature share the available intrinsic excitation when they are in thermal contact. We have shown that in this regime we reach a peculiar state of thermal equilibrium at scission in which the temperatures of the nascent fragments remain different in spite of the flow of E^* from the hot to the cold fragment. Rather unexpectedly, this implies that the total amount of intrinsic E^* available at scission is found in the fragment with the lower temperature. Our discovery of the energy-sorting mechanism may be considered as a new counter-intuitive manifestation of quantum-mechanical properties of microscopic systems. This entropy-driven E^*-sorting process appears to have similarities with Maxwell's demon [42] on the nucleonic level. However, the phenomenon is fully compatible with the second law of thermodynamics. This E^*-sorting effect explains very easily an issue that remained unsolved up to present when comparing the number of emitted neutrons as a function of fragment mass for different initial excitation energies. It was observed in asymmetric mass splits that the increase of intrinsic E^* of the fissioning nucleus appears as an increase of E^* in the heavy fission fragments, only.
Moreover, the complex features of the even-odd effect in fission-fragment yields as a function of initial excitation energy and Coulomb parameter of the fissioning system as well as of the mass asymmetry of the fragments can easily be explained by the eventual transfer of the last unpaired proton, generally from the light to the heavy fragment, at the last step of the energy-sorting process. The fact that the even-odd effect is governed by the ratio of the total intrinsic excitation energy at scission and by the temperature difference of the two nascent fragments lead us to propose a schematic dynamical model.
This finding represents an essential progress in the understanding of fission dynamics: The threshold behaviour of the asymmetry-associated even-odd effect establishes a relation between the speed of the energy transfer in the energy-sorting mechanism and the dynamical time, starting at the moment when the two fragments develop their individual properties, e.g. their final temperatures, and the moment when the resistance against the transfer of protons across the neck becomes inhibitive. There exists some experimental knowledge on the saddle-to-scission time e.g. by the pre-scission neutron multiplicity at higher excitation energy [43], but there is little knowledge on the time for intrinsic excitation-energy transfer between nuclei in thermal contact in the superfluid regime. Thus, the present work is a step forward in the development of new kinds of fast nuclear clocks. Detailed theoretical and experimental studies on pre-scission dynamics will allow extending the investigations on non-equilibrium processes between different superfluid mesoscopic objects in analogy to the supercurrent [44] in particle transfer. In the present case, the driving force is the entropy, in contrast to transfer reactions, which are driven by different Fermi levels. Our findings provide an

important constraint on the theoretical modelling of the last stage of fission in the superfluid regime [6], which represents still a considerable challenge.

Acknowledgements
This work was supported by the EURATOM 6. Framework Program “European Facilities for Nuclear Data Measurements” (EFNUDAT), contract number FP6-036434.

References

[1] E. Algin et al., Phys. Rev. C 78, 054321 (2008).
[2] A. V. Voinov et al., Phys. Rev. C 79, 031301(R) (2009).
[3] U. Mosel, H. Schmitt, Phys. Rev. C 4, 2185 (1971).
[4] U. Mosel, H. Schmitt, Nucl. Phys. A 165, 73 (1971).
[5] J. Maruhn, W. Greiner, Z. Phys. 251, 211 (1972).
[6] H. J. Krappe, S. Fadeev, Nucl. Phys. A 690, 431 (2002).
[7] H. J. Krappe, S. Fadeev, Nucl. Phys. A 645, 559 (1999).
[8] W. D. Myers, W. J. Swiatecki, Nucl. Phys. A 612, 249 (1997).
[9] N. Bohr, J. A. Wheeler, Phys. Rev. 56, 426 (1939).
[10] M. Asghar, R. W. Hasse, J. Phys. Colloques 45, C6-455 (1984).
[11] B. D. Wilkins, E. P. Steinberg, R. R. Chasman, Phys. Rev. C 14, 1832 (1976).
[12] I. Ragnarsson, R. K. Sheline, Phys. Scr. 29, 385 (1984).
[13] T. von Egidy, D. Bucurescu, Phys. Rev. C 72, 044311 (2005).
[14] U. Agvaanluvsan et al., Phys. Rev. C 79, 014320 (2009).
[15] A. A. Naqvi, F. Käppeler, F. Dickmann, R. Müller, Phys. Rev. C 34, 218 (1986).
[16] S. C. Burnett, R. L. Ferguson, F. Plasil, H. W. Schmitt, Phys. Rev. C 3, 2034 (1970).
[17] C. J. Bishop, R. Vandenbosch, R. Aley, R. W. Shaw Jr., I. Halpern, Nucl. Phys. A 150, 129 (1970).
[18] R. Müller, A. A. Naqvi, F. Käppeler, F. Dickmann, Phys. Rev. C 29, 885 (1984).
[19] M. Strecker, R. Wien, P. Plischke, W. Scobel, Phys. Rev. C 41, 2172 (1990).
[20] D. G. Madland, J. R. Nix, Nucl. Sci. Eng. 81, 213 (1982).
[21] S. Lemaire, P. Talou, T. Kawano, M. B. Chadwick, D. G. Madland, Phys. Rev. C 72, 024601 (2005).
[22] N. V. Kornilov, F.-J. Hambsch, A. S. Vorobyev, Nucl. Phys. A 789, 55 (2007).
[23] H. A. Bethe, Phys. Rev. 50, 332 (1939).
[24] J. Toke, W. U. Schröder, Annu. Rev. Nucl. Sci. 42, 401 (1992).
[25] S. Piantelli et al., Phys. Rev. C 78, 064605 (2008).
[26] F. Gönnenwein in Nuclear Fission Process, C. Wagemans ed., CRC Press Inc., (1991).
[27] K.-H. Schmidt et al., Nucl. Phys. A 665, 221 (2000).
[28] S. Steinhäuser et al, Nucl. Phys. A 634, 89 (1998).
[29] M. Caamano, F. Rejmund, K.-H. Schmidt, arXiv:0909.1059v2 [nucl-ex].
[30] B. L. Tracy et al., Phys. Rev. C 5, 222 (1972).
[31] J. P. Bocquet, R. Brissot, Nucl. Phys. A 502, 213c (1989).
[32] H. Naik, S. P. Dange, A. V. R. Reddy, Nucl. Phys. A 781, 1 (2007).
[33] W. Nörenberg, Proc. Symp. Phys. Chem. Fission, Rochester 1973, IAEA Vienna (1974), vol. 1, p. 547.
[34] G. Vladuca et al., Nucl. Phys. A 720, 274 (2003).
[35] http://www.cenbg.in2p3.fr/GEF
[36] G. Schütte, Z. Phys. A 283, 183 (1977).
[37] B. Bouzid, M. Asghar, M. Djebara, M. Medkour, J. Phys. G: Nucl. Part. Phys. 24, 1029 (1998).
[38] I. Tsekhanovich et al., Nucl. Phys. A 658, 217 (1999).
[39] I. Tsekhanovich et al., Nucl. Phys. A 688, 633 (2001).
[40] K.-H. Schmidt, B. Jurado, Phys. Rev. Lett. 104, 212501 (2010).
[41] F. Rejmund, A. V. Ignatyuk, A. R. Junghans, K.-H. Schmidt, Nucl. Phys. A 678, 215 2000).
[42] J. Earman, J. D. Norton, Stud. Hist. Phil. Mod. Phys. 29, 435 (1998).
[43] D. Hilscher, H. Rossner, Ann. Phys. Fr. 17, 471 (1992).
[44] I. Peter et al., Eur. Phys. J. A 16, 509 (2003).

Investigation of the prompt neutron properties from a Monte Carlo simulation of the fission fragment de-excitation

O. Serot, O. Litaize

CEA-Cadarache, Nuclear Energy Directorate, Physics Studies Laboratory,
Bldg. 230, F-13108 Saint Paul lez Durance, France
olivier.serot@cea.fr

Abstract: A Monte Carlo code named FIFRELIN (FIssion FRagment Evaporation Leading to an Investigation of Nuclear data) has been recently developed in order to investigate prompt fission neutrons and gamma properties. The available excitation energy of the fission fragments used for neutrons and gamma emission is calculated by accounting for their rotational energies. In addition, the fission fragment evaporation process is simulated using two main assumptions: (i) the partitioning of the excitation energy between primary fragments is performed by adopting a mass dependent temperature ratio law which has been established from physical grounds; (ii) a spin dependent excitation energy limit is considered for neutron emission. In the present paper, the spontaneous fission of ^{252}Cf is studied. We show that the main features of the prompt neutrons (energy spectrum, average neutron multiplicity, distribution of the prompt neutron multiplicity …) as well as the excitation energy available for prompt-gamma emission are nicely reproduced.

Introduction

In order to analyse or predict the various neutron, gamma and fission fragment related data in a user friendly way, we have developed a dedicated code named FIFRELIN (FIssion FRagment Evaporation Leading to an Investigation of Nuclear data). This code is based on a Monte Carlo approach of the FF deexcitation [1]. The basic ideas have been already developed by Lemaire et al. [2] and very recently by Randrup et al. [3]. In Lemaire's work two kind of hypothesis related to the partitioning of the FF initial excitation energy at the scission point are considered. The first one is an equipartition of the temperature between the two complementary fragments and the second one uses experimental results like mean neutron energy or average number of prompt neutrons as a function of the fission fragment mass to infer the initial excitation energy of each fragment. The first hypothesis is not able to reproduce the saw-tooth shape of the distribution of the average number of prompt neutrons as a function of fragment mass and we have definitively decided to not consider the second one because we try to have a predictive tool as much as possible and then experimental results can not be used as input parameters. In the present work various additional models have been developed and different hypothesis have been used to improve the agreement with experimental data. Up to now, only the ^{252}Cf spontaneous fission case has been studied.

Initial input data needed

In order to simulate the evaporation process, our Monte Carlo code needs some initial input data which are the mass and nuclear charge distributions of the fission fragments as well as their kinetic energy distributions: Y(A, Z, KE). These mass and kinetic energy distributions were taken from the measurement performed by Varapai [4] and are plotted in Fig.1.

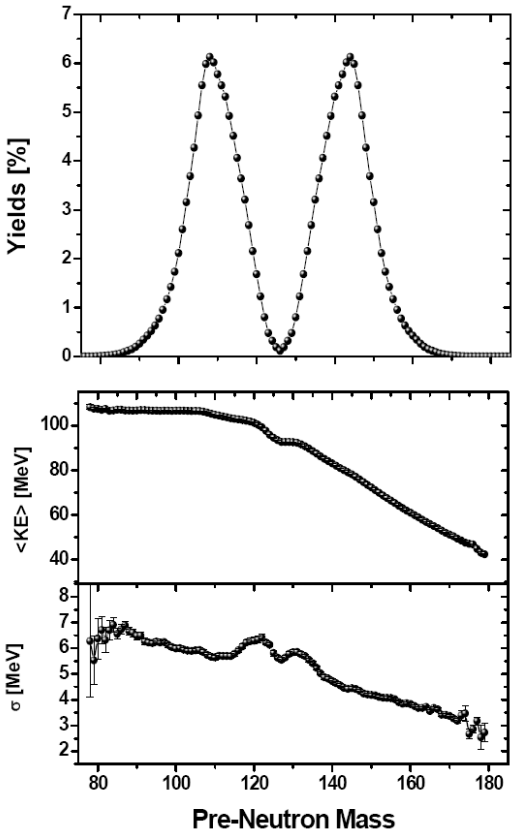

Figure 1. *Mass yield (top), average kinetic energy (middle) and width of the kinetic energy distribution (bottom) as a function of the pre-neutron mass (from Ref. [4]).*

The nuclear charge distribution within a mass chain is assumed to be:

$$\mathrm{Y(Z)} = \frac{1}{\sqrt{\mathrm{c}\pi}} e^{-(Z-Z_P)^2/c} \tag{1}$$

This distribution is characterised by the most probable charge Z_p and a width parameter $\mathrm{c} = 2\left(\sigma_Z^2 + 1/12\right)$ depending on the charge dispersion σ_z [5]. The most probable charges for light and heavy fragments are obtained within the Unchanged Charge Density assumption (UCD) corrected by a polarization function which depends on the mass number [5].

Calculation procedure

The calculation procedure is done in five steps which are described below.

Sampling of the light fragment
The first step consists in sampling (see previous section) the mass number A_L, the nuclear charge Z_L and the kinetic energy KE_L of the light fission fragment.

Sampling of the heavy fragment
It is then possible to determine the mass and charge of the heavy fragment (A_H=252-A_L and Z_H=98-Z_L), while its kinetic energy (KE_H) is sampled on the experimental kinetic energy distribution (Fig.1).

Determination of the total excitation energy at scission
From the two previous steps, the total excitation energy (TXE) available at scission can be deduced:

$$TXE \;=\; Q\text{-}TKE = B\left(A_L, Z_L\right) + B\left(A_H, Z_H\right) - B\left(A = 252, Z = 98\right) - \left(KE_L + KE_H\right) \tag{2}$$

where *B* are the atomic mass evaluations taken from [6].

Partitioning of the excitation energy between the two fragments
We know that the total excitation energy at scission is mainly composed of intrinsic excitation energy ($E^{*,SC}$), deformation energy ($E^{def,\,SC}$) and collective energy ($E^{coll,\,SC}$):

$$TXE = E^{*,SC} + \left(E^{def,SC}(\beta_{SC}) - E^{def,SC}(\beta_{GS})\right) + E^{Coll,SC} \quad (3)$$

Since after their full acceleration (i.e. after relaxation of the deformation energy), the fission fragments are rotating, it is believed that the total excitation energy is converted into intrinsic excitation energy and rotational energy. We can therefore write:

$$TXE = E^{*} + E_L^{Rot} + E_H^{Rot} \quad (4)$$

If we consider the nucleus as a Fermi gas, the intrinsic excitation energy is given by:

$$E^{*} = a_L T_L^2 + a_H T_H^2 \quad (5)$$

where a_L and a_H are the level density parameters of the light and heavy fragments which are calculated from the Ignatyuk's model [7]. T_L (T_H) is the light (heavy) fragment temperature.

Three different assumptions will be used concerning the temperature ratio ($R_T=T_L/T_H$):

- $R_T=1$; this assumption considers the same temperature for both fragments.
- $R_T=1.25$; it is assumed that the temperature of the light fragment is 25% higher than the heavy fragment one (this assumption has been already used for instance in Ref. [8]).
- $R_T \equiv R_T(A)$; here the ratio is assumed to be dependant of the fragment mass. This dependence is based on physical grounds and is plotted in Fig. 2. For mass split 78/174, the light fragment is assumed to have a spherical shape and then its temperature is lower than the heavy fragment one ($R_T=0.4$). For mass split 120/132, the situation is reversed and $R_T=1.6$. For symmetric mass split (126/126), the temperature is the same and therefore $R_T=1$.

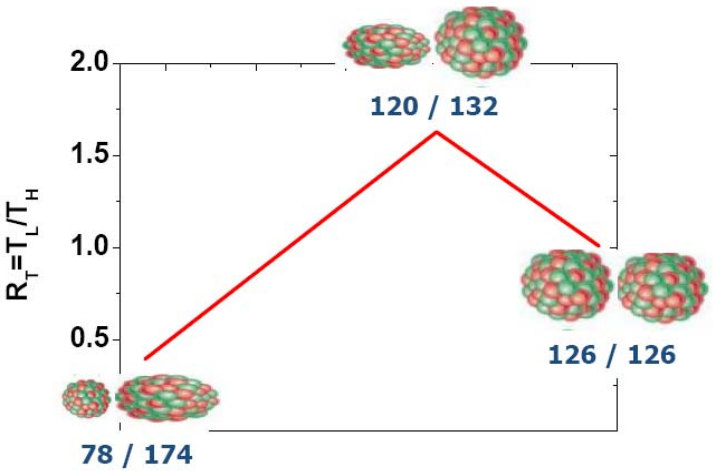

Figure 2. *Temperature ratio ($R_T=T_L/T_H$) law depending on the fragment mass and used in our Monte Carlo code.*

The rotational energy involved in Eq. (4) is approximated by the rotating liquid drop model:

$$E^{Rot} = \frac{\hbar J(J+1)}{2\Im} \quad (6)$$

where J and $\Im$ stand respectively for the total angular momentum and the moment of inertia. Both quantities are determined as follows:

- The fission fragment angular momentum is sampled from the following distribution [9]:

$$P(J) \propto (2J+1)\exp\left(-(J+1/2)^2/B^2\right) \quad (7)$$

  where B is almost equal to the root mean square value of $J+1/2$. We have adopted $B = 6\hbar$ for light fission fragment and $B = 7.2\hbar$ for the heavy one, in agreement with the Wilhelmy's observations [10].
- For the determination of the moment of inertia $\Im$, three cases were considered. The first one is based on the deformed rigid body model:

$$\Im_{rigid} = \frac{2}{5} AMR^2\left(1 + 0.31\beta + 0.44\beta^2\right) \quad (8)$$

Where *A*, *M* and *R* stand for the mass number, the nucleon mass and the radius ($R=1.2A^{1/3}$ *fm*). β is the quadrupole deformation parameter of the nucleus in its ground state which is taken from Ref. [11].
The second case is based on the fluid irrotational model, where the moment of inertia is given by:

$$\Im_{Irrot} = \frac{9}{8\pi} AMR^2\beta^2 \tag{9}$$

Lastly, we have considered an intermediate situation, where the moment of inertia is expressed as:

$$\Im = 1/2\,\Im_{rigid} \tag{10}$$

Table 1. *Survey of the total average neutron multiplicity calculated from various hypotheses.*

	$R_T=T_L/T_H$	$\Im$	$E^*_{\lim}$	$\overline{\nu_L}$	$\overline{\nu_H}$	$\overline{\nu_{Tot}}$
Case 1	1	-	S_n	1.82	2.44	4.26
Case 2	1.25	-	S_n	2.28	1.93	4.21
Case 3	1.25	$\Im = \Im_{Rigid}$	$S_n + E^{rot}$	2.18	1.83	4.01
Case 4	1.25	$\Im = \Im_{Irrot}$	$S_n + E^{rot}$	1.06	0.46	1.52
Case 5	1.25	$\Im = 0.5\,\Im_{Rigid}$	$S_n + E^{rot}$	2.07	1.71	3.78
Case 6	$R_T \equiv R_T(A)$	$\Im = 0.5\,\Im_{Rigid}$	$S_n + E^{rot}$	2.06	1.70	3.76
Experiment: Vorobyev et al. [13]				2.051	1.698	3.756

Neutron evaporation
Combining Eqs. (3) to (10) allows the determination of the excitation energy for each fission fragment. This energy will be used to evaporate prompt neutron and gamma. Assuming that the cross section of the inverse process of compound nucleus formation is constant, the energy ε (in the centre of mass frame) of a neutron emitted at a given temperature *T* is sampled over a Weisskopf spectrum [12]:

$$\phi(\varepsilon) = \frac{\varepsilon}{T^2} e^{-\varepsilon/T} \tag{11}$$

Note that the temperature in Eq. (11) is the temperature of the compound nucleus before emission. The neutron evaporation ends when the excitation energy is lower than an energy limit ($E^*_{\lim}$) which is given by:

$$E^*_{\lim}(J) = S_n + E^{rot}(J) \tag{12}$$

where S_n is the neutron energy separation. So, when neutron evaporation is no longer possible ($E^* < S_n + E^{rot}$), gamma deexcitation can start.

Results and discussion

As already said in the previous section, various cases have been considered concerning both the temperature ratio law (R_T) and the determination of the moment of inertia $\Im$. In each case, the average prompt neutron multiplicity for both fragments can be calculated and compared with the experimental data as shown in Table 1.

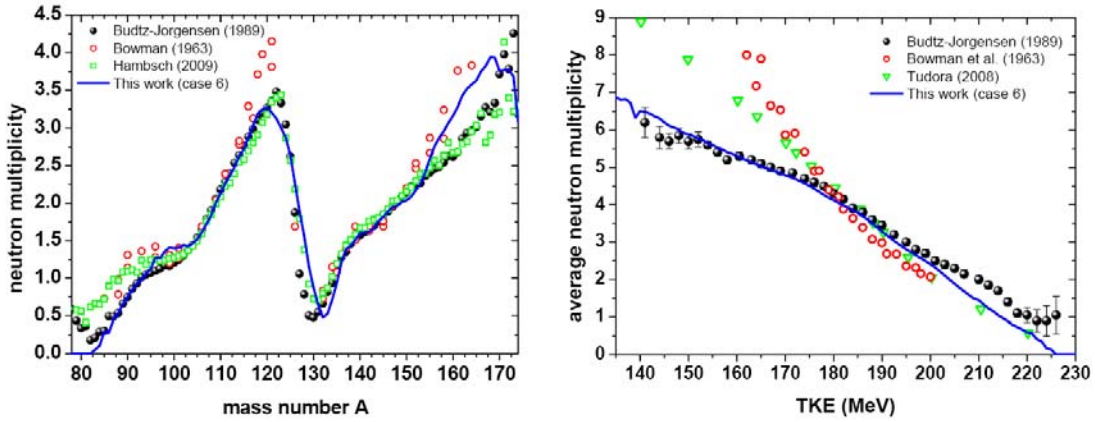

Figure 3. *Neutron multiplicity as a function of the fragment mass (left) and the total kinetic energy (right). Our calculations (performed with $R_T \equiv R_T(A)$ and $\Im = 0.5\,\Im_{Rigid}$) are compared with experimental data (Budtz-Jorgensen [14], Bowman [15], Hambsch [16]) and with the 'Point-by-Point' model (Tudora [17]).*

It is clear from Table 1, that cases 1 and 2 strongly overestimate the total average neutron multiplicity, meaning that the excitation energy limit is too low and then the rotational energy has to be taken into account. The impact of the moment of inertia (needed to calculate the rotational energy) is illustrated in the cases 2 to 5. It can be observed that $\Im = 0.5\,\Im_{Rigid}$ (case 5) is a good compromise to evaluate properly the $\overline{\nu_L}$, $\overline{\nu_H}$ and $\overline{\nu_{Tot}}$ quantities. Nevertheless, using a constant temperature ratio (R_T=*1.25)* does not allow to reproduce properly the neutron multiplicity as a function of the fragment mass (saw-tooth curve) [1].

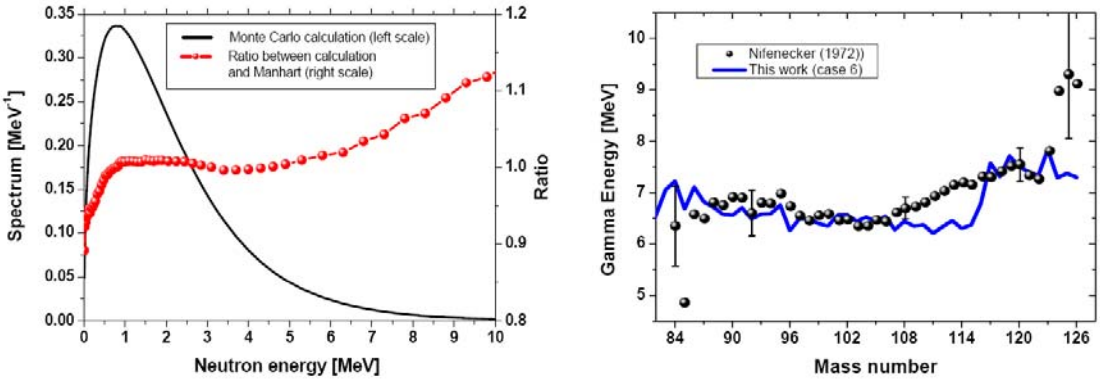

Figure 4. *Prompt neutron energy spectrum in the laboratory frame (left part of the figure) and total energy available for prompt gamma emission as a function of the light fragment mass (right part of the figure).*

The best case is clearly the last one (case 6). Indeed, within this model, various observables are nicely reproduced:

- The saw-tooth curve (left part of Fig. 3) and the neutron multiplicity as a function of the total kinetic energy (right part of Fig. 3) are in a very good agreement with Budtz-Jorgensen experimental data [14];
- The prompt neutron energy spectrum (left part of Fig. 4) is similar with the Manhart's evaluation [18], in particular in the region between 1 and 6 MeV;
- The total remaining energy available for prompt gamma emission (right part of Fig. 4) agrees well with Nifenecker experimental data [19];

- The neutron emission probabilities *P(ν)* for the light fragment, the heavy one and both of them (Fig. 5) follow the Vorobyev experimental data [13].

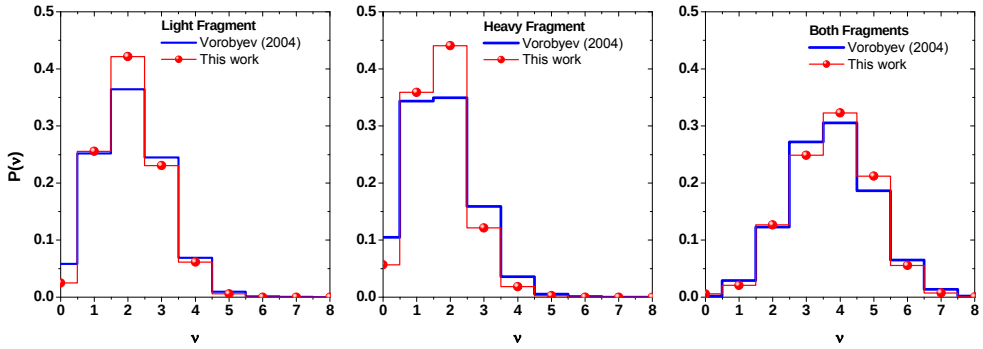

Figure 5. *Neutron emission probabilities for light fragment (left), heavy fragment (middle) and both fragments (right).*

Conclusion

A Monte Carlo code has been recently developed in order to investigate prompt fission neutrons and gamma properties. The available excitation energy of the fission fragments used for neutrons and gamma emission is calculated by accounting for their rotational energies. The main features of the prompt neutrons (energy spectrum, average neutron multiplicity, distribution of the prompt neutron multiplicity …) as well as the excitation energy available for prompt-gamma emission are nicely reproduced by using two main assumptions: (i) the partitioning of the excitation energy between primary fragments is performed by adopting a mass dependent temperature ratio law which has been established from physical grounds (see Fig. 2); (ii) a spin dependent excitation energy limit is considered for neutron emission (see Eq. (12)).

References

[1] O. Litaize and O. Serot, accepted for publication in Phys. Rev. C
[2] S. Lemaire et al., Phys. Rev. C72, 054608 (2005)
[3] J. Randrup and R. Vogt, Phys. Rev. C80, 024601 (2009) and these proceedings
[4] N. Varapai et al., Proc. Int. Workshop on Nuclear Fission and Fission Product Spectroscopy, Cadarache, France, May 11-14, 2005
[5] A.C. Wahl et al., Phys. Rev. C126, 1112 (1962)
[6] A.H. Wapstra et al., Nucl. Phys. A729, 129 (2003) and G. Audi et al., Nucl. Phys. A729, 337 (2003)
[7] A.V. Ignatyuk, G.N. Smirenkin, A.S. Tishin, Sov. Jour. of Nucl. Phys. 21, 255(1975)
[8] T. Ohsawa, Report INDC(NDS)-251, p. 71
[9] D. De Frenne, in 'The nuclear fission process', 1991, Ed. C. Wagemans, CRP Press, Boca Raton, USA, p. 475
[10] Wilhelmy et al., Phys. Rev. C5, 2041 (1972)
[11] RIPL-2, Report IAEA-TECDOC 1506 (2006)
[12] V. Weisskopf, Phys. Rev. 52, 295 (1937)
[13] A.S. Vorobyev et al., Proc. Int. Conf. on Nuclear Data for Science and Technology ND2004, Santa Fe, USA, Sept. 26-Oct. 1, 2004
[14] C. Budtz-Jørgensen et al., Nucl. Phys. A490, 307 (1988)
[15] H. R. Bowman, Phys. Rev. 129, 2133 (1963)
[16] F.-J. Hambsch et al., Proc. Int.Workshop on Compound Nuclear Reactions and Related Topics (CNR2009), Bordeaux, France, Oct. 5-8, 2009
[17] A. Tudora, Ann. Nucl. Ener. 35, 1 (2008)
[18] W. Manhart, Report IAEA-TECDOC 410 (1987) p. 158
[19] H. Nifenecker et al., Proc. Int. Conf. on Physics and Chemistry of Fission, Rochester, New-York, USA, Aug. 13-17, 1973.

^{237}Np fission cross section, new data and comparison to critical experiments

L. Tassan-Got[1)], L.S. Leong[1)], C. Paradela[2)], L. Audouin[1)], B. Berthier[1)], I. Duran[2)], L. Ferrant[1)†], S. Isaev[1)], C. Le Naour[1)], C. Stéphan[1)], D. Tarrio[2)], D. Trubert[1)†] and the n_TOF collaboration[3)]

1) Institut de Physique Nucléaire, CNRS/Université Paris Sud, 91406 ORSAY, France
2) Facultad de Física, Universidade de Santiago de Compostela,15782, Spain
3) n_TOF collaboration, CERN, Geneva, Switzerland
† Deceased
tassango@ipno.in2p3.fr

Abstract: Among the actinides, ^{237}Np is one of the most important components of the burn-up fuel. As it is a non-fissile isotope, ^{237}Np is a good candidate for being incinerated in fast neutron spectrum systems. In order to obtain the transmutation capabilities of this isotope under such a neutron flux, a more accurate measurement of the neutron-induced fission cross section is required. This contribution presents the final result of the ^{237}Np(n,f) cross section from threshold up to 1 GeV obtained by the n_TOF experiment, taking the ^{235}U(n,f) cross section as a reference. Contrary to other isotopes measured in the same conditions (^{233}U, ^{234}U, ^{238}U), in case of ^{237}Np significantly higher cross sections are found when compared to previous measurements. Critical experiments involving a significant amount of ^{237}Np make the multiplication factor k_{eff} very sensitive to the ^{237}Np(n,f) cross section and are useful benchmarks to test it. We checked the validity of our measurement by probing it against the Los Alamos critical experiment which consists of a spherical assembly of 6 kg of ^{237}Np surrounded by 62.5 kg of highly enriched uranium. Although most of fissions (86%) occur in uranium, the accuracy of determination of k_{eff} allows to discriminate different sets of the ^{237}Np(n,f) cross section, especially in the MeV region which is crucial for fast reactors. The k_{eff} has been computed with the MCNP5 code, first by using evaluated cross sections, and then by introducing the n_TOF ^{237}Np fission cross section. The latter improves the agreement between the simulation and the criticality measurement. Moreover a modification of the inelastic cross section of ^{235}U, as hypothesized by some authors to reconcile the simulation and the criticality experiment, hardly explains the discrepancy if the k_{eff} of a highly enriched uranium is kept constant.

Introduction

^{237}Np is one of the minor actinides produced in present nuclear reactors. Due to its long life time ($T_{1/2}$=2 Myr) it is considered as a long term waste and a possible candidate for incineration. Such a foreseen transmutation requires a better knowledge of cross sections.
This triggered several measurements of the neutron-induced fission cross section [1-5]. Although most of the measurements are in agreement with each other, the last data obtained at the CERN n_TOF facility [5] are about 5% to 6% higher than the others beyond the first chance fission threshold, as illustrated in figure 1. The same deviation shows up when those data are compared to the evaluated files (see figure 2), which is not surprising as the evaluations are based on the previous measurements. This singularity of the n_TOF measurement could lead one to consider that it is not reliable. However one should have in mind that several of the experimental results are not independent. For example the evaluation ENDF/B-7.0 [6] is based on Tovesson's data [3,4]. But those data have been renormalized to ENDF/B-6.8 at 14 MeV due to a lack of knowledge on the number of atoms in the targets. ENDF/B-6.8 is based essentially on Lisowski's measurement [1] which itself has been re-normalized to Meadows results [6] for similar reasons. All in all, despite small deviations, the three experiments give very similar values. In the n_TOF experiment, although the detection efficiency is reduced, the targets and all materials are well characterized so that no re-normalisation needed to be applied and the four neptunium targets delivered consistent data.

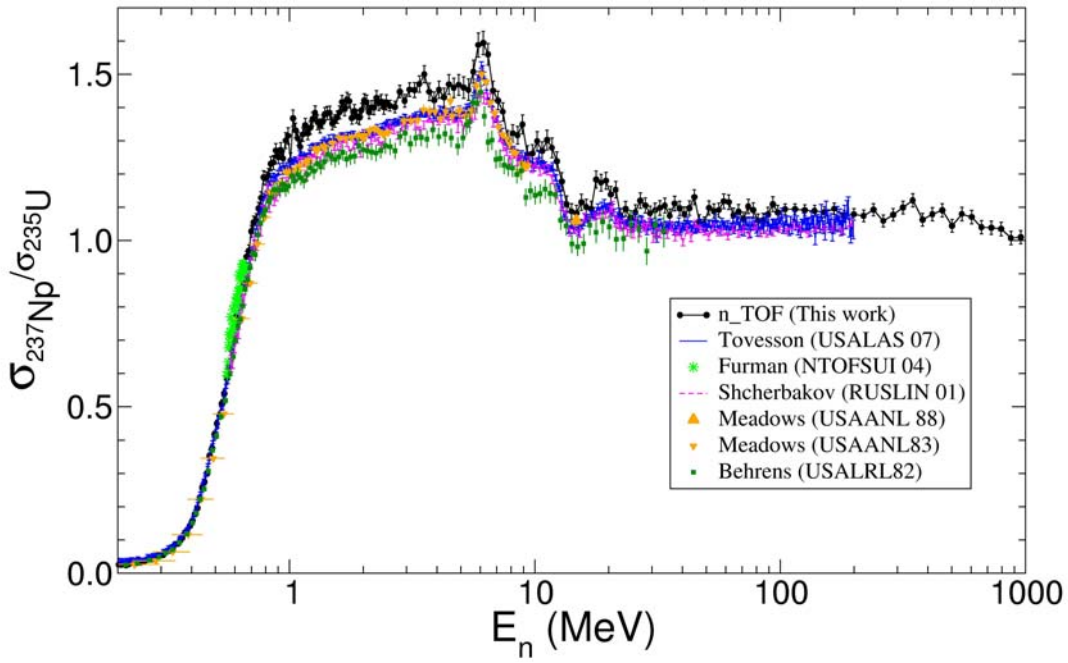

Figure 1 . *Ratio of neutron-induced fission cross sections of ^{237}Np and ^{235}U as measured at CERN n_TOF compared to previous measurements. Furman refers also to n_TOF data obtained with another detecting system.*

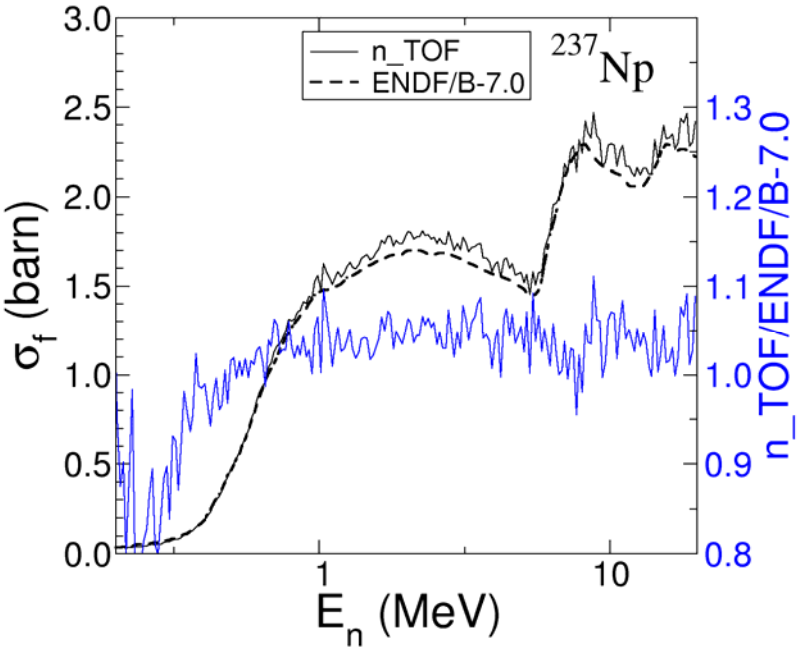

Figure 2 . *(n,f) cross section of ^{237}Np as measured at n_TOF (continuous black line), compared to the ENDF/B-7.0 evaluation (dashed line). The ratio is shown with a blue line, referred to the right hand scale.*

Therefore it is worth testing a situation where the fission cross section of ^{237}Np plays a significant role especially in the energy domain above or around the fission threshold, that's to say in the MeV region. We focus in this work on a critical experiment which has been performed at Los Alamos and proposed as a benchmark for neutron transport simulations [7]. The critical mass is

made of a neptunium sphere of 6 kg surrounded by hemispheric shells of Highly Enriched Uranium (HEU) to reach criticality. The multiplication factor k_{eff} has been accurately measured for a definite geometry. Although most of the fissions occur in the HEU mass (86%) the accuracy on k_{eff} is sensitive to the neptunium cross sections and allows testing the discrepancy between different fission cross section sets.
The next section briefly describes the critical set up and the comparison of our calculation of k_{eff} to previous ones when the evaluated cross sections (ENDF/B-6.8 and ENDF/B-7.0) are used. Then we compute again this multiplication factor when the n_TOF fission cross section of ^{237}Np is substituted for the standard one. Finally, instead of changing the ^{237}Np fission cross section we will modify the ^{235}U inelastic cross section, as this effect has been invoked by some authors to explain the difference between the simulation and the measurement.

Critical benchmark with neptunium

We give here only a brief description of the benchmark model which is an idealized representation of the true experiment, with some simplifications regarding the geometry of the fissile assembly and the surrounding materials. All the details concerning the geometry and the composition of materials can be found in reference [7]. The authors computed the small effects of these simplifications and corrected the measured value of k_{eff} to deliver an experimental-like one corresponding to the simpler geometry represented by the benchmark, which will only be considered in the following.
The benchmark set up, sketched in figure 3, is made of a neptunium sphere of 6 kg lying inside a lower HEU hollowed hemisphere made of several hemispheric shells of HEU. Other materials are present in small quantities as tungsten, nickel and aluminium claddings or liners. Another hollowed hemispheric HEU shell constitutes the upper part of the assembly. When the lower part is lifted and it joins the upper one criticality is reached.

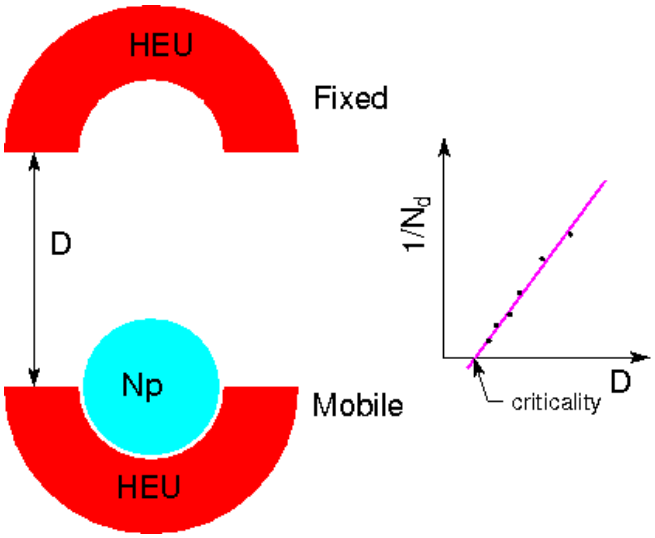

Figure 3 . *Left, schematic view of the neptunium benchmark experiment. Right, extraction of the critical distance from a series of sub-critical measurements.*

By definition the multiplication factor k_{eff} is the mean value of the number of neutrons created when one neutron is absorbed. In other words it is the number of neutrons at one generation divided by the number at the previous generation. If an internal source sends 1 neutron in the assembly, k_{eff} neutrons are present at the 1st generation, k_{eff}^2 at the 2nd, k_{eff}^3 at the 3rd, etc… In fact k_{eff} may vary along the first generations because the first neutrons do not necessarily sense the same parts of the assembly as the many neutrons of later generations, but this effect can be neglected when k_{eff} is close to 1.

Therefore the total number of neutrons generated by an initial one is:

$$N = 1 + k_{eff} + k_{eff}^2 + k_{eff}^3 + \ldots = \frac{1}{1 - k_{eff}} \qquad (1)$$

which is valid only for k_{eff} <1, otherwise N goes to infinity. A detector with an efficiency ε will detect a number of neutrons:

$$N_d = \varepsilon N = \frac{\varepsilon}{1 - k_{eff}} \qquad (2)$$

According to (2) by plotting $1/N_d$ versus the distance between the 2 parts of the system and linearly extrapolating it to 0 it is possible to find the distance for which criticality is reached: k_{eff} =1 and also the over-critical value of k_{eff} corresponding to contact, which can be confirmed also by kinetic measurements (increase in time of the flux).
The measurement has been performed by the authors of reference [7] and they found for the benchmark situation when the 2 parts are in contact:

$$k_{eff} = 1.0019 \pm 0.0036 \qquad (3)$$

They also computed this multiplication factor by using MCNP5 [8], which is a transport Monte Carlo code for neutrons. In this computation two sets of evaluated cross sections were used: ENDF/B-6.8 [7] and ENDF/B-7.0 [9]. The results are reported in table 1.

Table 1. *MCNP5 computation of K_{eff} done when the used cross section data set is ENDF/B-6.8 [7] or ENDF/B-7.0 [9]*

MCNP5	ENDF/B-6.8	ENDF/B-7.0
k_{eff}	0.9889	0.9956

With ENDF/B-6.8 the deviation amounts to 3.6 times the uncertainty, whereas with ENDF/B-7.0, which accounts for the recent measurement [3,4] of the ^{237}Np fission cross section, the discrepancy is still 1.8 times the uncertainty.

Simulation of the neptunium benchmark

We also simulated this benchmark by using MCNP5 driven by MURE [10]. The simulation has been done in the same conditions as in reference [7] to check its reliability. The results displayed in table 2, are very close to the ones previously obtained by other authors, as shown in table 1, which validates our calculation.

Table 2. *Our MCNP5 computation of the neptunium benchmark for validation purpose.*

MCNP5	ENDF/B-6.8	ENDF/B-7.0
k_{eff}	0.9889	0.9942

Now we keep the ENDF/B-7.0 data set for all cross sections except for the ^{237}Np fission cross section for which the n_TOF data set is substituted. The computation of the new multiplication factor gives:

$$k_{eff} = 1.0043 \qquad (4)$$

which exceeds now the experimental value but by an amount which is only 0.7 times the uncertainty. Therefore the simulation seems to confirm that the ^{237}Np fission cross section could

be higher than expected from previous measurements.

Inelastic cross section of ^{235}U

The discrepancy between the measurement and the simulation of k_{eff} using the ENDF/B-7.0 evaluated cross sections [9] has been tentatively explained as a possible deficiency in the inelastic cross section of ^{235}U. Indeed if the inelastic cross section on the highest excited levels is over-predicted the simulated neutron spectrum is slightly softer, as illustrated in figure 4, and the ^{237}Np fission rate drops leading to a k_{eff} reduction. This idea was corroborated by measurements of the ratio of fission rates induced in ^{237}Np and ^{235}U samples in a critical assembly with a fast neutron flux [9]. The simulated fission rate ratio ^{237}Np/^{235}U underestimates the experimental one by 2.5 %. Although this mismatch can also be accounted for by an underestimation of the fission cross section of ^{237}Np, we investigated a possible effect of the inelastic cross section by allowing it to vary.

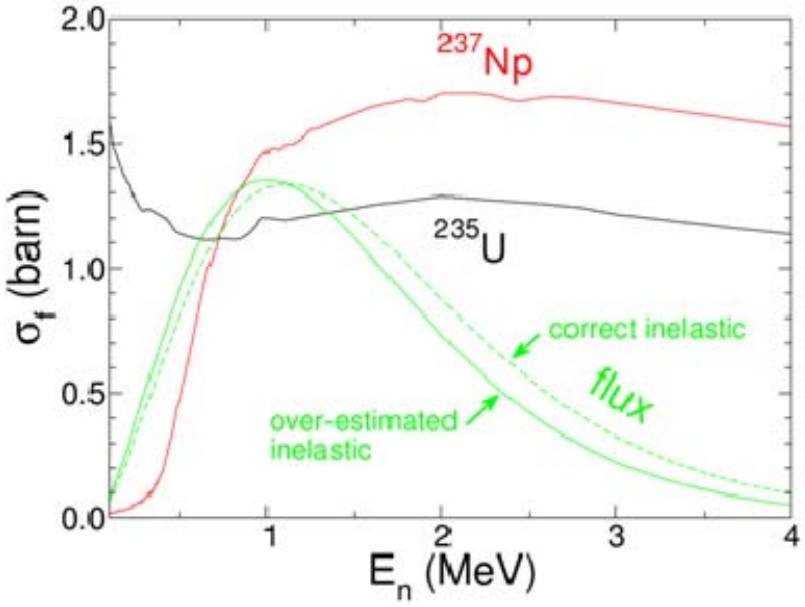

Figure 4. *Illustration of the effect of an incorrect inelastic cross section of ^{235}U reducing the fission rate in the neptunium sphere due to the fission threshold.*

We adopted a procedure based on a random modification of the cross sections related to the 35 excited levels of ^{235}U. We first select randomly how many levels will be affected, then the levels are selected randomly and the corresponding cross sections are multiplied by a random number lying between 0 and 2. However not all the cross section sets generated in this way are acceptable because they also modify the criticality of ^{235}U which is well known. Keeping this criticality unchanged, only those data sets will, therefore, be retained and applied to the neptunium benchmark. For each of the randomly generated cross section sets we computed the criticality of an assembly made of a sphere of HEU surrounded by a reflector made of a spherical shell of natural uranium [11]. Only the configurations keeping the computed k_{eff} within 0.00025 from the measured value are applied to the neptunium benchmark. This leads to keep 169 configurations among a few thousands which have bee generated.
Figure 5 shows the distribution of k_{eff} computed with the selected configurations for the benchmark. The measured value and the simulation using the n_TOF (n,f) cross section for ^{237}Np are also indicated. The distribution is centred around the original value of 0.9942. This is expected as the inelastic cross sections are varied symmetrically on average. The hypothesis of incorrect inelastic cross section would be explanatory only if some of the computed k_{eff} would be compatible with the measurement. Although this cannot be excluded from the distribution shown in figure 5, as we found one configuration approaching the measurement zone, the hypothesis of underestimation of the ^{237}Np fission cross section seems more likely.

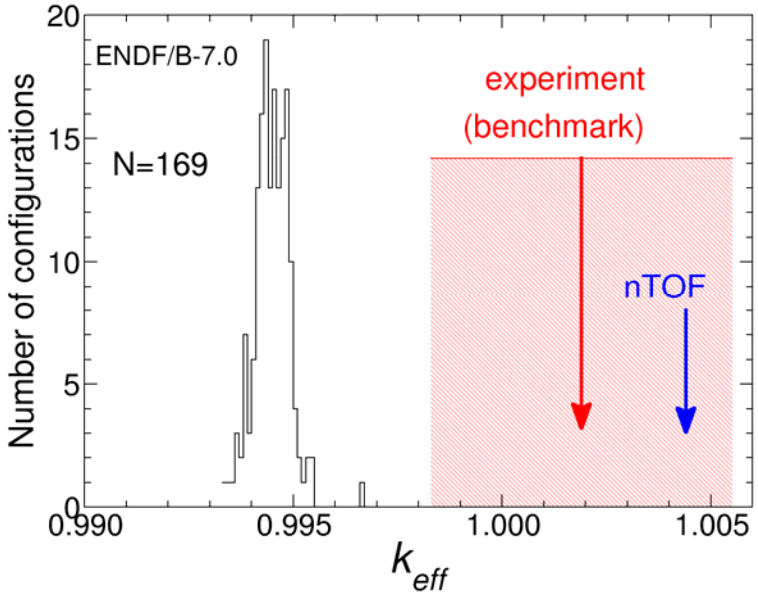

Figure 5. *Distribution of k_{eff} simulated by varying randomly the inelastic cross section of ^{235}U, constrained with the criticality of HEU. The red zone represents the interval of confidence of the measurement and the blue arrow is the result of the n_TOF $^{237}Np(n,f)$ cross section.*

Conclusion

The simulation of the neptunium critical benchmark indicates that the recent n_TOF measurement of the ^{237}Np(n,f) cross section, although higher than previous measurements and evaluations, is plausible as it is in better agreement with the measured k_{eff}. The hypothesis of a deficiency of the inelastic cross section in ^{235}U is less efficient in reconciling the simulation and the measurement although it cannot be completely discarded.

References

[1] P. Lisowski, J. Ullmann, S. Balestrini, A. Carlson, O. Wasson,and N. Hill, *Conference on* Nuclear Data For Science and Technology, Mito 1988, edited by S. Igarasi (Japan Atomic Energy Research Institute, 1998), p. 97.
[2] O. Shcherbakov et al., J. Nucl. Sci. Tech. Suppl. 2, 230, (2002).
[3] F. Tovesson and T. Hill, Phys. Rev. C 75, 034610 (2007).
[4] F. Tovesson and T. Hill, Nuclear Science and Engeneering 159,94 (2008)
[5] C. Paradela et al, Phys. Rev. C82, 034601 (2010)
[6] J. W. Meadows, Nucl. Sci. Eng. 85, 271 (1983)
[7] Russell D. Mosteller, David J. Loaiza,and Rene G. Sanchez, PHYSOR 2004, Chicago, Illinois, April 25-29, 2004
[8] MCNP — A General Monte Carlo N-Particle Transport Code, Version5, Volume I: Overview and Theory, -UR-03-1987, Los Alamos National Laboratory, (April 2003)
[9] M.B. Chadwick et al., Nucl. Data Sheets 107, 2931, (2006)
[10] MURE, http://www.nea.fr/tools/abstract/detail/nea-1845, April 2009
[11] Joseph L. Sapir, Russell Kidman, R. W. Brewer, LA-UR-98-1664, http://lib-www.lanl.gov/la-pubs/00418688.pdf

Total excitation energy partition between the light and heavy fragments forming a pair

A. Tudora[1)], C. Morariu[1)], C. Manailescu[1)], F.-J. Hambsch[2)], S. Oberstedt[2)]

1) University of Bucharest, Faculty of Physics, Bucharest-Magurele, POB MG-11, R-76900, Romania
2) European Commission, Joint Research Centre, Institute for Reference Materials and Measurements, Retieseweg 111, 2440 Geel, Belgium

anabellatudora@hotmail.com, atudora@gmail.com

Abstract: Two methods of the total excitation energy (TXE) partition between the light and heavy fragments forming a pair are analysed comparatively. The first one is based on the "classical" hypothesis of prompt neutron emission from fully-accelerated fission fragments at statistical equilibrium, both fragments having the same residual nuclear temperature distribution. The second method is based on the TXE partition according to the systematic behaviour of the experimental multiplicity ratio v_H/v_{pair} as a function of the heavy fragment mass number A_H, allowing parameterisations. In this case the fragments have different residual temperature distributions. The two TXE partition methods were applied for six fissioning systems: $^{233,235}U(n_{th},f)$, $^{239}Pu(n_{th},f)$, $^{237}Np(n_{5.5MeV},f)$, $^{252}Cf(SF)$, $^{248}Cm(SF)$ and fragment excitation energies, level density parameters, fragment and fragment pair temperatures were compared. Residual temperature ratios $RT=T_L/T_H$ with systematic behaviour versus A_H are obtained, as well as local and global parameterisations of $RT(A_H)$ for neutron induced fissioning systems. Average values of quantities characterising the prompt neutron emission are discussed, too. Interesting systematic behaviours of average quantities are obtained, e.g. a linear decrease of <RT> with the mass number of the fissioning nucleus and a linear decrease with the fissility parameter of the average C parameter. The validation of the $RT(A_H)$ parameterisations is made by Point by Point model calculations of the multi-parametric matrix $\nu(A,TKE)$, of all prompt neutron and gamma-ray emission quantities as a function of fragment mass, of total average prompt neutron multiplicity, spectrum and prompt neutron multiplicity distribution $P(\nu)$. The results are obtained in very good agreement with existing experimental data and evaluations. The global $RT(A_H)$ parameterisation extends the use of the PbP model allowing the prediction of prompt neutron emission quantities for fissioning systems without experimental prompt neutron emission data.

Excitation energies, level density parameters and temperatures of fragments

Two methods of the TXE partition between the light (LF) and heavy (HF) fragments forming a pair are analysed comparatively. The first one is based on the "classical" hypothesis of prompt neutron emission from fully-accelerated fission fragments (FF) at statistical equilibrium, both FF having the same residual nuclear temperature distribution [1, 2]. The second method is mainly based on the physical assumption of the TXE partition in the same ratio as the numbers of prompt neutrons emitted by the FF, leading to unequal residual temperatures of the FF. The use of this TXE partition in the frame of the PbP treatment was possible due to a very interesting behaviour deduced exclusively from experimental sawtooth $\nu(A)$ data that allowed us to develop parameterisations (see Refs. [3-6] and references therein).

If the experimental $\nu(A)$ data are represented as $\nu_H/(\nu_L+\nu_H)$ versus A_H, for all fissioning systems having experimental sawtooth data, a nice systematic behaviour is observed, consisting in the following features: a) a minimum of v_H/v_{pair} occurs at around A_H=130, b) an equal number of neutrons is emitted by the HF and LF forming a pair at around A_H=140 and c) the LF emits more neutrons than the HF only in the range A_H<140, while above A_H=140 the HF emits more neutrons than the LF. As an immediate consequence of this systematic behaviour, the fact that $\nu_H = \nu_L$ at around A_H=140 (where the FF mass yield distributions are maximum, too), validates again the Madland and Nix assumption made in the case of the Los Alamos (LA) "most probable fragmentation" approach [1].

In the present work the two TXE partition methods are analysed in the frame of the Point by Point (PbP) treatment. Taking into account the scarcity of sawtooth experimental data, for this

study we have chosen six fissioning systems having the best measured $\nu_{exp}(A)$ data, covering the neutron induced and spontaneous fission as follows: $^{233,235}U(n_{th},f)$, $^{239}Pu(n_{th},f)$, $^{237}Np(n_{5.5MeV},f)$, $^{252}Cf(SF)$ and $^{248}Cm(SF)$. In all cases the FF range was chosen in the usual manner of the PbP treatment [3-6]: the entire mass range covered by the experimental Y(A,TKE) distributions and at each A, this time 4 charge numbers are taken as the nearest integer values above and below the most probable charge obtained from the "unchanged charge distribution corrected with a possible charge polarization.

An example of the experimental sawtooth plotted as ν_H/ν_{pair} versus A_H is given in the upper part of Fig. 1 (different symbols), the interesting systematic behaviour, mentioned above, is visible and a simple parameterisation is plotted with the solid line.

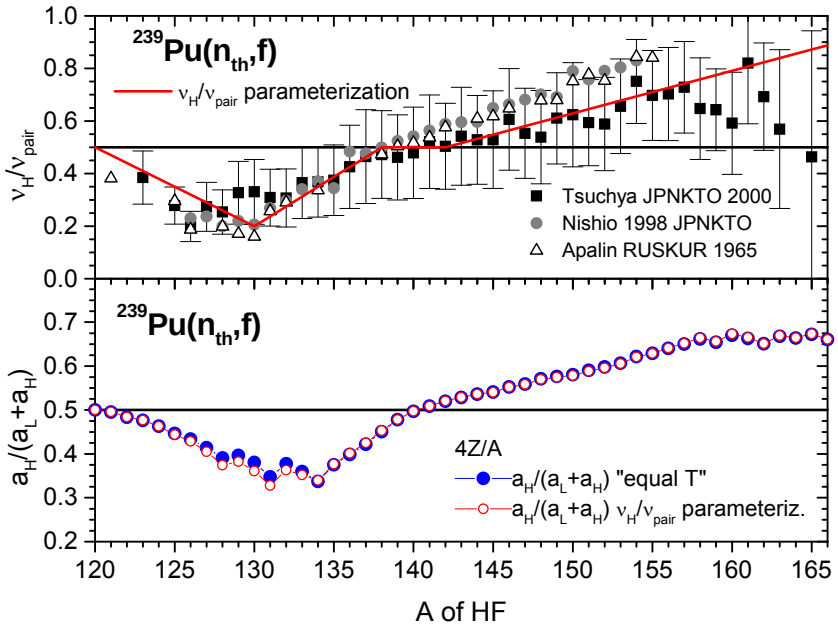

Figure 1. *ν_H/ν_{pair} parameterisation in comparison with experimental data taken from EXFOR (upper part) and the ratio a_H/a_{pair} obtained by using the two TXE partition methods (lower part).*

Fragment excitation energies E*(A) and level density parameters a(A) of the 6 fissioning systems were calculated in the frame of the super-fluid model [7]. An example of E*(A) is given in the upper part of Fig. 2 where the less pronounced sawtooth shape of E*(A) obtained in the case of the "equal T" method is visible. For all studied fissioning systems, the a(A) values obtained by the two methods are very close to each other as it can be seen in the lower part of Fig. 1 where almost in the entire mass range practically the two symbols (full and open circles) cover each other. Small differences are observed only in the mass range around 130. Looking at Fig. 1 it is easy to see that the ratio $a_H/(a_H+a_L)$ exhibits a similar behaviour as compared to the ν_H/ν_{pair} ratio but with a less pronounced minimum and shifted between A_H=129-134. We underline that the same behaviours are obtained for all 6 fissioning systems, Figs. 1 and 2 being only an example.

Comparison of the maximum values of the residual temperature distribution of FF obtained from the two TXE methods is given in the lower part of Fig. 2. Fragment temperature values T(A) of the ν_H/ν_{pair} parameterisation method are plotted with full circles and the temperatures of the "equal T" method with star symbols.

The good agreement between the a(A) values obtained by the two TXE partition methods allows to define an "equivalent temperature" of the FF pair, as follows: $TXE = a_L^* T_L^2 + a_H^* T_H^2 = (a_L^* + a_H^*) T_{equiv}^2$, where $a^*_{L,H}$ are the level density parameter values obtained in the case of the TXE partition method based on the ν_H/ν_{pair} parameterisation. The obtained equivalent temperature values plotted with open squares in the lower part of Fig. 2 are nerlz coinciding with the temperature values of the "equal T" method. To highlight these findings, the ratios between the equal T and equivalent T of the six studied fisioning systems are plotted together in Fig. 3. As it can be seen these ratios are practically 1 in almost the entire A_H range, only around A_H=130 differences between equivalent and equal T values are

of the order of 4% in the case of neutron induced fission and 6% in the case of the spontaneous fission (SF).

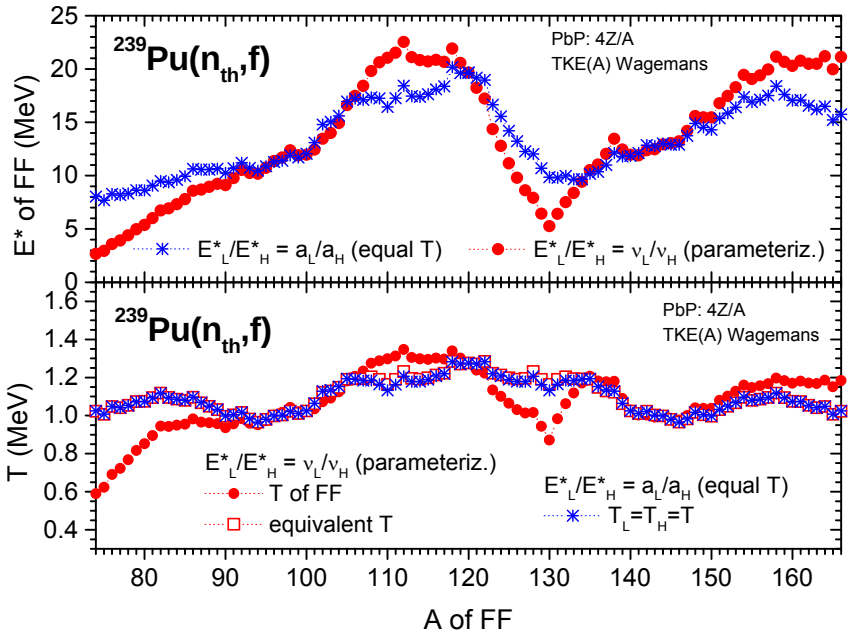

Figure 2. *Upper part: E* of FF obtained by the two TXE methods. Lower part: maximum values of the residual temperature distribution of FF obtained by using the ν_H/ν_{pair} parameterisation (fragment temperature plotted with full circles and equivalent temperature with open squares) in comparison with the "equal T" method (plotted with star symbols).*

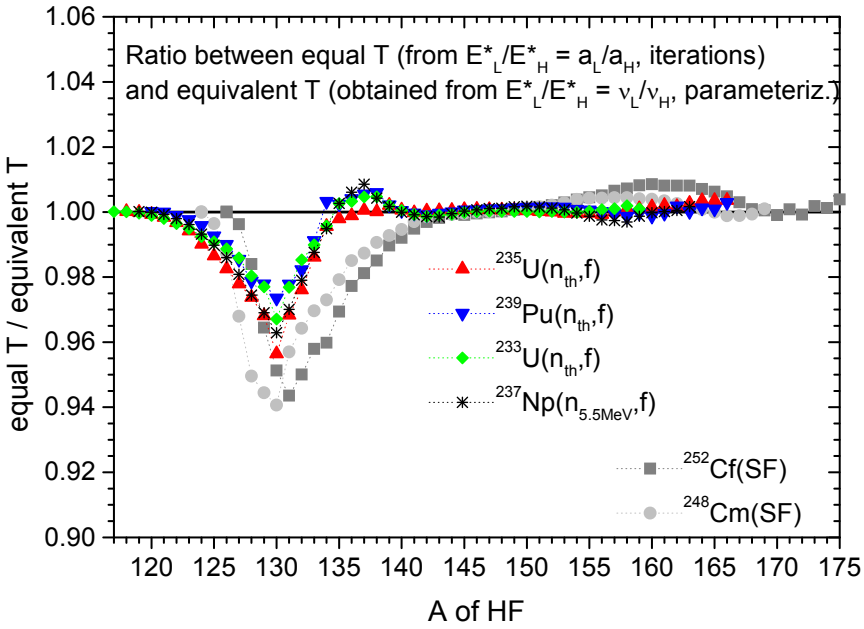

Figure 3. *Ratios between equal residual temperature and equivalent residual temperature from the ν_H/ν_{pair} parameterisation for the six studied fissioning systems.*

Fragment residual temperature ratios

The ratios between the maximum residual temperature of the LF and HF forming a pair as a function of A_H are plotted in Fig. 4 with different full symbols for the four studied neutron-induced fissioning systems. A very interesting behaviour of the fragment temperature ratio

$RT(A_H)$ is visible and has the following features: a) the maximum of $RT(A_H)$ occurs at A_H=130 and is around 1.5-1.6, b) in the A_H range between 135-145, the temperature ratio is approximately 1 (HF and LF having practically the same temperature) and c) for A_H>145 the decrease of RT is almost linear and the slope does not differ very much from one neutron induced fissioning system to another. This systematic trend allows parameterisations of RT as a function of A_H. Appropriate parameterisations of $RT(A_H)$ are plotted with different line shades in Fig. 4, too.

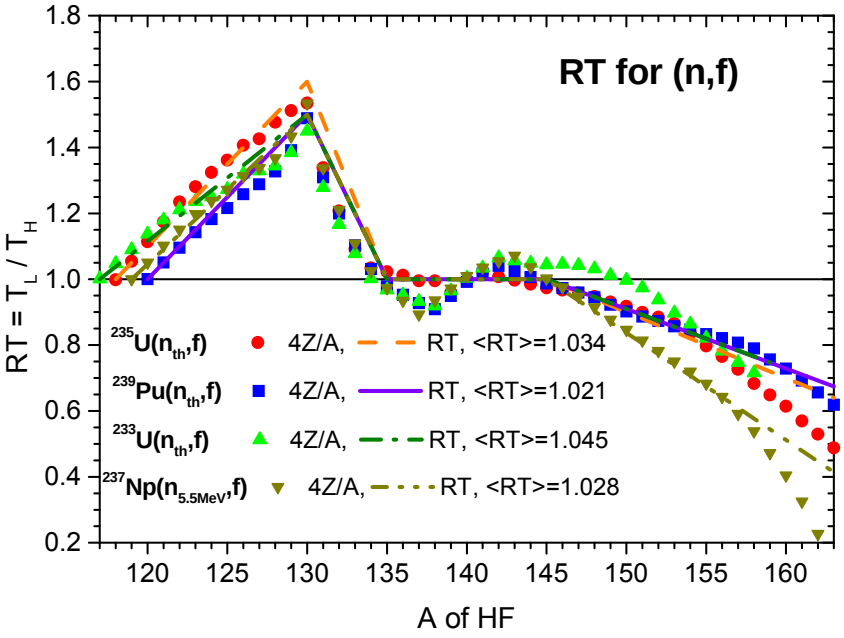

***Figure 4**. FF temperature ratios and parameterisations for neutron induced fission.*

The slopes and intercepts of the RT parameterisations (given with different line shades in Fig. 4) are plotted versus the fissility parameter in Fig. 5. Their almost constant values suggest that an unique RT parameterisation for the neutron-induced fissioning systems can be given taking for slopes and intercepts the values of the dashed lines plotted in Fig. 5.

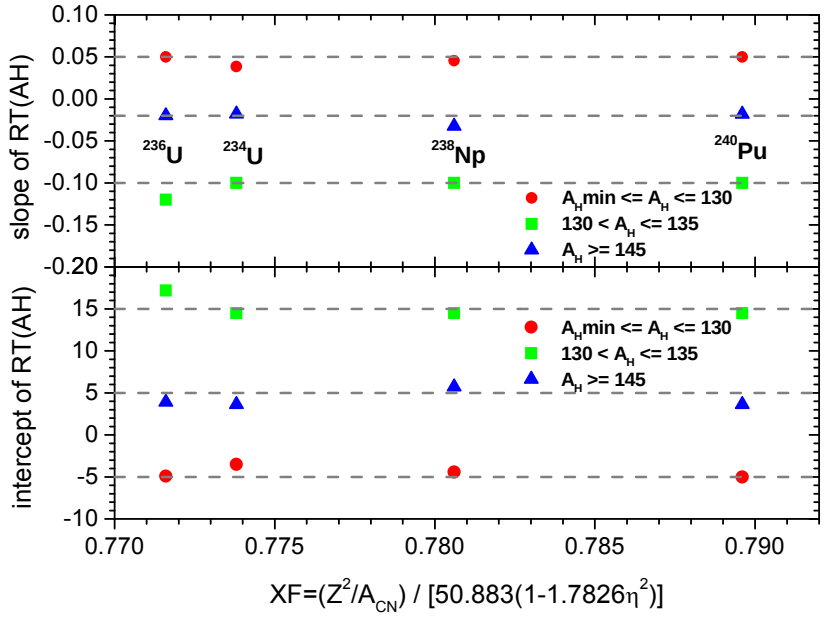

***Figure 5.** Slopes and intercepts of the RT parameterisations for neutron induced fission.*

Temperature ratios of the two studied SF systems are plotted in Fig. 6 and their behaviour differs from the RT behaviour of (n,f) as follows: a) the maximum of RT (placed around A_H=130) is higher than in the case of (n,f), b) the A_H range where RT is 1 is limited to one-two

mass units around A_H=145. Both SF systems have practically the same RT values in the A_H range above 134. The visible differences in the region A_H<134 are mainly due to the shifted minimum of experimental ν_H/ν_{pair} data in the case of ^{248}Cm(SF). Despite the facts mentioned above, RT parameterisations of the two SF systems can also be done, see the lines in Fig. 6 and the analytical expressions given in the figure, too.
In Figs. 4 and 6 also <RT> values averaged over the FF mass and charge distributions are given. In the case of (n,f) the <RT> values are close to 1 (not more than 6% higher), in the case of SF they are a little bit higher (about 15% above 1).

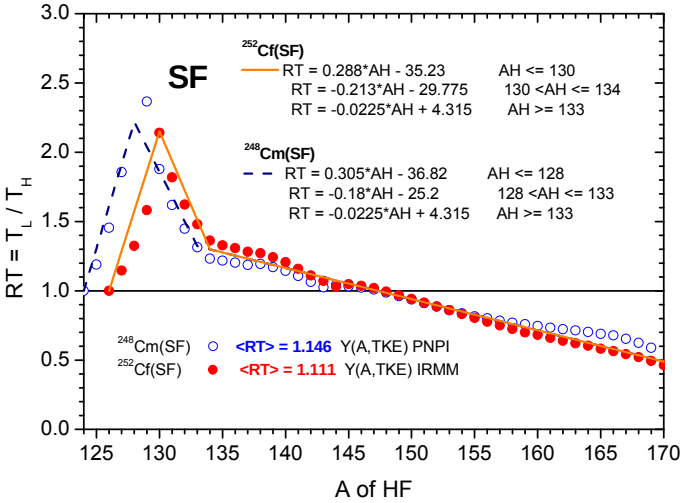

***Figure 6**. FF temperature ratios and parameterisations for spontaneous fissioning systems.*

Examples of PbP calculation of prompt neutron emission quantities using the TXE partition methods and new RT parameterisations

The TXE partition method based on the ν_H/ν_{pair} parameterisation was successfully used in the PbP model calculations of the multi-parametric matrix ν(A,TKE), of many quantities related to each fragment (such as ν(A), <ε>(A), E_γ(A) and so on), of average quantities (total average prompt neutron multiplicity and spectrum, <ν>(TKE) and so on) and the prompt neutron multiplicity distribution P(ν). Almost all fissioning systems having experimental FF distributions were studied in the frame of the PbP model (^{232,233,235,238}U(n,f), ^{231,233}Pa(n,f), ^{237}Np(n,f), ^{239}Pu(n,f), ^{240,242}Pu(SF), ^{244,248}Cm(SF), ^{252}Cf(SF)) with results reported in [3-6] and references therein.
For all fissioning systems the PbP calculations of ν(A) by using the two TXE partition methods showed that a less pronounced sawtooth shape of ν(A) is obtained in the case of the “equal T” method. An example is given in Fig. 7.
The total prompt neutron spectrum calculations with the two TXE partition methods lead to very close results, insignificant differences are observed only in the region of high prompt neutron energies. An example is given in Fig. 8 for the ^{233}U(n_{th},f) case, were also the result obtained by using the new RT parameterisation is plotted (with dotted line).
Even if the sawtooth shapes provided by the two TXE partition methods are different, the total average prompt neutron multiplicity is practically insensitive to the TXE partition (two examples are given in Table 1).

***Table 1.** Total average prompt neutron multiplicity from the two TXE partition methods*

TXE partition method	^{239}Pu(n_{th},f)	^{237}Np($n_{5.5MeV}$,f)
ν_H/ν_{pair} parameterisation	2.8678	3.4417
Equal T method	2.8686	3.4437

This fact is due to the very close ν(A) values given by the two methods in the fragment mass ranges where the FF mass distributions Y(A) have the highest values. Taking into account that in the A ranges where Y(A) have the highest values, the FF residual temperatures and excitation energies provided by the two TXE partition methods are also very close to each other (see for instance in Fig. 2 the very close values of E*(A) and T(A) in the A ranges 90-

105 and 135-150), total average prompt neutron and gamma-ray quantities insensitive to the TXE partition are expected.

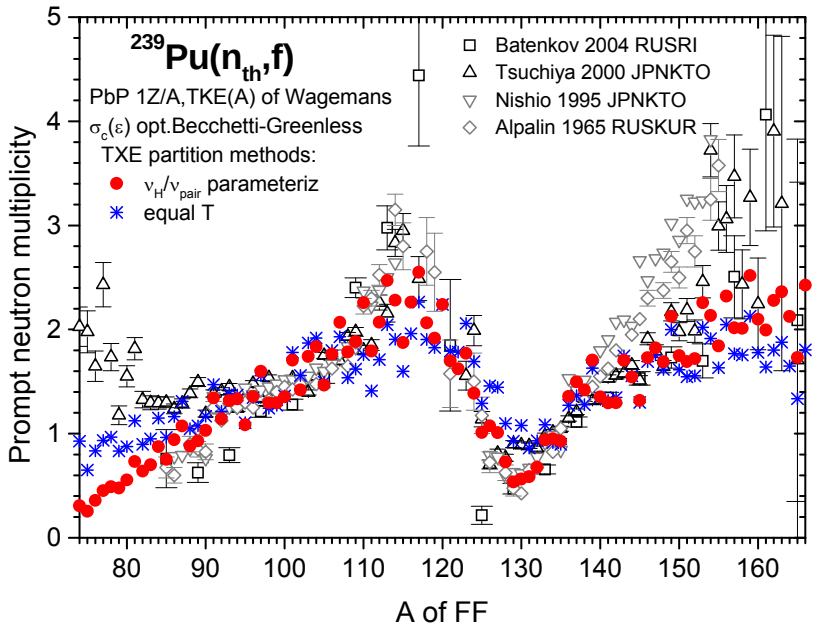

Figure 7. *$^{239}Pu(n_{th},f)$ sawtooth calculations using the two TXE partition methods, in comparison with experimental data from EXFOR*

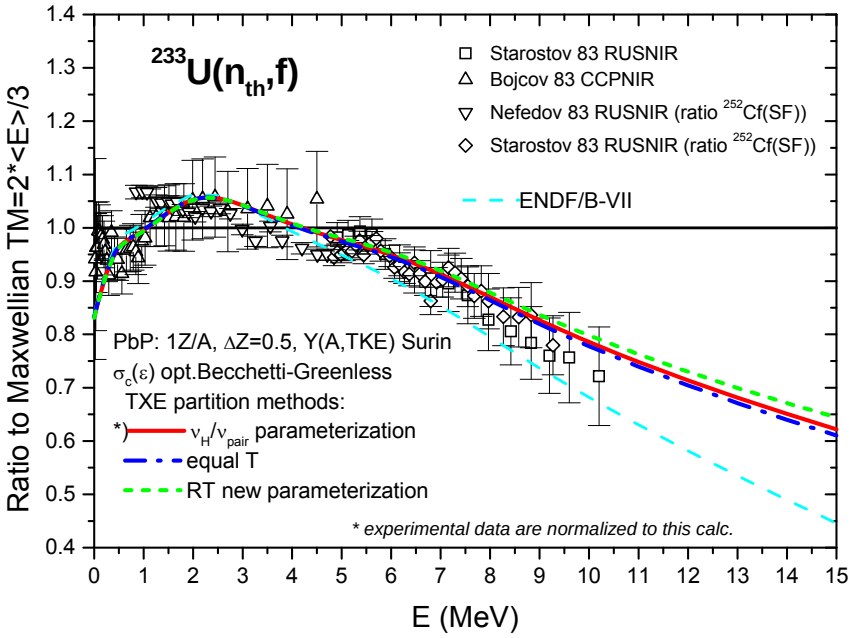

Figure 8. *$^{233}U(n_{th},f)$ PFNS calculations using the two TXE partition methods and the RT parameterization, in comparison with experimental data from EXFOR and ENDF/B-VII*

Average values of quantities related to the TXE partition between FF

Taking into account that in many cases the LA “most probable fragmentation” approach requiring average model parameters is used, the analysis of average values of quantities related to the TXE partition, part of them being also input model parameters, is useful and leads to interesting conclusions.

The average C parameter exhibits an interesting systematic trend consisting in a linear decrease with the fissility parameter as it can be seen in the upper part of Fig. 9, which also contains the linear fits. C is defined as $<C>=A_{CN}/<a>$ where A_{CN} is the mass number of the

fissioning nucleus and <a> = <a_L+a_H> is the fragment pair level density parameter averaged over the FF mass and charge distributions.
Average temperature ratios can be obtained in three manners: i) by averaging RT=T_L/T_H of fragment pairs over the FF mass and charge distributions (these <RT> values being given in Figs. 4 and 6), ii) by calculating the average temperature of the LF and HF groups (also by averaging over the FF mass and charge distributions) and defining the temperature ratio as <T_L>/<T_H>, iii) by calculating the average excitation energies and level density parameters of the LF and HF groups, the mean temperatures of the LF and HF groups being obtained by the relation $\overline{T}_{L,H} = \sqrt{< E^*_{L,H} > / < a_{L,H} >}$.

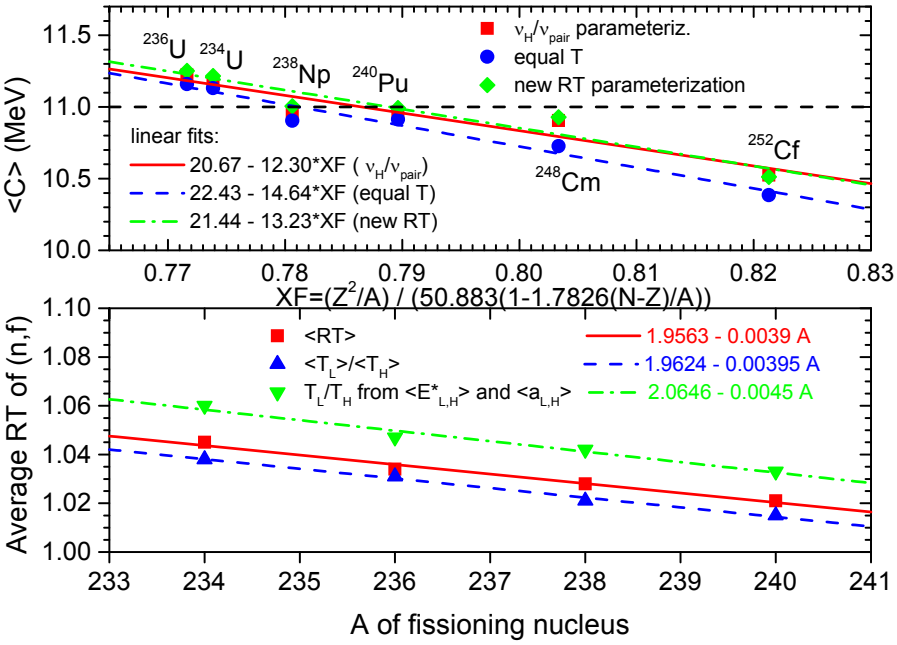

Figure 9. *Upper part: <C> as a function of the fissility parameter, lower part average RT as a function of the mass number of the fissioning nucleus. Linear decreases are visible in all cases.*

For all studied fissioning systems $< T_L > / < T_H > < \langle RT \rangle < \overline{T}_L / \overline{T}_H$.

Also a very interesting systematic behaviour of average temperature ratios as a function of the mass number of the fissioning system is observed in the case of neutron induced fission, their linear decrease is visible in the lower part of Fig. 9.

Conclusions

The comparative analyse of the two partition methods in the frame of the PbP treatment can be synthesized as follows:
- The very interesting systematic behaviour of experimental data concerning ν_H/ν_{pair} as a function of A_H leads to parameterisations that are used for the TXE partition between FF.
- The fragment pair residual temperature ratios RT as a function of A_H exhibit nice systematic behaviours that can be parameterised. RT(A_H) parameterisations were verified by the PbP model calculations of quantities characterising the prompt neutron emission. For neutron induced fissioning systems a general parameterization of RT(A_H) is proposed allowing the use of the PbP model to predict prompt neutron emission quantities of fragments in the absence of any experimental data.
- The maximum residual temperature ratios are practically 1 for fragment pairs with A_H in the range of a few mass units above and below 140 (where Y(A) are maximum, too). Consequently the average RT values are obtained only a little bit higher than 1. In other words the fragmentations occurring with great probability emit prompt neutrons at or near the thermodynamical equilibrium (the fragments having the same residual temperature distribution). For this reason when LA models with only one fragmentation (the so-called most

probable) are used, then the “classical” hypothesis [1] of the equal residual temperature is re-confirmed and also recommended.
- The level density parameter ratios $a_H/(a_L+a_H)$ as a function of A_H exhibit a similar behaviour as the experimental ν_H/ν_{pair} ratios, only the minimum is less pronounced and placed diffusely between A_H=129-134. And this fact is reflected in a less pronounced sawtooth behaviour of E*(A) and ν(A) in the case of the “equal T” method.
- The level density parameter values a(A) obtained by using the two TXE partition methods are close to each other almost in the entire FF mass range (except the region around A_H=130 and $A_H=A_{CN}$-130). As immediate consequence also the C parameter values are close to each other. The nearly equal values of a(A) allow to define an “equivalent temperature” of the FF pair with values practically equal with the temperature values of the “equal T” method. This fact allows not only to reduce the amount of calculations in the PbP model but also to treat the fissioning nucleus fragmentation in terms of FF pairs.
- The average temperature ratios defined as the ratio of average residual temperature of the LF and HF groups $\langle T_L\rangle/\langle T_H\rangle$, exceed 1 with no more that 6% in the case of neutron induced fission and with no more than 15% in the case of SF, being visibly lower than the value of 1.2 proposed in [8].
- The use of a linear RT function [9] for the ^{252}Cf(SF) case, leads to values of prompt neutron quantities very close to our results even if a higher average RT value of about 1.3 is obtained compared to our TXE partition method based on the ν_H/ν_{pair} parameterisation.
- The usual statement that “light fragments emit more neutrons than heavy fragments” is true and verified only in the case of average multiplicities of LF and HF groups. But a more attentive analysis of experimental sawtooth data shows that the LF emits more neutrons than the HF only for fragment pairs with A_H less than 140, for pairs with A_H above 140 the HF emits more neutrons than the LF.
- Both TXE partition methods lead to average excitation energies $\langle E^*_L\rangle$ higher than $\langle E^*_H\rangle$.
- Average values of the C parameter (obtained by both TXE partition methods) show a linear decrease with the fissility parameter.
- In the case of neutron-induced fissioning systems, average RT values exhibit a linear decrease with the mass number of the fissioning nucleus.

Acknowledgements
One of us (A.T.) wants to acknowledge the support of the EFNUDAT project (Contract No. 036434). Also a part of this work (referring to the prompt neutron emission of ^{239}Pu(n_{th},f) and ^{233}U(n_{th},f)) was done in the frame of the IAEA Research Contract No. 15805.

References
[1] D.G. Madland and J.R. Nix, Nucl. Sci. Eng. 81 (1982) 213-271.
[2] S. Lemaire, P. Talou, T. Kawano, M.B. Chadwick, D.G. Madland, Phys. Rev. C 72 (2005) 024601.
[3] A. Tudora, Ann. Nucl. Energy 33 (2006) 1030-1038.
[4] A. Tudora, Ann. Nucl. Energy 35 (2008) 1-10.
[5] A. Tudora, Ann. Nucl. Energy 37 (2010) 492-497.
[6] A. Tudora, F.-J. Hambsch, Ann. Nucl. Energy 37 (2010) 771-777.
[7] A. Ignatiuk in IAEA-RIPL1, Segment V, TECDOC-1034, 1998 (Chapter 5.1.4).
[8] P.Talou, International workshop on Nuclear Fission and Fission Product Spectroscopy, AIP Proceeding 1175 (2009) 261-268.
[9] O.Serot, private communication 2010.

Statistics vs. dynamics in fission: lights and shades from systems of intermediate fissility

E. Vardaci[1,2], A. Di Nitto[1,2], P. Nadtochy[2], A. Brondi[1,2], G. La Rana[1,2], R. Moro[1,2], A. Ordine[2], A. Boiano[2], M. Cinausero[4], G. Prete[4], V. Rizzi[4], N. Gelli[5], F. Lucarelli[5], G.N. Knyazheva[6], E.M. Kozulin[6], T.A. Loktev[6], S. Smirnov[6]

1) Dipartimento di Scienze Fisiche, Universitá di Napoli "Federico II", 80126 Napoli, Italy
2) Istituto Nazionale di Fisica Nucleare, 80126 Napoli, Italy
3) Dipartimento di Fisica and Istituto Nazionale di Fisica Nucleare, Padova, Italy
4) Laboratori Nazionali di Legnaro, Istituto Nazionale di Fisica Nucleare, Legnaro (Padova), Italy
5) Dipartimento di Fisica and Istituto Nazionale di Fisica Nucleare, Firenze, Italy
6) Flerov Laboratory of Nuclear Reactions, JINR,141980, Dubna

Emanuele.Vardaci@na.infn.it

Abstract: Systems of intermediate fissility are characterized by an evaporation residues cross section comparable or larger than the fission cross section, and by a relatively higher probability for charged particle emission in the pre-scission channel. In a theoretical framework in which time scale estimates of the fission process rely on statistical model calculations, the analysis of particle emission in the evaporation residues channel is the source of additional constraints on statistical and dynamical models. This contribution will focus on our statistical and dynamical analysis of a more complete set of data from the system ^{32}S + ^{100}Mo at E_{Lab} = 200 MeV. Statistical model fails in reproducing the whole set of data and no convincing estimate is possible of the fission time scale. In particular, while pre-scission multiplicities can be reproduced without delay, the model strongly overestimates proton and alpha particle multiplicities in the evaporation residues channel irrespective of the statistical model input parameters and prescriptions used for the level density and the transmission coefficients. The analysis of the same set of data with a three-dimensional Langevin dynamical model produces a very good agreement with the full set of data and indicates that one-body dissipation plays a dominant role in the fission process, implying a fission delay 23-25x10^{-21}s.

Introduction

A large variety of experimental studies of induced fission in heavy ion reactions [1] have shown that pre-scission multiplicities of light particles (neutrons, protons and alpha particles) increase monotonically with the bombarding energy, in contrast with the calculations of the standard statistical model (SM) which start from the complete thermalization of the compound system. Since the fission process is considered to be affected by nuclear dissipation [2], this result is considered as the evidence that fission is a slow process with respect to the lifetime for the evaporation of light particles. With increasing excitation energy, the particle decay lifetime decreases and becomes smaller than the time necessary for the build-up of the collective motion of the nuclear matter toward the saddle point. Consequently, fission does not compete as effectively as predicted by the SM in the early stage of the decay, and light particles, and possibly GDR γ-ray, emissions can occur with higher probability.
The overall cause of this transient effect is believed to be associated with the nuclear matter viscosity which slows down the collective flow of mass from the equilibrium to the scission point and does not allow the fission decay lifetime to be downscaled with the excitation energy as in the case of light particles evaporation. This is equivalent to consider that fission is delayed with respect to the picture of the SM in which the fission width has its full Bohr-Wheeler value already at the beginning of the decay. An energy domain has further been identified [3] above which the SM predictions begin to deviate from the data.
Several variants of the SM have been proposed in the literature to take explicitly into account time scales as well as nuclear viscosity. In the simplest fashion, known as the “neutron clock”

[1], the SM is modified so to include another free parameter, the fission delay τ_d : at the beginning of the evaporative cascade the fission decay width is kept to zero for a time τ_d. After τ_d the fission width is set to the full Bohr-Wheeler value. The time scale is defined by the light particle life time. This means that at the beginning of the decay cascade fission does not compete with light particle evaporation until a time τ_d has passed. Estimates of τ_d are obtained by the fit of the experimental multiplicities to the ones predicted by the SM which includes this new parameter.
Other refinements of the neutron clock approach have been proposed to distinguish between different time steps during the fission process [4]. The common approach is to split the path from the equilibrium-to-scission into two regions, the pre- and the post-saddle. The total fission delay is defined as the sum of τ_d and τ_{ssc}, where τ_{ssc} is the time necessary to travel the path from saddle to scission. The relevant observables are computed using τ_d and τ_{ssc} as free parameters, along with the other input parameters relative to the specific ingredients of the model, and fit to the experimental data. In spite of the extensive work, estimates of the fission time scales are however quite controversial. The reported values range from 0 [5] to 500 x 10^{-21} s [6], depending on the system and on the experimental probe. Furthermore, such estimates are weakened by the fact that different sets of input parameters can result in equally good fits within the same model [7, 8].
It must be pointed out that only neutron multiplicities have been measured in most of the studies and mostly for heavy systems (A > 200), and the lack of a sufficient number of constraints to the models could, in several cases, be the source of discrepancies. In order to withdraw a more consistent picture of nuclear dissipation it is crucial, in our opinion, to take into account simultaneously a larger number of observables and probes which can be expected to be sensitive to the nuclear dissipation and to try to reproduce the variety of observables with a unique set of input parameters.

Dissipation in systems of intermediate fissility

Systems of intermediate fissility (χ = 0.5-0.6) are very little studied although they offer several advantages. They are characterized by an evaporation residue (ER) cross section comparable or larger than the fusion-fission (FF) cross section, and by a shorter path in the deformation space from the saddle-to-scission point [9]. Consequently: 1) the input parameters of the models can be further constrained by the energy spectra and multiplicities of the light particles in the ER channel; 2) the effect of the fission delay over the fission and ER cross sections is much more pronounced with respect to heavier systems because the emission of a charged particle in the pre-saddle region strongly enhances the probability of producing an evaporation residue as consequence of both a reduction of the fissility and the large value of the angular momentum necessary to ignite fission. The use of the light particle multiplicities in the ER channel as further constraint grounds, however, also on the reliability of the statistical model to reproduce such multiplicities when all the necessary experimental constraints are given and this is not demonstrated yet.
We expect that the measurements of neutron and charged particle multiplicities and energy spectra in the two channels as well as the measurements of the cross sections of the channels themselves will allow more severe constraints onto the models. This should provide more reliable values of fission delay and of the friction parameter, and contribute to a better comprehension of the origin of nuclear viscosity. In this framework, the 8πLP collaboration has started a research program at the Laboratori Nazionali di Legnaro (Padova, Italy) aimed at studying the fission dynamics in systems of intermediate fissility.
In this presentation we will report on our analysis of the reaction 200MeV ^{32}S + ^{100}Mo leading to the composite system ^{132}Ce at E_x = 122 MeV and fusion angular momentum L_{fus} = 72$\hbar$, derived from the measured fusion cross section in the sharp cut-off approximation. We will show the inability of the SM to provide an estimate of the fission time scale when the evaporation residue channel is included as a further constraint in the procedure used to estimate the fission delay time. Afterwards, our study with an advanced realistic dynamical approach based on a three-dimensional (3D) Langevin approach [10] will be discussed. It will prove to be a method that better reproduces the overall multitude of data.

Experimental procedure and data analysis

For the system ^{32}S + ^{100}Mo at E_{lab} = 200 MeV we have measured the observables shown in Table 1. The experiment was performed at the XTU Tandem - ALPI Superconducting LINAC accelerator complex of the Laboratori Nazionali di Legnaro. A 200 MeV pulsed beam of ^{32}S of about 1 pnA intensity was used to bombard a self supporting ^{100}Mo target, 300 μg/cm thick. A beam burst with frequency of about 1.25 MHz and duration of about 2 ns was used.

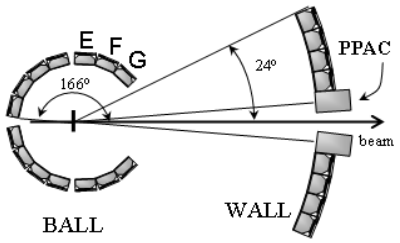

Figure 1. *Schematic layout of the 8πLp apparatus.*

We used the BALL and the WALL sections of the 8πLP apparatus [11], shown schematically in Figure 1, to detect light charged particles (LCP). The WALL consists of 116 telescopes placed at 60 cm from the target and covers an angular range from 2° to 24°. The BALL consists of 7 rings placed coaxially around the beam axis each with 18 telescopes which amount to a total number of 126 telescopes covering an angular range from 34° to 166°. The telescopes of the BALL are made out of a 300μm Si detector mounted in the flipped configuration (particle entering from the ohmic side) backed by a 3 mm CsI(Tl) crystal. The rings are labelled from A to G going from backward to forward angles. Each ring covers an angular opening of about 17°. The experimental method consists in measuring LCP in coincidence with both fission fragments and with the ER.

The fission fragments were detected in the telescopes of the ring F and G of the BALL. The Pulse Shape Discrimination technique allows the separation between heavy fragments and LCP stopping in the same detector. Evaporation residues were detected through 4 Parallel Plate Avalanche Counter modules (Figure 1). Each one covers a forward angle of 2.5° and 7.5° and subtends a solid angle of about 0.3 msr. A module consists of two coaxial PPACs mounted and operating in the same gas volume at a distance of 15 cm from each other. By adjusting the gas pressure, it is possible to stop the ER between the two PPACs, and let the lighter ions to impinge on the second PPAC. Consequently, ERs are sorted out from the first PPAC signals using the signals from the second PPAC as a veto.

In a separate experiment the ER cross section was measured by means of the electrostatic deflector of LNL and the FF cross section was measured with the double-arm time-of-flight spectrometer CORSET [12] at LNL as well.

For the system ^{32}S + ^{100}Mo at E_{lab} = 200 MeV we have measured most of the relevant quantities in the ER and FF channels: proton and alpha particle energy spectra and multiplicities, ER and FF cross sections as well as mass and total kinetic energy distributions of fission fragments. To extract the pre- and post-scission integrated multiplicities, particle energy spectra have been analyzed considering three evaporative sources: the composite nucleus prior to scission (CE) and the two fully accelerated fission fragments (F1 and F2). We used a well established procedure which employs the Monte Carlo statistical code GANES [13,14].

The full set of data is shown in Table 1 along with the results of the SM calculations performed with the code PACE2_N97 [15] and with a 3D Langevin dynamical code [10, 16] which implements the one-body and two-body dissipation models. The dynamical model is coupled with the statistical model Lilita_N97 to simulate the emission of LCP from ER and from the composite system before scission (pre-scission emission). The symbols are as follows: the multiplicities of the protons and alpha particles in the ER channel are, respectively, M_p and M_α (ER); M_p and M_α (PRE) are the prescission multiplicities. σ_{ER} and σ_{FF} are, respectively, the ER cross section and the FF cross section; <Mass> and σ_{Mass} are the mean and the standard deviation of the measured mass distribution, respectively; <TKE> and σ_{TKE} are the mean and the standard deviation of the measured TKE distribution, respectively.

Table 1. Comparison of measured observables (Exp.) and the best predictions of the code. One-body is obtained with full one-body dissipation, two-body with viscosity parameter μ = 0.46 TP.

	M*p* (ER)	Mα (ER)	M*p* (PRE)	Mα (PRE)	σ_{ER} (mb)	σ_{FF} (mb)	<Mass> (u)	σ_{Mass} (u)	<TKE> (MeV)	σ_{TKE} (MeV)
Exp.	0.9 (0.14)	0.56 (0.09)	0.055 (0.007)	0.038 (0.005)	828 (50)	130 (13)	66	15.4	90.9	11.4
SM	1.44	1.64	0.058	0.034	813	143				
OneBody	1.198	0.556	0.064	0.0399	786	150	65	14.6	82.1	7.2
TwoBody	1.18	0.57	0.059	0.031	758	178	65.5	14.9	79.4	7.3

Statistical model analysis

We analyzed the measured quantities in Table 1 with the SM implemented in the code PACE2. The original code has indeed been [15] extended with the inclusion of new options for the level density and the transmission coefficients as well as the possibility to account for a fission delay according to the prescription widely used in the literature [1]. The fission delay parameter τ_d is used in such a way that the fission probability is zero up to the time τ_d and has the full Bohr-Wheeler value subsequently.

If we limit our analysis to the FF channel only, namely, if we only try to reproduce the multiplicities in the FF channel as usually done [1], the data shown in Table 1 can be reasonably well reproduced assuming $a_\nu = A/9$, $a_f/a_\nu = 1.04$, liquid drop model (LDM) yrast line and optical model (OM) transmission coefficients [17-19], without any delay. The parameter a_ν is the Fermi gas level density parameter for particle evaporation and a_f is the level density parameter for fission.

From this result one could conclude that no transient effect takes place in this decay, in contrast with the systematics [3], although a different combination of input parameters does not exclude the presence of a relatively small fission delay. On the other hand, with the same parameters, the model strongly overestimates the ER particle multiplicities even though it reproduces the ER cross section. This is an evident contradiction: if the model is not able to reproduce the LCP multiplicities in the ER channel, once the ER cross section is well accounted for, the same model can not be supposed as a reliable tool to estimate the fission time scale through the pre-scission light particle multiplicities.

Table 2. *Summary of the SM parameters used in the calculations for the level density (a_ν),yrast line (YR) and the transmission coefficients (TC);*

Prescription	a_ν	YR	TC
a)	A/6	RS	OM
b)	A/12	LDM	OM
c)	A/6	RS	FS
d)	A/6	LDM	OM

In order to explore the possibility to reproduce the data in both channels with a unique set of input parameters we performed an extensive analysis with different prescriptions of the level density parameter and transmission coefficients. Calculations have been carried out adopting three different and well known prescriptions for the yrast line: 1) Gilbert Cameron [20], 2) LDM and 3) sharp rigid sphere (RS) with radius parameter r_0 = 1.2 fm. Different prescriptions have also been used for the level density parameter a_ν: 1) a constant value ranging from A/6 to A/12, 2) inclusion of shell effects [21] with a damping term [22] as a function of the excitation energy and 3) a temperature dependent prescription [23]. Transmission coefficients derived from: 1) optical model and 2) fusion systematics (FS) [24] have been used. Different values of fission delay and a_f/a_ν have been adopted to modulate particle-fission competition.

Calculations have been constrained by the sum of the measured evaporation residue and fission cross section $\sigma_{fus} = \sigma_{ER} + \sigma_{FF} = 958\,mb$.

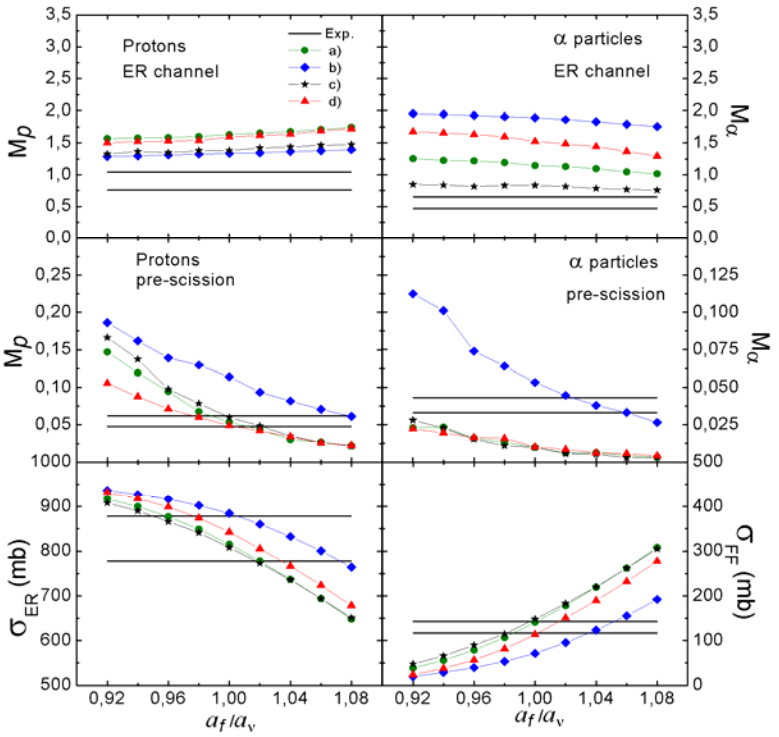

Figure 3. *Measured evaporative (ER) and pre-scission (PRE) charged particle multiplicities together with the FF and ER cross sections (full lines indicating lower and upper limits of the uncertainty), compared to the predictions of the statistical model (symbols connected by lines to guide the eye) using prescriptions: a), b), c) and d) reported in Table 2. See text for details.*

In Figure 3 we show the multiplicities for protons and alpha particles, in the ER and FF channels, as well as the measured channel cross sections, compared to the calculated values, as a function of the ratio a_f / a_ν. We report in the figure the results corresponding to the prescriptions labeled as a), b), c) and d), whose peculiarities are reported in Table 2. The prescriptions a), b), c) and d) presented here have been chosen among the many combinations for which calculations have been performed as they allow to explore the full range of variability of the calculated values of the observables under examination. No fission delay has been included in the calculations. From Figure 3 we infer that the SM strongly overestimates proton and alpha particle multiplicities in the ER channel for this system, irrespective of the input parameters and the prescriptions used for the level density and transmission coefficients. Same result is confirmed by the calculations performed with the well known codes Lilita_N97 [25] and Gemini [26]. Furthermore, the inclusion of a time delay to further suppress the fission does not change the overall pattern of the calculated data with respect to the experimental data. At the same time, the influence of nuclear deformation would further enhance the statistical model particle multiplicities predictions, resulting in a larger overestimation. On the other hand, the comparison of the measured proton and alpha particle energy spectra with the SM shows no evidence of nuclear deformation.

It should be pointed out that the overestimate in the ER channel found for the present compound system was found also in other systems of similar mass. We have in fact compared experimental data taken from the literature with the predictions of our code PACE2_N97. Indeed in the literature there are only few systems for which the ER channel LCP multiplicities have been measured. From calculations performed by us, once again we find that the SM overestimates protons and alpha particle multiplicities in the ER channel which makes us to suspect that the SM is behaving surprisingly at variance with what expected.

Dynamical model analysis

These contradictory results outline the necessity of considering dynamical models. Recently we have coupled the Lilita_N97 code with a dynamical model [10] which describes the fission process by using a 3D Langevin stochastic approach. This coupling was necessary in order to allow the evaporation of light particles from the composite system during the evolution along trajectories in the phase space. At the moment we have performed several sets of calculations for the system ^{32}S + ^{100}Mo at E_{Lab} = 200 MeV assuming different prescriptions of transmission coefficients and level densities for particle evaporation, and by modulating the values of the strength of the one-body and two-body dissipation schemes. From Table 1 we see that the model is able to reproduce most of the measured quantities, including the ones in the ER channel, assuming full one-body dissipation, and with a viscosity parameter μ independent upon the temperature but dependent on the deformation of the fissioning system. In order to obtain a similar agreement with two-body dissipation, the unrealistic value of viscosity parameter μ = 0.24 TP had to be used, as already found in Ref. [27]. The full one-body dissipation implies a transient times for fission in the range of 23-25 x 10^{-21}s.

Conclusions

Our study on the system 200MeV ^{32}S + ^{100}Mo highlights the inadequacy of the SM in describing the LCP particle multiplicities in the ER channel. Same analysis performed on data from literature in the region of mass number A ≈ 150 and excitation energy E_x ≈ 100-200 MeV, for the ER channel, provides similar conclusions. This result pours some shade on the application of the SM in studies designed to investigate on the presence of transient effects. These findings also repropose the problem of the reliability of the SM in describing the compound nucleus decay and have a relevant impact on the extraction of the fission delay time through the use of the SM. The dynamical approach to fission decay is instead very promising in describing both fission and evaporation residues channel within the same model and consequently sheds some light on the physics of the fission process.

References

[1] P. Paul and M. Thoennesen, Ann. Rev. Nucl. Part. Sci. 44, 65 (1994).
[2] A. Kramer, Physica (Amsterdam) 7, 284 (1940).
[3] M. Thoennessen and G. F. Bertsch, Phys. Rev. Lett. 71, 4303 (1993).
[4] J. P. Lestone et al, Nucl. Phys. A 559, 277 (1993).
[5] J. P. Lestone et al, Phys. Rev. C59, 1540 (1999).
[6] D. J. Hofman, B. B. Back, and P. Paul, Nucl. Phys. A599, 23c (1996).
[7] A. Chatterjee et al., Phys. Rev. C52, 3167 (1995).
[8] I. Diószegi et al., Phys. Rev. C61, 24613 (2000).
[9] M.G. Itkis, A. Ya. Rusanov, Phys. Part. Nucl., 29 160 (1998).
[10] P.N. Nadtochy et al. Phys. Rev. C65, 064615 (2003).
[11] E. Fiorettto et al., IEEE Trans. Nucl. Scie., 44, 1017 (1997).
[12] M. Kozulin et al., Prib. Tekh. Eksp. 1, 51 (2008); Instrum. Exp. Tech. 51, 44 (2008).
[13] R. Lacey et al., Phys, Rev. C37, 2540 (1988) and Phys, Rev. C37, 2561 (1988).
[14] G. La Rana et al., Eur. Phys. J. A16, 199 (2003).
[15] PACE2_N97 is a modified version of the original PACE2 by A. Gavron, Phys. Rev. C21, 230 (1980).
[16] A. Di Nitto, PhD. Thesis, University of Naples, Italy (2009), www.infn.it
[17] J. R. Huizenga and G. Igo, Nucl. Phys. 29, 462 (1961).
[18] F.G. Perey, Phys. Rev. 131, 745 (1963).
[19] D. Willmore and P. E. Hudson, Nucl. Phys. 55, 673 (1964).
[20] A. Gilbert and A. G. W. Cameron, Can. J. Phys. 43, 1446 (1965).
[21] S. K. Kataria, V.S. Ramamurthy and S.S. Kapoor, Phys. Rev. C18, 549 (1978).
[22] A. V. Ignatyuk et al, Yad. Fiz. 21, 485 (1975), [Sov. J. Nucl. Phys. 21, 255 (1975).
[23] J. P. Lestone, Phys. Rev. C52, 1118 (1995).
[24] L. C. Vaz et al., Z. Phys. A318, 231 (1984).
[25] Lilita_N97 is an extensively modified version of the original Lilita program made by J. Gomez del Campo and R. G. Stockstad, ORNL Report No. TM7295, 1981 (unpublished).
[26] R. J. Charity, Computer code GEMINI (unpublished).
[27] Wada et al. *Phys. Rev.* Lett. 70, 3539 (1993).

Re-absorption and scattering of scission neutrons by the fission fragments

T. Wada[1)], R. Nishioka[1)], T. Asano[2)]

1) Dept. Pure and Applied Physics, Kansai University, 3-3-35 Yamate-cho, Suita 564-8680, Japan
2) RCNP, Osaka University, 10-1 Mihogaoka, Ibaraki 567-0047, Japan
wadataka@kansai-u.ac.jp

Abstract: A formulation is given to investigate the angular distribution of scission neutrons. The effects of the re-absorption and scattering by the fission fragments are taken into account by means of the S-matrix. Results are given for two simple models: the purely absorptive model and the optical potential model. Dependence on the magnitude of the absorption and on the separation between fragments is discussed.

Introduction

Neutron emission is one of the important processes to understand the dynamics of nuclear fission. Pre-scission neutrons give us the information on the time scale of fission through the competition between neutron emission (Γ_n) and fission (Γ_f) [1]. On the other hand, post-scission neutrons give us the information on the deformation of the fission fragments through the partition of the excitation energy between the fragments. These components can be separated by taking the kinematical condition into account; post-scission neutrons are emitted from the moving source (fully accelerated fragments) while the pre-scission neutrons are emitted from the source at rest. Besides these two components, there is another important source of neutron, i.e. scission neutrons. The importance is more prominent in low energy fission like spontaneous fission and thermal neutron induced fission, since we can neglect the pre-scission particle emission.

At the moment of scission, the neck that has connected the two fission fragments ruptures, then the neck protuberances are absorbed rapidly by the fragments. On this abrupt change of nuclear shape, it is probable that nucleons are left behind in the neck region and are observed as particle emission. From the energetic consideration, neutrons are the most probable to be emitted in this process. Attempts have been made to estimate the fraction of scission neutrons [2, 3], they reported that 10-20% of the total neutron yield could be scission neutrons. It is also attempted to estimate the number of scission neutrons theoretically [4]. They assumed a sudden change of the nuclear shape at the moment of scission and estimated the fraction of neutrons that are left in the continuum. The results depend on the nuclear shape such as the neck radius before scission. If we extract the reliable number of scission neutrons from experiments, we can get information on the nuclear shape at the time of scission. The angular distribution of the scission neutron is a key to separate it from other neutron components as well as the energy spectrum.

The emission of scission neutrons is supposed to be isotropic in the lowest order approximation. However, since they are emitted in the close vicinity of the fission fragments, the final angular distribution of the scission neutrons is disturbed with the re-absorption and the scattering by the fragments. In this paper, we present a formulation to calculate the angular distribution of the scission neutrons taking account of the effect of the re-absorption and the scattering by the fission fragments. In the next section, a new formulation is given to calculate the angular distribution of the scission neutrons in which the effect of the re-absorption and the scattering is taken into account in term of the S-matrix. Then we show the results with simple models, a purely absorptive model and an optical model with square well potentials, to demonstrate the qualitative features of our formalism. Finally, a summary is given.

Formalism

First, we assume a simple configuration; the fissioning nucleus is separated into two identical fragments leaving some fraction of neutron wave function around the midpoint of the fragments. Since the scission neutrons are emitted from a compact region outside of the

fragments, this emission is simply expressed by an outgoing spherical wave expanding from the origin. Now, we rewrite this outgoing wave in a new coordinate system; the coordinates measured from the center of one fragment. The outgoing wave with the wave number k is expanded as

$$\frac{1}{R}\exp(ikR) = ik\sum_l (2l+1)\, j_l(kr_<)h_l^{(1)}(kr_>)P_l(-\cos\theta_1) \tag{1}$$

where $\boldsymbol{R} = \boldsymbol{\rho} + \boldsymbol{r}_1$, $R = |\boldsymbol{R}|$, $\rho = |\boldsymbol{\rho}|$, $r_1 = |\boldsymbol{r}_1|$, $r_> = \max(r_1, \rho)$, $r_< = \min(r_1, \rho)$, and θ_1 is the angle between $\boldsymbol{\rho}$ and $\boldsymbol{r}_1$. $\boldsymbol{\rho}$ indicates the center of one fragment and $\boldsymbol{r}_1$ is the position measured from the center of the fragment. Because we assume a symmetric fission here, the center of the other fragment lies at $-\boldsymbol{\rho}$. Though the neutrons emitted isotropically in $\boldsymbol{R}$, they are expressed as a sum of partial waves in the new coordinates. The emitted neutrons are scattered by the potentials that represent the effects of the fragments. The range of the potential is about the size of the fragment. Again for simplicity, we assume the spherical potential with the radius a.
In our setting, the scission neutrons are emitted well outside of the fragments, i.e. emission points of scission neutrons are outside of the interaction range of the fragments. Thus, when we treat the points in the interaction range of a fragment whose center is situated at $\boldsymbol{r}$, we have $\rho > r$. The scission neutrons interact with this fragment, some of them are scattered and some of them are re-absorbed, i.e. the initial wave is modified. We assume here that the effect can be expressed in terms of an *S*-matrix,

$$j_l(kr) \to j_l(kr) + \frac{i(1-S_l)}{2}h_l^{(+)}(kr)$$

where r is taken to be outside of the interaction range of the fragment, but still satisfies $\rho > r$. Inserting this "asymptotic" form in Eq. (1), the modification of the initial wave by the right fragment is expressed as

$$\begin{aligned}\frac{1}{R}\exp(ikR) &\to ik\sum_l (2l+1)\left(j_l(kr_1) + \frac{i(1-S_l)}{2}h_l^{(+)}(kr_1)\right)h_l^{(1)}(k\rho)P_l(-\cos\theta_1) \\ &= \frac{1}{R}\exp(ikR) - \frac{k}{2}\sum_l (2l+1)(1-S_l)h_l^{(+)}(kr_1)h_l^{(1)}(k\rho)P_l(-\cos\theta_1)\end{aligned} \tag{2}$$

Thus, the additional wave that is emitted from the right fragment is expressed as

$$-\frac{k}{2}\sum_l (2l+1)(1-S_l)h_l^{(+)}(kr_1)h_l^{(1)}(k\rho)P_l(-\cos\theta_1)$$

We call this wave the "scattered wave" from the right fragment. In the same manner, we get the scattered wave from the left fragment,

$$-\frac{k}{2}\sum_l (2l+1)(1-S_l)h_l^{(+)}(kr_2)h_l^{(1)}(k\rho)P_l(\cos\theta_2)$$

where $\boldsymbol{R} = -\boldsymbol{\rho} + \boldsymbol{r}_2$, $r_2 = |\boldsymbol{r}_2|$ and θ_2 is the angle between $\boldsymbol{\rho}$ and $\boldsymbol{r}_2$.
In the asymptotic region ($R \to \infty$), r_1 and r_2 are also large, $r_1, r_2 \to \infty$. In this case, we can use the asymptotic form of $h_l^{(+)}$. By noting the following relations,

$$h_l^{(+)}(kr_1) \to \frac{1}{kr_1}\exp\left(ikr_1 - \frac{il\pi}{2}\right) \to (-i)^l \frac{\exp(ikR)}{kR}\exp(-i\vec{k}\cdot\vec{\rho})$$

$$h_l^{(+)}(kr_2) \to \frac{1}{kr_2}\exp\left(ikr_2 - \frac{il\pi}{2}\right) \to (-i)^l \frac{\exp(ikR)}{kR}\exp(i\vec{k}\cdot\vec{\rho})$$

the sum of the three waves, the initial wave, the scattered wave from the right fragment and the scattered wave from the left fragment, is expressed as,

$$\begin{aligned}\Psi_k(R,\theta) \to \frac{1}{R}\exp(ikR)\Bigg\{1 &- \frac{1}{2}\sum_l (2l+1)(1-S_l)(-i)^l h_l^{(1)}(k\rho)P_l(-\cos\theta)\exp(-ik\rho\cos\theta) \\ &- \frac{1}{2}\sum_l (2l+1)(1-S_l)(-i)^l h_l^{(1)}(k\rho)P_l(\cos\theta)\exp(ik\rho\cos\theta)\Bigg\}\end{aligned}$$

where θ denotes the angle between $\boldsymbol{R}$ and $\boldsymbol{\rho}$. The angular distribution of scission neutron is given as

$$R^2\left|\Psi_k(R,\theta)\right|^2 \rightarrow f_k(\theta)$$

$$f_k(\theta)=\left|1-\frac{1}{2}\sum_l(2l+1)(1-S_l)(-i)^l h_l^{(1)}(k\rho)P_l(-\cos\theta)\exp(-ik\rho\cos\theta)\right.$$
$$\left.-\frac{1}{2}\sum_l(2l+1)(1-S_l)(-i)^l h_l^{(1)}(k\rho)P_l(\cos\theta)\exp(ik\rho\cos\theta)\right|^2 \quad (3)$$

Equation (3) gives the angular distribution of mono-energetic neutrons with wave number k. When necessary, we can average it over the energy distribution of the fission neutrons,

$$f(\theta)=\int dk\, w(k) f_k(\theta) \quad (4)$$

where $w(k)$ is a weight function.

Results

As an example, we consider the fission of ^{236}U that corresponds to the neutron induced fission of ^{235}U. As was mentioned earlier, we here consider the symmetric fission for simplicity. An important quantity in the calculation is $k\rho$ that comes from the separation between the fragments. To determine the value of ρ, we utilize the systematics of the average total kinetic energy (TKE) of the fragments. From a systematic study of TKE, Zhao et al. derived the elongation parameter β which is the ratio between the average distance between the fragments $D(A_1, A_2)$ to the contact distance $r_0(A_1^{1/3} + A_2^{1/3})$ [5].

$$\overline{TKE}=Z_1Z_2e^2/D(A_1,A_2)$$
$$\beta=D(A_1,A_2)/r_0(A_1^{1/3}+A_2^{1/3})$$

The average distance between the fragments is determined so that the corresponding point charge Coulomb energy is equal to the average TKE. They found that the value of β stays constant over a wide mass range of the fissioning nuclei. They obtained β = 1.53 for the asymmetric fission in U region and β = 1.33 for the compact symmetric fission in Fm region. In our formulation, ρ is calculated as $\rho = \beta\, r_0\, (A/2)^{1/3}$, where A is the mass number of the fissioning nucleus and r_0 = 1.17 fm.

In our formulation, the key quantity to determine the angular distribution of the scission neutron is the S-matrix S_l, which can be calculated in several ways. In the following, we apply simple models for the calculation of S_l to examine the qualitative features of the formulation.

Purely absorptive model

In this model, S_l is given as the following,

$$S_l=\begin{cases}0 & l<l_{\max}\\ 1 & l>l_{\max}\end{cases}$$

The quantity l_{max} is given as $l_{max} = ka$, where k is the wave number of the emitted neutron and a is the radius of a fragment, $a = r_0\,(A/2)^{1/3}$. It is known that this absorptive model corresponds to a completely absorptive sphere in the semi-classical limit, i.e. when l_{max} approaches to infinity. For 1 MeV neutron, k is about 0.22 fm^{-1}, that gives ka = 1.3 for the case of the fission of U. That means only very few partial waves (l = 0, 1) contribute to the absorption. Consequently, the wave nature of neutron shows up.

Figure 1 shows the results with this model for the case of the symmetric fission of ^{236}U. The elongation parameter is taken as β = 1.53. The angular distribution is presented in the polar plot, i.e. the abscissa represents the fragment axis, the axis that connects the centers of the fragments, and the ordinate represents the direction perpendicular to the fragment axis. The radius for each direction represents the strength of the neutron emission $f(\theta)$ to that direction. Since we have the axial symmetry, we only plot for the value of θ from 0 to π. The solid line

shows the result when both fragments are taken into account while the dashed line denotes the case when we only take account of the right fragment. The dotted line shows the result when we only take account of the s-wave component (from both fragments). Results are normalized to the value at θ = π/2. For the dashed line and the dotted line, the same normalization as in the case of the solid line is used. The results show that we observe more neutrons along the fragment axis than in the direction perpendicular to it. This is true even when we only take account of the s-wave component. It is to be noted that the results show that we observe more neutrons on the same side of the fragment.

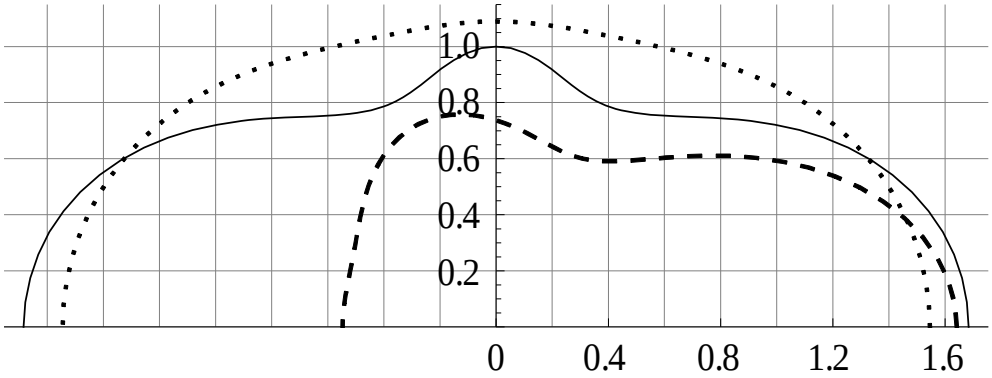

Figure 1. *Angular distribution with the purely absorptive model: Both fragments (solid line), both fragments but s-wave component only (dotted line), and right fragment only (dashed line).*

Optical model

In the analysis of nuclear reactions, a local complex potential is frequently used to incorporate with the loss of flux due to the coupling to the reaction channels. Woods-Saxon shape is commonly used to describe the scattering of a nucleon from a nucleus. Here, however, we use a square well potential for the calculation of S_l, since we get an analytical solution in this case. For a square well potential with the depth V_0 and the width a, S_l is given as the following,

$$S_l = \frac{u_l^{(-)}(a)}{u_l^{(+)}(a)} \cdot \frac{D_{in} - D^{(-)}}{D_{in} - D^{(+)}}$$

$$D_{in} = \frac{du_l(a)}{dr} \Big/ u_l(a), \quad u_l(r) = qr\, j_l(qr), \quad q = \sqrt{k^2 + \frac{2mV_0}{\hbar^2}}$$

$$D^{(\pm)} = \frac{du_l^{(\pm)}(a)}{dr} \Big/ u_l^{(\pm)}(a), \quad u_l^{(\pm)}(r) = kr\, h_l^{(\pm)}(kr)$$

Similar solutions can be obtained with the complex square well potential $V_0 + \mathrm{i}W_0$.

Figure 2 shows the angular distribution of mono energetic scission neutrons for the case of the square well optical potential with the elongation parameter β = 1.53. The depth of the real part of the potential V_0 is 40 MeV in this calculation and the strength of the imaginary part W_0 is 5 MeV. Taking account of the mirror symmetry, we hereafter plot only for the value of θ from 0 to π/2. The left panel shows the dependence on the energy of the emitted neutrons. The dashed curve is for E_n = 0.5 MeV, the solid curve 1.0 MeV, and the dotted curve 1.5 MeV. The right panel shows the convergence with the partial wave summation for E_n = 1.0 MeV case. The dotted curve represents the results when we take account of s- and p-waves only, the dotted curve is when we include up to d-wave, and the solid curve is the sum of all the contributing partial waves.

Finally, Figure 3 shows the results of energy averaged cases. The distribution $w(k)$ is taken as,

$$w(k) = \exp\left(-\hbar^2 k^2 / 2m\right)$$

The left panel shows the dependence on the strength of the imaginary potential; the dotted curve is for no imaginary part case (W_0 = 0), the solid curve is for W_0 = 5 MeV, and the dashed curve is for W_0 = 20 MeV. It is to be noted that the result tells us that we observe more neutrons along the perpendicular axis as we increase the strength of the absorption. In the

right panel, we show the dependence on the distance between the fragments that is represented with β. The dotted curve is for a compact scission configuration β = 1.33, the solid curve is for β = 1.53, and the dashed curve is for a more elongated case β = 1.65.

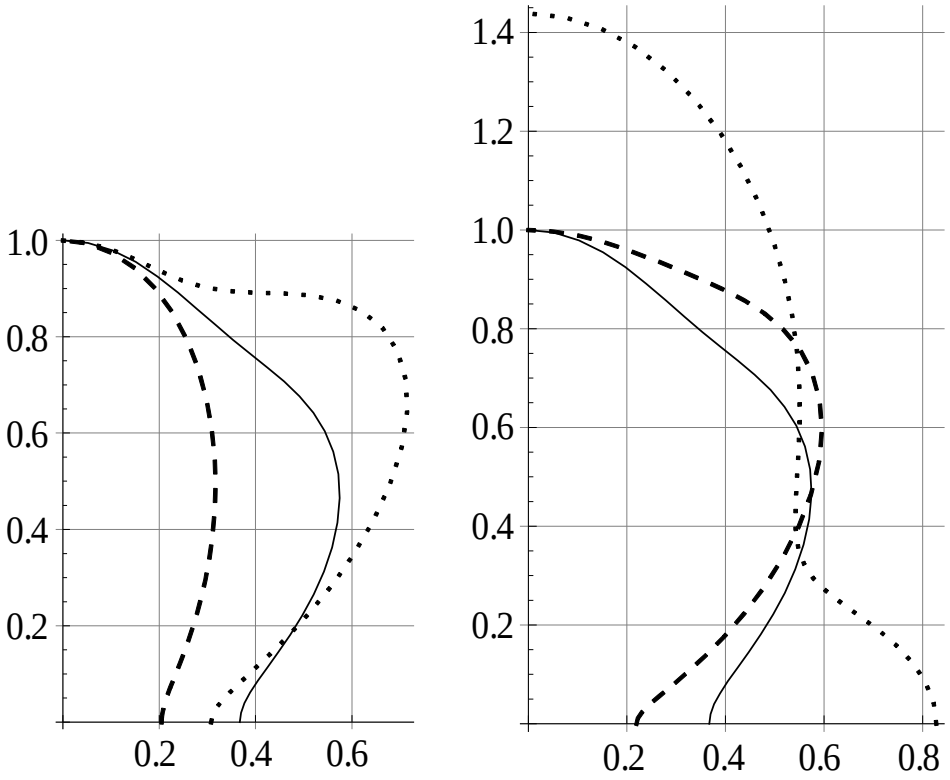

Figure 2. *Angular distribution with the square-well optical potential: (left) Energy dependence: E_n = 0.5 MeV (dashed line), 1.0 MeV (solid line), and 1.5 MeV (dotted line), (right) Convergence with the partial wave summation: s- and p-waves (dotted line), up to d-wave (dashed line), the sum of all partial waves (solid line).*

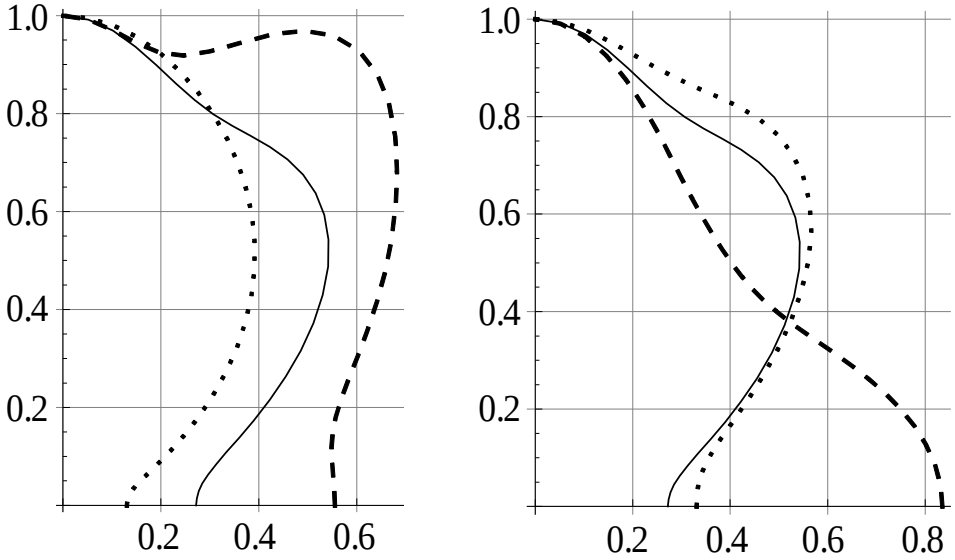

Figure 3. *Angular distribution with the square-well optical potential: (left) Dependence on the imaginary part: W_0 = 0 MeV (dashed line), 5.0 MeV (solid line), and 20.0 MeV (dotted line), (right) Dependence on the distance between the fragments: β = 1.33 (dashed line), β = 1.53 (solid line), and β = 1.65 (dotted line).*

Altogether, the results show strong interference effect among the components from different sources, i.e. scattered waves from the fragments and the original one. When many partial waves contribute, they tend to add up destructively and the semi-classical picture works. In the case of the emission of scission neutrons, the number of partial waves is rather small and it makes the intuitive interpretation of the results difficult.

Summary

The effects of the re-absorption and scattering by the fission fragments on the angular distribution of scission neutrons have been investigated in the framework of the time-independent scattering theory. A formulation to calculate the angular distribution of scission neutrons is given. With a purely absorptive assumption, the formula shows a strong interference effect for low energy neutrons. Preliminary results with optical model type potentials are given. They also show a strong interference effect among the wave functions from different sources.
The information on the angular distribution of the scission neutrons is very important to separate them from other neutron sources. Further investigation with more realistic potentials is necessary and is under progress. It is also desirable to investigate it with a complementary approach, e.g. a time-dependent framework taking account of the wave packet nature of the scission neutrons.

Acknowledgements
The authors would like to express their gratitude to Dr. N. Carjan for inspiring this work and also for many discussions. They also would like to thank Prof. M. Ito for encouragement.

References
[1] D. Hilscher and H. Rossner, Ann. Phys. Fr. 17 (1992) 471;
D. J. Hinde, D. Hilscher and H. Rossner, Nucl. Phys. A538 (1992) 243c.
[2] C.B. Franklyn, C. Hofmeyer, D.W. Mingay, Phys. Lett. B 78 (1978) 564.
[3] N.V. Kornilov et al., Nucl. Phys. A 686 (2001) 187.
[4] N. Carjan, P. Talou, O. Serot, Nucl. Phys. A 792 (2007) 102.
[5] Y. L. Zhao et al., Phys. Rev. C62 (2000) 14612.

AUTHOR INDEX

European Commission

EUR 24802 EN – Joint Research Centre – Institute for Reference Materials and Measurements
Title: THEORY - 1 Proceedings of the Scientific Workshop on Nuclear Fission Dynamics and the Emission of Prompt Neutrons and Gamma Rays. 27 – 29 September, 2010. Sinaia, Romania
Author(s): Franz-Josef Hambsch and Nicolae Carjan
Luxembourg: Publications Office of the European Union
2011 – 172 pp. – 21.0 x 29.7 cm
EUR – Scientific and Technical Research series – ISSN 1018-5593 (print version), ISSN 1831-9424 (online version)
ISBN 978-92-79-20048-9 (print version)
ISBN 978-92-79-20049-6 (pdf version)
doi:10.2787/4298 (print version)

Abstract
The THEORY - 1 workshop was held from Sept., 27 – 29, 2010 at Hotel International, Sinaia, Romania. These proceedings collect the full papers summarising the contributions to this workshop.

The mission of the JRC is to provide customer-driven scientific and technical support for the conception, development, implementation and monitoring of EU policies. As a service of the European Commission, the JRC functions as a reference centre of science and technology for the Union. Close to the policy-making process, it serves the common interest of the Member States, while being independent of special interests, whether private or national.

JRC
EUROPEAN COMMISSION

LA-NA-24802-EN-C

Publications Office

ISBN 978-92-79-20048-9

9 789279 200489